U. S. Department of Energy
1000 Independence Avenue, S.W.
Washington, D.C. 20585

Fiscal Year 2019: Third Quarter

Progress Reports:
Advanced Battery Materials Research (BMR) Program
&
Battery500 Consortium

Released September 2019
for the period of April – June 2019

Approved by

Tien Q. Duong, Program Manager
Advanced Battery Materials Research Program & Battery500 Consortium
Vehicle Technologies and Electrification Program
Energy Efficiency and Renewable Energy

TABLE OF CONTENTS

Advanced Battery Materials Research Program

Battery500 Consortium Program

TABLE OF FIGURES

TABLE OF TABLES

A MESSAGE FROM THE MANAGER: ADVANCED BATTERY MATERIALS RESEARCH PROGRAM AND BATTERY500 CONSORTIUM

This document summarizes the activities of the BMR Program principal investigators performed April 1, 2019, through June 30, 2019. A few notable achievements from the BMR investigators this quarter are summarized below:

- **Brookhaven National Laboratory** (Yang's group) used X-ray fluorescence microscopy and X-ray absorption spectroscopy to study the chemical composition and distribution of sulfur species in cycled cathodes recovered from Li-S pouch cells. Experiments showed significant area-dependent variations possibly due to non-uniform solvent depletion.
- **University of Washington** (Jen's and Yang's groups) investigated the effectiveness of a quasi-solid-state (QSS) electrolyte design toward self-discharge in Li-S coin cells. The QSS system was found to be more resistant to continued degradation caused by the redistribution of sulfur species during prolonged rest.
- The **General Motors** team (Xiao, Sheldon, Qi, and Cheng) investigated the effect of external pressure on the microstructure of electroplated mossy lithium. The results show that the thickness of mossy lithium layer on the plating side of Li | Li symmetric cells decreases with increasing pressure.
- The **Stanford** group (Bao and Cui) designed and tested artificial solid electrolyte interphases (SEI) based on self-healable dynamic polymers and single-ion conducting elastomers. The results demonstrated that improved dynamicity in the polymers enables stable lithium deposition, which is a deviation from the long-standing concept in solid electrolytes stating that high modulus is important to prevent dendrites.
- The **Daikin** group (Sunstrom, Hendershot, and Falzone) conducted thickness measurements of 200 mAh NMC-532 Li-ion cells containing three different electrolytes (EMC/EC, EMC/EC/HFE, EMC/HFE/FEC). Cells containing only fluorinated ether (HFE), and no FEC, displayed the largest thickness increase when cycled to 4.6 V. The increase was not attributed to gassing.
- **Lawrence Berkeley National Laboratory** (Persson's group) is developing models to understand the role of amorphous coatings on lithium cell performance. *Ab initio* molecular dynamics calculations and density-based spatial clustering were used to differentiate the vibrational and translational motions for lithium trajectories. The models suggest that the oxygen content of a coating is one of the limiting factors for lithium diffusion.
- **Argonne National Laboratory** (Johnson's group), which is developing blended composite anodes for Na-ion batteries, reported a high-performance phosphorus-based anode using high-energy ball milling. The anode achieved a high reversible capacity of 2000 mAh/g, high initial Coulombic efficiency of > 90%, and excellent cycle stability. A U. S. patent application was filed.

Highlights from the Battery500 Consortium team include the following:

- **Keystone Project 1 (Materials and Interfaces):** An ether-based liquid electrolyte was developed to give much improved performance over the standard carbonate-based electrolytes in Li||NMC-811 cells.

- **Keystone Project 2 (Electrode Architectures):** Advancement in understanding the importance of Li-anode architectures was made. The role of isolated lithium metal in determining capacity loss was confirmed by a new chemical analysis method.
- **Keystone Project 3 (Cell Fabrication, Testing and Diagnosis):** Li||NMC pouch cells achieved 250 cycles at 350 Wh/Kg with less than 20% fade.

We encourage you to follow our progress as we proceed. Our next report is expected to be available in December 2019.

Sincerely,

Tien Q. Duong

Tien Q. Duong
Manager, Advanced Battery Materials Research Program & Battery500 Consortium
Vehicle Technologies and Electrification Program
Energy Efficiency and Renewable Energy
U.S. Department of Energy

TASK 1 – Liquid/Polymer Solid-State Electrolytes

Summary and Highlights

The BMR Program goal is to develop long-life batteries superior to commercial Li-ion systems in terms of cost, vehicle range, and safety. The BMR Program addresses the fundamental problems of electrode chemical and mechanical instabilities that have slowed development of affordable, high-performance, automotive batteries. The aim is to identify electrode/electrolyte materials that yield enhanced battery performance and lead to greater acceptance of electric vehicles (EVs). Currently, the U. S. Department of Energy (DOE) Vehicle Technologies Office (VTO) supports ten projects in the BMR Program under this Electrolytes Task. These projects can be categorized into three general topics:

- **Liquid.** The projects for liquid electrolyte aim to develop electrolyte formulations, based on fluoro-chemistries, to achieve significantly improved operating voltage, increased durability, and increased energy density of Li-ion batteries at a reasonable cost. Nonaqueous polyelectrolyte solutions with high Li^+ transference numbers will be developed to achieve high rate capabilities at room temperature. In addition, electrolytes with new polymer binders bearing a pentafluorophenyl group on the backbone will be designed, synthesized, and tested.
- **Polymer.** The targets of polymer electrolyte (PE) projects include inorganic/polymer and polymer/gel hybrid electrolytes that have flexibility, mechanical strength, thermal stability, high ionic conductivity, stable interfaces against lithium metal, and polysulfide-trapping capability enabling energy density Li-S batteries, with comparable cycle life.
- **Self-Forming & Self-Healing.** The self-forming, self-healing electrolyte projects are focused on developing and implementing Li-metal-based metal fluorite and metal iodide batteries, capable of energy densities > 400-500 Wh/kg and 1000 Wh/L.

Highlights

At the Daikin group, interim cells for analysis were delivered to Idaho National Laboratory (INL) to complete the final deliverable for FY 2019. Thickness measurements of 200 mAh NMC-532 cells at 4.6 V as a function of electrolyte reveal a measurable increase in the swelling of the cell (non-gassing) at high voltage. Cells that contain only fluorinated ether (hydrofluoroether, HFE), and without fluoroethylene carbonate (FEC), result in the largest thickness increase. These 4.6-V cells with HFE reported last quarter also contain the highest amount of dissolved metals deposited on the anode (nickel, manganese, cobalt).

The Lawrence Berkeley National Laboratory (LBNL) group focused on building lab capabilities to perform rigorous transference number measurements based on concentrated solution theory. The team found that the steady-state condition is difficult to consistently satisfy. Next quarter, they will study the source of this instability using 3-electrode cells with a gold micro-reference electrode, and will further study the effect of the preconditioning cycle on steady-state current measurements. This quarter, the team also developed a setup for thermodynamic factor and electrolyte activity coefficient measurements in a liquid-liquid concentration cell.

At Argonne National Laboratory (ANL), the team has been working to elucidate the beneficial effects of partially fluorinated ethers (PFE) for Li-S batteries, using seven fluorinated ethers with similar structures. They found that the solid electrolyte interphase (SEI) formed with electrolytes containing PFE solvents is distinctly different from that in the typical 1,3-dioxolan : dimethoxyethane (DOL:DME). The previously reported compound 7 and new compound 8 displayed the best Coulombic efficiency (CE) among the seven compounds tested, with values up to 96% without the commonly employed additive $LiNO_3$. The conclusions drawn can aid in development and discovery of new PFE-based solvents for Li-S based batteries.

At University of Maryland (UMD), Li-S full cells were fabricated and evaluated. The discharge curve shows one sloping plateau around 2 V, which represented a solid-state type conversion of Li_2S_8 to Li_2S. The charging curve shows only one plateau, which is often seen in the most common electrolyte based on 1:1 vol DOL and DME. They found that cell capacity has been continuously increasing, which is distinct from the tendency of batteries to lose capacity after cycling. It is observed that capacity doubled after 100 cycles. Due to irreversibility of the side reaction, CE over 100% was attained in the initial 40 cycles. Thereafter, the cell gave high reversible discharge/charge capacities in the following cycles with efficiency above 98%, exhibiting good electrochemical performance over 100 cycles.

The University of Washington (UW) group has additionally tested the robustness of the quasi-solid-state (QSS) design towards self-discharge, to which Li-S batteries are particularly susceptible. They have found that the QSS system is more resistant to continued degradation caused by redistribution of sulfur species during prolonged rest. In addition, they are testing improved gel cathode formulations with the goal of minimizing required thickness for high loading, and reducing the cathode charge transfer overpotential. Furthermore, they studied the effect of adding polyvinylidene fluoride (PVDF) into the polysulfides trapping PENDI-350. Cathode with sulfur loading of 3.7 mg/cm^2 and PENDI-350/PVDF as binder was fabricated. It shows stable capacity around 800 mAh/g after 32 cycles; CE was higher than 98%. Although capacity is stable, it needs improvement. More systematic investigation of the failure mechanism of polypropylene (PP) binder is in progress.

At West Virginia University (WVU), the composite solid electrolytes consisting of the silane-coated $Li_{6.28}La_3Al_{0.24}Zr_2O_{12}$ (s@LLAZO) nanofibers and the cross-linked polyethylene glycol diacrylate (PEGDA) polymer were further studied. The performance of composite solid electrolytes based on the hydrogen-treated $Li_{0.33}La_{0.57}TiO_3$ nanofibers was also investigated with half cells and full cells.

The Stanford University group has designed and tested artificial SEI with two distinct concepts that can enable stable deposition of metallic lithium. The two concepts are based on self-healable dynamic polymers and single-ion conducting elastomers. Interestingly, their results clearly demonstrate that improved dynamicity in the polymers enables stable lithium deposition, which is a deviation from the long-standing concept in solid electrolytes that high modulus is important to prevent dendrites.

The LBNL group studied the effect of Li-metal purity and failure mechanisms. Last year, they found that density of lithium protrusions increased with current density in an analogous block copolymer electrolyte, and that protruding structures were nucleated in the POSS-PEO-POSS (5-35-5) triblock (where POSS is acryloisobutyl polyhedral oligomeric silsesquioxane, and PEO is polyethylene oxide) in the vicinity of these impurity particles. They plated planar lithium at a low current density to use the electrolyte to “filter” out impurity particles (impurity particles do not go through the electrolyte). The goal of this treatment is to reduce nucleation of lithium protrusions by reducing the concentration of impurity particles at the electrode-electrolyte interface. The cells were cycled at a constant current density to determine effects of treatment on lifetime. The treated cells passed an average of 52-390% more charge before failure, compared to control cells. Further work is under way to determine the nature of this improvement.

At Stony Brook University (SBU), cell design B was constructed with four interface variations to determine the impact of elevated temperature. As observed during the long-term cycling study, cell design B I shows CE of between 90 and 100% throughout the testing regime. At higher temperature, the team found that the efficiency value stabilizes more rapidly to its final value, which may be attributed to a more rapidly constituted SEI. In addition, the decrease in impedance with rising temperatures has been attributed to the elevated temperatures facilitating formation of the SEI as well as an increase in conductivity. The impedance of an as-constructed cell was measured at 30, 40, 50, and then 30 C, sequentially. Strikingly, on returning to a lower temperature, the impedance value reverts to a larger magnitude; however, the impedance does not assume the value observed prior to any heating. The aforementioned result bears similarity to the decrease in impedance observed after initial charging of cells containing composite LiI solid electrolyte with $LiI(3\text{-hydroxypropionitrile})_2$ additive.

At Rutgers University, the group investigated two pathways toward improved single-cell performance: first, deposition of excess, nonfluorinated lithium salts to investigate limiting effects of Li^+ depletion, and second, incorporation of the project's nanolayered multicomponent electrode composition to address both F^- and Li^+ ion transport. It was determined that excessive amounts of Li^+ enrichment did not equate to higher cell performance; however, this limitation was likely mechanical because at these compositions the mechanical integrity became unstable. The approach of nanolayered multicomponent electrode modifications proved that enabling localized source and improved transport of F^- anions resulted in better cell performance when combined with optimized cell designs developed last quarter.

Task 1.1 – Advanced Lithium-Ion Battery Technology: High-Voltage Electrolyte (Joe Sunstrom, Ron Hendershot, and Alec Falzone, Daikin)

Project Objective. The project objective is to identify electrolyte formulations, based on fluoro-chemistries, that will allow significantly improved operating voltage, increased durability, and increased energy density of Li-ion batteries at a reasonable cost. The project seeks to understand the conditions under which the electrolyte degrades, the effect on battery performance, and solutions that can overcome current limitations of the electrolyte. Gassing in Li-ion batteries is one of the most common failure mechanisms and poses the greatest safety risk in consumer devices. This project aims to investigate gas composition as a function of cathode material, electrolyte formulation, and operating voltage, and proposes optimal cell compositions at decomposition voltages.

Project Impact. Developing an understanding of the operating conditions in which gasses form in Li-ion batteries enables the project to propose optimized cell compositions, which operate at higher voltages for a longer period. Different fluorinated electrolyte components and additives may suppress and/or eliminate gas generation at or above hypothesized decomposition voltages. To investigate these topics, it is imperative that the project utilize multiple approaches, including, but not limited to: cathode material, electrolyte composition, operating voltage, and cycle number.

Approach. The evolving composition of the electrolyte in the battery will be examined by various analytical instruments to study volatiles [gas chromatography – mass spectrometry (GC-MS)/thermal conductivity detector (TCD)], liquid [liquid chromatography MS (LC-MS)], and solid [time-of-flight secondary ion mass spectrometry (TOF-SIMS), thermogravimetric analysis MS (TGA-MS), X-ray photoelectron spectroscopy (XPS), and auger electron spectroscopy (AES)] electrolyte decomposition products during battery operation. In the first year, the team addressed the gas composition and kinetics for both hydrocarbon and fluorocarbon as a function of several charge/discharge conditions. In the second year, the project will transition into analysis of the solid-state electrolyte (SSE) decomposition components of its tested batteries to obtain valuable information about SEI layer formation and how it manifests change in both the anode (graphite) and cathode (LCO and NMC). The third year is focused on measuring changes in the solid-state structure of the cathode following high-voltage operation. The project aims to quantify any dissolved metal ions originating from the cathode and deposited on the anode using inductively coupled plasma – mass spectrometry (ICP-MS). It will also study changes in the cathode structure using powder X-ray diffraction (XRD).

Out-Year Goals. Work will progress toward understanding how electrolyte formulation and cell operation affect the stability of transition metals (TMs) in the cathode structure. Specifically, the project aims to quantify metal ions, if any, dissolved into solution as a function of operating parameters (that is, voltage, time, etc.) and electrolyte formulation. In addition, measurements will be made using powder XRD to detect changes in the crystal structure of the cathode (LCO and NMC). Understanding effects on the solid-state structure in Li-ion batteries will provide valuable information on the required cathode chemistry for increased performance at high voltage.

Collaborations. The project has initiated a collaboration with Dr. Y. Cui (Stanford University) for cryogenic transmission electron microscopy (cryo-TEM) measurements on solid battery components.

Milestones

1. Film composition (elemental) versus time/voltage – Milestone 2.2. (Q1, FY 2019; Completed)
2. Battery thickness (non-gas) versus time/voltage – Milestone 2.3. (Q3, FY 2019; Completed)
3. Metal dissolution versus time/voltage – Milestone 3.1. (Q4, FY 2019; In Progress)

Progress Report

Interim cells for analysis were delivered to INL late this quarter to complete the final deliverable of the fiscal year. NMC-532 cells were chosen due to their performance in both calendar and cycle life tests. Cells with the baseline hydrocarbon (ethyl methyl carbonate : ethylene carbonate, or EMC/EC, 80:20) and best-to-date fluorinated (EMC/HFE/FEC/EC 60:20:15:5) electrolytes were submitted for analysis. Cells will be returned and deconstructed post-mortem for surface analysis and dissolved metal experiments.

Thickness measurements of 200 mAh NMC-532 cells at 4.6 V as a function of electrolyte reveal a measurable increase in the swelling of the cell (non-gassing) at high voltage. Cells that contain only fluorinated ether (HFE), and without FEC, result in the largest thickness increase. These 4.6 V cells with HFE reported last quarter also contain the highest amount of dissolved metals deposited on the anode (nickel, manganese, cobalt). Table 1 displays the overall thickness increase of the pouch cell following a cycle life test.

Table 1. Thickness measurements were taken before and after a cycle life test (200 cycles at .7C).

Cathode		Voltage	Electrolyte	Overall Cell Thickness Change (%)
NMC-532		4.6 V	EMC:EC	22.2
NMC-532		4.6 V	EMC:EC:HFE	24.0
NMC-532		4.6 V	EMC:HFE:FEC	20.2

Real-time measurements show that cell thickness increases on charging and decreases while discharging, as seen in Figure 1. The left panel of Figure 1 shows a cell cycled at 4.6 V with the baseline hydrocarbon electrolyte (80:20 EMC/EC); the right panel depicts a cell with fluorinated electrolyte (60:20:20 EMC/HFE/FEC).

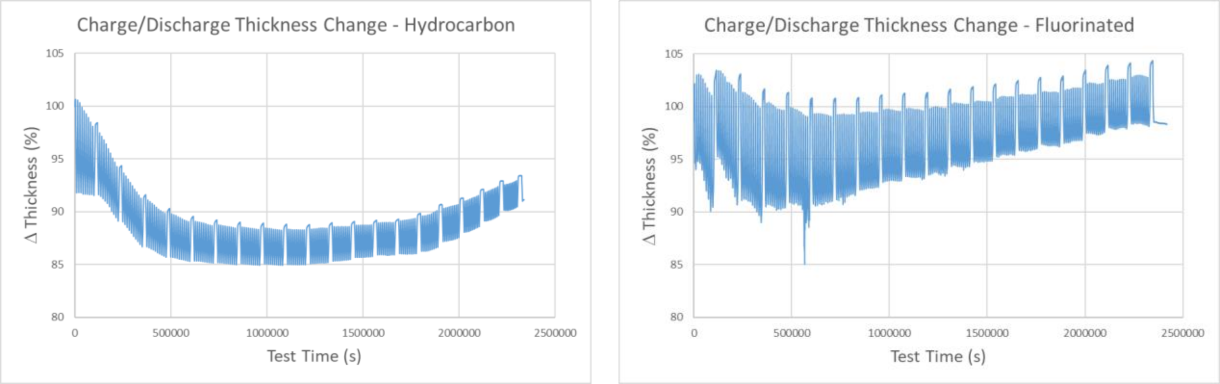

Figure 1. Thickness changes of cells as a function of cycle number, between 3.0 V and 4.6 V.

On charging, both pouch cells gain 3-5% of overall thickness as lithium inserts into the graphite. As the cells lose capacity due to cathode/electrolyte degradation at high voltage, there is a measurable loss in Δ thickness as a function of cycle number. Physical contact with the pouch cell causes a slight compression at the interface, resulting in the negative feature in both graphs. This loss is overcome as the cycle life test progresses.

Additional efforts this quarter have focused on fabrication and testing of sample cylinders for custom gas mixtures. These will allow for molar quantification of gasses as a function of cathode/electrolyte/voltage identified in cells in FY 2017-2018. Along with gas quantification efforts, graphite anodes from NMC-532 cells were submitted for ICP-MS analysis, along with anodes from NMC-622 cells. Results are expected to be analyzed early next quarter.

Patents/Publications/Presentations

Presentation

- DOE VTO Annual Merit Review (AMR), ES312, Arlington, Virginia (June 10–13, 2019): “Daikin Advanced Lithium Ion Battery Technology – High Voltage Electrolyte”; A. J. Falzone, J. Sunstrom, C. A. Meserole, R. Hendershot, et al.

Task 1.2 – Multi-Functional, Self-Healing Polyelectrolyte Gels for Long-Cycle-Life, High-Capacity Sulfur Cathodes in Lithium-Sulfur Batteries

(Alex Jen and Jihui Yang, University of Washington)

Project Objective. The project objective is to develop self-healing and polysulfide-trapping polyelectrolyte gels containing room-temperature ionic liquid (RTIL) for the Li-S battery system. The battery design will be able to achieve gravimetric and volumetric energy densities of ≥ 800 Wh/kg and ≥ 1000 Wh/L, respectively.

Project Impact. The Li-S battery system is currently hampered by poor capacity retention, primarily caused by dissolution of polysulfide reaction intermediates in typical organic electrolytes, as well as poor electrical contact between insulating sulfur and the conductive carbon matrix. This project aims to produce a high-capacity, long-cycle-life Li-S battery system by using rational molecular design strategies to address each capacity loss mechanism directly. A long-cycle-life Li-S battery system with the capability of doubling Li-ion energy density would enable production of lighter, longer range EVs at a cost affordable to the average U. S. household.

Approach. The team will develop Li-S coin cells that utilize self-healing, interpenetrated ionomer gel electrolytes in both the cathode and separator. The team will synthesize necessary starting materials and fabricate components of these gels while testing their relevant electrochemical and mechanical properties. All components will be combined into interpenetrating structures, which will be tested both alone and in cell configurations. Device performance data will be collected and used to further optimize designs of both material and cell, culminating in an optimized Li-S battery design capable of doubling the energy density of traditional Li-ion batteries. The team is focusing on (1) design and synthesis of a variety of precursors for gel electrolytes, (2) fabrication and testing of both reference materials and novel materials made from these precursors, and (3) iterative validation and improvement of design principles through both materials and device testing.

Out-Year Goals. Work will progress toward developing structure-property relationships for the self-healing, interpenetrated gel ionomer electrolyte and its individual components, as well as successful incorporation of such an electrolyte into a working Li-S cell. The team plans to demonstrate significant improvements in both capacity and retention when using the project's novel materials, as compared to state-of-the-art reference systems.

Collaborations. This project funds work at UW. Dr. A. Jen, principal investigator (PI), focuses on design, synthesis, and testing of novel materials, as well as device-based verification of design principles. Dr. J. Yang (co-PI) focuses on optimization of device fabrication and testing, as well as investigation of failure mechanisms in devices using novel materials. Pacific Northwest National Laboratory (PNNL) facilities will be used for detailed characterization study and device operation.

Milestones

1. Provide detailed cell performance data for practical-loading cells containing currently best materials designs, along with conclusions regarding the origin of performance details. (Q2, FY 2019; Completed)
2. Provide detailed cell performance data for concept cells containing currently best materials designs, which should meet performance targets. (Q4, FY 2019)

Progress Report

Multifunctional Ionomer Gels / Gel Cathode. Previously, the project demonstrated a nitrate-free QSS Li-S design, in which solvate ionogel (SIG) electrolytes are crosslinked *in situ* within the pores of a C/S cathode and Celgard 2500 separator. QSS cells showed good specific capacity and retention at sulfur loadings of ~ 1 mg$_S$/cm^2, matching or outperforming control cells with liquid organic electrolyte and PVDF binder. This quarter, the team has additionally tested the robustness of the QSS design toward self-discharge, to which Li-S batteries are particularly susceptible. A reference cell, fabricated using PVDF binder in the cathode and liquid organic electrolyte (1M LiTFSI in DOL:DME 1:1v/v + 1 wt% $LiNO_3$), was also tested for comparison. After two "formation cycles" at C/20, cells were cycled at C/10 until the 7th discharge, at which point 300 mAh/g$_S$ capacity was discharged, followed by a 100-hour rest. Discharge was then resumed, and cycling continued as normal.

Figure 2a depicts the results. The cell with organic electrolyte ("OE") lost 185 mAh/g$_S$ (18.3%) to self-discharge relative to the previous cycle, while the QSS cell lost only 108 mAh/g$_S$ (8.9%). Interestingly, the OE cell recovered 63 mAh/g$_S$ in the following cycle, bringing the total two-cycle loss to 12.1%, while the QSS cell lost an additional 44 mAh/g$_S$, for a similar total of 12.5%. However, the OE charge/discharge capacities rapidly diverged after this point, strongly suggesting an accelerated redox shuttle effect. The QSS cell did not exhibit this behavior, instead cycling its remaining capacity stably with a CE of ~ 98%. This result is especially encouraging given the lack of anode-passivating additives in the QSS system. Hence, while the team has observed that both designs are similarly susceptible to irreversible capacity loss during self-discharge, the QSS system has been found to be more resistant to continued degradation caused by the redistribution of sulfur species during prolonged rest.

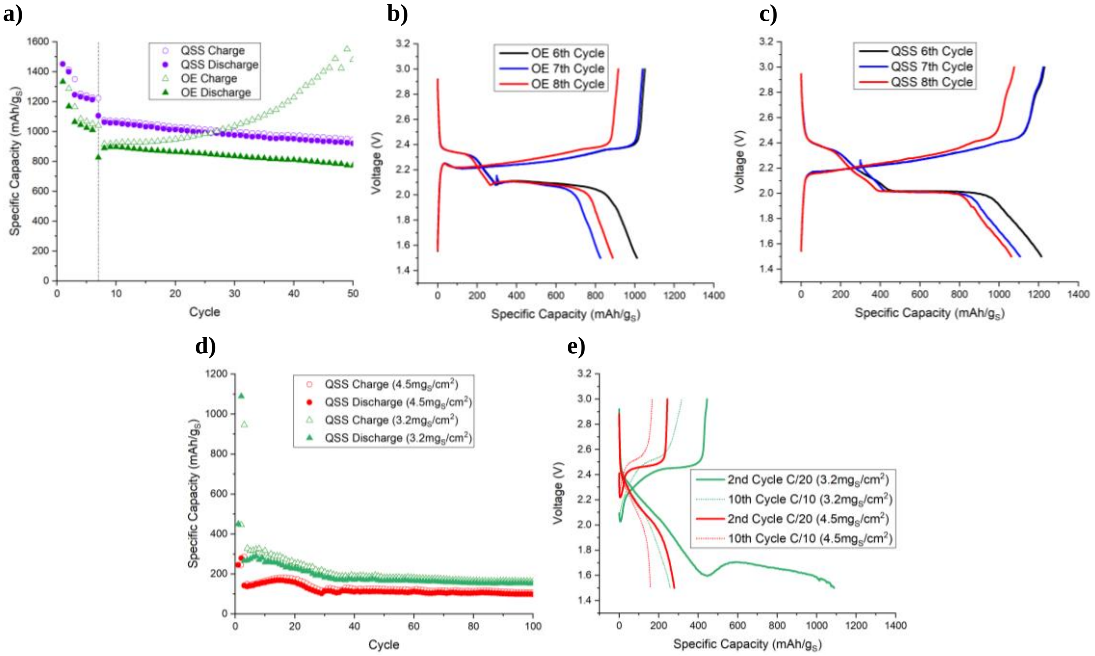

Figure 2. (a) Cycling performance of quasi-solid-state (QSS) and organic electrolyte (OE) cells, with a 100-hour rest during 7th cycle discharge. Some irreversible capacity loss is observed for both designs, but the OE cell exhibits accelerated redox shuttling after the self-discharge test, while the QSS cell continues to cycle stably. (b) OE voltage profiles for the 6th, 7th, and 8th cycles. (c) QSS voltage profiles for the 6th, 7th, and 8th cycles. (d) Cycling performance of two representative high-loading QSS cells. Available capacity is quite low at C/10 due to large internal resistance in the thick cathodes. (e) 2nd and 10th voltage profiles for the representative high-loading cells. Increasing resistance during discharge prevents the cells from accessing their lower plateau capacity, especially at C/10.

Examining the voltage profiles of each cell before, during, and after the self-discharge test (Figure 2b-c) provides some insight into the cause of capacity loss. First, the team finds that the general shape and voltage of each discharge/charge region remains mostly unaffected following self-discharge; however, in each case, the irreversible capacity loss is mostly localized to the lower plateau, corresponding to the conversion of soluble polysulfides into insoluble Li_2S_2 and Li_2S. Prior literature suggests that the lower plateau capacity is often limited by the passivation of conducting surfaces with these insoluble products, rather than the total availability of reducible sulfur. The project's previous galvanostatic intermittent titration technique (GITT) results also support this interpretation. In light of this, the capacity that is irreversibly lost by both cells following self-discharge may be related to the disproportionation of soluble polysulfides during the rest period, resulting in the production of insoluble sulfides and accelerated passivation of cathode surfaces. Further study is needed to confirm this mechanism and investigate its prevention.

The team also focused significant effort this quarter on fabricating and testing QSS cells with higher cathode areal loadings, with the goal of attaining reasonable performance at 4-5 mg_S/cm^2. Since the project's gel cathodes are blade coated from a precursor-containing slurry, the team was able to achieve increased loading simply by casting films at increased height. However, the downside of this "cure in place" method is that high loading cathodes were exceptionally thick—over 0.5 mm in some cases. Predictably, this produced significant internal resistance in the final QSS cells. As shown in Figure 2d, the capacity available during the initial two cycles at C/20 was commonly much larger than that available at C/10, which was generally 100-200 mAh/g_S in all cases. Examining the voltage profiles in Figure 2e reveals that the cause of this low capacity is an inability to reach the lower plateau prior to the safety cutoff of 1.5V, due to rapidly growing internal resistance during the initial stages of discharge. The team is testing improved gel cathode formulations with the goal of minimizing required thickness for high loading, and reducing the cathode charge transfer overpotential.

Self-Healing Materials. Previously, the team fabricated high-loading sulfur cathode after optimizing the cathode components, including ratio between PENDI-350 and tri-Py, choice of carbon-based conductive additives, current collector, and the loading amount of S/C composites. Sulfur cathode with loading of 4.2 mg/cm^2 was achieved (PENDI-350 : tri-Py = 1:1). Although the cathode exhibited high and stable cycling capacity around 810 mAh/g in the first several cycles, sudden drop happened in the following cycles. Therefore, the team has focused research this quarter on understanding the failure mechanism of cathode, including studies of lower CE and cathode cracking in this system.

CE is related to the dissolution of lithium polysulfides and therefore capacity retention. In the project's design, PENDI-350 is used to trap the polysulfides. First, pure PENDI-350 is used as binder to compare with reference binder PVDF. As shown in Figure 3a, cathode with PENDI-350 as binder shows better capacity retention and much higher CE than in the case of PVDF. Specifically, the trends of capacity change are different. The dramatic capacity decrease in the first several cycles of cathode with PVDF as binder implies the quick dissolution of the polysulfides into the electrolyte. Then, the shuttle effect becomes more significant, leading to constant decay of capacity and lowering of the CE. On the contrary, cathode with PENDI-350 as binder has stable capacity around 1000 mAh/g in the first three cycles, which implies significant trapping of the polysulfides. The CE stays constant around 98%, even after around 60 cycles. The capacity stays almost constant after 30 cycles. Therefore, the team believes these two cathodes have different capacity failure mechanisms. Cathode with PVDF as binder loses capacity due to the dissolution of the polysulfides. Although cathode with PENDI-350 as binder traps polysulfides efficiently, cathode cracking can lead to the loss of sulfur by isolation. To prove this, scanning electron microscopy (SEM) images of these cathodes were taken after 20 cycles. As shown in Figure 3b, cathode with PVDF as binder showed continuous surface without significant cracking. However, there is cracking with a 15-μ width in the surface of cathode when PENDI-350 is used as binder, most likely due to its higher rigidity. In addition, the morphologies of the two films are quite different: in the case of cathode using PENDI-350 binder, the surface is smoother. This suggests better compatibility of PENDI-350 binder with C/S composite, possibly resulting in a layer of PENDI-350 film formation on the surface of cathode during the cycling process.

Second, due to the different failure mechanism, it is possible that the mechanical integration of electrode materials can be improved by adding PVDF into PENDI-350. As shown in Figure 3c, after adding PVDF (with weight ratio between PVDF and PENDI-350 as 1:3), the capacity retains around 962 mAh/g after 40 cycles with sulfur loading of 2.5 mg/cm^2. However, the CE is worse than pure PENDI-350. The team believes that although PVDF helps improve the mechanical integration, it may also interfere with interactions between PENDI-350 and PENDI-350 or between PENDI-350 and S/C composite. The SEM image of cathode with PENDI-350/PVDF as binder after 20 cycles is shown in Figure 3c. It is found that the surface of cathode is less smooth than the cathode with pure PENDI-350 as binder. This suggests that less polymer film is formed on the surface of cathode, which means part of PENDI-350 may dissolve into the electrolyte. The lack of PENDI-350 may lead to dissolution of the polysulfides and low CE. Therefore, the team can simply increase the thickness of sulfur cathode to alleviate the dissolution problem of PENDI-350.

As shown in Figure 3d, the cathode with sulfur loading of 3.7 mg/cm^2 and PENDI-350/PVDF as binder was fabricated. It shows stable capacity around 800 mAh/g after 32 cycles. Also, the CE was higher than 98%, which may be due to the trapping effect of PENDI-350 and the physical blocking of thick cathode. Therefore, by improving the mechanical property and alleviating the dissolution of PENDI-350, high-loading sulfur cathode with high-capacity retention and CE has been achieved. Although the capacity is stable, it needs improvement. A more systematic investigation of the failure mechanism of PP binder is in progress.

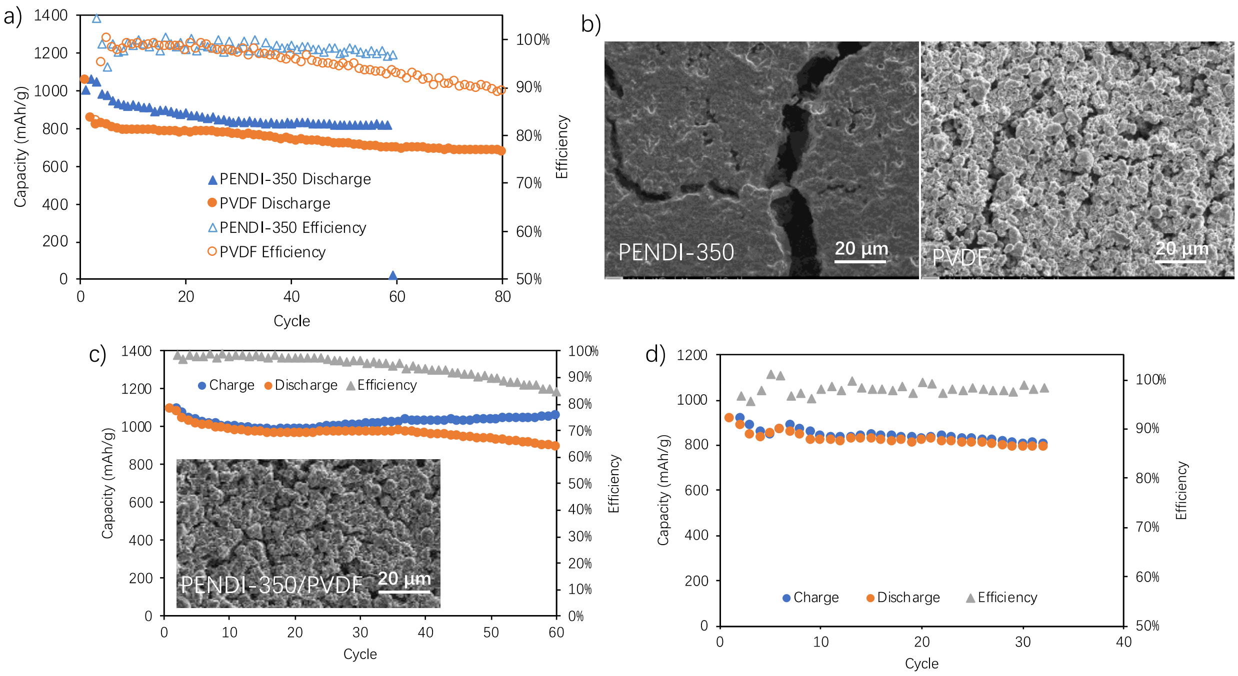

Figure 3. (a) Cycling performances of sulfur cathodes with PENDI-350 (2.0 mg$_S$/cm^2) and PVDF (3.1 mg$_S$/cm^2) as binder, respectively. (b) Scanning electron microscopy (SEM) images of cathodes with PENDI-350 and PVDF as binder after 20 cycles. (c) Cycling performance of sulfur cathode with PENDI-350/PVDF as binder, and the SEM image of the cathode after 20 cycles. (d) Cycling performance of sulfur cathode with PENDI-350/PVDF.

Patents/Publications/Presentations

Publications

- Hubble, D., J. Qin, F. Lin, I. A. Murphy, S.-H. Jang, J. Yang, and A. K.-Y. Jen. "Designing Lithium Solvate Ionogels with Very High Conductivity and Lithium Transference Number." *Journal of Materials Chemistry A* 6 (2018): 24100–24106. doi: 10.1039/C8TA08808J.
- Qin, J., F. Lin, D. Hubble, Y. Wang, Y. Li, I. A. Murphy, S.-H. Jang, J. Yang, and A. K.-Y. Jen. "Tuning Self-Healing Properties of Stiff, Ion-Conductive Polymers." *Journal of Materials Chemistry A* 7 (2019): 6773–6783. doi: 10.1039/C8TA11353J.
- Li, Y.,* I. A. Murphy,* Y. Chen, F. Lin, X. Wang, S. Wang, D. Hubble, S.-H. Jang, K. T. Mueller, C. Wang, A. K.-Y. Jen, and J. Yang. "A Multi-Functional Interface Derived from Thiol-Modified Mesoporous Carbon in Lithium-Sulfur Batteries." *Journal of Materials Chemistry A* 7 (2019): 13372–13381. doi: 10.1039/C9TA02743B.

Presentations

- 233rd Electrochemical Society (ECS) Meeting, Seattle, Washington (May 13–17, 2018): "Rationally-Designed Solvate Ionogel Electrolytes for Improved Lithium-Sulfur Battery Performance"; D. Hubble, J. Qin, F. Lin, I. A. Murphy, Y. Li, S-H. Jang, J. Yang, and A. K-Y. Jen. Poster.
- 233rd ECS Meeting, Seattle, Washington (May 13–17, 2018): "Tunable Surface Modification of Mesoporous Carbon Particles for Polysulfide Trapping in Lithium Sulfur Batteries"; I. A. Murphy, Y. Li, Y. Chen, F. Lin, X. Wang, S. Wang, D. Hubble, S-H. Jang, K. T. Mueller, C. Wang, J. Yang, and A. K-Y. Jen. Poster.
- 233rd ECS Meeting, Seattle, Washington (May 13–17, 2018): "Tuning Self-Healing Property of Stiff Supramolecular Polymer for Flexible Electronics"; J. Qin, F. Lin, Y. Wang, D. Hubble, Y. Li, J. Yang, and A. K-Y. Jen. Poster.
- BMR Electrolytes Meeting, Berkeley, California (October 11–12, 2018): "Multifunctional, Self-Healing Polyelectrolyte Gels for Long-Cycle-Life, High-Capacity Sulfur Cathodes in Li-S Batteries"; D. Hubble, J. Qin, F. Lin, I. A. Murphy, Y. Li, S-H. Jang, J. Yang, and A. K-Y. Jen.

Task 1.3 – Construct and Test Lithium-Metal/Composite Electrolyte/Lithium-Metal Symmetric Cells (Nianqiang (Nick) Wu, West Virginia University; Xiangwu Zhang, North Carolina State University)

Project Objective. The project objective is to develop SSEs based on the highly conductive inorganic nanofibrous network in the polymer matrix for lithium batteries.

Project Impact. The team will conduct research and development (R&D) on solid-state inorganic nanofiber-polymer composite electrolytes that will not only provide higher ionic conductivity, improved mechanical strength, and better stability than the PEO polymer electrolyte, but also exhibit better mechanical integrity, easier incorporation, and better compatibility with the Li-metal anode than the planar ceramic membrane counterparts. The proposed inorganic nanofiber-polymer composite electrolytes will enable practical use of high-energy-density, high-power-density Li-metal batteries, and Li-S batteries.

Approach. Integration of the highly Li^+-conductive inorganic nanofiber network into the polymer matrix not only provides the continuous Li^+ transport channels, but also kinetically inhibits crystallization from the amorphous state of polymer electrolyte. The inorganic nanofibers will be fabricated with an electrospinning technique; the ionic conductivity of inorganic nanofibers will be improved by chemical substitution or doping. Highly ionic-conductive polymers will be developed by cross-linking and/or creation of a block-copolymer structure. The composition and microstructure of the composite electrolyte will be designed to suppress the lithium dendrite formation.

Out-Year Goals. Work will progress toward synthesis of the inorganic nanofibers and polymer matrix. The goal is to find the optimal synthetic route to achieve the desirable conductivity.

Collaborations. This project funds work at WVU and North Carolina State University (NCSU). Dr. N. Wu at WVU serves as PI, and Dr. X. Zhang at NCSU acts as co-PI. P. Zheng and X. Gao (Ph.D. student at WVU), H. Yang (Postdoctoral Fellow at WVU), B. Liu (Ph.D. student at WVU), C. Yan (Ph.D. student at NCSU), and M. Dirican (Postdoctoral Fellow at NCSU) contributed to the project.

Milestones

1. Construct Li-metal/composite electrolyte/Li-metal symmetric cells – Subtask 3.1. (Q4, FY 2019; Completed)
2. Construct Li-metal/composite electrolyte/cathode cells. Test specific energy, energy density, cycle life time, specific discharge pulse power, specific regeneration pulse power, and recharge rate of full cells – Subtask 3.2. (Q4, FY 2019; Completed)
3. Optimize composite electrolytes to achieve best performance of the battery full cells. Overall performance of the full cells will be analyzed – Subtask 3.3. (Q4, FY 2019; 80% Completed)

Progress Report

This quarter, the composite solid electrolytes consisting of the silane-coated $Li_{6.28}La_3Al_{0.24}Zr_2O_{12}$ (s@LLAZO) nanofibers and the cross-linked PEGDA polymer were further studied. The performance of composite solid electrolytes based on the hydrogen-treated $Li_{0.33}La_{0.57}TiO_3$ nanofibers was also investigated with half cells and full cells.

Optimize the Composite Electrolytes

Silane-Coated LLAZO-Incorporated Cross-Linked Polymer Composite Electrolytes for Li-S Batteries. Solid electrolytes were then prepared by polymerization of s@LLAZO-40PEGDA-10mPEG precursor sandwiching between two quartz plates with the controlled thickness (~ 40 µm). Considering slower kinetics of Li-S redox reactions than those of Li-ions, an additional 10 wt% poly(ethylene glycol) dimethyl ether (mPEG) was added in the polymer precursor to improve ionic conductivity. The composite solid electrolyte was then used to construct the Li-S batteries. A retained capacity of 760 mAh g^{-1} was obtained at initial cycles at a current density of 0.1 C at room temperature. However, the cycling stability was not improved much in all-solid state Li-S batteries as compared to the liquid electrolyte (DME/DOL(LiTFSI)) based Li-S battery. The capacity decreases to 500 mAh g^{-1} after 80 cycles, which is similar to the cycling stability of Li-S battery with liquid electrolyte at 0.2 C. Advanced cathode designs with confined polysulfides diffusion is being designed to improve cycling stability of all-solid-state Li-S batteries.

Cross-Linked PEGDA-LisTFSI Polymer Electrolytes. Cross-linked polymer electrolytes were further studied in Li-ion batteries. The propylene carbonate (PC, 50-100 wt%) plasticizer was added in the prepolymer solution. All the as-prepared samples are denoted as LisTFSI-PEGDA-xPC, where x represents the weight ratio of PC plasticizer based on the total weight of polymer electrolyte. At room temperature, the non-plasticized LisTFSI-PEGDA polymer electrolyte showed the lowest ionic conductivity of 5.16×10^{-6} S cm^{-1}. LisTFSI-PEGDA-100PC demonstrated the highest room-temperature ionic conductivity of 2.5×10^{-4} S cm^{-1}. Dynamic mechanical analysis (DMA) tests were conducted to determine the glass transition temperatures and mechanical strength of the LisTFSI-PEGDA-xPC polymer. After addition of the PC plasticizer, the values of Young's modulus of samples were reduced, as shown in Table 2. It is noted that the sample with 100 wt% PC plasticizer was unable to undergo the DMA test due to its extremely weak mechanical properties.

Table 2. Electrochemical and mechanical properties of LisTFSI-PEGDA-PC polymer electrolytes.

Sample	Ionic conductivity (S cm^{-1}, 25 ˚C)	Activation Energy (eV)	T_g (˚C)	Young's Modulus (MPa)
LisTFSI-PEGDA	5.16×10^{-6}	0.62	0	8.34
LisTFSI-PEGDA-50PC	2.16×10^{-5}	0.20	-30	5.09
LisTFSI-PEGDA-75PC	6.92×10^{-5}	0.18	-40	1.76
LisTFSI-PEGDA-100PC	2.5×10^{-4}	0.17	-	-

To investigate the electrochemical performance of LisTFSI-PEGDA-75PC polymer electrolyte in Li|$LiFePO_4$ batteries, CR2032 coin type cells were assembled. At the first cycle, the cell delivered capacity of 93 mAh g^{-1} at a current density of 0.2 C at room temperature. The relatively low capacity might be due to the high bulk resistance and low ionic conductivity of the LisTFSI-PEGDA-75PC polymer electrolyte (6.92×10^{-5} S cm^{-1}) used in the solid-state batteries. In addition, the charge-discharge profiles of solid-state Li|LisTFSI-PEGDA-75PC|LFP cell showed a high overpotential, which also indicated the strong reaction barrier due to slow Li^+ ion mobility. Therefore, the LisTFSI-PEGDA-75PC polymer electrolyte was not able to demonstrate high performance in solid-state Li-ion batteries. In the future, a higher amount of plasticizer (100-200 wt%) will be investigated in the LisTFSI-PEGDA polymer electrolyte, and the resultant polymer electrolyte will be incorporated with electro-spun PVDF mat to provide strong mechanical support.

PVDF-HFP/LiTFSI/LLATO/Li_3PO_4 Polymer Composite Electrolytes. The interface stability between the electrolyte and the electrode was identified through galvanostatic cycling testing of Li|PVDF-HFP/LiTFSI/LLTO|Li and Li|PVDF-HFP/LiTFSI/H-LLTO|Li symmetric cells to mimic the lithium stripping and plating process. The symmetric cell was tested at a current density of 0.5 mA cm^{-2} under a 0.5-hour cycling period at room temperature. Figure 4a shows the time-dependent voltage profile with positive voltages during lithium stripping and negative voltages during lithium plating. At room temperature, the Li|PVDF-HFP/LiTFSI/LLTO|Li cell showed a large polarization voltage of ± 340 mV. In contrast, the Li|PVDF-HFP/LiTFSI/H-LLTO|Li cell showed a much smaller voltage of ± 115 mV without short-circuiting for over 300 h.

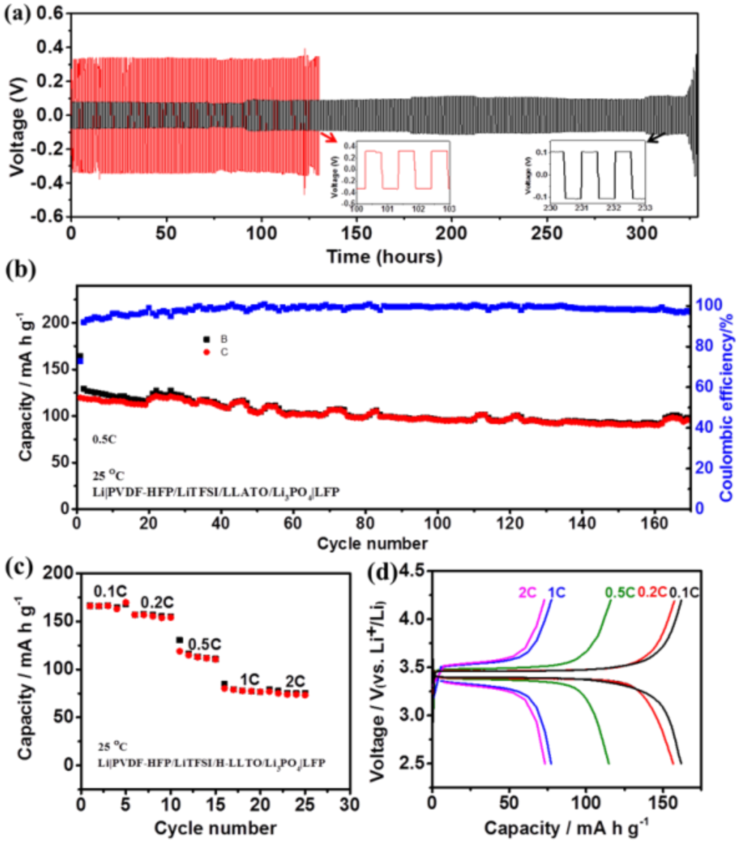

Figure 4. (a) Voltage profiles of Li||Li symmetric cells with PVDF-HFP/LiTFSI/LLTO and PVDF-HFP/LiTFSI/H-LLTO 500 composite electrolyte. (b) Cycling performance of Li|PVDF-HFP/LiTFSI/H-LLTO 500|LFP coin cell at 0.5 C at 25°C. (c) Rate capability and (d) corresponding charge/discharge profiles of the Li|PVDF-HFP/LiTFSI/H-LLTO 500 |LFP coin cell at 0.1 C, 0.2 C, 0.5 C, 1 C, and 2 C, respectively.

The performance of Li||LFP full cell based on the H-LLTO-containing composite electrolyte was tested between 2.5 V and 4.2 V. The cell exhibited stable cycling performance at 0.5C. The initial discharge capacity was 120 mAh g^{-1} and still remained at 95.2 mAh g^{-1} after 170 cycles, showing 80% retention of the first cycle's discharge capacity (Figure 4b). The CE remained over 97% after 170 cycles. Also, the Li/PVDF-HFP/H-LLTO 500°C/LFP cell revealed high rate capacity (162, 153, 114, 80, and 73 mAh g^{-1} at 0.1, 0.2, 0.5, 1, and 2C, respectively). The capacity was recovered to 158 mAh g^{-1} when the C rate decreased from 2C to 0.1C after 25 discharge/charge cycles. The typical charge/discharge voltage profiles at 0.1, 0.2, 0.5, 1, and 2 C are shown in Figure 4c.

Patents/Publications/Presentations

The project has no patents, publications, or presentations to report this quarter.

Task 1.4 – High Conductivity and Flexible Hybrid Solid-State Electrolyte (Eric Wachsman, Liangbing Hu, and Yifei Mo, University of Maryland)

Project Objective. The project objective is to develop flexible hybrid electrolyte with garnet nanofibers to achieve the following: (1) flexible, with greater mechanical strength (~ 10 MPa) and thermal stability than polymer electrolytes; (2) high room-temperature ionic conductivity, ~ 0.5 mS/cm; (3) stable interface with lithium metal and effective blocking of lithium dendrites at current densities up to 3 mA/cm^2; and (4) battery performance with Li-S chemistry with an energy density of ≥ 450 Wh/kg (and ≥ 1000 Wh/L) and maintaining ≥ 80% of capacity up to 500 cycles.

Project Impact. Instability and/or high resistance at the interface of lithium metal with various solid electrolytes limit(s) the use of the metallic anode for batteries with high energy density, such as Li-air and Li-S batteries. The critical impact of this endeavor will be focused on developing a new type of SSE that is highly conductive, highly flexible, and electrochemically stable. The new SSE will enable Li-metal anodes with excellent interfacial impedance and blocking of lithium dendrite formation.

Approach. The project will synthesize garnet nanofibers, fill the porous region with polymer electrolyte, and characterize the flexible hybrid membrane properties. The flexible hybrid SSE microstructure will be determined using focused ion beam / scanning electron microscopy (FIB/SEM) and integrated with electrochemical methods to investigate the properties and stability with Li-metal anode.

Out-Year Goals. The project will develop a fundamental understanding of the mechanism of Li-ionic diffusion in garnet nanofibers and their mechanical properties, as well as these properties for hybrid garnet-fiber/polymer hybrids. Work will progress toward study of the electrode assembly during electrochemical cycling of the anode.

Collaborations. This project funds work at UMD, College Park. Dr. E. D. Wachsman (PI) will focus on optimizing the garnet network to achieve high ionic conductivity and flexibility using FIB/SEM and electrochemical impedance spectroscopy (EIS) characterization. Dr. L. Hu (co-PI) focuses on synthesis of the hybrid electrolyte and on test for Li-metal anode with the hybrid electrolyte. Dr. Y. Mo (co-PI) will lead efforts on computational modeling of the garnet nanofiber hybrid electrolytes for fundamental mechanistic understanding.

Milestones

1. Modeling of lithium dendrite protection: Understand lithium dendrite growth and protection effect of polymer and interphase layers on garnet nanofiber. (Q1, FY 2019; Completed December 2018)

2. Fabricate porous mixed electron/ion conductor: Fabricate and evaluate porous framework of mixed electron and ion conductor (to fill sulfur cathode). (Q2, FY 2019; Completed)

3. Li-S full cell with hybrid SSE: Fabricate and evaluate Li-SSE-S full cell with a size of 1 cm by 1 cm. (Q3, FY 2019; Completed)

4. Full cell performance: Achieve full cell of 10 mAh and energy density of 450 Wh/kg. (Q4, FY 2019; In progress)

Progress Report

Li-S full cells were fabricated and evaluated this quarter. The hybrid electrolyte was prepared as reported previously. The cathode was prepared by adding 1 M Li_2S_8 catholyte into a conductive carbon substrate with area of 1.27 cm^2. The polysulfide catholyte was prepared by mixing stoichiometric amounts of sulfur and Li_2S in a 1,3-dioxolane (DOL) and 1,2-dimethoxyethane (DME) solution (50:50 vol) with 1 M lithium bis(trifluoro-methanesulfonyl)imide and 2 wt% lithium nitrates. The mixed precursor solution was stirred at 65ºC for 48 h in a glove box. Electrochemical testing of the full cell was carried out with standard CR2032 cell using 175-µm-thick Li-metal counter electrode. Four pieces of stainless-steel spaces (0.2-mm thick) were used to achieve good contact between the electrolyte and electrodes. The electrochemical performance of the Li-S cell was analyzed with a battery cycler (Arbin Instruments) in the voltage window of 1.5–3.0 V at 0.1 mA/cm^2. Figure 5 shows voltage profiles of the full Li-S cell. The discharge curve shows one sloping plateau around 2 V, which represented a solid-state type conversion of Li_2S_8 to Li_2S. The charging curve shows only one plateau, which is often seen in the most common electrolyte based on 1:1 vol DOL and DME. The hybrid electrolyte prevented polysulfide anion diffusion and avoided the shuttle effect issues. Figure 6 shows cell capacity and cycling stability of the cell. The team found of interest that that cell capacity has been continuously increasing, which is distinct from the tendency of batteries to lose capacity after cycling. It is observed that capacity doubled after 100 cycles. Due to the irreversibility of the side reaction, CE over 100% was attained in the initial 40 cycles. Thereafter, the cell gave high reversible discharge/charge capacities in the following cycles with efficiency above 98%, exhibiting good electrochemical performance over 100 cycles.

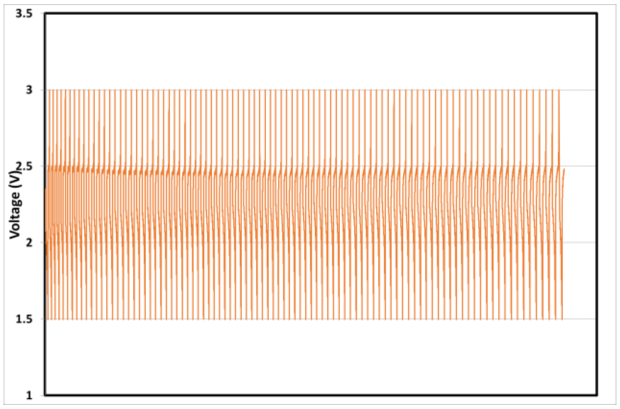

Figure 5. Charge-discharge profiles of Li-S cell using hybrid electrolyte at 0.1 mA/cm^2. Temperature: 22°C.

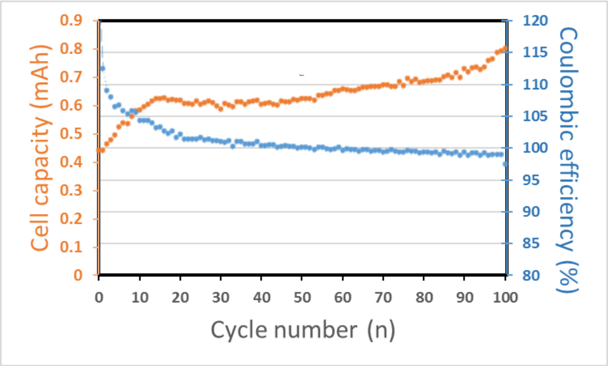

Figure 6. Cycling stability of Li-S cell using hybrid electrolyte at 0.1 mA/cm^2. Temperature: 22°C.

Patents/Publications/Presentations

The project has no patents, publications, or presentations to report this quarter.

Task 1.5 – Self-Forming Thin Interphases and Electrodes Enabling 3D Structured High-Energy-Density Batteries
(Glenn Amatucci, Rutgers University)

Project Objective. The project objective is to develop and implement a novel *in situ* formed Li-metal-based metal fluoride battery that will enable packaged 10-mAh batteries of energy densities > 1000 Wh/L and > 400 Wh/kg at 12 V.

Impact. Successful realization of 3D batteries formed *in situ* with a practical approach to large-scale fabrication would address some of the DOE EV performance goals, including: (1) areal capacity increase, (2) improved rates, and (3) designs to enable high-voltage unit cells.

Approach. The project is divided into two main tasks that focus on advance of the self-forming chemistry concurrent to cell design and fabrication. The self-forming chemistry task is comprised of three subtasks encompassing the negative and positive reactive current collectors, and the bi-ion glass conductor. The cell design and fabrication are targeting development and integration of the bipolar configuration to achieve the 12-V single-cell goal.

Out-Year Goals. Work will continue toward improving reactive current collectors and cell design to optimize electrochemical performance of the cell stack in terms of energy density both gravimetric and volumetric, as well as capacity retention on cycling. A secondary focus will be implementation of bipolar design within the cell structure.

Collaborations. All project tasks will be performed at Rutgers University.

Milestones

1. Design and fabricate 10-mAh cell stack that achieves 12 V and delivers energy densities of 1400 Wh/L and 600 Wh/kg per cell stack. (Q1, FY 2019; In progress)
2. Establish negative current collector compositions that enable high efficiency of lithium plating and stripping in excess of 95% during the *in situ* formation step and > 99% during subsequent cycles. (Q2, FY 2019; In progress)
3. Achieve < 30% increase in electrolyte impedance after 50 cycles as characterized by EIS. (Q3, FY 2019)
4. Establish positive current collector compositions that achieve 90% of the theoretical energy density based on complete utilization of the initial amount of the positive reactive current collector. (Q4, FY 2019)
5. *Deliverables:* Deliver 12 baseline and 12 improved packaged cells with 10-mAh capacity. Improved cells will offer > 1000 Wh/L and > 400 Wh/kg, and output voltage of 12 V.

Progress Report

Last quarter, the team focused on optimization of the cell microstructural design to promote F^- and Li^+ ion diffusion and to maximize interaction of the formation electrolyte with the reactive current collector, to ultimately enhance cell performance. During this effort, the team returned to development of the single-cell configuration and also evaluated the effect of three main parameters (that is, electrode spacing, electrode aspect ratio, and orientation of the electrodes within the cell). These modifications resulted in significant progress in the single-cell performance, with a 116% and 60% improvement in positive utilization and electrode pairs' energy density, respectively, relative to the original design. The resulting 54% positive electrode utilization and 1318 Wh/L electrode pair energy density yielded the best single-cell configuration performance, up to this quarter. In addition, thicker layers of electrolyte, providing an excess reserve of F^- and Li^+ ions, were also investigated last quarter along with the three structural variables for the 12-V cell configuration. This resulted in positive electrode utilization of 44% and electrode pairs' energy density of 1059 Wh/L, an increase of 19% and 21%, respectively, relative to the first quarter design with modified electrode aspect ratio only.

Moving into this quarter, the project goals were to further address diffusion and transport by incorporating the optimized microstructural cell design advances (last quarter) along with the nanolayered multicomponent compositional modifications (Q2, FY 2018) in a combined study. The team's approach to overcoming transport and subsequent capacity limitations has focused on optimizing cell design, composition, and cycling protocols. This rationale was based on the hypothesis that cell performance was limited by F^- ions availability and accessibility to the reactive current collectors. However, deeper examination of the results has highlighted the potential underlying barrier of irreversibility caused by localized Li^+ ion depletion as well. As such, this quarter, the team investigated two pathways toward improved single-cell performance: (1) deposition of excess, non-fluorinated lithium salts to investigate limiting effects of Li^+ depletion, and (2) incorporation of the project's nanolayered multicomponent electrode composition to address both F^- and Li^+ ion transport.

Pathway 1. In an effort to improve formation efficiency, the single-cell configuration with optimized cell design from last quarter was tested with three different quantities of localized Li^+ enrichment without an associated F^- enrichment: a standard Li^+ enrichment composition, and 1.8x and 3.3x the standard Li^+ enrichment amount. Figure 7 shows the resulting positive electrode utilization for the first cycle of the unenriched and enriched lithium compositions for the single-cell configuration. Following electrolytic formation, the cells were cycled between 1.5 and 3.5 V. The standard Li^+ dopant had an advantageous outcome for the first cycle, reaching the highest positive electrode utilization for the single-cell design at 89%. This was a 65% increase in utilization relative to an unenriched cell with optimized cell design (60-μ electrode spacing and 4 times smaller electrode aspect ratio with the new orientation, as described in more detail in last quarter's report). Further enrichment, both the 1.8x and 3.3x compositions, had detrimental impact on the positive electrode utilization and performance. Physical review of each cell revealed adding excessive Li^+ ion enrichment structurally compromised the mechanical integrity of the cell by loss of adhesion.

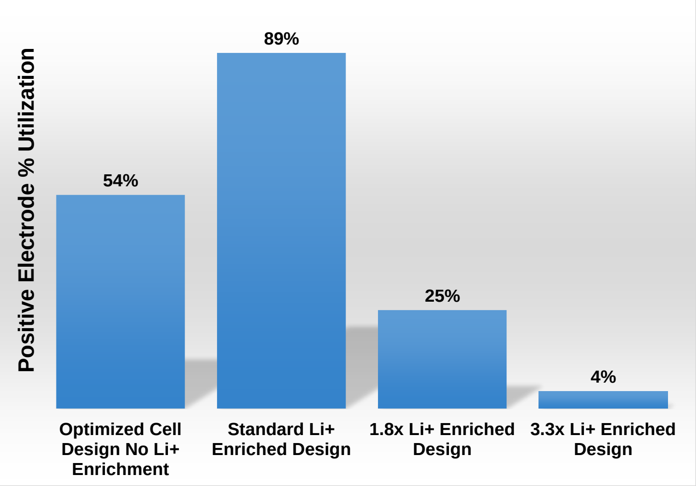

Figure 7. Positive electrode utilization (%) for single-cell configurations with different Li-ion dopant quantities, in the first cycle. The cells were cycled between 1.5 V and 3.5 V.

Pathway 2. The second method of ion enrichment consisted of incorporation of the nanolayered multicomponent electrode compositions into newly optimized cell structures. As mentioned, the goal is to further improve accessibility of the active material and address both Li^+ and F^- ion limitation. Figure 8 depicts the positive electrode utilization results of an optimized cell design with and without the nanolayered feature. With this addition, the positive electrode utilization increased to 82%, which was a growth of almost 52%. In addition, irreversible losses were improved, achieving second cycle positive electrode utilization of 69%, as compared to 35% with the standard Li^+ dopant enrichment method of pathway 1. However, capacities were 8% lower than the standard Li^+ enrichment design of pathway 1 and failed to attain higher results. The team concluded that the nanolayered multicomponent electrode structurally provided more pathways for access to F^- ions and maintained conductivity pathways, but were deficient in Li^+ ions as the Li^+ to F^- ratio was kept at a constant. Moving forward, the nanolayered multicomponent electrode systems of pathway 2 should be combined with the Li-ion enrichment of pathway 1 to reach the greatest capabilities.

Overall, the team combined compositional modifications and the structurally optimized cell design from last quarter to improve availability and transport pathways of the F^- and/or Li^+ ions to reach optimal cycling performance. The project's two approaches included Li-ion enrichment to provide excess lithium for improved cycling reversiblity and incorporation of the nanolayered multicomponent electrode system for improved accessibility and fluorination of active material. Individually, each modification yielded certain improvements. The Li^+ enrichment studies indicated that excessive amounts of Li^+ enrichment did not equate to higher cell performance; however, this limitation was likely mechanical, as at these compositions mechanical integrity became unstable. The approach of nanolayered multicomponent electrode modifications proved that enabling localized source and improving transport of F^- anions resulted in higher cell perfomance when combined with the optimized cell designs developed last quarter. This resulted in better cycling retention capabilities than the enrichment studies, but slightly lower starting capacities, which means that each modification independently addresses the identified barriers to maximize cell performance and reach the milestones (one for efficiency, the other for reversibility). Moving forward, the team will evaluate the impact of lithium doping and nanolayered multicomponent system combined together with the optimized cell design.

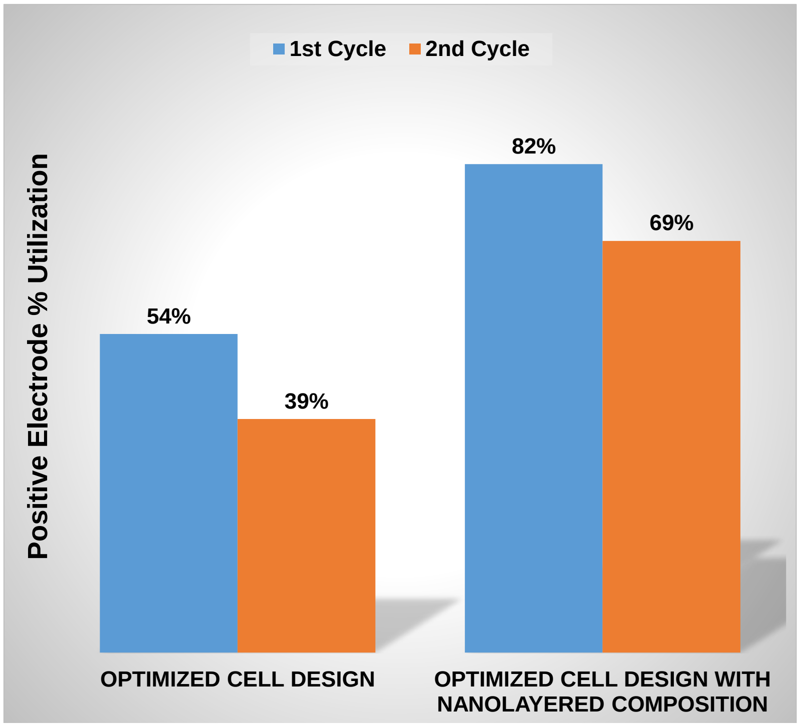

Figure 8. Positive electrode utilization (%) of optimized single cell designs, without and with nanolayered multicomponent electrodes in the first two cycles. Cells were cycled between 1.5 V and 3.5 V.

Patents/Publications/Presentations

The project has no patents, publications, or presentations to report this quarter.

Task 1.6 – Dual Function Solid-State Battery with Self-Forming, Self-Healing Electrolyte and Separator

(Esther Takeuchi, Stony Brook University)

Project Objective. The project objective is to demonstrate a solid-state rechargeable battery based on a Li-metal anode and iodine cathode with a self-forming, self-healing electrolyte and separator with high gravimetric and volumetric energy density.

Project Impact. This program will enable demonstration of the proposed rechargeable battery with improved power capability, high energy density, and a self-forming, self-healing SSE/separator. Technical insight will be gained regarding improved conductivity of the solid lithium iodide (LiI) based electrolyte, power capability of the proposed system, the self-healing nature of the LiI layer, the nature of the electrode-electrolyte interfaces, and feasibility of the system to reach the DOE targets.

Approach. The proposed concept is a dual function rechargeable solid-state battery utilizing LiI combined with silver iodide (AgI) as the electrolyte, with lithium metal (and small quantities of silver metal) as the anode and iodine as the cathode and with a self-forming, self-healing separator/electrolyte. The battery will be assembled in the discharged state where the anode and cathode will be created during the first formation (charge) step. Initially, silver ion (Ag^+) will diffuse toward the negative electrode and be reduced to silver metal (Ag^0), and iodine ion (I^-) will be oxidized to elemental iodine (I_2) at the cathode side. As the formation of the battery continues, lithium ion (Li^+) will form a Li-metal layer at the anode, with generation of iodine at the cathode. LiI will remain and serve as both the separator and electrolyte.

Out-Year Goals. This is a multiyear program where the effort is divided into three major tasks.

- Year 1 involves electrolyte preparation and characterization including preparation of SSEs and conductivity measurements.
- Year 2 will focus on cell construction and testing including both *in situ* and *ex situ* analysis.
- Year 3 will focus on cell characterization. Under the program, cycle life, efficiency, energy density, and the functional capacity of cells will be determined.

Collaborations. This project collaborates with A. Marschilok and K. Takeuchi of SBU.

Milestones

1. Destructive analysis of construction A cells. (Q3, FY 2019; Completed)
2. *In situ* analysis of select construction A/B cells. (Q4, FY 2019; Initiated)

Progress Report

Destructive Analysis of Cell LiI Cells. The milestone for this quarter was to perform destructive analysis of construction A cells. Last quarter, the XRD of pristine and charged cells was reported, affirming the formation of the charge product iodine. SEM / energy dispersive X-ray spectroscopy (SEM/EDS) was also conducted to show morphology of cycled cells (Figure 9).

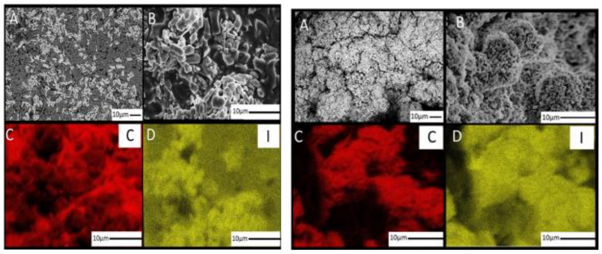

Figure 9. Scanning electron microscopy / energy dispersive X-ray spectroscopy analysis of cells post charge. Left side images are of the cathode side of the cell. Right side images are of the anode side of the cell.

Determine Impact of Elevated Temperature on construction B cells. Cell design B included the composite LiI solid electrolyte with LiI(3-hydroxy-propionitrile)$_2$ additive, as reported in previous quarters. Cell design B was constructed with four interface variations: B-Interface I (B-I), B-Interface II (B-II), B-Interface III (B-III), and B-Interface IV (B-IV). Variation of the interface was studied to evaluate its effects on CE during charge-discharge cycling. It was observed that the CE could be significantly impacted by the interfacial modification, with the improvement retained over 10 cycles. Cycling at elevated temperatures was conducted this quarter, where three different cell design B cell constructs (I, III, and IV) were compared with cell design A I. The CE of cells over 10-12 cycles at higher and lower depths of discharge (DoD) is reported in Figure 10. Interestingly, at higher DoD, the cell types that contain a lithium interface, that is, B I and A I, continue to exhibit a significant increase in efficiency over the first 10 cycles, as reported last quarter. At lower DoD cycling, the sequential improvement is smaller before stabilizing at values similar to that observed during longer term cycling. In contrast, cell types that did not contain an additional lithium interface, that is, B III and B IV, show minute improvement and deterioration at lower and higher DoD, respectively, before stabilizing at values similar to that observed during longer term cycling. Notably, as observed during the long-term cycling study, cell design B I shows CE of 90-100% throughout the testing regime. The propensity to stabilize more rapidly to its final value at heightened temperatures may be attributed to a more rapidly constituted SEI.

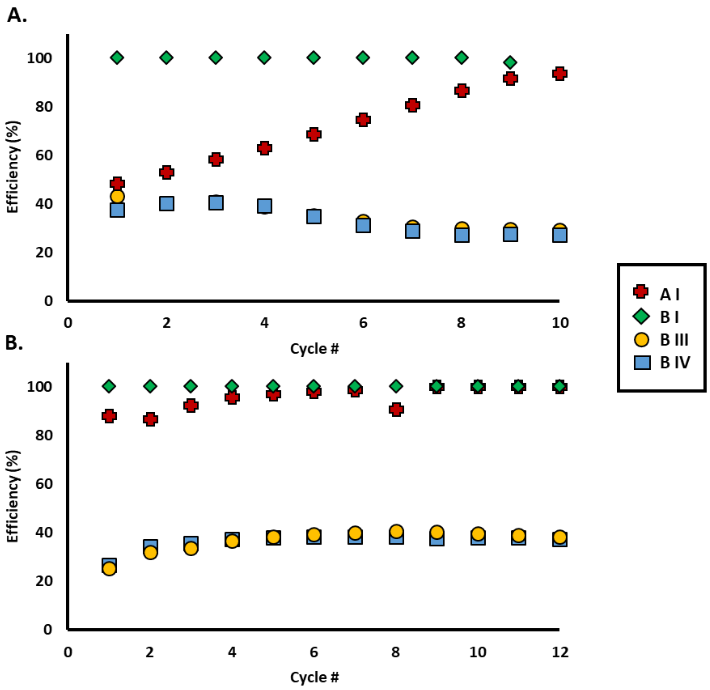

Figure 10. Coulombic efficiency under extended cycling of solid-state cells of cell designs B I, B II, B III, and B IV compared with cell design A I charging to higher (a) and lower (b) depths of discharge at 40°C.

Demonstration of the Effect of Elevated Temperatures on Cell Impedance. As reported in Figure 11, impedance measurements were carried out on cell types B I, B III, and A I prior to charging, after charging, and when fully discharged after a period of cycling at various temperatures. As temperature is increased, a precipitous decrease in impedance is observed. Notably, there is little to no variation in the magnitude of impedance between the diverse cell types. The decrease in impedance with rising temperatures has been attributed to the elevated temperatures facilitating the formation of the SEI as well as increase in conductivity.

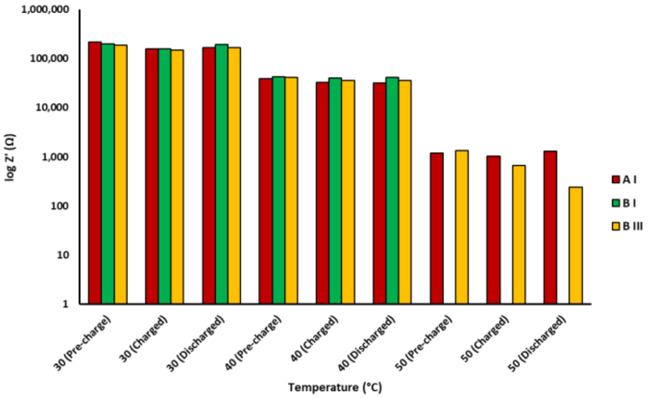

Figure 11. Impedance measurements at elevated temperature prior to charging, charged, and fully discharged for cell designs B I, B III, and A I.

Demonstration of Permanency of the Effect of Elevated Temperatures. The response to elevated temperature in the absence of any charge cycling was investigated on a B III cell type. As reported in Figure 12, the impedance of an as-constructed cell was measured at 30, 40, 50, and then 30C, sequentially. As observed when cycling at raised temperature, impedance decreased as a result of the higher temperature. Strikingly, on returning to a lower temperature, the impedance value reverts to a larger magnitude; however, the impedance does not assume the value observed prior to any heating. The aforementioned result bears similarity to the decrease in impedance observed after initial charging of cells containing composite LiI solid electrolyte with LiI(3-hydroxypropionitrile)$_2$ additive. Analogously, the decrease may be attributed to the formation of the interface, which in this instance is facilitated by the greater temperatures.

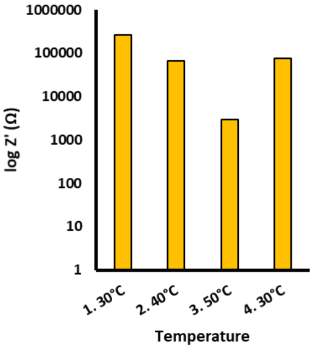

Figure 12. Direct measurement of Impedance of B III cell design at various temperatures in sequence prior to charging.

Patents/Publications/Presentations

Publications

- Abraham, A., M. R. Dunkin, J. Huang, B. Zhang, K. J. Takeuchi, E. S. Takeuchi, and A. C. Marschilok. "Interface Effects on Self-Forming Rechargeable Li/I_2 Based Solid State Batteries." *MRS Communications* 9 (2019): 657–662.
- Stackhouse, C. A., A. Abraham, K. J. Takeuchi, E. S. Takeuchi, and A. C. Marschilok. "Progress and Outlook on Few Component Composite Solid State Electrolytes." *MRS Advances* 1-6, (2019). Advance online publication. doi: 10.1557/adv.2019.264.

Presentations

- DOE VTO AMR, Arlington, Virginia (June 10–13, 2019): "Dual Function Solid State Battery with Self-Forming, Self-Healing Electrolyte and Separator"; E. S. Takeuchi, K. J. Takeuchi, A. C. Marschilok, A. Abraham, C. Stackhouse, A. M. Bruck, M. R. Dunkin, J. Huang, and P. F. Smith.
- National Institutionalized Research and Career Development Award Meeting, Poster Session: Chemistry and Biochemistry, Ann Arbor, Michigan (Summer): *Award received* – "Lithium Iodide Based Batteries: Complex Interfacial Chemistry and Progress In Self-Healing"; C. A. Stackhouse, A. Abraham, M. Dunkin, J. Huang, B. Zhang, A. C. Marschilok, E. S. Takeuchi, and K. J. Takeuchi.

Task 1.7 – High-Conductivity, Low-Temperature Polymer Electrolytes for Lithium-Ion Batteries (Bryan D. McCloskey, University of California at Berkeley)

Project Objective. Design of electrolytes with enhanced transport properties compared to conventional liquid organic electrolytes is key to improving the rate at which a Li-ion battery can be discharged or charged. Ideally, electrolytes would allow high mobility for lithium ions and disallow mobility of inactive ions (for example, the counteranion of the Li^+). However, current liquid electrolyte compositions usually provide higher mobility for the counteranion than Li^+, which results in high concentration polarization that disallows fast charging, particularly in batteries that employ thick porous electrodes, as is necessary for EVs to provide high energy densities. The project objective is to develop a high Li^+ transference number (t_{Li}, the fraction of ionic current carried by Li^+ in an electrolyte of uniform composition) polymer-based electrolyte that, when used in a Li-ion battery, can support current rate capabilities sufficient for EV propulsion at room temperature.

Impact. Development of practical high t_{Li} polymer-based electrolytes for Li-ion batteries would enable safer Li-metal and graphitic anode cycling and thicker porous electrode designs, leading to improved specific and volumetric battery energy densities consistent with the EV Everywhere Grand Challenge. High-energy anode and cathode materials, such as lithium metal, silicon, and high-voltage layered or spinel structures, could be enabled by electrolytes with high t_{Li} and large operating voltage windows, such as those based on sulfones, as proposed here.

Approach. Lowering the operating temperature of polymer electrolytes has been cited as an important challenge to their viability as Li-ion battery electrolytes. The project will address this challenge by using Li^+ neutralized anionically charged polymers as salts in conventional liquid solvents. Using these so-called polyelectrolyte solutions, initial results indicate that the project can access t_{Li} values typical of single-ion conducting polymer electrolytes ($t_{Li} > 0.9$) and conductivity values (> 1 mS/cm at room temperature) that approach those of traditional battery electrolytes.

Out-Year Goals. The optimization of transport and stability properties of these polyelectrolyte systems, through understanding of appropriate polymer and solvent design, is the objective. The goal is to develop new polyelectrolyte compositions that provide superior transport properties (specifically, higher t_{Li} and conductivity) than conventional liquid electrolytes and enable use of high-energy electrode materials, such as lithium metal.

Collaborations. Collaborations on this project include V. Battaglia (porous electrode preparation) and K. Persson (atomistic modeling) at LBNL.

Milestones

1. Complete synthesis and characterization of a new Li^+-neutralized charged polymer (pFTO) with a triflate-like ion ($-CF_2-SO_{3-}$) appended to the polymer backbone to improve ion dissociation. (Q1, FY 2019; Completed October 2018)
2. Complete nuclear magnetic resonance (NMR) transport and viscosity measurements of pFTO dissolved in carbonate-based solvents. Progress measure: Publish an article describing transport properties of polyelectrolyte solutions comprised of sulfonated polysulfone-co-poly(ethylene oxide) in carbonate-based solvents. (Q2, FY 2019; Progress measure completed November 2018)
3. Complete electrochemical transport measurements of pFTO in symmetric cells with Li-metal electrodes and SSEs. (Q3, FY 2019)
4. Complete characterization of rate capabilities of cells comprised of lithium metal, a porous NMC cathode, and pFTO-containing carbonate solutions during electrochemical cycling. (Q4, FY 2019)

Progress Report

Last quarter, the team reported on the synthesis and initial characterization of triflimide-based styrene (PS-LiTFSI) and acrylate (PA-LiTFSI) ionomers and polyelectrolyte solutions of these polymers in carbonate mixtures. They highlighted the promising conductivity of over 1 mS/cm for the project's PS-LiTFSI and PA-LiTFSI systems in a 2:1 EC / dimethyl carbonate (DMC) mixture as well as the order of magnitude higher self-diffusion coefficients for lithium species over the polymer backbone in these solutions.

This quarter, the team focused on building the lab's capabilities to perform rigorous transference number measurements based on concentrated solution theory. They designed the measurement setup based on the modified Balsara-Newman approach that requires four independent measurements: the bulk electrolyte conductivity, κ, obtained via impedance measurements; the ideal transference number, $t_{+,id}$, from lithium symmetric cell measurements of steady state currents under an applied polarization; the total salt diffusion coefficient, D, obtained from restricted diffusion measurements in a lithium symmetric cell; and the electrolytes thermodynamic factor, T_f, measured by a decay in liquid junction potential in a concentration cell as concentration gradients relax. From these measurements, one can determine the true cation transference number, t_+^0, which relates the fraction of current carried by positively charged lithium species to the total ionic current. The team focused on building and verifying the setup with traditional liquid electrolytes, laying the groundwork for polyelectrolyte solution measurements.

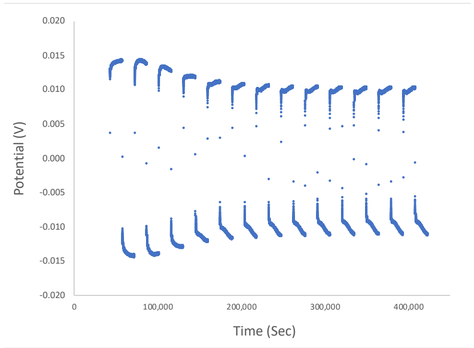

Figure 13. Potential (V) versus time (s) for 0.5 M LiTFSI in EC/DMC = 2 on charging and discharging for 4 h preconditioning cycles at 20 μ/cm².

Initial efforts focused on achieving reproducible transference number measurements using the Bruce-Vincent steady-state current for solutions of LiTFSI salt in EC/DMC. The steady-state current technique for measuring the transference number assumes both that the electrolyte behaves ideally, and that a steady-state current can be consistently achieved on polarization. Due to the reactivity of lithium metal, unless a very stable passivating SEI layer is formed, the steady-state condition is difficult to consistently satisfy. To address this issue, the team tried a number of constant-current cell preconditioning treatments as well as additives to build a stable SEI layer with LiTFSI in EC/DMC. From Figure 13, it is clear that even after 12 charge and discharge cycles at 20 μA/cm², a stable current-potential response is not achieved for this electrolyte combination. Continual growth of the interfacial resistance, as measured by impedance between cycles, suggests continued reactions at the lithium surface. To test the stability of a liquid electrolyte solution closer to LiTFSI in PEO solid electrolyte systems frequently studied in literature by the steady-state current method, the team also studied LiTFSI in tetraglyme. While the LiTFSI in tetraglyme appeared more repeatable from cell to cell, still a perfectly stable current-voltage response was not achieved during precondition. Despite the observed interfacial instability in the LiTFSI in tetraglyme system, the team performed steady-state current measurements on cells preconditioned for 6 cycles, by polarizing the cells at an applied potential of ± 10 mV for 4 h while recording the cell current. While the current appears to start tapering off after about an hour, a true steady state is not achieved. Additionally, the current achieved after 4 h at 10 mV applied potential continues to decrease with cycle, indicating that the system continues to change, likely due to reaction at the Li-metal surface (see Figure 14). Next quarter, the team will study the source of this instability using 3-electrode cells with a gold micro-reference electrode, which

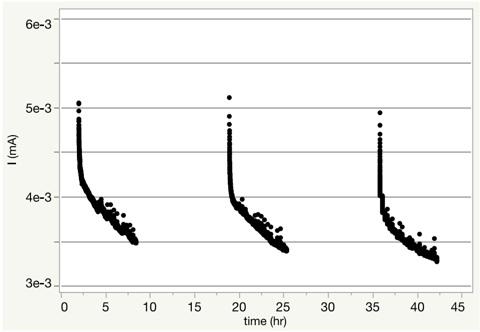

Figure 14. Current (mA) versus time (h) for 0.5 M LiTFSI in tetraglyme polarized for 4 h at 10 mV.

is a well-established technique already developed in the project's laboratory for another project; they will also further study the effect of the preconditioning cycle on steady-state current measurements. Using this method, the team will characterize the stability of the polyelectrolyte solutions against lithium metal while performing steady-state transport property measurements.

In addition to studying the reproducibility of transference number measurements via the steady-state current method in lithium symmetric cells, this quarter the team developed a setup for thermodynamic factor and electrolyte activity coefficient measurements in a liquid-liquid concentration cell. Custom low-volume U-cells with a fine borosilicate glass frit were fabricated by Adams & Chittenden, and a dry-bath block machined for the cell to ensure consistent temperature control during experiments (see Figure 15). This setup will be used to quantify the non-idealities of the polyelectrolyte solutions over a broad concentration range. Next quarter, the team will run reliability and reproducibility tests on this setup with standard liquid electrolytes; once the method has been verified, they will perform full characterization of the triflimide-based polyelectrolyte solutions. The team will also simultaneously continue to study the cycling and rate capabilities of the polyelectrolyte in carbonate solution against Li-metal anodes and porous NMC cathodes.

Figure 15. Concentration cell setup designed for low-volume characterization of liquid electrolyte non-idealities.

Patents/Publications/Presentations

Publication

- Fong, K. D., J. Self, K. D. Diederichsen, B. M. Wood, B. D. McCloskey, and K. A. Persson. "Ion Transport and the True Transference Number in Nonaqueous Polyelectrolyte Solutions for Lithium-Ion Batteries." *American Chemical Society Central Science* (2019). Available online.

Presentation

- American Physical Society Spring Meeting, Boston, Massachusetts (2019): "Molecular Dynamics Simulations of Ion Transport in High Transference Number Polyelectrolytes for Li-Ion Batteries"; K. D. Fong, J. Self, K. D. Diederichsen, K. A. Persson, and B. D. McCloskey.

Task 1.8 – Advanced Polymer Materials for Batteries
(Zhenan Bao and Yi Cui, Stanford University)

Project Objective. This project will develop new polymer materials for batteries. The team will develop polymer coatings with specific mechanical properties that can accommodate the volume expansion and contraction of the Li-metal anode associated with deposition and stripping (charging and discharging).

Project Impact. The cycling stability and CE of Li-metal electrodes will be increased by implementation of a polymer-based protective layer that functions as an artificial SEI with desired properties. The improved performance will enable further development toward practical utilization of Li-metal anodes with higher cycling efficiency and less susceptibility to dendrite-based failure.

Approach. The project uses soft polymer coatings with dynamic crosslinking to give the resulting polymers liquid-like rheological properties and stretchable and self-healing properties. In previous work, the project has shown that such coatings resulted in uniform deposition/stripping of lithium metal and improved cycling stability of Li-metal electrodes. To understand the design rules for effective polymer coatings, the team chose a few representative polymers to systematically understand structure property relationships. Here, the team investigates the correction between surface energy of the polymer and exchange current for lithium deposition.

Out-Year Goals. Work will progress toward the correlation between dielectric constant and exchange current. These findings will enable further understanding and development of various polymer coatings for protecting Li-metal anodes.

Collaborations. There are no active collaborations this quarter.

Milestones

1. Identify at least two different types of self-healing polymers (SHPs) with promise to suppress dendrites. (Q2, FY 2019; Completed)

Progress Report

Rational design of the electrode-electrolyte interphase is essential to stabilize electrodeposition of metallic lithium. Thus, it is important to design an artificial interfacial layer that can accommodate the stress generation due to the volume changes during battery operation and at the same time maintain ionic continuity. This report describes the design of artificial SEI with two distinct concepts that can enable stable deposition of metallic lithium. The two concepts are based on self-healable dynamic polymers and single-ion conducting elastomers.

Dynamic Polymeric Architectures

The team hypothesizes that stimuli-responsive polymeric architectures can be effective in preventing morphological instabilities during electrodeposition compared to covalently bonded rigid polymers and crosslinked elastomers, when used as artificial interfaces between the electrode and electrolyte. The fundamental working mechanism of the dynamic polymeric coatings can arise from the spontaneous structural response of the polymer in response to the roughening electrode during electrodeposition. As the polymer coating is free to flow, if there is a ‘hotspot’ (uneven deposit) on the surface of the lithium metal, the dynamic polymer coating can rearrange and cover these regions, resulting in increased overpotential. Thus, successive Li^+ ions deposit on the flatter regions resulting in uniformity of deposition. Furthermore, the tortuous pathway in the polymeric interface can enable uniform distribution of lithium ions during charging process, thus leading to uniform deposition.

The team is synthesizing a series of different supramolecular polymers that will be designed comprising various content of noncovalent interactions and polymer entanglements using polymerization of soft polymer (having low Tg) with urea linkages. The team varied the chemical structure of the SHP comprising a polymer soft block, and the urea linkages were formed using diisocyanate units. Two different hard block units were utilized in this work, specifically, isophorone (IPDI) and bis methylene diphenyl units (MDI). These units enable different strength of hydrogen bonding in the supramolecular polymer network. The MDI block can form pi-pi stacking and also quadrupolar H-bonding at each site, while the IDPI unit forms weaker H-bonding due to steric hindrance and low symmetry of the molecule. Thus, the synthesized polymers will help the team understand the effect of the entanglements and dynamic bond formation in the coatings for stabilizing electrodeposition.

The team performed frequency-dependent oscillatory shear measurements to analyze mechanical and molecular properties of supramolecular polymers. Specifically, they utilized a strain of 1% and at different temperatures and finally performed Time – Temperature Superposition to obtain the rheology at a wider frequency range. The high-frequency regime corresponds to the elastic behavior of the material, while the low frequency corresponds to the viscous effects. It can be seen from Figure 16 that the polymers with just the IPDI units behave like a viscoelastic liquid, while adding the MDI groups make the polymers harder. In fact, at a content of MDI=50% ratio, there is a crossover from viscoelastic liquid to viscoelastic solid. Thus, the gel-point of the different supramolecular polymers is at MDI=50%. Thus, in the current set of polymers, the team can systematically understand the effect of the polymer relaxation timescales on the stability of electrodeposition. Relation between the mechanical properties of polymer electrolyte and electrodeposition has been studied in the past; however, very little is known on the role of polymer coating mechanics in the electrodeposition.

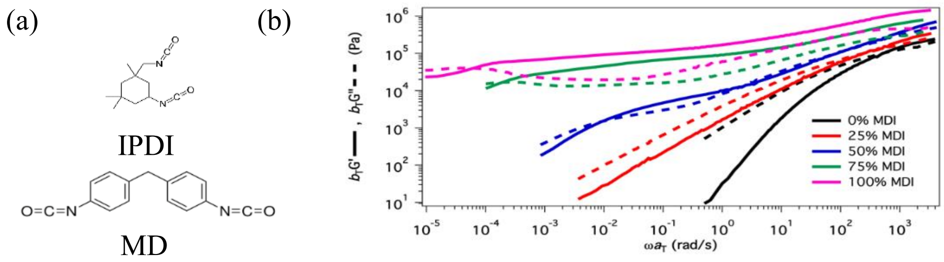

Figure 16. (a) Chemical structure of IPDI (weak H–bonding) and MDI (strong H–bonding) moieties in polymer backbone. (b) Oscillatory shear measurements at 1% strain for different self-healing polymers.

The team analyzed electrochemical characteristics of the SHP using CE measurements in Li|| SHP@Cu cells. In this measurement, a fixed amount of lithium was deposited onto the copper electrode, followed by repeated stripping and plating for shorter timeframes. Thereafter, the amount of lithium remaining from the copper electrode was quantified for obtaining the CE of electrodeposition. The electrolyte utilized in this experiment was 1 M $LiPF_6$ in EC/DMC with 10% FEC. Figure 17b compared the CE of the different polymer coatings with varying H-bonding strength. It is observed that the CE of the lithium deposition is higher for the polymer-coated copper compared to the bare. It is important to note that in previous reports, polymer coatings have been shown to be effective in only ether-based electrolytes and not in carbonate-based systems that are more desirable for high-voltage batteries. Thus, improved CE with the current polymer coating is interesting and encouraging. The figure also shows that values for all the coatings demonstrate a trend that at lower levels of MDI content, the polymer coating shows higher CE than those with higher MDI content. Also, it is apparent that the CE is higher for the polymers below the gel-point in comparison to stiffer polymers. The results clearly demonstrate that improved dynamicity in the polymers enables stable deposition, which is a deviation from the long-standing concept in solid electrolytes that states that high modulus is important to prevent dendrites.

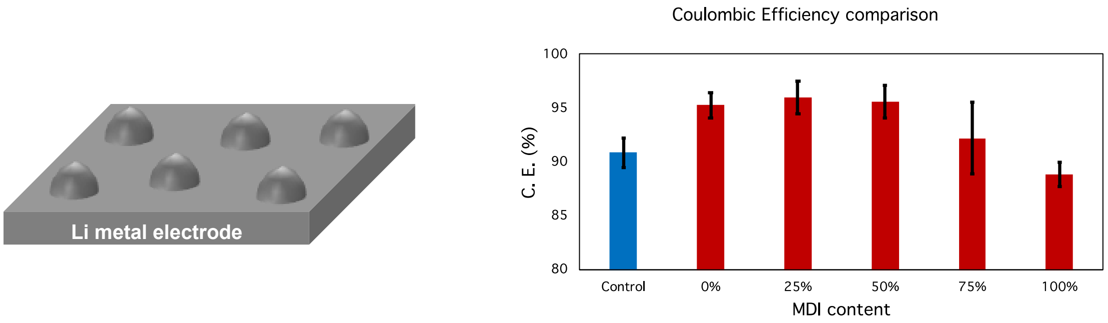

Figure 17. (a) Schematic showing the polymer coating on Li-metal electrode. (b) Coulombic efficiency comparisons of the self-healing polymer with varying H-bonding strengths in the co-polymer.

Patents/Publications/Presentations

Presentation

- DOE VTO AMR, Arlington, Virginia (June 10–13, 2019): "Stabilizing Lithium-Metal Anode by Interfacial Layer"; Z. Bao.

Task 1.9 – Improving the Stability of Lithium-Metal Anodes and Inorganic-Organic Solid Electrolytes (Nitash Balsara, Lawrence Berkeley National Laboratory)

Project Objective. The project objective is to establish a new hybrid electrolyte that will be stable against cells with a Li-metal anode.

Project Impact. Polymer electrolytes offer increased stability in lithium batteries in comparison to more widely used liquid electrolytes. Nanostructured electrolytes containing both soft, ion-conducting domains and rigid, nonconducting domains offer the opportunity to tune both mechanical and electrical properties separately. Such electrolytes are conveniently made by block copolymer self-assembly. Most of the block copolymer electrolytes studied thus far comprise organic polymer chains for both the conducting and rigid domains. The team hopes to synthesize new electrolytes that simulataneously have high transport properties and have greater stability against lithium in comparison to organic diblock copolymers.

Approach. First, the team synthesizes hybrid diblock copolymers by incorporating monomers that contain an inorganic component. Then, electrolytes are prepared by mixing these diblock copolymers with salt. Electrochemical and mechanical characterization of these materials is performed before carrying out cycling X-ray tomography (XRT) experiments. The combination of these approaches enables rational design of materials that exhibit improved stability against lithium metal.

Out-Year Goals. The project will synthesize a new hybrid electrolyte that is designed to be stable against lithium metal. The material is a block copolymer wherein acryloisobutyl polyhedral oligomeric silsesquioxane (POSS) is covalently bonded to the chain. The second block is a conventional polymer electrolyte, PEO. Electrochemical characterization of this polymer will include measurement of all transport properties including conductivity, diffusion coefficient, and the transference number. The stability against lithium metal will be evaluated by cyclic voltammetry (CV), while its applications as an electrolyte will be evaluated and visualized using cycling XRT experiments on symmetric Li-hybrid-Li cells.

Collaborations. There are no active collaborations this quarter.

Milestones

1. Determine limiting current in solid electrolytes. (Q1, FY 2019; Completed)
2. Determine the nature of lithium/electrolyte interface. (Q2, FY 2019; Completed)
3. Study the effect of lithium metal purity and failure mechanisms. (Q3, FY 2019; Completed)
4. Determine parametric range over which stable lithium electrodeposition is obtained. (Q4, FY 2019)

Progress Report

The Q3 milestone to study the effect of lithium metal purity and failure mechanisms was completed. Impurities in the Li-metal electrode material were imaged using XRT at beamline 8.3.2 at the Advanced Light Source, as shown in Figure 18.

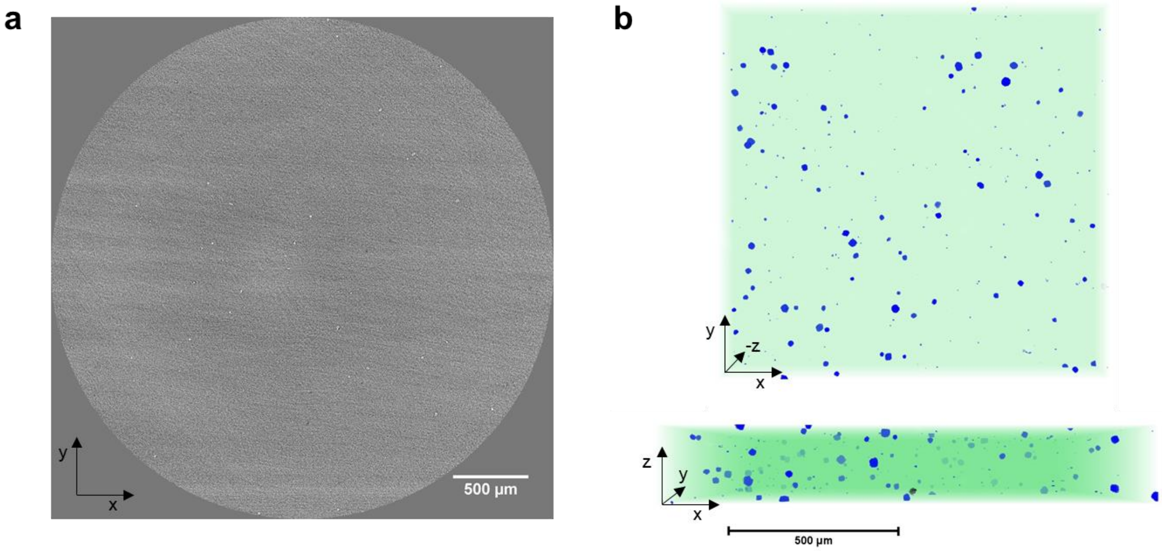

Figure 18. (a) Impurities are present in lithium as-received. Cross-sectional slice through cell with additional cross section of pure lithium showing impurity particles. (b) Reconstruction of volume of lithium as-received with highlighted impurity particles and a volume density.

Last year, the team found that density of lithium protrusions increased with current density in an analogous block copolymer electrolyte (Figure 19). They also found that protruding structures were nucleated in the POSS-PEO-POSS (5-35-5) triblock in the vicinity of these impurity particles (Figure 20). As a result, the team hypothesized a treatment for lithium symmetric cells containing a block copolymer electrolyte to move impurity cells away from the electrode-electrolyte interface. This may be accomplished by plating planar lithium at a low current density to use the electrolyte to "filter" out impurity particles (impurity particles do not go through the electrolyte). A schematic is shown in Figure 21a. The goal of this treatment is to reduce nucleation of lithium protrusions by reducing concentration of impurity particles at the electrode-electrolyte interface. Figure 21b shows a plot of current, voltage, and time during a treatment step; Figure 21c shows a cross-section by XRT of a cell before this treatment. Figure 21d-e shows treatment results: most impurity particles are successfully removed from the interface, although some remain adhered.

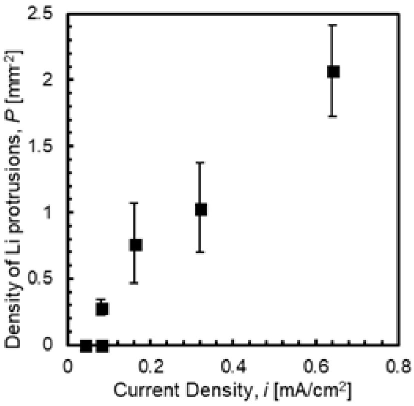

Figure 19. Correlation between current density and defect density in failed cells. The areal density of protruding defects, P, increases with current density.

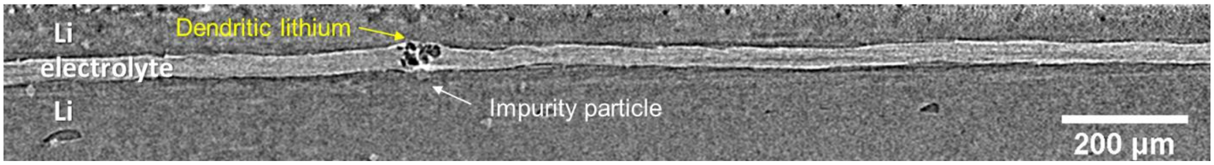

Figure 20. Slice through a reconstructed volume imaged using X-ray tomography. This Li/POSS-PEO-POSS/Li cell was cycled at 0.175 mA cm^{-2} and failed after 17 cycles.

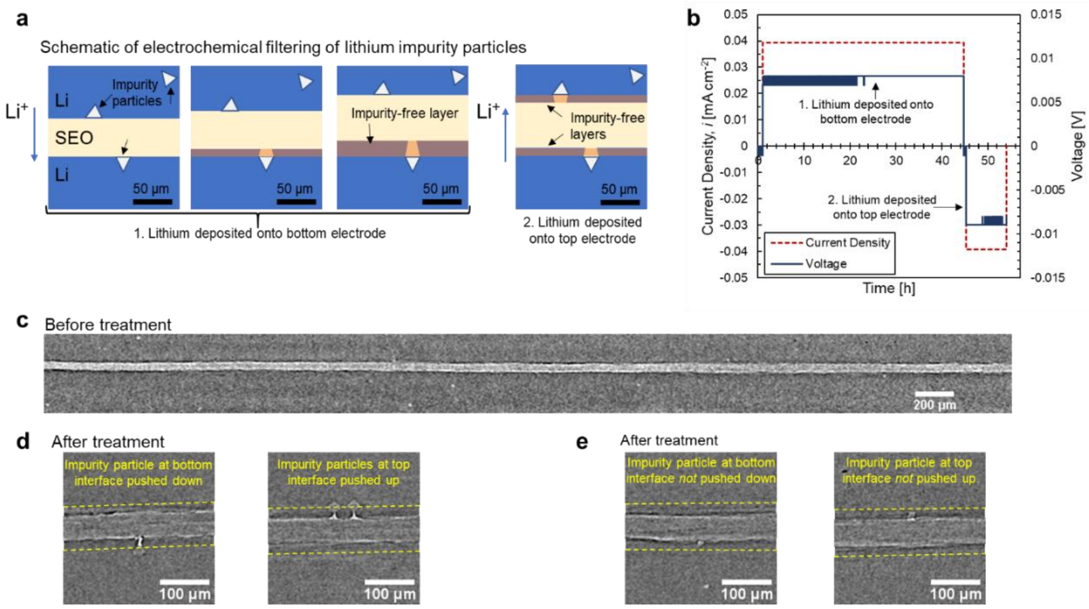

Figure 21. Strategy of the electrochemical filtering treatment to push impurity particles away from the interface. (a) Schematic of the electrochemical filtering treatment. After symmetric cell fabrication, some impurity particles, shown as white triangles, lie at the electrode-electrolyte interface. Step 1: with a sufficiently low current density, new planar lithium, highlighted in orange, can be deposited onto the bottom electrode to create a layer free of impurity particles. Step 2: by reversing the direction of current, planar lithium may be plated on to the upper electrode, such that both electrodes have a layer of impurity-free lithium at the electrode-electrolyte interface. (b) Current density and voltage of one electrochemical treatment over time. Lithium was charged at 0.04 mA cm^{-2} for 43.75 h (8.5 μm of lithium calculated) and discharged at the same current density for 8.75 h (1.7 μm of lithium calculated). (c) Slice through a reconstructed volume of a symmetric cell as-fabricated after 14 conditioning cycles. No inhomogeneities were observed at the interfaces. (d) Slices through a reconstructed volume of the symmetric cell in (c) after an electrochemical filtering treatment. Yellow dashed lines indicate the calculated height of lithium after the treatment. This cell charged a calculated 38 μm of lithium, and discharged a calculated 19 μm of lithium. Impurity particles are visibly pushed away from the electrode-electrolyte interface. (e) Slices through a reconstructed volume of the symmetric cell in (d) after an electrochemical filtering treatment. Yellow dashed lines indicate the calculated height of lithium after the treatment. Some impurity particles still remain adhered to the polymer electrolyte after the treatment.

The cells were then cycled at a constant current density to determine the effects of treatment on lifetime. The treated cells passed an average of 52-390% more charge before failure as compared to control cells. Further work is under way to determine the nature of this improvement.

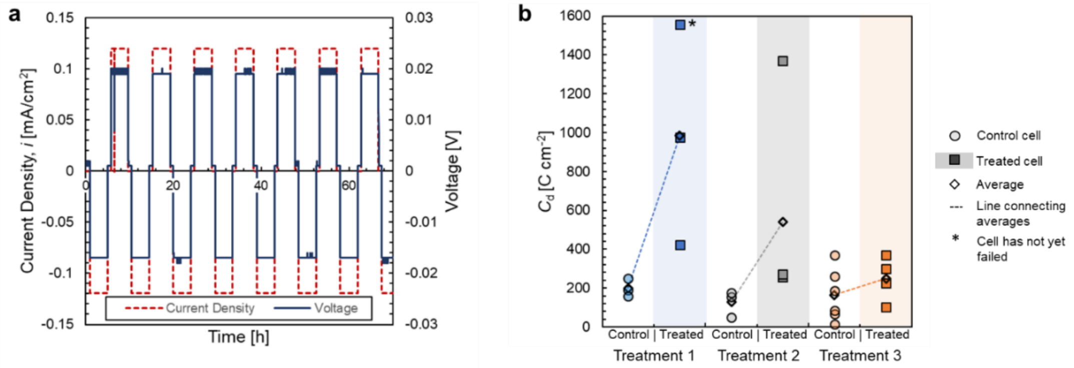

Figure 22. Galvanostatic cell cycling example and results. (a) Current density and voltage of the first cycles at 0.12 mA cm^{-2} for one cell. During each cycle, current was applied for 4 h at -0.12 mA cm^{-2} (2.3 μm of lithium calculated), no current was applied for 45 min, current was applied for 4 h at 0.12 mA cm^{-2}, and no current was applied for 45 min. (b) Charge passed before failure, C_d, plot for each group's control and treated cells. Details of the electrochemical filtering treatment are found in Figure 21. The transparent circles indicate control cells, while the filled-in squares indicate treated cells. Hollow diamonds indicate the average of cells in the column. Dashed lines connect the averages of control and treated cells in each group. The asterisk indicates a cell that has not yet failed. Treatment 1 cells were cycled at 0.12 mA cm^{-2}, while Treatment 2 and 3 cells were cycled at 0.175 mA cm^{-2}.

Patents/Publications/Presentations

Presentations

- Berkeley Electrochemistry Seminar Series, Berkeley, California (May 20, 2019): "Dissolution of Lithium Metal in Poly(ethylene oxide)"; M. Galluzzo.
- Berkeley Electrochemistry Seminar Series, Berkeley, California (June 24, 2019): "Factors Influencing Lithium Protrusion Nucleation and Cycle Life in Solid Polymer Electrolytes for Battery Applications"; J. Maslyn.

Task 1.10 – Electrolyte/Binder for High Efficiency Lithium-Sulfur Battery: New Materials Design and Computation
(Zhengcheng Zhang, Larry A. Curtiss, and Ahn Ngo, Argonne National Laboratory)

Project Objective. Li-S batteries have received great attention because sulfur exhibits an order of magnitude higher theoretical capacity than that achievable with intercalation-type cathode materials in Li-ion batteries and is considered as a promising battery chemistry to power long-range, low-cost EVs. Sulfur is abundant in nature and nontoxic, which leads to low cost of the cell and environmental benefits. However, low active material utilization and poor cycle life hinder the practical application of Li-S batteries. The project objective is to develop new electrolyte materials to help overcome these challenges and enable high-efficiency Li-S batteries for vehicle application.

Project Impact. Development of novel functional electrolytes tailored for Li-S electrochemistry will enable improved materials utilization and longer cycle life as needed to take advantage of the high potential capacity of Li-S batteries to power long-range, low-cost EVs.

Approach. This project takes a new approach, combining organic synthesis and quantum chemistry computations to obtain an in-depth understanding of the interaction of the discharged lithium polysulfides with the electrolyte solvents and the lithium salt, aiming to develop new electrolyte materials for Li-S batteries. Based on the team's previous study, the fluorinated-ether-based electrolytes have shown very limited Li_2S_x solubility, and at the same time could effectively passivate the lithium anode surface, affording a reversible electrochemistry with high CE. However, the low active material utilization compromises its advantages of high theoretical capacity and energy density. To overcome this, the team will investigate boron-containing fluorinated polyethers as a new class of electrolytes for Li-S batteries. To further improve the cycle life, the project also proposes to design and synthesize new polymer binders bearing a pentafluorophenyl group on the backbone. First principles density functional theory (DFT) and wave-function based quantum chemistry methods will be employed to provide accurate atomic/molecular level insight into the experimental studies. The team will also employ *ab initio* molecular dynamics (AIMD) simulations of the solvents for different finite temperatures and concentrations. The AIMD simulations will provide information on the structures of the electrolytes based on the fluorinated ethers synthesized in the experimental part of this project.

Out-Year Goals. The out-year goals are to find electrolytes that promote longer cycle life through electrolytes to reduce material loss.

Collaborations. This project engages in collaboration with Prof. A. Salehi at University of Illinois at Chicago (UIC).

Milestones

1. Design and synthesis of new fluorinated borate electrolytes and baseline studies of sulfur utilization, CE, and cycle life. (Q1, FY 2019; Completed, December 30, 2018)
2. Quantum chemical calculations of the chemical stability and reactivity properties of new borate and fluorinated ethers solvents and with electrode surfaces. (Q2, FY 2019; Completed, March 30, 2019)
3. Electrochemical characterization of performance of various fluorinated ether electrolytes in Li-S cells. (Q3, FY 2019; Completed, June 30, 2019)
4. Correlation of experimental and theoretical results on Li-S cells with ether decomposition during cell operation. (Q4, FY 2019; Initiated).

Progress Report

Partially fluorinated ethers (PFEs) have been reported a number of times as beneficial co-solvents and additives for batteries using Li-S chemistries. Unfortunately, there are few reports describing the structural/chemical basis for this improvement. As such, the team has been working to elucidate these properties using seven fluorinated ethers with similar structures. Shown in Figure 23 are the eight compounds chosen for this investigation; synthesis and purification were carried out in the project's lab, followed by cell testing in electrolyte formulations of DOL:PFE (1:1) with 1 M LiTFSI.

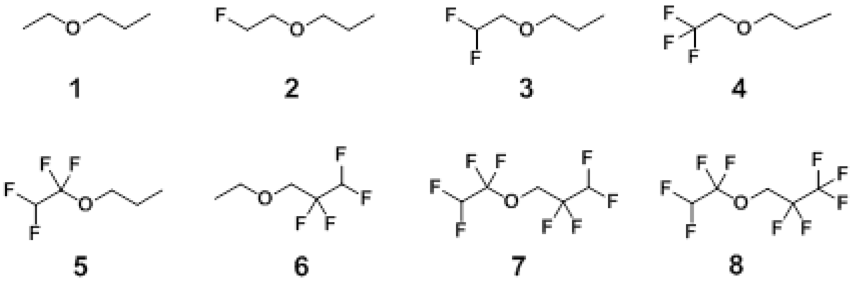

Figure 23. Structures of the eight partially fluorinated ethers considered in this study.

This study showed the influence of structural characteristics of PFE co-solvents on CE (Figure 24) and specific discharge capacity retention in Li-S electrochemical cells. It was shown that high-functioning PFE solvents possess a higher number of fluorine and that the fluorine is also in close proximity to the oxygen of the ether. The PFEs that displayed the best cycling behavior (4, 7, and 8) possess both of these characteristics. Compounds 5 and 6, while showing better performance than the baseline, did not outperform compound 4, despite the fact that they both possessed four fluorine atoms versus the three in compound 4. This observation suggests that the degree of fluorination is not the only determining factor in the higher performance previously observed for compound 7 (TTE). Even the most fluorinated PFE studied, compound 8, fell just short of the bar set by 7, despite containing nine fluorine atoms versus the eight fluorine atoms of compound 7.

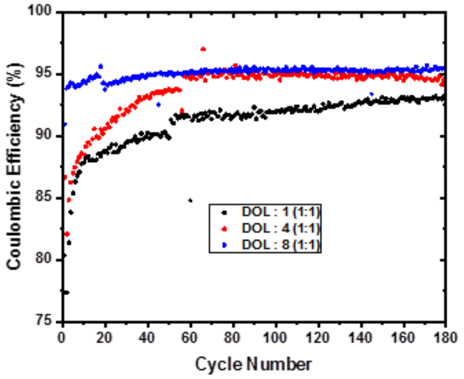

Figure 24. Coulombic efficiency of Li-S cells with partially fluorinated ether electrolytes 1, 4, and 8.

Post-test analysis of cycled lithium metal used as the anode showed a distinct difference in surface morphology by SEM/EDS analysis, with electrolytes using 4 and 7 producing large aggregates. Analysis of the elemental composition of these aggregates showed them to be higher in carbon, fluorine, and oxygen than the more uniform SEI observed for the DOL:DME electrolyte sample. Spectra collected of the lithium SEI by Fourier transform infrared (FTIR) showed that formulations using 3, 7, and 8 have similar chemical structural composition in the aggregates. The FTIR spectra for the SEI formed with 3, 7, and 8 were distinctly different from those collected for the baseline electrolyte DOL:DME and also possessed peaks not observed in any of the initial electrolyte components. This implies that the SEI formed with electrolytes containing PFE solvents is distinctly different from that in the typical DOL:DME. The previously reported compound 7 and new compound 8 displayed the best CE among the seven compounds tested, with values up to 96% without the commonly employed additive $LiNO_3$. The conclusions drawn from this study can aid in development and discovery of new PFE-based solvents for Li-S based batteries.

Patents/Publications/Presentations

Publication

- "Li-S Battery with Partially Fluorinated Ether Electrolytes: Interplay between Capacity, Coulombic Efficiency and Li Anode SEI Formation"; under revision.

TASK 2 – DIAGNOSTICS

Summary and Highlights

To meet the goals of the VTO Multi-Year Program Plan and develop lower-cost, abuse-tolerant batteries with higher energy density, higher power, better low-temperature operation, and longer lifetimes suitable for the next-generation of EVs, hybrid EVs (HEVs), and plug-in hybrid EVs (PHEVs), there is a strong need to identify and understand structure-property-electrochemical performance relationships in materials, life-limiting and performance-limiting processes, and various failure modes to guide battery development activities and scale-up efforts. In pursuit of batteries with high energy density, both high cell operating voltages and demanding cycling requirements lead to unprecedented chemical and mechanical instabilities in cell components. Successful implementation of newer materials such as silicon anode and high-voltage cathodes also requires better understanding of fundamental processes, especially those at the SEI of both anode and cathode.

This Task takes on these challenges by combining model system *ex situ*, *in situ*, and *operando* approaches with an array of start-of-the-art analytical and computational tools. Three subtasks are tackling the chemical processes and reactions at the electrode/electrolyte interface. Researchers at LBNL use *in situ* and *ex situ* vibrational spectroscopy and far- and near-field scanning probe spectroscopy to understand the structure of active materials and the physio-chemical phenomena at electrode/electrolyte interfaces, particularly those of the high-voltage cathodes. GM is developing a number of *in situ* diagnostic techniques, including atomic force microscopy (AFM), nanoindentor, dilatometer, and stress-sensor, to be combined with atomic/continuum modeling schemes to investigate and understand the coupled mechanical/chemical degradation of the SEI layer on Li-metal anode. ANL aims to develop high-conductivity ceramic electrolytes through cation doping and then stabilize the electrode/electrolyte interfaces though co-sintering. Subtasks at Brookhaven National Laboratory (BNL) and PNNL focus on the understanding of fading mechanisms in electrode materials, with the help of synchrotron-based X-ray techniques (diffraction and hard/soft X-ray absorption) at BNL and high-resolution transmission electron microscopy (HRTEM) and spectroscopy techniques at PNNL. UC San Diego (UCSD) is developing advanced diagnostic tools, including scanning transmission electron microscopy / electron energy loss spectroscopy (STEM/EELS), *operando* Bragg coherent diffraction imaging (BCDI) and *ab initio* computation, to probe anion redox and oxygen evolution in Li-excess NMC materials. At LBNL, model systems of electrode materials with well-defined physical attributes are being developed and used for advanced diagnostic and mechanistic studies at both bulk and single-crystal levels. These controlled studies remove the ambiguity in correlating a material’s physical properties and reaction mechanisms to its performance and stability, which is critical for further optimization. The final subtask at Stanford University / Stanford Linear Accelerator Center (SLAC) develops and utilizes a correlative X-ray microscopy platform to investigate the lithiation dynamics and understand factors that determine the rate capability and degradation mechanisms in cathode materials. The diagnostics team not only produces a wealth of knowledge that is key to development of next-generation batteries, it also advances analytical techniques and instrumentation that have a far-reaching effect on material and device development in a variety of fields.

Highlight. The highlight for this quarter is as follows:

- BNL (Yang’s group) used X-ray fluorescence (XRF) microscopy and X-ray absorption spectroscopy (XAS) to study the chemical composition and distribution of sulfur species in cathodes recovered from high-energy-density Li-S pouch cells, which showed significant area-dependent variations in both.

- The General Motors team (Xiao, Sheldon, Qi, and Cheng) investigated the effect of external pressure on the microstructure of electroplated mossy lithium. The results show that the thickness of mossy lithium layer on the plating side of Li | Li symmetric cells decreases with increasing pressure.
- PNNL (Wang's group) used cryo-TEM techniques to characterize the structure and chemistry of electrochemically deposited lithium metal and the associated SEI. The results show deposited lithium in ribbon-like configurations along with a uniform layer of SEI on the edges.

Task 2.1 – Model System Diagnostics for High-Energy Cathode Development
(Guoying Chen, Lawrence Berkeley National Laboratory)

Project Objective. This project will use a rational, nonempirical approach to design and synthesize next-generation high-energy, high-voltage cathode materials. Combining a suite of advanced diagnostic techniques with model cathode materials and model electrode/electrolyte interfaces, the project will perform systematic studies to achieve the following goals: (1) obtain new insights into solid-state chemistry, particularly cationic and/or anionic redox activities during charge and discharge of high-capacity lithium TM oxides, (2) gain fundamental understanding on cathode/electrolyte interfacial chemistry and charge transfer process as a function of operating voltage, (3) reveal performance- and stability-limiting properties and processes in high-energy, high-voltage cathodes, and (4) develop strategies to mitigate the structural and interfacial instabilities.

Impact. The project will improve the commercial viability of next-generation high-energy cathode materials. The findings will enable more stable high-voltage cycling of existing Li-TM oxides as well as development of novel high-capacity cathode materials for advanced Li-ion batteries.

Approach. The project will prepare crystal samples of Li-stoichiometric and Li-excess TM oxides with well-defined physical attributes. It will perform advanced diagnostic and mechanistic studies at both bulk and single-crystal levels. Global properties and performance of the samples will be established from the bulk analyses, while the single-crystal-based studies will utilize time and spatially resolved analytical techniques to probe the material redox transformation process and failure mechanisms under battery operating conditions.

Out-Year Goals. In the out-years, the project will obtain fundamental knowledge on performance-limiting physical properties, phase transition mechanisms, parasitic reactions, and transport processes that prevent cathode materials from delivering higher capacities and achieving more stable cycling at high voltages. It will develop approaches to mitigate cathode structural and interfacial instabilities during high-voltage operation. Further, it will design and synthesize optimized Li-TM oxide cathodes as well as novel high-energy electrode materials.

Collaborations. This project collaborates with the following: G. Ceder, K. Persson, M. Doeff, B. McCloskey, and P. Ross (LBNL); V. Srinivasan (ANL); D. Nordlund and Y. Liu (Stanford Synchrotron Radiation Lightsource, SSRL); C. Wang (PNNL); C. Grey (University of Cambridge); and A. Huq and J. Nanda (Oak Ridge National Laboratory, ORNL).

`Milestones

1. Understand the interplay between cationic and anionic redox processes in model TM oxides. (Q1, FY 2019; Completed)

2. Characterize interfacial processes and surface changes on anion-active model oxides. (Q2, FY 2019; Completed)

3. Evaluate the effect of particle size/morphology on oxygen redox chemistry and kinetics. (Q3, FY 2019; Completed)

4. Develop design strategies to improve performance of anion-active oxide cathodes. (Q4, September 2019; On schedule)

Progress Report

This quarter, the effect of particle size on oxygen redox behavior in Li-excess TM rock-salt cathodes was evaluated on $Li_{1.3}Nb_{0.3}Mn_{0.4}O_2$ (LNMO) model compound. Due to cation disordering in the crystal structure, LNMO crystals tend to grow in a spherical shape without defined facets on the surface. The subsequent ball milling process needed for carbon coating further adds complexity in particle size and morphology control. Here, LNMO samples with different particle sizes were obtained by simply varying ball milling energy. Starting from the as-synthesized micron-sized LNMO single crystals (LNMO_AS, Figure 25a), a two-step ball milling procedure was used to prepare carbon-coated LNMO samples with an average particle size of ~ 400 nm and 50 nm, referred to as LNMO_L and LNMO_S, respectively. The crystals were first ball milled for 12 h at 100 rpm for LNMO_L and 300 rpm for LNMO_S, followed by each ball milling with acetylene black (8:2 wt ratio) for 12 h at 100 rpm. As shown in Figure 25b-c, carbon was uniformly distributed on the LNMO particles in both cases. XRD patterns (Figure 25d) show visible peak broadening on LNMO_S, whereas no changes were observed on the larger-sized LNMO_L sample.

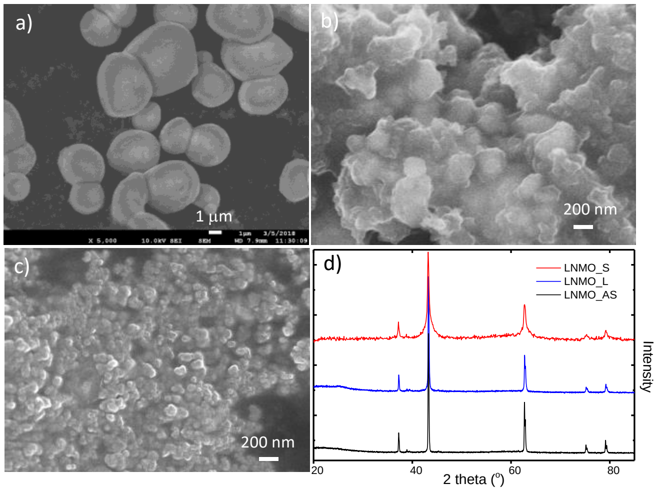

Figure 25. (a-c) Scanning electron microscopy images and (d) X-ray diffraction patterns of as-synthesized LNMO_AS and carbon-coated LNMO_L and LNMO_S samples.

Figure 26 compares the electrochemical performance of the samples. At a current density of 10 mA/g, significantly lower first-cycle discharge capacity along with higher polarization was observed on LNMO_L (Figure 26a). While the low-voltage slopy region (arising from oxidation of Mn^{3+} to Mn^{4+}) is nearly identical on first-charge, the plateau region associated with oxygen activities is significantly shorter on LNMO_L. This is consistent with the known inferior kinetic properties of oxygen redox as compared to cation redox, resulting in a larger particle size impact in the former. On the dQ/dV profiles (Figure 26b), the broad manganese oxidation peak is similar in both samples. A doublet feature was observed in the oxygen oxidation region around 4.5 V on LNMO_S. This corresponds to oxygen oxidation at the lower voltage and oxygen loss at the higher voltage, according to the project's previous studies on LNMO. On the other hand, only a single peak was seen on LNMO_L, suggesting that lattice oxygen redox and oxygen loss occur simultaneously in larger particles. Lowering the current density from 10 to 2.5 mA/g significantly increases discharge capacity and reduces polarization voltage gap in LNMO_L, as shown in Figure 26d. On the dQ/dV profiles (Figure 26e), the single peak at about 4.5 V also split into a doublet, although the ratio of the high/low voltage peaks is much lower compared to that in the LNMO_S sample. Cycling performance during

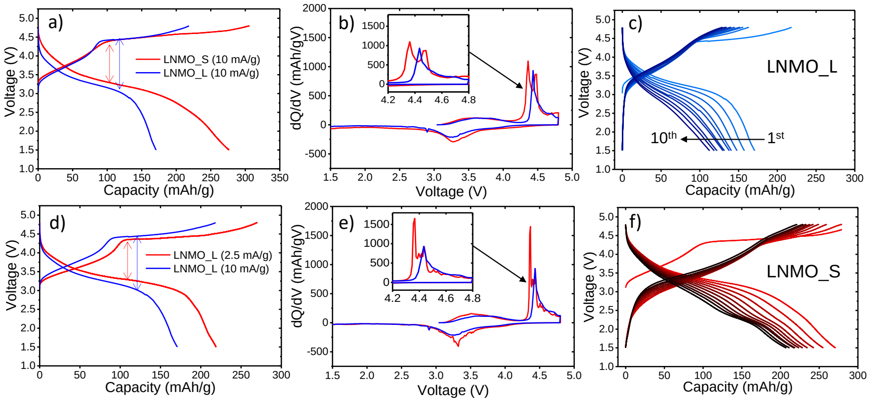

Figure 26. (a/d) First-cycle voltage profiles. (b/e) First-cycle dQ/dV profiles of LNMO half cells. (a-b) Comparison of LNMO_L and LNMO_S at the same rate. (d/e) Comparison of LNMO_L at different rates. (c/f) Voltage profiles of half cells during the first 10 cycles at a current density of 10 mA/g.

the first 10 cycles is shown in Figure 26e-f. Capacity decay was observed on both LNMO_L and LNMO_S cathodes, but the retention was improved in the latter. These results indicate that compared to TM cation redox, oxygen redox is more sensitive to kinetic factors such as particle size and current density. These parameters, therefore, can be used to tune the behavior of oxygen redox in Li-rich TM oxide cathodes, especially the balance between oxygen redox/oxygen loss and subsequent capacity/stability of the cathodes.

Patents/Publications/Presentations

Publications

- Chen, D., W. H. Kan, and G. Chen. "Understanding Performance Degradation in Cation-Disordered Rock-Salt Oxide Cathodes." *Advanced Energy Materials* (2019): 1901255. doi: 10.1002/aenm. 201901255.
- Yan, P., M. Su, J. Zheng, N. Song, A. Devaraj, B. Liu, Y. Wang, G. Chen, X. Li, Z. Xu, K. Amine, J-G. Zhang, and C-M. Wang. "Anionic Redox Enhanced Vacancy Injection and Condensation in Bulk Lattice of Layered Cathodes." *Nature Nanotechnology* 14 (2019): 602. doi: 10.1038/s41565-019-0428-8.
- Shen, H., E. Yi, L. Cheng, M. Amores, G. Chen, S. Sofie, and M. M. Doeff. "All Solid-State Battery Design Considerations for Electric Vehicles." *Sustainable Energy & Fuels* 3 (2019): 1647. doi: 10.1039/C9SE00119K.

Presentations

- 235th ECS Meeting, Dallas, Texas (May 2019): "Unraveling the Origin of Performance Degradation in High-Capacity Cation-Disordered Oxide Cathodes"; D. Chen and G. Chen.
- International Battery Association (IBA) 2019, La Jolla, California (March 2019): "Li-Rich Rock-Salt Oxides as High-Energy LIB Cathodes"; G. Chen.

Task 2.2 – Interfacial Processes – Diagnostics
(Robert Kostecki, Lawrence Berkeley National Laboratory)

Project Objective. This collaborative project will develop and apply advanced experimental methodologies to study and understand the mechanism of operation and degradation of high-capacity materials for rechargeable cells for PHEV and EV applications. The objective is to develop and apply *in situ* and *ex situ* far- and near-field optical multi-functional probes and synchrotron-based advanced X-ray techniques to obtain detailed insight into the active material structure and physio-chemical phenomena at electrode/electrolyte interfaces at a spatial resolution corresponding to the size of basic chemical or structural building blocks. Through an integrated synthesis, characterization, and electrochemistry effort, the project aims to develop a better understanding of electrode and electrolyte materials so that rational decisions can be made as to their further development into commercially viable cathode materials.

Project Impact. Instability and/or high resistance at the interface of battery electrodes limits electrochemical performance of high-energy density batteries. A better understanding of the underlying principles that govern these phenomena is inextricably linked with successful implementation of high-energy-density materials in Li-based cells for PHEVs and EVs. Pristine and cycled composite and thin-film model electrodes are investigated using state-of-the-art techniques to identify, characterize, and monitor changes in materials structure and composition that take place during battery operation and/or storage. The proposed work constitutes an integral part of the concerted effort within the BMR Program, and it supports development of new electrode materials for high-energy, Li-metal-based rechargeable cells.

Approach. The pristine and cycled composite electrode and model thin-film electrodes will be probed using various surface- and bulk-sensitive techniques, including FTIR, attenuated total reflectance (ATR)–FTIR, near-field infrared (IR) and Raman spectroscopy and microscopy, and scanning probe microscopy to identify and characterize changes in materials structure and composition. Novel *in situ/ex situ* far- and near-field optical multifunctional probes in combination with standard electrochemical and analytical techniques are developed to unveil the structure and reactivity at interfaces and interphases that determine materials electrochemical performance and failure modes.

Out-Year Goals. In the out-years, the project aims to (1) understand the factors that control charge/discharge rate, cyclability, and degradation processes, (2) design and apply new diagnostic techniques and experimental methodologies capable of unveiling the structure and reactivity at hidden or buried interfaces and interphases that determine material, composite electrode, and full-cell electrochemical performance and failure modes, and (3) propose effective remedies to address inadequate Li-metal-based battery calendar/cycle lifetimes for PHEV and EV applications.

Collaborations. Electrode materials and composite solid electrolytes tested under different cycling regimes by V. Battaglia and M. Doeff (LBNL) will be studied. The diagnostic studies will be carried out in sync with other diagnosticians in this research program.

Milestones

1. Manufacture model thin-film and composite LLZO and lithium thiophosphate (LPS) SSEs by pulsed laser deposition (PLD) as model systems for fundamental electrochemical studies of Li-metal battery systems. (Q1, FY 2019; Completed)
2. Characterize the bulk and surface structure of lithium anode, NMC cathode electrodes, and SSEs and the relationship to electrochemical and interfacial properties. (Q2, FY 2019; On schedule)

3. Characterize the chemistry of SSE/Li and electrolyte/cathode interfaces with *ex situ* near-field IR, XAS, and XPS. (Q3, FY 2019; Completed)
4. Design and develop new XAS/XPS experimental setup to characterize *in situ* solid/solid (for example, NMC/SSE and Li/SSE) interfaces. *Go/No-Go Decision*: Demonstrate feasibility of *in situ* measurements of solid-solid electrochemical interfaces. (Q4, FY 2019; On schedule)

Progress Report

Li-metal batteries are among the most promising candidates of high-energy-density devices for advanced energy storage. However, uncontrollable lithium dendrite growth induces poor cycling efficiency and severe safety concerns, dragging Li-metal batteries out of practical applications. This quarter, the team investigated a carbon-nitrogen modified stainless steel mesh (CNSSM), which favors homogeneous Li-metal nucleation and growth of a dense lithium film when employed as an anode in Li-metal battery.

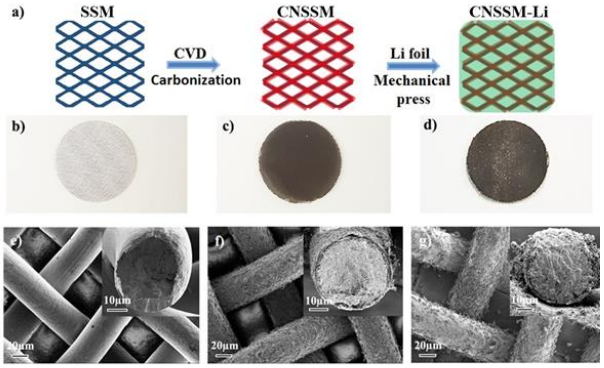

Figure 27. (a) Schematic illustration of the fabrication process of carbon-nitrogen modified stainless-steel mesh and lithium (CNSSM-Li) composite electrode. Digital camera images of (b) SSM, (c) CNSSM, and (d) CNSSM-Li composite electrode. Scanning electron microscopy image top views and cross-sections (insets) of (e) SSM, (f) CNSSM, and (g) CNSSM-Li composite electrode.

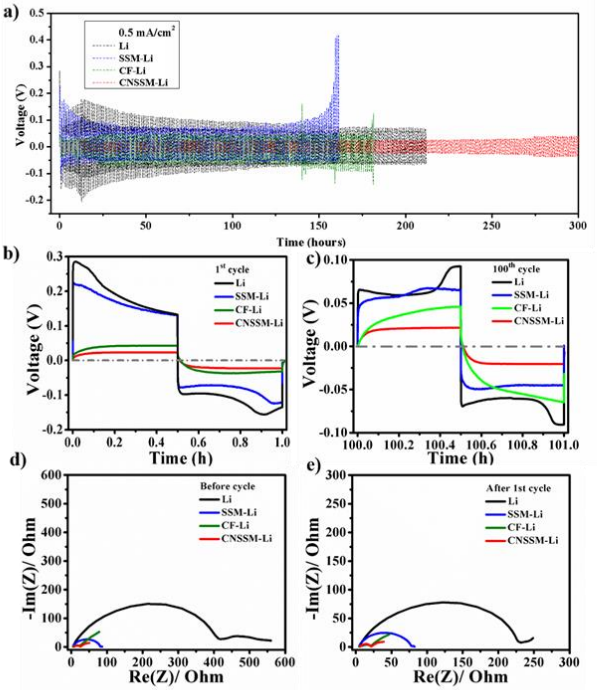

Figure 28. (a) Lithium electrodissolution/electrodeposition cycles for symmetrical Li/Li cells using pristine lithium foil electrode, SSM-Li, CF-Li, or CNSSM-Li electrodes at ±0.5 mA cm^{-2}. Corresponding voltage profiles of (b) the 1st and (c) the 100th cycles. (d) Nyquist plots of the symmetrical cells before cycling and (e) after 1st cycle. Frequency range: 10 kHz – 100 mHz.

Figure 27a shows a schematic representation of the fabrication process of the CNSSM and the final carbon-nitrogen modified stainless steel mesh and lithium (CNSSM-Li) composite electrode. The stainless steel mesh (SSM) was first carbonized and covered with a dense functional layer, then pressed onto lithium foil via mechanical pressing. Digital camera images of SSM, CNSSM, and CNSSM-Li are shown in Figure 27b-d, and the corresponding SEM images are given in Figure 27e-g. After carbon-nitrogen coating, the surface of the CNSSM became rougher, and an outer layer can be clearly seen in the cross-sectional SEM image (Figure 27f inset). The grains in the outer zone appear larger owing to the permeation of carbon atoms from the surface, leading to the formation of Fe_3C. Figure 27g shows a top-view SEM image of the CNSSM-Li electrode. The CNSSM partly penetrated into the foil, and the bare lithium can be seen through the void of the modified mesh.

The cycling performance of lithium, SSM-Li, CF-Li, and CNSSM-Li symmetric cells at a current density of 0.5 mA cm^{-2} are presented in Figure 28a. The CNSSM-Li composite efficiently stabilizes the cycling of lithium metal and significantly limits the increase of voltage hysteresis (Figure 28b-c). The modification contributes to a lower nucleation overpotential, leading to homogeneous nucleation and thus limited surface area growth with plating. The lithiophilic functional group from CNSSM-Li tends to bond strongly to lithium ions and immobilize them on the surface, promoting a uniform plating at its initial stages. The interfacial resistance (Figure 28d-e) of both CF-Li and the CNSSM-Li composite electrode remain low (24 Ω cm^2) and the cells maintain at low resistances after the 1st cycle. This report summarizes the project's efforts toward Milestone 3.

Patents/Publications/Presentations

The project has no patents, publications, or presentations to report this quarter.

Task 2.3 – Advanced *In Situ* Diagnostic Techniques for Battery Materials
(Xiao-Qing Yang and Seong-Min Bak, Brookhaven National Laboratory)

Project Objective. The primary objective of this project is to develop new advanced *in situ* material characterization techniques and to apply these techniques to support development of new cathode and anode materials with high energy and power density, low cost, good abuse tolerance, and long calendar and cycle life for beyond Li-ion battery systems to power PHEVs and battery electric vehicles (BEVs). The diagnostic studies will focus on issues relating to capacity retention, thermal stability, cycle life, and rate capability of beyond Li-ion battery systems.

Project Impact. The VTO Multi-Year Program Plan describes the goals for battery: "Specifically, lower-cost, abuse-tolerant batteries with higher energy density, higher power, better low-temperature operation, and longer lifetimes are needed for development of the next-generation of HEVs, PHEVs, and EVs." The knowledge gained from diagnostic studies through this project will help U. S. industries develop new materials and processes for next-generation Li-ion batteries in the effort to reach these VTO goals.

Approach. This project will use the combined synchrotron-based *in situ* X-ray techniques (XRD; and hard and soft XAS) with other imaging and spectroscopic tools such as HRTEM and MS to study the mechanisms governing performance of electrode materials.

Out-Year Goals. In the out years, the project will complete development of diagnostic techniques using X-ray pair distribution function (x-PDF), XRD, and XAS combined with neutron diffraction and neutron PDF (n-PDF), as well as STEM imaging and transmission X-ray microscopy (TXM) for cathode materials studies. It will then apply these techniques to study the structural changes of various new cathode and anode materials.

Collaborations. The BNL team will work closely with material synthesis groups at ANL (Drs. Shin and Amine) for the high-energy composite and at PNNL for the S-based cathode and Li-metal anode materials, and with ORNL on neutron scatterings. This project will also collaborate with industrial partners at GM and Johnson Controls, as well as with international collaborators.

Milestones

1. Complete the *ex situ* soft x-ray absorption (sXAS) studies at oxygen K-edge of novel organic disulfide cathode material (1,2,4,5,6,7,9,10-octathia bis cyclopenta antraquinone-3,8-dithone, or TPQD) for Li-S batteries at different charged and discharged states. (Q1, FY 2019; Completed)
2. Complete the *ex situ* sXAS studies at sulfur K-edge of novel organic disulfide cathode material (TPQD) for Li-S batteries at different charged and discharged states. (Q2, FY 2019; Completed)
3. Complete XAS studies of sulfur electrode harvested from failed high-energy Li/S pouch cells after multiple cyclings. (Q3, FY 2019; Completed)
4. Complete the spatially resolved XAS at sulfur K-edge and imaging of sulfur-based chemical species using XRF on the Li-metal anode in a cycled high-energy Li/S pouch cell. (Q4, FY 2019; In progress)

Progress Report

This quarter, the third milestone was completed. BNL has been focused on the *ex situ* X-ray microprobe. XRF and sulfur K-edge XAS studies of high-energy-density Li-S pouch cells were conducted. The chemical information of the sulfur species regarding composition and distribution was studied using XRF. Figure 29 depicts XRF and XAS spectra results from R1-R3 regions (Figure 29a) of the cycled sulfur cathode. Figure 29b shows XRF image collected at R1 (7×7 mm) below an energy of 2469 eV, which only detects sulfur species with relatively low absorption energies. Apparently, this area is covered mainly by the low-valence sulfur species (in yellow color), with randomly distributed uncovered spots (in blue color). Further XAS analysis reveals that the low-valence sulfur species (from yellow area) are composed of lithium polysulfides and lithium sulfides; the high valent species (from blue spots) are mainly sulfone and sulfate (Figure 29d). When the X-ray beam energy is increased to 2480 eV, more sulfur species with a wider valence range from S^{2-} to S^{4+}can be detected. In contrast to XRF at 2469 eV, more uniform mapping was observed at 2480 eV (Figure 29c). It means that the whole R1 area is evenly covered by sulfur species with a wider valance range. The comparison in Figure 29b-c presents variation of the sulfur species in both oxidation states and distribution in the local R1 area, which suggests random distributed reaction areas in the region. Similar results, that is, randomly distributed reaction areas, were observed in the R3 region (Figure 29h-j). However, more significant differences were found in the center region of the electrode (R2). Compared to R1 and R3, R2 experiences much more serious inhomogeneous reactions as proved by the uneven XRF mappping at both 2469 and 2480 eV (Figure 29e-f). In addition, high contents of sulfone from TFSI, and S^{6+} from SO_4^{2-}, were detected by XAS (Figure 29g), from either the residual of LiTFSI salt or oxidation of the sulfur species by $LiNO_3$. This may be caused by earlier solvent depletion in R2 compared to R1 and R3 regions, exacerbating polarization and thus decreasing the reaction extent locally.

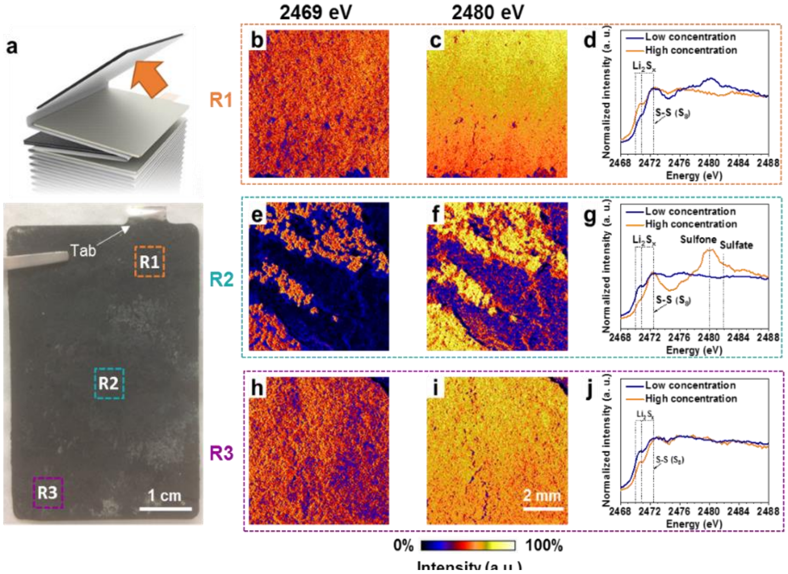

Figure 29. (a) Digital photograph for sulfur cathode obtained from the cycled pouch cell (schematic illustration) with indicating boxes for three selected spots of interest; outer region nearby electrode-tab (R1), central region (R2), and outer corner region (R3). Corresponding mappings of X-ray fluorescence (XRF) microscopy at two different energy levels (2469 and 2480 eV) to investigate the status and distribution of sulfur species at the regions of R1 (b-c), R2 (e-f), and R3 (h-i). X-ray absorption spectra (d/g/j) within an energy scanning range of 2468–2488 eV at two strong contrasted areas in XRF image (Figure 28b/f/h), respectively.

Patents/Publications/Presentations

Publications

- Shadike, Z., H-S. Lee, C. Tian, K. Sun, L. Song, E. Hu, I. Waluyo, A. Hunt, S. Ghose, Y. Hu, J. Zhou, J. Wang, P. Northrup, S-M. Bak, and X-Q. Yang. "Synthesis and Characterization of a Molecularly Designed High-Performance Organodisulfide as Cathode Material for Lithium Batteries." *Advanced Energy Materials.* doi: 10.1002/aenm.201900705, Publication Date: April 10, 2019.
- Lin, R., E. Hu, M. Liu, Y. Wang, H. Cheng, J. Wu, J-C. Zheng, Q. Wu, S-M. Bak, X. Tong, R. Zhang, W. Yang, K. A. Persson, X. Yu, X-Q. Yang, and H. L. Xin. "Anomalous Metal Segregation in Lithium-Rich Material Provides Design Rules for Stable Cathode in Lithium-Ion Battery." *Nature Communications.* doi: 10.1038/s41467-019-09248-0, Publication Date: April 9, 2019.
- Liu, D., Q. Yu, S. Liu, K. Qian, S. Wang, W. Sun, X-Q. Yang, F. Kang, and B. Li.* "Evolution of Solid Electrolyte Interface on TiO_2 Electrodes in an Aqueous Li-Ion Battery Studied Using Scanning Electrochemical Microscopy." *Journal of Physical Chemistry C* 123, no. 20 (2019): 12797–12806. doi: https://doi.org/10.1021/acs.jpcc.9b01412, Publication Date: May 1, 2019.
- Qiu, Q-Q., Z. Shadike, Q-C. Wang, X-Y. Yue, X-L. Li, S-S. Yuan, F. Fang, X-J. Wu, A. Hunt, I. Waluyo, S-M. Bak,* X-Q. Yang,* and Y-N. Zhou.* "Improving the Electrochemical Performance and Structural Stability of the $LiNi_{0.8}Co_{0.15}Al_{0.05}O_2$ Cathode Material at High-Voltage Charging through Ti Substitution." *ACS Applied Materials & Interfaces* 11, no. 26 (2019): 23213–23221. doi: 10.1021/acsami.9b05100, Publication Date: June 11, 2019.

Presentations

- The Minerals, Metals, and Materials Society (TMS) Annual Meeting & Exhibition, San Antonio, Texas (March 10–15, 2019): "Identification and Visualization of Chemical Outliers through Scientific Data Mining in Nanoscale Spectro-Microscopic Study of NMC Electrode"; E. Hu, Y. Liu, H. Xin, and X-Q. Yang. Invited.
- U. S.–China Clean Energy Research Center for Clean Vehicles (CERC-CVC), Xining, China (June 23, 2019): "Understanding Capacity Fade in High-Nickel Content Cathode Materials for Lithium Batteries"; R. Lin, Z. Shadike, S-M. Bak, E. Hu, H. Xin, X. Huang, Y. H. Shin, H-S. Lee, Y. S. Chu, Y. Liu, and X-Q. Yang.* Invited.

Task 2.4 – Advanced Microscopy and Spectroscopy for Probing and Optimizing Electrode-Electrolyte Interphases in High-Energy Lithium Batteries
(Shirley Meng, University of California at San Diego)

Project Objective. The proposed research aims to develop advanced microscopy and spectroscopy tools to probe, understand, and optimize the anion activities that govern the performance limitations such as capacity and voltage stabilities in high-energy Li-excess TM (such as nickel, cobalt, manganese) oxides cathode materials. The approach uniquely combines atomic resolution STEM, EELS, *operando* BCDI, and first-principles computation to probe anion redox and oxygen evolutions in Li-excess NMC materials. Furthermore, the project will track the lithium and oxygen dynamics under electrochemical testing via *operando* neutron diffraction, which will enhance understanding of the overall structural changes due to anion activities. Ultimately, this will home in on the synthesis efforts to produce the modified materials with optimum bulk compositions and surface characteristics at large scale for consistently good performance. The above-mentioned characterization tools will be extended to diagnose various anode types, such as Li-metal anode.

Project Impact. If successful, this research will enable *operando* imaging at the single-particle level by advanced microscopy imaging and high-energy-resolution oxygen K-edge EELS. This work will provide an in-depth understanding of anion activities in high-voltage electrode materials, which can lead to significant improvement in stabilizing operation voltage and electrode-electrolyte interface for future generation high-energy-density electrodes.

Approach. This unique approach combines STEM/EELS, *operando* BCDI, and *ab initio* computation as diagnostic tools for probing anion redox and oxygen evolutions in Li-excess NMC materials. This allows for pinning down the atomistic/molecular mechanism of anion oxidation and determining the speciation compositions and surface characteristics for enabling high rate and long life in the proposed materials. Neutron enables the characterization of bulk material properties to enhance and further optimize high-energy electrode materials.

Out-Year Goals. The goal is to improve the cycle life and efficiency of Li-excess NMC materials through the modification of both the cathode and the electrolyte. Single particle behavior of the modified Li-excess NMC with new electrolytes will be characterized.

Collaborations. This work funds collaborations on EELS (M. Chi, ORNL), neutron diffraction (K. An, ORNL), and sXAS (M. Doeff, LBNL). It supports collaborative work with Z. Liu and Y. Xia at Ningbo Institute of Materials Technology and Engineering in China. It also supports collaboration with the Battery500 Consortium.

Milestones

1. Benchmarking new electrolyte performance with the optimized cathode materials. (Q1, FY 2019; Completed)
2. Conducting XPS characterization of anion evolution on modified Li-excess NMC. (Q2, FY 2019; Completed)
3. Carrying out STEM/EELS characterization on modified Li-excess NMC single particle using optimized electrolyte. (Q3, FY 2019; Completed)
4. Performing EELS and XPS characterization of SEI on electrochemically deposited lithium metal with new electrolyte systems. (Q4, FY 2019; In progress)

Progress Report

Performance Improvement of Li-Rich Layered Oxide with Electrolyte Additive LiBOB

As reported last quarter, a novel electrolyte with LiBOB additive (lithium bis(oxalato) borate) is introduced to further optimize the electrochemical performance of modified $Li[Li_{0.144}Ni_{0.136}Co_{0.136}Mn_{0.544}]O_2$ (denoted as LR-NCM). The baseline electrolyte used in this study is 1 M $LiPF_6$ in EC:DMC=3:7 by volume (denoted as Baseline in Figure 1); the novel electrolyte is 0.98 M $LiPF_6$ + 0.02M LiBOB in EC:DMC=3:7 by volume (denoted as 2% LiBOB). The cycling performances of LR-NCM with different electrolyte are shown in Figure 30a-b. All the cells were charge/discharged at C/20 (1C=250 mAh/g) for two cycles and C/10 for the rest of the cycles. After 50 cycles in the Baseline electrolyte, LR-NCM delivers a specific capacity of 264 mAh/g (82.2% retention). In comparison, LR-NCM cycled in 2% LiBOB exhibits 279 mAh/g (88.0% retention) after 50 cycles, which improves the capacity retention of LR-NCM significantly. The hysteresis of LR-NCM during cycling is determined by the difference of average charging voltage and discharging voltage in each cycle. Both samples have around 0.82 V hysteresis in the first cycle due to the oxygen redox activation process. From second cycle, both samples' hysteresis drops to 0.48 V and decreases to around 0.4 V at 10th cycle. After that, LR-NCM cycled in 2% LiBOB has relatively lower hysteresis compared with that of LR-NCM cycled in the Baseline electrolyte. Rate performance of LR-NCM in the two electrolytes is also compared in Figure 30c-e. The same cycling procedure was applied to two LR-NCM cells starting with 5 cycles of C/20, then 5 cycles of C/10, C/5, C/3, 1C at each rate separately, then C/10 for extended cycling. In the rate change steps (especially at the 10th and 20th cycles), LR-NCM in the Baseline electrolyte shows larger capacity drop than in 2% LiBOB. When changing back to C/10 rate, LR-NCM cycled in 2% LiBOB electrolyte shows much higher (over 10 mAh/g) specific capacity.

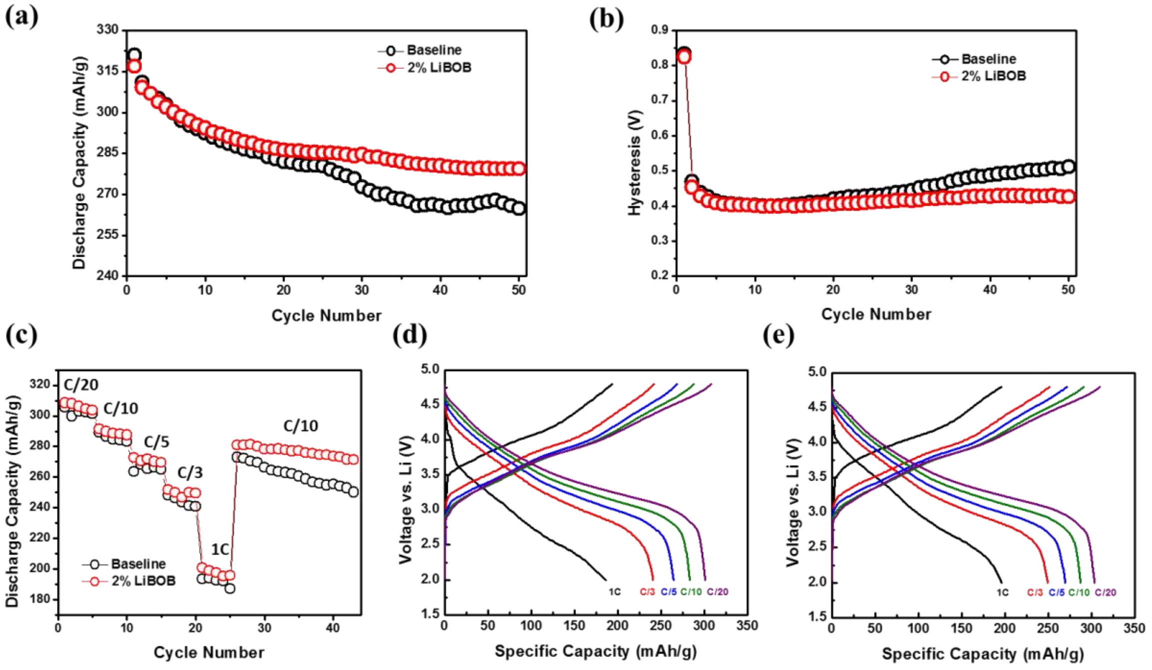

Figure 30. Electrochemical performance of LR-NCM in different electrolyte. (a) Discharge capacity and (b) voltage hysteresis of LR-NCM cycled in different electrolyte. (c). Rate performance of LR-NCM in different electrolyte. (d). Voltage profiles of LR-NCM cycled in the Baseline electrolyte. (e). Voltage profiles of LR-NCM cycled in 2% LiBOB electrolyte. Two activation cycles of C/20 were applied to the cells in (a) and (b) at the beginning of cycling.

STEM and EELS Comparison of Cycled Li-Rich Layered Oxides in Different Electrolyte

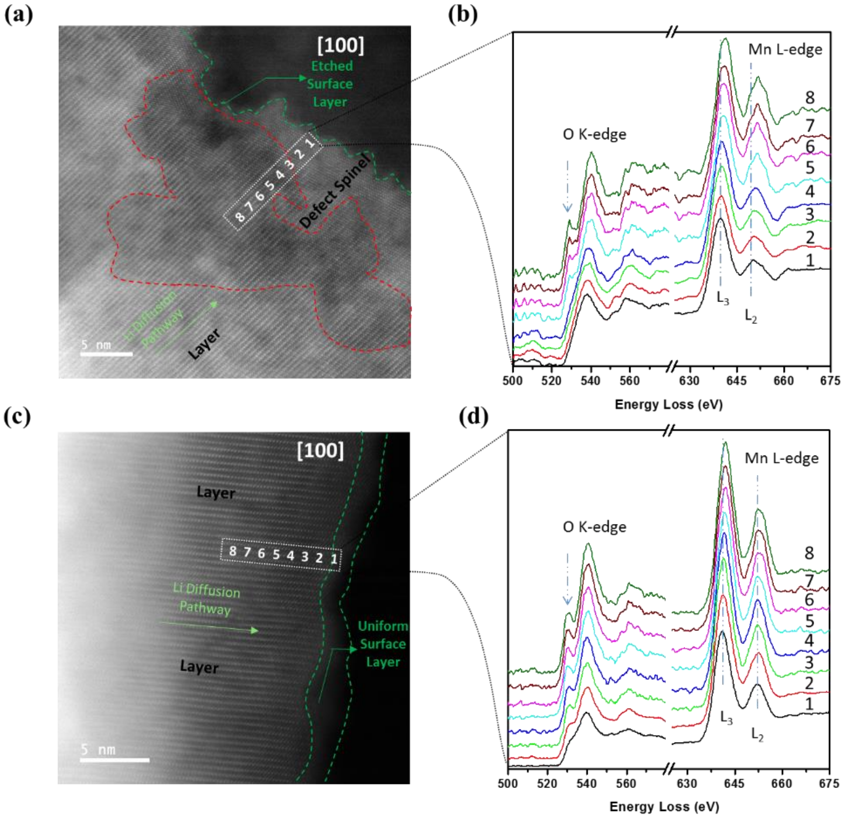

Figure 31. Scanning transmission electron microscopy / high-angle annular dark-field images of the (a) cycled LR-NCM in the Baseline electrolyte and (c) cycled LR-NCM in 2% LiBOB electrolyte. Spatially resolved electron energy loss spectra from the surface to the bulk of the (b) cycled LR-NCM in the Baseline electrolyte and (d) cycled LR-NCM in 2% LiBOB electrolyte.

STEM / high-angle annular dark-field (HAADF) images were collected for the samples cycled 50 times in different electrolyte to explain the performance improvement at atomic scale. For the sample cycled in the Baseline electrolyte (Figure 31a), the team clearly observed bulk structural degradation, which is featured by the nucleation of nanovoids in the bulk lattice, as representatively revealed by the red dashed circle. TM ions were found in the lithium layer in the subsurface regions, forming a defect spinel structure that is different from the layered structure in bulk. In addition, an etched surface was observed, which can be attributed to the defective cathode electrolyte interfacial (CEI) layer formed during cycling in the Baseline electrolyte. In sharp contrast, the cycled sample obtained from 2% LiBOB electrolyte shows uniform contrast across the entire grain (Figure 31c), which corresponds to a well-defined layered structure after 50 cycles. The formation of a more uniform CEI layer well prevents the structural transformation and degradation from particle surface to bulk. Spatially resolved EELS was also used at a step of ~ 0.8 nm from the surface to bulk, and the spectra are presented in Figure 31b/d. The data points are aligned with the HAADF image to indicate where each spectrum was taken. There is a clear oxygen pre-peak in the oxygen K-edge obtained from bulk of the particle cycled in the baseline electrolyte. This pre-peak starts to decrease when it comes to the interface region of the spinel-like phase, and disappears completely in the near surface. The disappearance of the pre-peak can be ascribed to the oxygen vacancy formation and reduction of neighboring TM, which is verified by both L_3/L_2 peak intensity ratio and peak shift in the manganese L-edge. The same spectra evolution was only found in a thin surface region (less than 2 nm) for the cycled sample in 2% LiBOB electrolyte. From the STEM/EELS results, it is clear that structrual degradation and composition changes occur in the sample where the CEI is not well formed, which impedes the lithium diffusion pathway and reduces the amount of active material during cycling. As a result, electrolyte additive LiBOB shows an improvement in both the rate performance and cycling stability of LR-NCM.

Patents/Publications/Presentations

Publications

- Zhao, E., M. Zhang, Y. S. Meng, et al. “Local Structure Adaptability through Multi Cations for Oxygen Redox Accommodation in Li-Rich Layered Oxides.” *Energy Storage Materials* (2019). In revision.
- Qiu, B., M. Zhang, Y. S. Meng, et al. “Structural Metastability and Reversibility in Anionic Redox-Based Li-Rich Layered Oxide Cathode.” *Joule* (2019). In submission.

Task 2.5 – *In Situ* Diagnostics of Coupled Electrochemical-Mechanical Properties of Solid Electrolyte Interphases on Lithium-Metal Rechargeable Batteries

(Xingcheng Xiao, General Motors; Brian W. Sheldon, Brown University; Yue Qi, Michigan State University; and Y. T. Cheng, University of Kentucky)

Project Objective. The project objective is to develop a comprehensive set of *in situ* diagnostic techniques combined with atomic/continuum modeling schemes to investigate and understand the coupled mechanical/chemical degradation of the SEI layer / lithium system during lithium cycling. The goal of this understanding is to develop a new coating design strategy to achieve dendrite-free, high-cycle efficiency and extend the cycle life of high-energy-density batteries with lithium as the anode for EV application.

Project Impact. The fundamental understanding of the coupled mechanical/chemical degradation of the SEI layer during lithium cycling will enable the project to identify the desirable mechanical properties on SEI/lithium as a system and also the specific transport properties that enable the homogenous lithium stripping/plating while avoiding the mossy structure. Furthermore, it will allow the project to develop a highly impactful strategy to protect lithium metal and achieve dendrite-free high cycle efficiency, which can dramatically increase the energy density of lithium batteries for EV applications.

Approach. Different *in situ* techniques, including AFM, nano-indentor, dilatometer, and stress-sensor, will be developed to investigate the mechanical compatibility between SEI and soft lithium and the relationship between surface morphology and current density distribution that results in an inhomogeneous lithium plating/stripping process. Multiple strategies will be developed to tailor the mechanical and transport properties of SEI and to properly engineer the protective coating/lithium interface.

Out-Year Goals. The out-year goals involve using *in situ* electrochemical tools to reveal failure mechanisms of SEI/lithium as a whole electrode system, including correlating mechanical failure mechanisms of SEI/lithium, morphology evolution, cycle efficiency, and transport properties of SEI. Then, the project will develop continuum framework to establish the failure modes of SEI layer on lithium metal and provide the governing mechanical/material properties of SEI responsible for the critical failure mode based on the experimental results and atomic-scale simulation.

Collaborations. Prof. H. Gao (Brown University) and Dr. Q. Zhang (GM) will be the key researchers involved in continuum simulation and postmortem analysis. Dr. C. Wang (PNNL), Dr. W. Yang (LBNL), and Dr. J. Xiao (PNNL) will be collaborators on advanced *in situ* analysis and electrolyte additives.

Milestones

1. Determine coating design window required to achieve mechanically stable coating on lithium metal. (Q1, FY 2019; Completed)
2. Determine impact of stress on morphological evolution of coated Li-metal surface, and identify failure modes of protective coatings on lithium. (Q2, FY 2019)
3. Vary coating modulus and investigate its impact on interfacial strength and cycle efficiency, and develop coating with desirable mechanical and transport properties. (Q3, FY 2019)
4. Establish a design strategy of protective coatings as artificial SEI on Li-metal electrode to achieve high cycle efficiency (> 99.8%). (Q4, FY 2019)

Progress Report

The Influence of External Pressure on the Microstructure of Electroplated Mossy Lithium has been Studied Using Li | Li Symmetric Cells. After 8 cycles, the stripping side of the cell under the pressure of 0.05 MPa consists of a porous mossy matrix with many lithium chunks, as shown in Figure 32a. A similar porous mossy matrix was also found on the stripping side of the cells under the pressure of 0.11 and 0.17 MPa. However, lithium chunks were not found on the stripping side of the cells under high pressure, as shown in Figure 32b-c. The microstructure on the plating side of Li | Li symmetric cells under different pressures consists of porous matrix and heterogeneously distributed lithium dendrites, as shown in Figure 33.

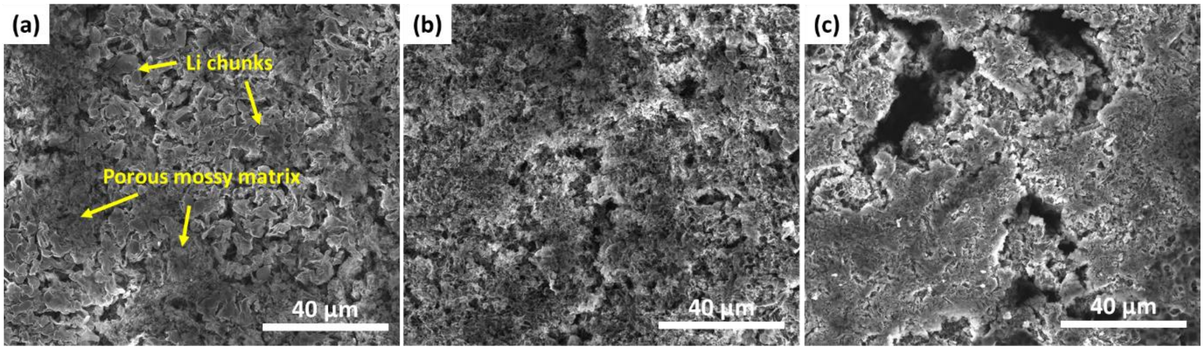

Figure 32. The microstructure of mossy lithium on the stripping side of Li | Li symmetric cells under different pressures: (a) 0.05 MPa, (b) 0.11 MPa, and (c) 0.17 MPa. Current density is 1 mA/cm^2; areal capacity of plating and stripping is 4 mAh/cm^2.

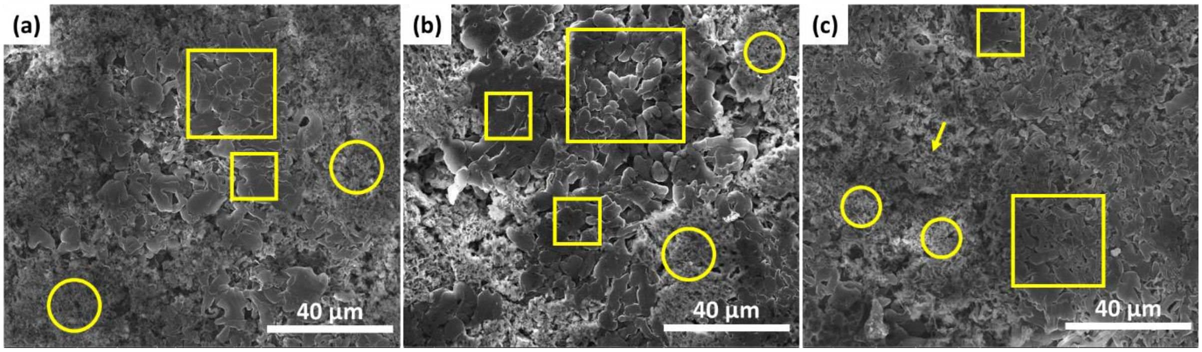

Figure 33. The microstructure of mossy lithium on the plating side of Li | Li symmetric cells under different pressures: (a) 0.05 MPa, (b) 0.11 MPa, and (c) 0.17 MPa. The square regions indicate lithium chunks, and the circled regions indicate porous mossy matrix. Current density is 1 mA/cm^2; areal capacity of plating and stripping is 4 mAh/cm^2.

External pressure also influences the thickness of mossy lithium layers. As shown in Figure 34, the average thickness of the mossy lithium layer on the plating side of Li | Li symmetric cells decreases with increasing pressure. The mossy lithium layer of the cell under a pressure of 0.05 MPa has an average thickness of 79.6 μm, which is about 1.6 times larger than that of the cell under a pressure of 0.17 MPa. The distinct thickness may cause different electronic conductivities of the mossy layers, which will be investigated by using electrochemical atomic force microscopy.

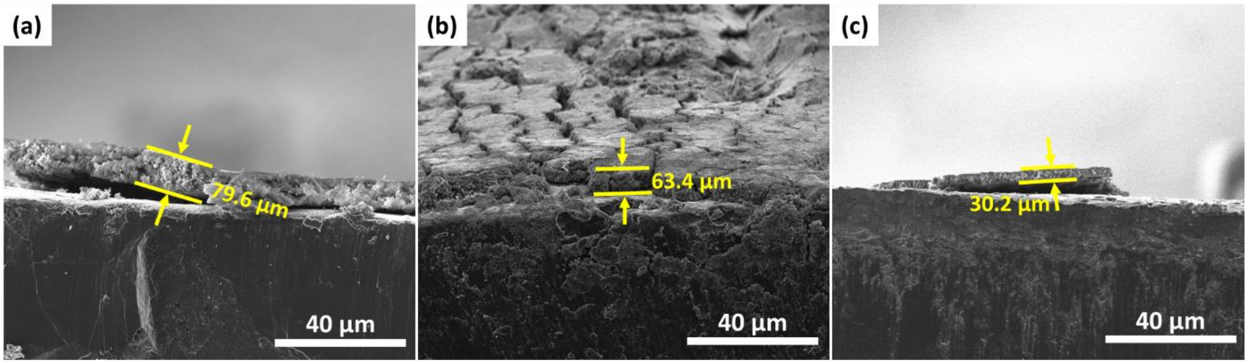

Figure 34. Cross-sectional images of mossy lithium layer on plating side of Li | Li symmetric cells under different pressures: (a) 0.05 MPa, (b) 0.11 MPa, and (c) 0.17 MPa. Current density is 1 mA/cm^2; areal capacity of plating and stripping is 4 mAh/cm^2.

The Team Further Investigated Stress Evolution of Lithum Metal Electrode with *In Situ* Curvature Measurement (MOSS) on these PEO-Protected Electrodes. It showed that the suppressed initial transient stress for the first 3 cycles is associated with surface (SEI/Li inclusion) phenomena. These observations suggest that PEO may suppress an additional reaction associated with SEI formation during the initial phase of plating, and the stress behavior becomes "growth-stress-dominant" instead. If this is true, then it may explain why PEO electrodes tend to cycle longer than the unprotected electrodes. To further investigate the effect of PEO on Li-metal anode, more MOSS measurements were carried out along with post-mortem investigation.

As shown in Figure 35, the stress evolution from MOSS measurements indicates that PEO-protected electrodes tend to suppress the compressive initial transient stress associated with surface layer formation. The post-mortem images after cycling show a distinctive SEI layer on top of the bulk lithium metal, which shows a brittle feature that is thicker than typical SEI formed on lithium metal. The results indicate that swelled PEO layer from the liquid electrolyte may suppress these initial transient stresses, as the soft PEO matrix buffers the stress from SEI formation within. Further analysis using XPS may show what comprises this surface layer. The team also plans to look into much harder artificial SEI layers such as LiF, which would also allow investigation of effects of mechanical properties of artificial SEIs on the stress evolution and performance of Li-metal anodes.

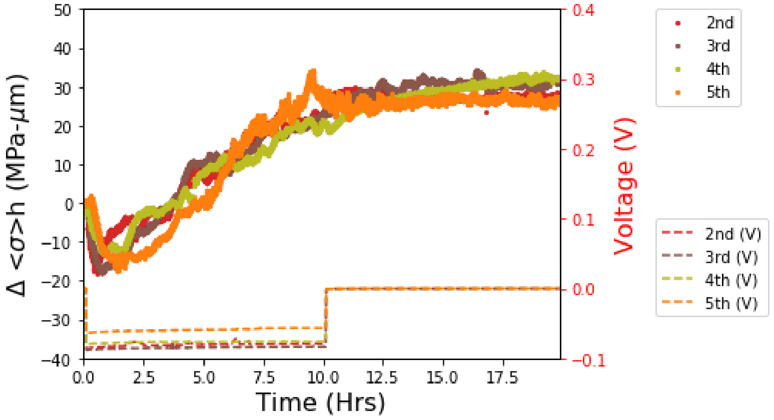

Figure 35. Change in stress-thickness versus time for respective cycles in MOSS cell. Dotted lines indicate MOSS data; dashed lines indicate voltage profile.

Patents/Publications/Presentations

Publication

- Wang, Y., D. Dang, M. Wang, X. Xiao, and Y-T. Chen. "Mechanical Behavior of Electroplated Mossy Lithium at Room Temperature." *Applied Physics Letter* (2019). Accepted.

Task 2.6 – Microscopy Investigation on the Fading Mechanism of Electrode Materials (Chongmin Wang, Pacific Northwest National Laboratory)

Project Objective. This work will use a combination of *ex situ*, *in situ*, *operando* and cryo HRTEM and spectroscopy to probe the fading mechanism of both lithium and silicon as high-capacity anode as well as Ni-rich NMC as high-capacity cathode. For high-capacity anode, the research task will focus on revealing how lithium and silicon interact with liquid electrolyte to critically affect their fading process. For the Ni-rich NMC cathode, the project will focus on delineating the structural and chemical evolution of the Ni-rich NMC regarding dependence on operating voltage, charge rate, and chemistry of electrolyte.

Project Impact. Success of this project will further improve the energy density of Li-ion batteries and accelerate market penetration of EVs required by the DOE EV Everywhere program. The proposed characterization work focuses on atomic-level structural and chemical analysis and direct correlation with battery fading properties. The work can be directly used to guide the designing of electrode materials with tailored microstructure and chemistry for enhanced properties of increasing the energy density of Li-ion batteries and to accelerate market acceptance of EVs, especially for PHEV as required by the EV Everywhere Grand Challenge.

Approach. Aberration-corrected STEM-HAADF and cryo-TEM imaging combined with EELS / energy-dispersive X-ray spectroscopy (EDX) chemical analysis will be used to probe the microstructural and chemical evolution of both cathode and anode. TOF-SIMS, nano-SIMS, and XPS will be used to explore the chemistry and the thickness of SEI layer on cathode and anode material. These characterization results will be used to guide the materials optimization process and establish a solid knowledge base on the correlation between materials selections and structure evolution in the Ni-rich NMC layered cathode materials.

Out-Year-Goals. This project has the following out-year goals:

- Multi-scale *ex situ*/*in situ* and *operando* TEM and cryo-TEM investigation of failure mechanisms for energy-storage materials and devices. Atomic-level *in situ* TEM and STEM imaging to help develop fundamental understanding of electrochemical energy-storage processes and kinetics of electrodes.
- Extension of *in situ* TEM capability for energy storage technology beyond lithium ions, such as Li-S, Li-air, Li-metal, sodium ions, and multi-valence ions.

Collaborations. This project collaborates with G. Chen (LBNL); J. Nanda (ORNL); K. Amine (ANL); D. Wang (Pennsylvania State University); A. Manthiram (University of Texas at Austin, UT Austin); W. Tong (LBNL); G. Liu (LBNL); Y. Cui (Stanford University); J. Zhang (PNNL); J. Liu (PNNL); X. Xiao (GM); S. Meng (UCSD); and S. Whittingham (State University of New York, SUNY, at Binghamton).

Milestones

1. Resolve the true structural nature of the intragranular cracks in Ni-rich NMC and answer questions on the origin of such cracking behavior. (Q1, FY 2019; Completed)
2. Reveal the true structural and chemical information of Si-anode/liquid-SEI layer by integration of cryo-TEM and EELS. (Q2, FY 2019; Completed)
3. Determine the critical factor that controls the correlation between charging rate and fading behavior of Ni-rich NMC. (Q3, FY 2019; Completed)

1. Reveal the true structural and chemical information of Li-metal anode/liquid-SEI layer by cryo-TEM and EELS. (Q4, FY 2019; On schedule)

Progress Report

Lithium metal has been regarded as the most attractive anode material for rechargeable batteries due to its low electrode potential and high theoretical specific capacity compared with other electrode materials used today. However, dendritic growth of lithium metal and low CE during cycling of batteries are the two critical issues that need to be addressed for using lithium metal as anode. To address these critical issues, a fundamental understanding on the formation mechanism of lithium dendrite is needed. The current understanding is limited to ensemble studies using low-resolution TEM due to the instability of organic liquid electrolyte at room temperature under electron beam irradiation during the imaging. Cryo-TEM techniques, which are mostly used in structural biology studies, were demonstrated recently as an effective approach to studying battery materials.

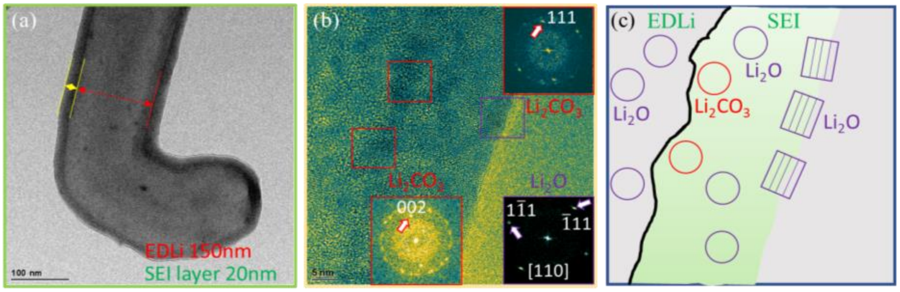

Figure 36. Atomic-resolution transmission electron microscopy (TEM) of electrochemically deposited lithium metal (EDLi) and SEI interface. (a) Bright-field TEM image of the EDLi at a low magnification. (b) Atomic-resolution image of the EDLi and SEI interface. (c) Schematic of the observed SEI formed on EDLi.

This quarter, the team used cryo-TEM techniques to characterize detailed structure and chemistry of electrochemically deposited lithium metal (EDLi) and the associated SEI. Lithium metal was directly deposited onto a copper TEM grid in a coin cell by applying a current of 2 mA cm^{-2} for 5 min. 1.2 M $LiPF_6$ in 3:7 w/w EC/EMC with 5 wt% vinylene carbonate (VC) as the electrolyte. After deposition, the TEM grid was taken out from the copper foil and slightly rinsed with DOL to remove trace lithium salt in the glove box. Then, the TEM grid with deposited lithium metal was placed in a sealed bag fulfilled with argon. The sealed bag was plunged directly into a bath of liquid nitrogen after removal from the Ar-filled glovebox until the lithium metal reached low temperature. Then, the copper TEM grid with EDLi in the sealed bag was loaded onto a pre-cooling Gatan cryo-holder using a cryo-transfer station to ensure the entire process occurred under a cryogenic environment. TEM observations were performed on 300 kV FEI Titan monochromated STEM equipped with a probe aberration corrector under low dose condition.

Figure 36a is a cryo-TEM image showing the typical morphology of lithium metal. It is seen that EDLi exhibits ribbon-like configurations with a diameter of ~ 150 nm. Along the edges of the lithium metal, a uniform SEI is present with a thickness of ~ 20 nm. Figure 36b shows atomically resolved TEM images showing the EDLi, SEI, and its interface structures. High-resolution image reveals that the EDLi contains small crystalline domains dispersed randomly throughout amorphous matrix. Those small crystalline domains were confirmed as Li_2O. The interface between EDLi and SEI is not atomically sharp and irregular in shape. Small crystalline domains randomly dispersed in the amorphous SEI matrix. Fast Fourier transform (FFT) patterns as shown from the red color-coded regions indicate that the small crystalline domains along the interface are mainly Li_2CO_3, while others are mainly Li_2O. Crystalline Li_2O of relatively large sizes are noticed to address on the surface of the SEI, as shown from the purple color-coded region and those large Li_2O grains with the same zone axis of [110]. The SEI formed on EDLi in VC electrolyte is schematically summarized in Figure 36c.

Patents/Publications/Presentations

Publications

- Yan, P., J. Zheng, Z-K. Tang, A. Devaraj, G. Chen, K. Amine, J-G. Zhang, L-M. Liu, and C. Wang. "Injection of Oxygen Vacancies in the Bulk Lattice of Layered Cathodes." *Nature Nanotechnology* 14 (2019): 602–608.
- Mo, R., F. Li, X. Tan, P. Xu, R. Tao, G. Shen, X. Lu, F. Liu, L. Shen, B. Xu, Q. Xiao, X. Wang, C. Wang, J. Li, G. Wang, and Y. Lu. "High-Quality Mesoporous Graphene Particles as High-Energy and Fast-Charging Anodes for Lithium-Ion Batteries." *Nature Communications* 10 (2019):1474.
- Ryu, J., J. H. Seo, G. Song, K. Choi, D. Hong, C. Wang, H. Lee, J. H. Lee, and S. Park. "Infinitesimal Sulfur Fusion Yields Quasi-Metallic Bulk Silicon for Stable and Fast Energy Storage." *Nature Communications* 10 (2019): 2351.
- Song, G., J. Y. Cheong, C. Kim, L. Luo, C. Hwang, S. Choi, J. Ryu, S. Kim, W-J. Song, H-K. Song, C. Wang, I-D. Kim, and S. Park. "Atomic-Scale Combination of Germanium-Zinc Nanofibers for Structural and Electrochemical Evolution." *Nature Communications* 10 (2019): 2364.
- Niu, C., H. Pan, W. Xu, J. Xiao, J-G. Zhang, L. Luo, C. Wang, D. Mei, J. Meng, X. Wang, Z. Liu, L. Mai, and J. Liu. "Self-Smoothing Anode for Achieving High-Energy Lithium Metal Batteries under Realistic Conditions." *Nature Nanotechnology* 14 (2019): 594–601.

Presentation

- Materials Research Society (MRS) Spring Meeting, Phoenix, Arizona (April 2019): "Advanced *In Situ* and *Ex Situ* S/TEM Probing of Interfacial Process in Rechargeable Batteries."

Task 2.7 – Correlative Microscopy Characterization of Electrochemical Hotspots in Oxide Electrodes (Yi Cui, William Chueh, and Michael Toney; Stanford/SLAC)

Project Objective. This project aims to develop and utilize a correlative microscopy platform to investigate the lithiation dynamics of lithium- and manganese-rich (LMR) NMC and NCA, with the specific goal of understanding factors that determine the rate capability and degradation mechanisms at the single primary particle length scale. By developing a nanoscale and single-particle understanding of lithiation, the project addresses specific engineering problems including electrochemical hotspot, electrode utilization, safety, and capacity/voltage fade.

Project Impact. Fundamental insights from this new diagnostic capability are expected to increase the power density and cycle life of oxide electrodes by improving electrode utilization, reducing electrochemical hotspots, decreasing capacity and voltage fade, and enhancing safety, which all improve the viability of Li-ion batteries for vehicle transportation. By understanding lithiation at the single-particle level, this project's success will contribute to improving on-vehicle battery management, such as charging/discharging protocol, and state-of-charge and state-of-health monitoring.

Approach. As stated, the project aims to develop a correlative microscopy platform to investigate the lithiation dynamics of LMR-NMC and NCA, with the goal of understanding factors that determine the rate capability and degradation mechanisms at the single primary particle length scale. On recharging time, the specific phenomena to be addressed include nonuniform current distribution and the correlation between surface property and the local lithiation rate. On degradation, phenomena to be addressed include correlating local chemistry and phases to capacity and voltage fading.

Out-Year Goals. Develop X-ray microscopy to investigate NMC and LMR-NMC cathodes at the single primary particle and single secondary particle level.

Collaborations. Commercial battery electrode particles are being supplied by Samsung.

Milestones

1. Quantify the local structure of Li-rich layered oxides using local X-ray probe. (Q1, FY 2019; Completed)
2. Assess the effect of synthesis condition of anion redox. (Q4, FY 2019)
3. Assess the effect of oxygen vacancies on anion redox. (Q4, FY 2019)

Progress Report

This quarter, the team continued to develop the soft X-ray microscopy characterization of NMC-111 platelets. This particle morphology enables 2D microscopy resolving lithium migration along the conduction planes of layered oxide. The electrochemistry and diffraction patterns are shown in Figure 37. In general, the rate capability is poor compared to agglomerates prepared via co-precipitation synthesis, likely due to the long diffusion path along the width of the platelet and small active area (that is, side wall of the platelets). The team's efforts focused on spectro-microscopy. Specifically, they are using nanoscale XAS at the nickel L-edge to monitor the state-of-charge (SOC). By characterizing discharged and charged NMC-111, the team shows that they can successfully resolve SOC at the tens of nanometer length scale (Figure 38). As would be expected, the fully charged and discharged particles are uniform in SOC. Beam-induced damage was non-existent despite repeated imaging, pointing to the stability of the platelets under soft X-ray imaging condition.

Moving toward *operando* X-ray microscopy experiments, the team has developed a new *in situ* cell that enables the electrochemistry of a ~ 1 nAh NMC-111/Li half cell to be precisely controlled. Initial electrochemistry shows comparable rate-capability as coin cells. The team has also optimized dispersion of the platelet particles on the project's *in situ* cell.

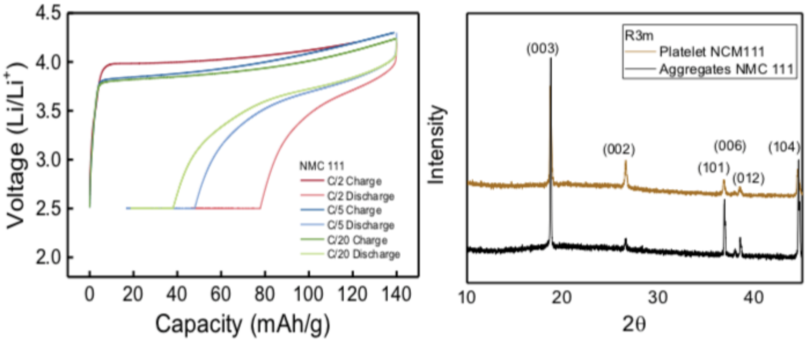

Figure 37. Electrochemistry and diffraction patterns of NMC-111.

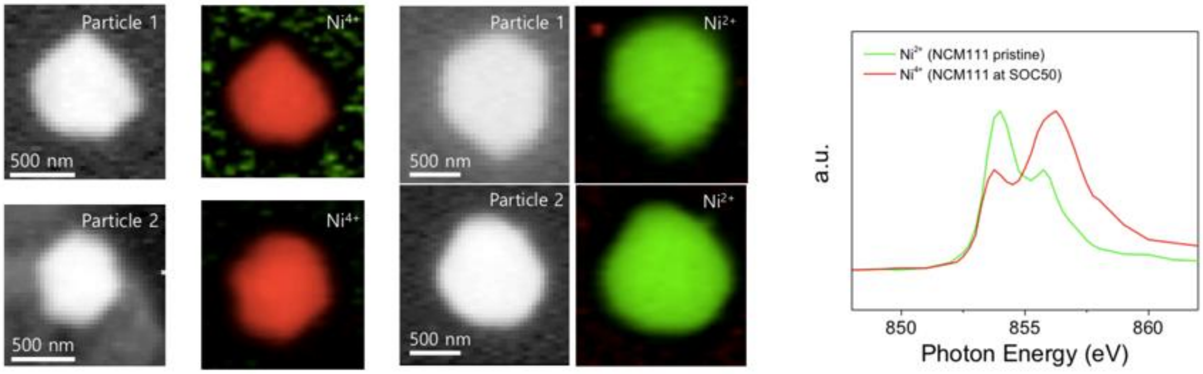

Figure 38. Scanning transmission X-ray microscopy images of platelet NMC-111 in the charged and discharged states. (Right) Corresponding X-ray absorption spectroscopy at the nickel L absorption edge.

Patents/Publications/Presentations

Presentations

- 22nd International Conference on Solid State Ionics (SSI-22), Pyeongchang, Korea (June 18, 2019): W. C. Chueh. Keynote.
- European MRS Meeting, Nice, France (May 29, 2019): W. C. Chueh.

Task 2.8 – Investigate the Impact of Doping on the Structural Stability and Conductivity of Solid Electrolytes
(Zonghai Chen, Argonne National Laboratory)

Project Objective. The project objective is to develop high conductivity ceramic electrolyte through cation doping and to stabilize the structure and cathode/electrolyte interface through cation doping and co-sintering between electrolyte and cathode.

Project Impact. Development of structurally, chemically, and electrochemically stable high conductivity solid electrolytes can significantly improve (1) volumetric energy density and (2) safety characteristics of lithium batteries, and will accelerate the penetration of EVs.

Approach. The project approach is multi-fold: (1) understanding the physics behind the transformation between the low conductivity phase and the high conductivity phase; (2) investigating the bonding strength of the cathode/electrolyte interface using model systems; and (3) developing electrolytes with high ionic conductivity and good bonding to cathodes through cation doping.

Out-Year Goals. The project has the following out-year goals:

- Using $Li_7La_3Zr_2O_{12}$ (LLZO) as a model material to investigate the pathway of path transformation during the synthesis of the solid-state electrolyte.
- Investigating the impact of cation doping on the kinetics of phase transformation.
- Initiating the research activity on the co-sintering of cathode/electrolyte model system for a chemically/mechanically strong interface.

Collaborations. The project collaborates with Dr. A. Ngo (ANL), Dr. L. Curtiss (ANL), Dr. V. Srinivasan (ANL), Dr. Y. Ren (ANL), Dr. J. Libera (ANL), Dr. T. Li (Northern Illinois University), and Dr. D. Chen (University of Houston).

Milestones

1. Developing *in situ* high-energy XRD capability to investigate the phase transformation of ceramic electrolytes. (Q1, FY 2019; Completed)
2. Investigating the tetragonal/cubic phase transformation of LLZO. (Q2, FY 2019; Completed)
3. Investigating the impact of bonding between LLZO and cathode materials. (Q3, FY 2019; Partially completed)
4. Synthesizing W-doped LLZO for investigation on structural stability and mechanical stability. (Q4, FY 2019; Ongoing)

Progress Report

A functional solid-solid interface requires: (1) good chemical compatibility to ensure long-term performance of the interface, and (2) good mechanical stability to tolerate the mechanical strain across the interface when the lattice of the cathode contracts/expands during operation while the electrolyte does not. To achieve mechanical stability, a proper process is needed to trigger the inter-diffusion of atoms between the cathode material and electrolyte without scarifying the functionality of both materials. A possible approach to achieve this is to co-sinter both materials at an elevated temperature to form strong bonding between two oxide materials.

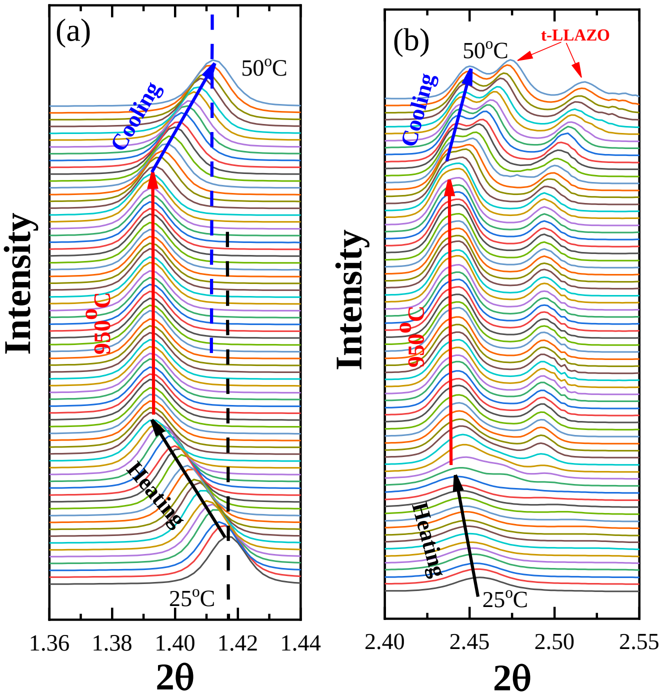

Figure 39. Evolution of high-energy X-ray diffraction patterns during the co-sintering of LNMC622-LLAZO at 950^{o}C, showing (a) the evolution of (003) peak of NMC-622, and (b) formation of tetragonal phase after co-sintering.

The first co-sintering effort was conducted using a mixture of $LiNi_{0.6}Mn_{0.2}Co_{0.2}O_2$ (NMC-622) and the $Li_7La_{3-x}Al_xZr_2O_{12}$ (LLAZO) precursor as the model material. The mixture was heated from room temperature to 950^{o}C with a heating rate of 10^{o}C/min, and maintained at 950^{o}C for 5 h before being cooled to room temperature with a controlled cooling rate of 20^{o}C/min. The high-energy XRD patterns were continuously collected during the whole course of the co-sintering process. Figure 39a illustrates the evolution of XRD pattern between 1.36^{o} and 1.44^{o} (λ=0.1173Å), showing the shifting of the (003) peak during the whole process. The XRD data indicate that the layered structure was maintained during and after the co-sintering process. However, the c lattice of NMC-622 was slightly expanded after the co-sintering process, suggesting that some doping element was successfully inserted into the lattice of NMC-622. On the other hand, Figure 39b shows the evolution of XRD patterns between 2.4^{o} and 2.55^{o}, showing the disappearance of the electrolyte precursor during heating, and the appearance of tetragonal LLAZO phase during the cooling process. Since the ionic conductivity of t-LLAZO is substantially lower than that of c-LLAZO, the formation of t-LLAZO at the interface of CEI will have detrimental impact on the charge transfer kinetics at the solid-solid interface, and hence is highly undesired.

Therefore, this effort will continue next quarter by co-sintering a cathode and a cubic LLZO electrolyte (instead of a precursor) with an emphasis on suppressing the formation of the tetragonal phase after co-sintering.

Patents/Publications/Presentations

The project has no patents, publications, or presentations to report this quarter.

TASK 3 – MODELING

Summary and Highlights

Achieving the performance, life, and cost targets outlined by VTO will require moving to next-generation chemistries, such as higher capacity Li-ion intercalation cathodes, silicon and other alloy-based anodes, Li-metal anode, and sulfur cathodes. However, numerous problems plague development of these systems, from material-level challenges in ensuring reversibility to electrode-level issues in accommodating volume changes, to cell-level challenges in preventing cross talk between the electrodes. In this task, a mathematical perspective is applied to these challenges to provide an understanding of the underlying phenomenon and to suggest solutions that can be implemented by the material synthesis and electrode architecture groups.

The effort spans multiple length scales from *ab initio* methods to continuum-scale techniques. Models are combined with experiments, and extensive collaborations are established with experimental groups to ensure that the predictions match reality. Efforts also focus on obtaining parameters needed for the models, either from lower-length scale methods or from experiments. Projects also emphasize pushing the boundaries of the modeling techniques used to ensure that the task stays at the cutting edge.

In the area of intercalation cathodes, effort is focused on understanding working principles of high nickel layered materials with an aim of understanding structural changes and associated changes in transport properties. Coatings, an effective strategy for high-voltage operation, are being explored with the aim of providing a rational design approach for new coating materials. In parallel, design of liquid electrolytes and gaining understanding of their behavior are used to determine their usability at high voltages. In addition, focus is paid to the assembling of porous electrodes with particles to predict the conduction behavior and impact of heterogeneities on electrode behavior. Efforts this quarter were aimed at examining the electrolyte formulations for silicon anodes to ensure lower SEI resistance and developing a framework to model amorphous coatings.

In the area of Li-metal anodes, the focus is on understanding how materials can be designed to prevent dendrite growth using continuum modeling approaches, combined with calculations on mobility in solid conductors. The results are used to guide materials development by providing the properties needed to prevent dendrites while also achieving the energy and power goals. Models are also starting to examine the role of the SEI on the morphology of the dendrite and to describe the mechanical-electrochemical coupled effects that are critical for dendrite formation. Finally, models are being developed to examine the solid-cathode interface in Li-metal based systems, where interface debonding issues are known to limit cycling. This quarter, models examined the focusing of current in solid electrolytes due to defects and examined the nucleation and growth of dendrites in solid electrolytes.

Task 3.1 – Design of High-Energy, High-Voltage Lithium Batteries through First-Principles Modeling (Kristin Persson, Lawrence Berkeley National Laboratory)

Project Objective. This project supports VTO programmatic goals by developing next-generation, high-energy cathode materials and enabling stable cathode operation at high voltages through target particle morphology design, functional coatings, and rational design of electrolytes. The end-of-project goals include: (1) understanding of the factors that govern charge transport in nonaqueous, superconcentrated liquid electrolytes (2) new fundamental understanding of the Li-ion dynamics in Si-Sn electrode alloys (and their native oxides), with a design focus on improving stability of the silicon electrode through tin alloying, and finally (3) critical surface and coating design and optimization strategies that will improve cycling of Li-ion battery cathodes by reducing cathode degradation from oxygen loss.

Project Impact. To enhance performance of Li-ion systems, improvements on the cathode and the electrolyte side are needed. This project is aimed to result in an improved understanding of the atomistic mechanisms underlying surface behavior and performance of the Li-ion cathode materials, with the ultimate goal being to suggest strategies, such as coatings, surface protection, and particle morphology design. Furthermore, fundamental studies of electrolyte conductivity and transport mechanisms, as a function of solvent and salt concentrations, and components will be conducted.

Approach. First-principles calculations, both static and dynamic approaches, are used to model solid-state electrode material thermodynamics and kinetics. Liquid electrolytes are modeled through coupled classical molecular dynamics (MD) and first-principles methods to accurately capture solvation structure as well as reactivity of the liquid system.

Out-Year Goals. For the electrolyte development, work will be aimed toward understanding the atomistic interactions underlying the performance of lithium electrolytes specifically elucidating conductivity (as a function of salt concentration) and impact on the charge transport mechanisms at play. Stable interfaces will be determined by focusing initially on degradation mechanisms related to release of surface oxygen at high charge. Tuning particle morphology and coating materials—both of crystalline as well as amorphous structure—will be explored using the Materials Project. Li-ion conduction mechanisms and electrode stability of Si-Sn alloys will be determined, in addition to the reactivity and ionic conduction of the native oxide surface phases.

Collaborations. This project is highly collaborative between BMR PIs G. Chen (LBNL), G. Ceder (LBNL), and V. Srinivasan (ANL). Cathode design and synthesis will be performed by Chen and Ceder, surface design by Persson, and electrolyte design and testing by Persson and Srinivasan.

Milestones

1. Finish benchmarking of algorithms for obtaining reliable solvation structures and ionic conductivity in highly concentrated liquid electrolytes. (Q1, FY 2019; Completed)

2. Identify Li-ion conduction mechanisms in Si-Sn alloy anode, using first-principles modeling. (Q2, January 2019; In progress)

3. Evaluate SiO_2 and SnO_2 as surface phases from the perspective of ionic conduction and reactivity with lithium. (Q3, April–July 2019)

4. Conduct first evaluation of amorphous oxygen-retention and lithium diffusion enhancing coatings using the Materials Project infrastructure. (Q4, July–November 2019)

Progress Report

This project is aimed toward amorphous coating design that will improve performance of Li-ion battery cathodes. Amorphous coating layers tend to be conformal, with reduced grain boundaries, or other defective regions that exist in polycrystalline coating layers. Therefore, amorphous coatings are expected to reduce the diffusion of metal and/or oxygen ion transport, and effectively suppress corrosion.[1] In this report, the team presents a methodology that can analyze lithium and oxygen diffusion mechanisms in amorphous coating materials.

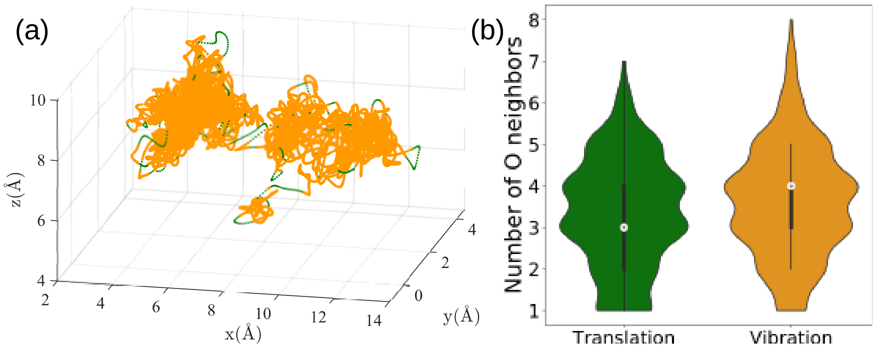

Figure 40. (a) Trajectory of one lithum atom in amorphous structure for 40 ps. Yellow and green dots represent vibrational and translational motions, respectively. (b) Number of oxygen neighbors during lithium translational and vibrational motions. The white dots represent the median values.

Figure 40a shows the trajectory of one lithium atom in the AIMD simulations for 40 ps. The team implemented a density-based spatial clustering (DBSCAN) to differentiate the vibrational and translational motions for lithium trajectories, which are represented by the yellow and green dots in Figure 40a, respectively. For each time step, the team also analyzed the number of nearest neighbors for the lithum atom during the vibrational and translational motions to elucidate the limiting factors for lithium and oxygen diffusion. Figure 40b shows that the number of nearest oxygen neighbors during translation is smaller than that during vibration, which implies that the oxygen content of the coating is one of the limiting factors for lithium diffusion.

An additional project goal is the study of the specific modes of transport in superconcentrated electrolytes via validated classical MD simulations, for which time scales are commensurate with relevant diffusional modes. The diffusion of Li^+ in superconcentrated $LiBF_4$/propylene carbonate electrolyte has been speculated as differing from $LiPF_6$ in propylene carbonate due to specific ion-hopping processes.[2] Figure 41 shows the diffusion constants for the ionic species, computed herein as a function of concentration from 1 M to 3 M. The employed methodology can allow both qualitative and quantitative agreement with experiment[3] for $LiBF_4$ in propylene carbonate, which will allow further analysis and elucidation of the specific modes of transport and conductivity.

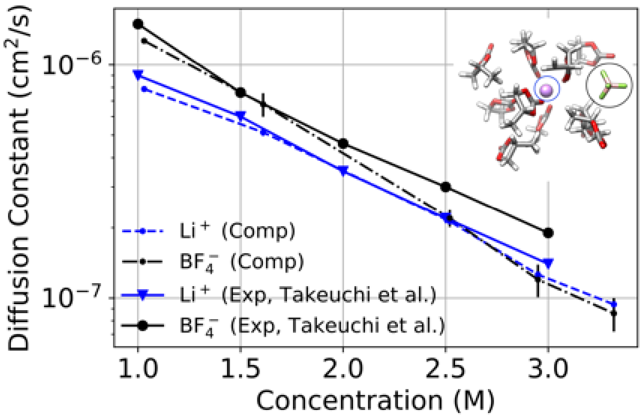

Figure 41. Computed and experimental diffusion constants of Li^+ and BF_4- in propylene carbonate as a function of concentration.

[1] Aykol, M., and K. A. Persson. "Oxidation Protection with Amorphous Surface Oxides: Thermodynamic Insights from *Ab Initio* Simulations on Aluminum." *ACS Applied Materials & Interfaces* 10, no. 3 (2018): 3039–3045.

[2] Hwang, S., et al. "Ionic Conduction and Solution Structure in $LiPF_6$ and $LiBF_4$ Propylene Carbonate Electrolytes." *The Journal of Physical Chemistry C* 122, no. 34 (August 30, 2018): 19438–46. doi: 10.1021/acs.jpcc.8b06035.

[3] Takeuchi, M., et al. "Ion–Ion Interactions of $LiPF_6$ and $LiBF_4$ in Propylene Carbonate Solutions." *Journal of Molecular Liquids* 148, no. 2–3 (September 2009): 99–108. Doi: 10.1016/j.molliq.2009.07.003.

Patents/Publications/Presentations

Presentation

- 2019 DOE VTO AMR, Arlington, Virginia (June 10–13, 2019): "Predicting and Understanding Novel Electrode Materials From First-Principles"; K. A. Persson.

Task 3.2 – Understanding and Strategies for Controlled Interfacial Phenomena in Lithium-Ion Batteries and Beyond
(Perla Balbuena and Jorge Seminario, Texas A&M University; Partha Mukherjee, Purdue University)

Project Objective. The project objective is to evaluate and characterize interfacial phenomena in lithiated silicon and Li-metal anodes and to develop guidelines for potential solutions leading to controlled reactivity at electrode/electrolyte interfaces of rechargeable batteries using advanced modeling techniques based on first principles.

Project Impact. Understanding SEI growth on constantly evolving silicon surfaces and on highly reactive Li-metal surfaces is expected to allow definition of the electrolyte properties required in high-performance cells. Strategies to control the silicon anode instability and pulverization issues and the well-known safety and short effective lifetimes of Li-metal anodes will be developed by tuning the electrolyte composition, structure, dynamic, and stability, as well as that of the electrode morphology and interactions with the electrolyte, based on multiple characterizations of interfacial phenomena.

Approach. A comprehensive multiscale modeling approach, including first-principles *ab initio* static and dynamics, classical MD, and coarse-grained mesoscopic models, will focus on the roles of the electrolyte's chemical, structural, and dynamical properties and of the electrode micro- and nano- structure on the formation and evolution of the SEI layer and the associated electrochemical performance on silicon and on Li-metal anodes.

Out-Year Goals. Work will progress toward characterizing lithiation and SEI formation at silicon surfaces as well as the subsequent cracking and reforming events under the most realistic modeling conditions. Similarly, the project will investigate electrolyte effects on reactivity and dendrite formation in Li-metal surfaces. The project aims to capture how the chemistry of the various electrolyte components (mainly liquids, but also solid polymers and gels) affects the main issues that influence the electrode performance.

Collaborations. This project funds work at Texas A&M University (TAMU) and Purdue University. The team has collaborated with Prof. G. Somorjai (UC Berkeley), Prof. S. Yassar (UIC), and Dr. V. Murugesan (PNNL).

Milestones

1. Complete analysis of anode macroscopic effects during cycling. (Q1, FY 2019; Completed)
2. Complete study of improved electrolytes for silicon anodes. (Q2, FY 2019; Completed)
3. Complete study of improved electrolytes for lithium anodes. (Q3, FY 2019; Completed)
4. Complete evaluation of alternative charging strategies for lithium anodes. (Q4, FY 2019)

Progress Report

Additive Cation in the Electrolyte for Dendrite Suppression in Li-Metal Anodes. Dendrite growth can be initiated by uneven electrodeposition on the electrode. Here, the team assumes spatially varying intrinsic reaction kinetics on the electrode, as illustrated in Figure 42. The center region, between the two dashed lines, has an intrinsic reaction rate of k_c, as opposed to the reaction rate of k_I in adjoining regions. k_c is varied while keeping k_I constant. For each case, the morphology shown at the top is obtained without the cationic shield (CS) effect, while the lower one incorporates the dynamic impact of the CS effect. Figure 42a shows the evolved morphologies at $k_c = 5k_I$ and self-diffusion barrier $E_a = 0.2$ eV. Because of the relatively high reaction rate, the center region has much faster growth than other regions; thus, a protrusion is formed. In contrast, the lower morphology indicates that the dendrite growth, initiated in the center region, is significantly suppressed attributable to the CS effect. In the presence of additive M^+ ions, the electrostatic repulsion hinders the deposition of metal lithium atoms at the dendrite tip, which leads to relatively uniform electrodeposition. Figure 42b shows the morphologies at $k_c = 5k_I$ and $E_a = 0.4$ eV. Inspecting the morphologies in Figure 42a-b, it can be seen that as the surface self-diffusion barrier increases, the metallic deposit becomes less compact with a slightly larger protrusion height for Figure 42b(upper) as compared to Figure 42a(upper).

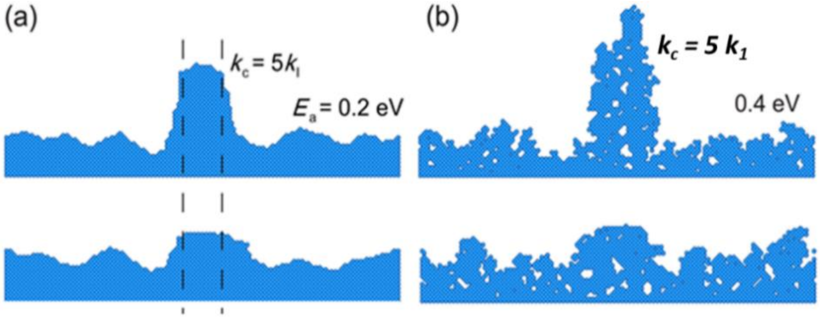

Figure 42. Inhomogeneity-induced electrodeposition morphologies in the reaction-kinetics-limited regime. (a) $k_c = 5k_I$ and the surface diffusion barrier $E_a = 0.2$ eV. (b) $k_c = 5k_I$ and $E_a = 0.4$ eV. The upper morphology is without the cationic shield (CS) effect, and the lower morphology has the CS effect. Protrusion height decreases with the shielding effect. (Mukherjee, Verma, and Hao; work in progress)

Effects of Electrolyte Composition on Li^+ Electrodeposition on Clean and Native Films—Covered Lithium Surfaces. The team completed the first part of the analysis of passivation effects of lithium surfaces covered by native films produced by environmental impurities. A manuscript is under review that reports the project's findings that were also presented at the AMR meeting in June 2019. Briefly, the team examined using AIMD simulations of the interfacial behavior at three surfaces: Li/Li_2O; Li/LiOH, and Li/Li_2CO_3 in contact with a 1 M solution of LiTFSI in DME. This work was in collaboration with Dr. V. Murugesan (PNNL) on soft landing and XPS experiments to analyze the TFSI decomposition on lithium surfaces. The experimental work showed two main compositions of the native films: lithium oxide and LiOH. Since both surfaces have some Li_2CO_3, simulations were done using 1-nm films of the oxide, hydroxide, and carbonate, respectively, on top of the lithium surface. Some passivation behavior was evident in all cases. In addition, AIMD showed the charge storage and transfer effects in each of the films. The hydroxide and carbonate molecular crystals are easier to amorphize and reorient under the charge transfer events than the oxide phase; a clear electron exchange with the surface was observed during the entire simulation, whereas the oxide film is able to store and transfer electrons to the electrolyte phase without major structural changes. Current AIMD simulations explore the effect of the electrolyte composition on lithium cation electrodeposition. Initial results show a marked difference in a solution based on EC versus DME solvents. Other simulations characterized the effect of the anion-cation distance on the surface. This new knowledge will be used to clarify many issues regarding why certain electrolytes are more effective than others.

Patents/Publications/Presentations

Publications

- Sharifi-Asl, S., F. A. Soto, Y. Yuan, T. Foroozan, P. Abbasi, R. Deivanayagam, R. Rojaee, B. Song, A. Salehi-Khojin, K. Amine, J. Lu, P. B. Balbuena, and R. Shahbazian-Yassar. "Anti-Oxygen Leaking $LiCoO_2$." *Advanced Functional Materials* (2019): 1901110.
- Alaminsky, R. J., and J. M. Seminario. "Sigma-Holes from Iso Molecular Electrostatic Potential Surfaces." *Journal of Molecular Modeling* 25 (2019).
- Galvez-Aranda, D. E., and J. M. Seminario. "*Ab Initio* Study of the Interface of the Solid-State Electrolyte $Li_9N_2Cl_3$ with a Li-Metal Electrode." *Journal of the Electrochemical Society* 166 (2019): A2048-A2057.
- Kamphaus, E. P., S. Angarita-Gomez, X. Qin, M. Shao, M. Engelhard, K. Mueller, V. Murugesan, and P. B. Balbuena. "Role of Inorganic Surface Layer on Solid Electrolyte Interphase Evolution at Li-Metal Anodes." *ACS Applied Materials & Interfaces*. Under review.
- Hao, F., A. Verma, and P. P. Mukherjee. "Electrodeposition Stability of Metal Electrodes." *Energy Storage Materials* 20, no. 1 (2019).

Presentations

- 235th ECS, Dallas, Texas (May 28, 2019): "Elucidating Interfacial Phenomena in Li-Metal Based Batteries"; P. B. Balbuena. Invited.
- 235th ECS, Dallas, Texas (May 27, 2019): "Analysis of Solid-State Electrolytes for Li-ion Batteries using a Multiscale Molecular Dynamics Approach"; J. M. Seminario, D. Galvez, V. Ponce, L. Selis, C. Vicharra, F. Gallo, and M. Gamero.
- 1st CIBIQ, Santander, Spain (June 18, 2019): "*Ab Initio* Study at the Interface of a Solid-State Electrolyte with a Li-Metal Electrode for a Design Based on Nanobatteries"; J. Seminario, D. Galvez, V. Ponce, L. Selis, C. Roman, F. Gallo, and M. Gamero. Invited lecture.
- ICTP School, Cartagena, Colombia (June 1, 2019): "Atomistic Classical and Quantum Simulations of Nanobatteries – Theory"; J. Seminario, D. Galvez, V. Ponce, L. Selis, C. Roman, F. Gallo, and M. Gamero; Plenary lecture.
- DOE VTO Annual Merit Review Meeting, Arlington, Virginia (June 13, 2019): Perla B. Balbuena.
- 235th ECS Meeting, Dallas, Texas (May 26–30, 2019): "'Dead' Lithium: Interface Evolution and Characterization"; D. Tewari, S. P. Rangarajan, and P. P. Mukherjee.
- 235th ECS Meeting, Dallas, Texas (May 26–30, 2019): "Mechanistic Investigations of Interfacial Stochasticity in Lithium Metal Anodes"; A. Verma and P. P. Mukherjee.

Task 3.3 – Electrode Materials Design and Failure Prediction (Venkat Srinivasan, Argonne National Laboratory)

Project Objective. The main project objective is to develop computational models for understanding the various degradation mechanisms for next-generation Li-ion batteries. This year's goal is to use the continuum-based mathematical model to (1) investigate interfacial stability between electrodes and ceramic-based SSEs, and (2) experimentally measure and understand the impedance observed at the cathode/SSE interface. Ceramic-based SSEs are expected to enable high energy density and liquid-free, safe, next-generation Li-ion batteries. Li-metal anodes should be incorporated due to their substantially larger specific capacity, as compared to present day graphite-based anodes. During deposition, lithium dendrite growth through the SSEs and subsequent short circuit has been a major issue, limiting successful implementation of SSEs. Similarly, on the cathode side, diffusion of TMs into the SSEs along with delamination between cathode and SSE lead to increased interfacial resistance. The developed computational model will be used to investigate the impact of microstructural (grain size), physical (mechanical stiffness), and transport (conductivity) properties of the SSE on the overall interfacial degradation observed at both the cathode and anode sides. Due to the SOC-dependent electrochemical and mechanical properties of the cathode, an attempt will be made to experimentally measure the SOC-dependent impedance at the cathode/SSE interface. The main focus will be to elucidate interfacial issues, observed at both anode and cathode sides, and to devise strategies to enable successful implementation of SSE in next-generation Li-ion batteries.

Project Impact. Findings from this research will give a better understanding of the factors, at the cathode/SSE interface, limiting the cycle life of solid-electrolyte-based Li-ion batteries. These results will help to enable incorporation of cathode particles within SSEs.

Project Approach. The approach used here is to develop mesoscale models, based on continuum modeling, to describe the critical processes in the materials, and combining them with electrochemical, microscopic, and spectroscopic data to ensure parameter estimation and model validation. The model is then used to provide insights on impact of material properties on performance and life and as guidance for design of new materials.

Out-Year Goals. At the end of this project, a computational framework will be presented that is capable of estimating delamination and impedance at cathode/SSE interface.

Collaborations. This project collaborates with L. A. Curtiss, A. T. Ngo, and C. M. Phatak at ANL.

Milestones

1. Investigate impact of grain-interior (GI) / grain-boundary (GB) microstructure on overall dendrite growth observed at SSE/lithium interface. (Q1, FY 2019; Completed)
2. Analyze effect of delamination at the cathode/SSE interface as a mode of degradation. (Q2, FY 2019; Completed)
3. Investigate impact of grain size of the electrolyte on the mechanical degradation occurring at the cathode/SSE interface. (Q3, FY2019; Completed)
4. *Go/No-Go Decision*: Estimate SOC-dependent impedance at cathode/SSE interface. If not possible, proceed with impedance measured at fixed SOC. (Q4, FY 2019; In progress)

Progress Report

Investigate the Impact of Grain Size of the Electrolyte on the Mechanical Degradation Occurring at the Cathode/SSE Interface. Last quarter, the team demonstrated that the lithium insertion/extraction induced swelling and contraction of the NMC-based cathode material, which can lead to delamination at the cathode/SEI. This loss of interfacial contact can eventually lead to a decrease in the total amount of electrochemically active surface area, effectively reducing the discharge capacity of the solid-electrolyte cells. Impact of solid-electrolyte microstructure on the interfacial delamination induced capacity fade has been investigated in the present quarter. Different LLZO microstructures have been generated with various grain sizes. Figure 43a-b shows two such LLZO/NMC interfaces, where the average LLZO grain size has been assumed to be around 150 nm and 75 nm, respectively. By conducting charge-discharge cycle on top of these LLZO/NMC microstructures, interfacial delamination induced capacity fade has been estimated. From Figure 43c, it is evident that the magnitudes of capacity fade decrease with smaller grain sizes. This can be attributed to the fact that within LLZO microstructures with smaller grains, there exist multiple GB domains. The GBs demonstrate smaller elastic modulus, and higher deformability, as compared to the GIs. With a larger number of mechanically soft GB domains, the ceramic electrolyte is able to better accommodate the volume changes experienced by the cathode materials. Hence, within LLZO microstructures with small grains, smaller magnitude of strain energy evolves at the interface, which leads to less interfacial delamination, and subsequently lesser capacity fade.

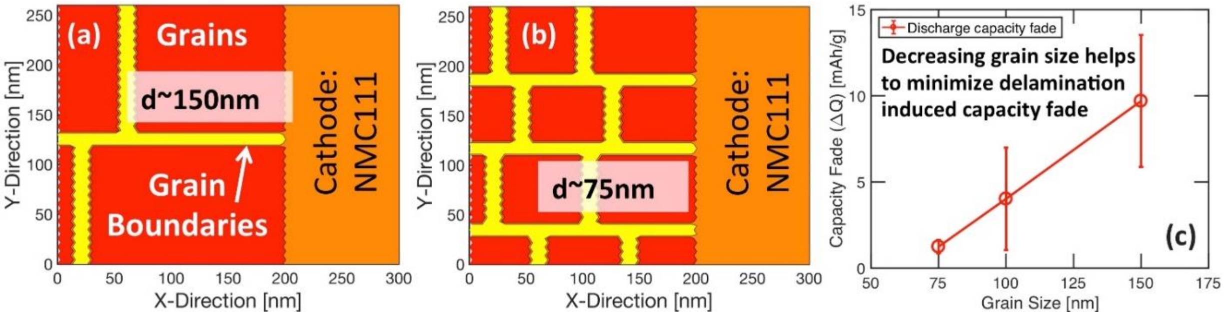

Figure 43. (a) Computational domain with large grain size of approximate diameter around 150 nm. (b) Computational domain with smaller grain sizes of diameter ~ 75 nm. In both (a) and (b), the orange portion indicates cathode (NMC-111), the red domain denotes grain interior, and the yellow region stands for the grain boundary. (c) Capacity fade due to interfacial delamination as observed in different LLZO microstructures with various grain sizes. Decreasing the grain size helps to minimize capacity fade.

Continuing earlier efforts, the team also investigated the impact of long-term cycling on the interfacial delamination induced capacity fade. All the LLZO/cathode microstructures, with different electrolyte grain sizes, have been subjected to 10 constant current – constant voltage (CCCV) charge and constant current (CC) discharge cycles. The applied current density for the CC process is 1A/m^2, whereas the cutoff voltage during charging has been assumed to be 4.4 V. The CV process has been stopped as soon as the current becomes less than 10% of the initial applied current density. The performance curves for the 1st, 3rd, and 9th cycles have been demonstrated in Figure 44a; overall capacity fade is shown in Figure 44b. The LLZO microstructures with smaller grains experience capacity fade at a slower rate. Analysis of interfacial delamination induced capacity fade with different LLZO grain sizes concludes the milestone for this quarter.

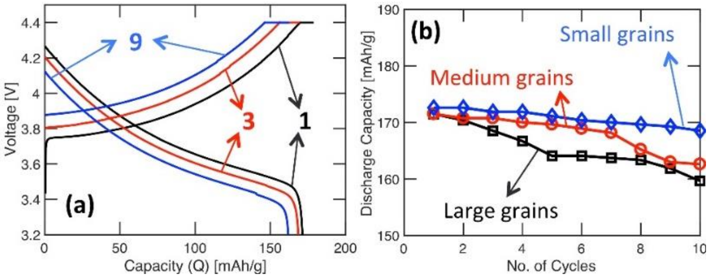

Figure 44. (a) The voltage versus capacity performance curves as observed during the 1st, 3rd, and 9th constant current – constant voltage (CCCV) charge and CC discharge cycle as observed in the LLZO microstructures with large grain sizes. (b) Interfacial delamination induced capacity fade observed in three different LLZO microstructures with large, medium and small grain sizes. The rate of capacity fade is much less in the smaller grain, due to the limited mechanical degradation observed there.

Patents/Publications/Presentations

Publication

- Barai, P., K. Higa, A. T. Ngo, L. A. Curtiss, and V. Srinivasan. "Mechanical Stress Induced Current Focusing and Fracture in Grain Boundaries." *Journal of the Electrochemical Society* 166 (2019): A1752–A1762.

Presentation

- 235th ECS Meeting, Dallas, Texas (May 2019): "Impact of Solid-Electrolyte-Interphase (SEI) Stiffness on Lithium Dendrite Growth"; P. Barai and V. Srinivasan.

Task 3.4 – First-Principles Calculations of Existing and Novel Electrode Materials
(Gerbrand Ceder, Lawrence Berkeley National Laboratory)

Project Objective. Solid-state batteries are promising to achieve high energy density. The project objective is to determine the design principles needed to create SSEs with high Li-ion conductivity while also achieving stability against common Li-ion cathodes and Li-metal anodes.

Project Impact. The project will lead to understanding the factors that control Li-ion motion in crystalline and amorphous solids and will develop strategies to create stable interfaces against lithium metal and high-voltage cathode materials. The understanding of such processes is necessary to determine design principles to develop reliable all solid-state batteries.

Approach. High-throughput computation method is used to screen suitable solid electrolyte with high electrochemical stability and high ionic conductivity, by incorporating Nudged Elastic Band (NEB) and an AIMD method. Meanwhile, DFT is used to calculate bulk elastic constants of materials, surface energies, and interface decohesion energies of GBs. Thermodynamic interface stability is assessed from *ab initio* computed grand potential phase diagrams in which the lithium voltage can be controlled. Kinetic limits for solid electrolyte decomposition are assessed by topotactic lithium insertion and removal from the solid electrolyte.

Out-Year Goals. Future goals include the following: (1) gain insight into what creates high Li-ion conduction in sulfide and oxide solids, and (2) develop stable, processable solid-state conductors that can be applied in all solid-state batteries.

Collaborations. There are no current collaborations.

Milestones

1. Modeling of the Li_2S-P_2S_5 phase diagram for SSEs: solid phases correctly modeled. (Q1, FY 2019; Completed)
2. Modeling of the Li_2S-P_2S_5 phase diagram for SSEs: include correct modeling of amorphous phase. (Q2, FY 2019; Completed)
3. Model Li-ion conductivity in amorphous LPS (Li-P-S) systems and glass ceramics. (Q3, FY 2019; Completed)
4. Develop understanding on which structural and compositional features make LPS an excellent ionic conductor. (Q4, FY 2019)

Progress Report

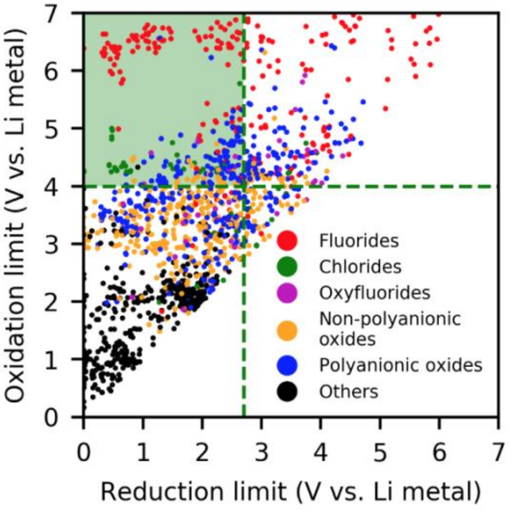

Figure 45. Electrochemical stability windows of 1,600 phase-stable materials categorized by anion chemistry.

The instability of the LPS/cathode interface is one of the main sources of the interfacial resistance in all-solid-state batteries that deteriorates cell performance. The origin for the instability includes the electrochemical decomposition of LPS at high voltage and the chemical reaction between LPS and oxide cathodes. One way to mitigate these issues is use of a cathode coating that acts as a buffer layer between the cathode and LPS. However, the coating composition has yet to be optimized. An ideal cathode coating should have the following: (1) an oxidation stability limit above 4 V, and a reduction limit below 2.7 V to overlap with the stability window of LPS, and (2) low chemical reactivity with both the cathode and LPS. The team has conducted a high-throughput computational screening for cathode coating materials among all Li-containing compounds in the project's internal database, focusing on electrochemical stability, chemical stability, and ionic conductivity. Figure 45 shows the electrochemical stability of stable Li-containing materials categorized by their anion chemistries. It is observed that fluorides have the highest oxidation limits, followed by chlorides, polyanionic oxides, and non-polyanionic oxides. Compounds in the ''Others'' category (for example, bromides, nitrides and phosphides) generally have the lowest oxidation limits, below 2.5 V. The green box in Figure 45 represents the stability window of interest, which contains 302 compounds, most of which are halides, polyanionic oxides, and non-polyanionic oxides.

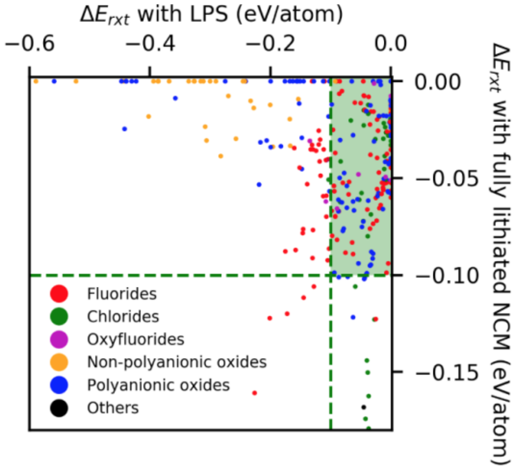

Figure 46. Chemical reaction energy ΔE_{rxt} with LPS and fully lithiated NCM for the 302 screened materials enclosed in the green box in Figure 45.

The calculated chemical reactivity of these candidate coatings with LPS and a typical oxide cathode $LiNi_xCo_yMn_{1-x-y}O_2$ (NCM) is plotted in Figure 46. The team found that although the non-polyanionic oxides have a low reactivity (defined by $|\Delta E_{rxt}|$) below 50 meV/atom with oxide cathodes, they often have high reactivity above 100 meV/atom with the LPS electrolyte. In contrast, in the green box in Figure 46 defined by reactivity below 100 meV/atom with both NCM and LPS, the 184 compounds mostly consist of halides and polyanionic oxides. This observation indicates that halides and polyanionic oxides are promising cathode coatings that may outperform the state-of-the-art non-polyanionic cathode coatings. Due to the ease of synthesis and application of oxides, the team considers polyanionic oxides to be the next-generation cathode coating materials that can effectively protect LPS from high-voltage oxide cathodes. In the polyanionic oxide category, some lithium phosphates and lithium borates are particularly appealing because of their high oxidation limits above 4.5 V plus reasonable ionic conductivity.

Patents/Publications/Presentations

Presentations

- International Union of Pure and Applied Chemistry (IUPAC) Meeting, Paris, France (July 10, 2019): "DRX, A Route to Co-Free Cathodes."
- International Conference on Materials for Advanced Technologies (ICMAT) Meeting, Singapore (June 26, 2019): "A Materials Perspective on the Future of Energy Storage in the Grid and Transportation: Insights from Basic Science."

Task 3.5 – Dendrite Growth Morphology Modeling in Liquid and Solid Electrolytes (Yue Qi, Michigan State University)

Project Objective. The project goal is to develop a validated model to predict lithium dendrite morphology evolution in both liquid and solid electrolytes during electrodeposition and stripping to accelerate the adoption of Li-metal electrodes in current and emerging battery technologies. To achieve this goal, the project has four objectives: (1) formulate a general framework that captures the electrochemical-mechanical driving forces for lithium morphology evolution; (2) consider the role of the nm-thin SEI in liquid electrolytes as well as the microstructures of µm-thick solid electrolytes for lithium morphology evolution; (3) connect micron-scale phase-field models and atomic-scale DFT-based simulations via parameter- and relationship-passing to predict lithium dendrite nucleation and growth kinetics and morphology; and (4) validate the key input parameters and main conclusions of the multi-scale model as new capabilities are being developed step-by-step.

Project Impact. This atomically informed, fully coupled, electrochemical-mechanical dendrite morphology evolution model will allow the project to design the desired properties of artificial SEI coatings, the microstructure of solid electrolyte materials, and the corresponding battery operating conditions, so as to avoid dendrite growth during cycling. It will accelerate design of durable and safe lithium anodes for Li-S, Li-air, and all-solid Li-ion batteries. Thus, it directly impacts such emerging technologies that aim to meet the DOE target of the high-energy-density battery cells (> 350 Wh/kg) for EV applications and to push the cost below $\$100/\text{kWh}_{\text{use}}$.

Approach. A multiscale model approach is taken to connect micron-scale phase-field models and atomic-scale DFT-based simulations via parameter- and relationship-passing.

Out-Year Goals. The second-year goal is to establish the model to simulate metallic lithium precipitation in solid electrolytes while further developing understanding of lithium dendrite growth in liquid electrolytes. To reach this goal, mechanical and electrochemical driving forces for lithium dendrite growth in solid electrolytes will be coupled in phase-field model, while DFT is used to address the lithium plating tendency in various solid electrolyte and coating materials. Validation of the model will come from experiments to correlate the distinctive transport properties of artificial SEI layers with their impact on lithium dendrite morphology.

Collaborations. This project collaborates with UMD, Sandia National Laboratories (SNL), PNNL, University of Arkansas, and University of Houston.

Milestones

1. Identify an ideal microstructure of LLZO to avoid lithium dendrite growth. (Q1, FY 2019. It was predicted a coating layer, such as LiPON, between the Li/LLZO, will be more efficient in resisting lithium dendrite. A *Go* decision was made to experimentally vary this prediction.)
2. Develop a fully coupled Li/SEI/liquid electrolyte dendrite morphology model. (Q2, FY 2019; Completed)
3. Illustrate the relationship between Li/SEI interface roughness, adhesion, and dendrite morphology in a liquid electrolyte. (Q3, FY 2019; Completed)
4. Determine the effect of multicomponent SEI layer on dendrite morphology in a liquid electrolyte. (Q4, FY 2019; In progress)

Progress Report

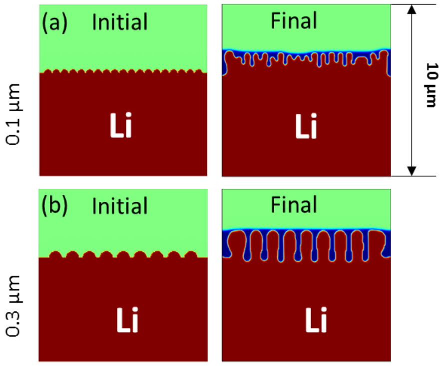

Figure 47. Phase field model of lithium growth induced Li/coating delamination.

The project's lithum charge transfer reaction energy landscape model has shown that the charge transfer step occurs under a perfect SEI layer, represented by Li_2CO_3. This quarter, the team further illustrates the lithium electrodeposition and its relationship with the SEI or the coating layer in a liquid electrolyte.

The impact of Li/coating interface roughness and adhesion was modeled by an extended explicit phase-field model. As shown in Figure 47, the coating layer (green) is mathematically described by an additional order parameter moving concurrently with the growing Li-metal phase (brown) in a 10 × 10 μm^2 half-cell. It is assumed that the coating layer is Li-ion conductive and electronic insulate, and that any space created in-between coating and lithium metal due to interfacial delamination can be filled in immediately by a liquid electrolyte (blue). The Li-ion diffusion coefficient in the coating layer was set to be 1/10 of that in a liquid electrolyte. The surface energy of 0.3 J/m^2 and interfacial adhesion energy of 0.05 J/m^2 were used based on the DFT results of Li-metal/Li_2CO_3 interface. Initially, the coating layers have complete contact with Li-metal surfaces. The initial interface roughness was described by half-spherical asperities with different sizes (0.02 ~ 1 µm) and densities (0.1 ~ 4 / μm^2). Constant voltage condition of -0.1 V was applied for all lithium plating simulations. The simulation results show that the detached area and delamination volume increase as the initial surface asperity size increases for both the single and multiple asperities. Neighboring asperities tend to merge and smooth out to reduce the surface roughness for small asperity size (Figure 47a), while large asperities remain and grow separately (Figure 47b). Therefore, an initial smooth interface will be beneficial to prevent Li/coating interface delamination.

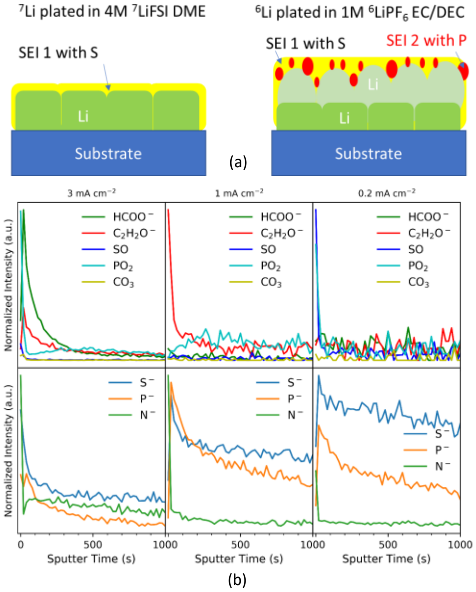

Figure 48. (a) Isotope exchange experiment and (b) the time-of-flight secondary ion mass spectrometry depth profile of the SEI.

To further figure out the SEI and lithium evolution, an isotope exchange experiment was designed. The process is to first deposit a ~ 5-µm ^7Li layer in an ether electrolyte (4 M ^7LiFSI DME) and then to deposit another ~ 5-µm ^6Li layer in carbonate electrolyte (1 M $^6LiPF_6$ EC/DEC) under a range of current density from 0.2 to 3 mA cm^{-2}. The SEM images of the top view of the lithium electrodes showed that the second lithium layer was indeed formed on first lithium layer. Smaller, round-shaped lithium chunks were formed when the high current density was applied. Small lithium chunks result in high surface area, which would consume more electrolyte and lead to lower CE. TOF-SIMS depth profile was used to analyze the SEI composition in the top ~100 nm, as shown in Figure 48b. Organic components are generally located near the surface of SEI, as indicated by organic species $HCOO^-$ and $C_2H_2O^-$. The inorganic species, sulfur and phosphorus, are from the two independent lithium salts, ^7LiFSI and $^6LiPF_6$, respectively. Thus, sulfur indicates the pre-formed SEI on the first ^7Li layer, and phosphorus indicates the SEI formed during the second ^6Li layer deposition. For all the samples, sulfur and phosphorus have close intensities. Therefore, the team concludes that the second lithium deposition mainly occurs underneath the pre-formed SEI layer. The top SEI layer has mixed compositions from the pre-formed SEI (sulfur) and the newly formed SEI (phosphorus). This indicates that electrolyte decomposition reactions continue to occur inside, instead of on top, of the pre-formed SEI layer; this is either because the electrolyte molecules diffuse into the preformed SEI or the pre-formed SEI layer cracks due to lithium deposition (as shown in the schematic in Figure 48a).

Patents/Publications/Presentations

Publications

- Wan, J., J. Xie, X. Kong, Z. Liu, K. Liu, F. Shi, A. Pei, W. Chen, J. Chen, H. Chen, X. Zhang, L. Zong, J. Wang, L-Q. Chen, J. Qin, and Y. Cui. "Ultrathin, Flexible, Solid Polymer Composite Electrolyte Enabled with Aligned Nanoporous Host for Lithium Batteries." *Nature Nanotechnology*. doi.org/10.1038/s41565-019-0465-3 (2019).
- Li, G., Z. Liu, D. Wang, X. He, S. Liu, Y. Gao, A. AlZahrani, S. H. Kim, L-Q. Chen, and D. Wang. "Electrokinetic Phenomena Enhanced Lithium-Ion Transport in Leaky Film for Stable Lithium Metal Anodes." *Advanced Energy Materials*. doi: 10.1002/aenm.201900704. Publication Date (Web): April 29, 2019.
- Tian, H-K., Z. Liu, Y. Ji, L-Q. Chen, and Y. Qi. "Interfacial Electronic Properties Dictate Li Dendrite Growth in Solid Electrolytes." *Chemistry of Materials* (2019). Under review.
- Liu, Z., Y. Li, Y. Ji, Q. Zhang, X. Xiao, Y. Yao, L-Q. Chen, and Y. Qi. "Dendrite Free Li – Lesson Learned from the Li and Mg Electrodeposition Morphology Simulations." Pending submission (2019).
- Xu, B., Z. Liu, J. Li, X. Huang, B. Qie, T. Gong, L. Tan, X. Yang, D. Paley, X. Liao, Q. Cheng, H. Zhai, X. Chen, L-Q. Chen, C-W. Nan, Y-H. Lin, and Y. Yang. "Engineering Interfacial Adhesion for High-Performance Lithium Metal Anode." Pending submission (2019).
- Xu, J., H-K. Tian, J. Qi, Q. Zhang, Y. Qi, and X. X. Xiao. "Mechanical and Electronic Stabilization of Solid Electrolyte Interphase with Sulfite Additive for Lithium Metal Batteries." *Journal of the Electrochemical Society*. Submitted.

Presentation

- 235th ECS Meeting, Dallas, Texas (May 2019): "Atomically-Informed Phase-Field Modeling of Li and Mg Electrodeposition Morphologies"; Y. Qi, Y. Li, Z. Liu, Y. Yan, and L. Q. Chen. Invited.

Task 3.6 – First-Principles Modeling and Design of Solid-State Interfaces for the Protection and Use of Lithium-Metal Anodes
(Gerbrand Ceder, University of California at Berkeley)

Project Objective. The project objective is to determine the design principles that control the solid electrolyte/lithium electrode interfaces by determining the reaction products stemming from pairing solid electrolytes and lithium metal. The project will conduct rigorous analysis based on computing electrolyte phase-diagrams closed and open to lithium. Li-ion transport properties in bulk electrolytes and interfacial products will be assessed through AIMD and NEB calculations. Simultaneously, a robust framework will be developed to identify factors controlling lithium dendrite propagation within solid electrolytes and interfacial products by accounting for irregularities, defects, and GBs, through a model that includes elements of fracture mechanics, thermodynamics, and electrochemistry.

Project Impact. The project will lead to understanding of the complex evolution of lithium metal/SEI during electrochemical cycling. The understanding of this process is necessary to determine design principles to develop reliable all solid-state batteries.

Approach. By incorporating NEB and AIMD methods, high-throughput computation is used to screen candidate solid electrolyte with high electrochemical stability and high ionic conductivity. DFT is used to calculate bulk elastic constants of materials, surface energies, and interface decohesion energies of GBs; continuum theory (elastic-plastic-fracture mechanics) is used to assess the resilience of solid electrolytes and grain/particle boundaries toward lithium dendrite growth and propagation. The finite element method is used to couple several physical processes, including electrochemical deposition, ionic diffusion, thermal expansion, and mechanical contacting.

Out-Year Goals. The out-year goals include the following: (1) obtain design criteria for solid electrolytes that can resist unstable lithium propagation by computing elastic properties, surface energies, and decohesion energies, and (2) adapt fracture mechanics models describing crack propagation to lithium dendrite propagation in different scenarios.

Collaborations. There are no collaborative activities this quarter.

Milestones

1. Development of high-throughput framework to screen SSE materials based on phase stabilities. (Q1, FY 2019; Completed)
2. Adapt fracture models that describe crack propagation in materials to lithium dendrite propagation in perfect crystal with cracks. (Q2, FY 2019; Completed)
3. Adapt fracture models that describe crack propagation in materials to lithium dendrite propagation in perfect crystal with GBs. (Q3, FY 2019; Completed)
4. Adapt fracture models that describe crack propagation in materials to lithium dendrite propagation in pressed/porous electrolyte. (Q4, FY 2019; On target)

Progress Report

Deposition Boundary Traction Diffusion Potential Effects

Field concentration effects at sharp conductor defects lead to increased deposition rates and subsequent stress/ pressure concentrations. However, local stress intensification is not decoupled from the transport fields and surface deposition rates. The team has included the effects of the boundary traction at the conductor/metal electrode interface in metal-filled defects that arise from increased localized deposition rates. The stress and transport fields are coupled at said interfaces using a boundary diffusion potential term.

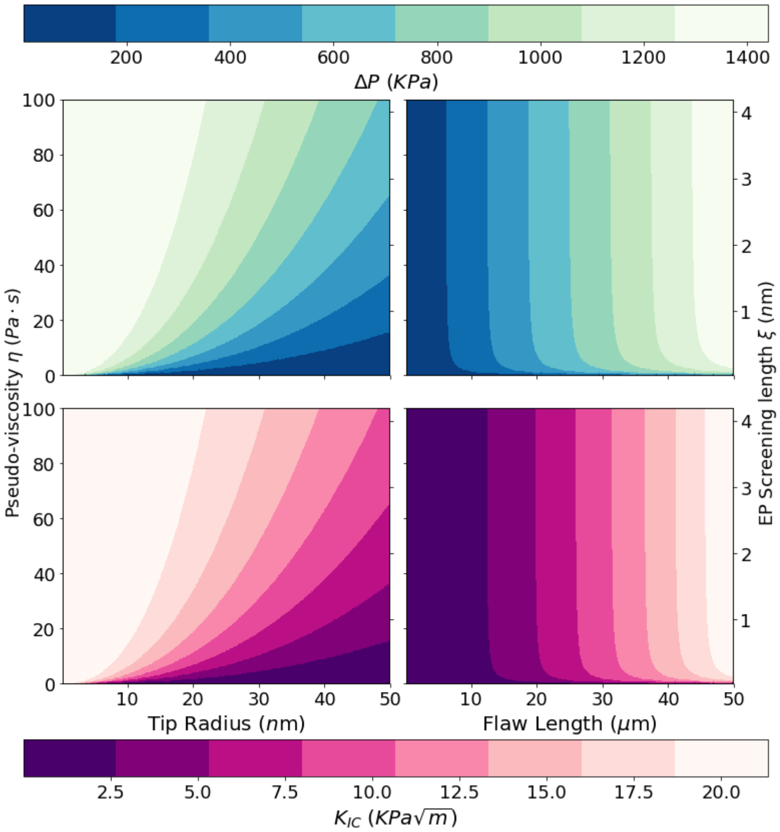

Figure 49. Pressure increase and stress intensity factor versus crack geometry. Values for an ionic conductor with $\lambda = 1\times10^{-6}$ S/cm, and current density $i_0 = 10$ mA/cm^2. Values in terms of tip radius are calculated for a flaw length L = 50 μm, and values in terms of length are calculated using a tip radius of $r_0 = 5$ nm.

The results from this initial model show that deposition hotspots are quickly counterbalanced by ionic redistributions in response to the boundary traction term. This limits the maximum pressure that can occur at defect tips to a saturation value determined by the length of the defect only. Furthermore, when the results of the coupled model are used to determine the stress intensity factor (SIF) for internally pressurized cracks, the team obtains values for SIFs that fall short of the fracture criteria determined from the fracture toughness of common inorganic solid ionic conductors. This leads to the conclusion that deposition at isolated cracks (ignoring possible side reactions and more complex electrode kinetic effects) cannot drive fracture. This level of analysis dispels a set of experimentally proposed models that rely on deposition drive fracture by individual defects.

Future work will require the team to investigate the role of other possible phenomena that can accurately reflect experimental observations of fractured ionic conductors after electrical cell failure. These effects include interface reduction reaction in pores and grain boundaries, in addition to bulk strain fields in the ionic conductor from several deposition hot spots. Doing so requires extending the project's electrochemical, mechanical, and fracture models to include polycrystalline and/or porous domains as well as chemically caused embrittlement at these internal interfaces.

Patents/Publications/Presentations

The project has no patents, publications, or presentations to report this quarter.

Task 3.7 – Large-Scale *Ab Initio* Molecular Dynamics Simulations of Liquid and Solid Electrolytes (Lin-Wang Wang, Lawrence Berkeley National Laboratory)

Project Objective. The project objective is to use AIMD simulations and other computational approaches to study the discharging mechanism in Li-S battery, especially for polysulfide interaction with liquid electrolyte solvent molecules, and cathode materials, as well as lithium diffusion mechanisms in various systems. The long-term goal is to use such theoretical understanding to provide guidance to develop better electrolyte and cathode systems to overcome the bottlenecks that prevent commercialization of the Li-S battery.

Project Impact. Making the Li-S battery a commercial reality will have a major impact on society and also help to realize the VTO goal of 500 km per charge for EV. However, the nature of chemical reaction makes it different from the traditional intercalation-based Li-ion battery. The molecular nature of Li_2S_n also allows solvation in the electrolyte. To address these problems, it is essential to have fundamental studies and understandings of the underlying mechanisms. The theoretical simulation can also play an important role in discovering and designing new cathode materials.

Approach. One major issue is solvation of Li_2S_n molecules in the electrolyte. The project seeks to solve this problem by both understanding the Li_2S_n-electrolyte interaction and discovering better cathode materials for optimal Li_2S_n-cathode binding. More specifically, it aims to develop reliable methods that combine classical force field (CFF) simulations with *ab initio* calculations to study thermal dynamic properties of Li_2S_n in different electrolytes, as well as interactions with different species within the electrolytes. It will also study Li_2S_n interaction with different cathode materials, especially for 2D cathode materials comprised with light elements in the right-upper corner of the periodic table. The goal is to have sufficient binding energy between the Li_2S_n molecules and the cathode material, so that, thermodynamically, the Li_2S_n will not be dissolved in the electrolyte. To study Li_2S_n-electrolyte interaction, the project must accurately calculate molecule entropy inside the solvent, which is a rather challenging task. It plans to use the bicanonical method to carry out the calculation. To design new cathodes, the project plans to focus on lightweight 2D materials. Genetic algorithm combined with DFT will be used to explore the structure and morphology of the Li_2S_n cluster on top of the 2D material. The stability of the solid electrolyte will be investigated by studying the surface reaction of such electrolytes.

Out-Year Goals. In outgoing years, the project will further develop the computational methods for more accurate entropy and interaction energy calculations for the electrolyte. This is a critical capability for studying the battery system. The project will also explore different cathode materials and morphologies. In particular, there is a vast space to explore using 2D materials as Li-S battery cathodes. Stability of the solid electrolyte is another topic to be investigated.

Collaborations. The project will collaborate with G. Liu and Y. Cui for cathode design. It has also collaborated with Prof. F. Pan of Beijing University for lithium battery research in general.

Milestones

1. Develop reliable ways to calculate the diffusion barrier of lithium in either crystal or amorphous structure. (Q1, FY 2019; Completed)
2. Continue calculation of Li_2Sn/cathode binding energies, and phase diagrams, discovering new adequate cathode materials and morphologies. (Q2, FY 2019; Initiated)
3. Investigate the solid electrolyte, its pathways and surface stabilities, and electrolyte/anode interface. (Q3, FY 2019)
4. Develop method to calculate Li-ion chemical energy in liquid electrolyte with *ab initio* calculations. (Q4, FY 2019)

Progress Report

Using AIMD simulation, the team has investigated the lithium diffusion in liquid electrolyte, especially when the Li$^+$ ion is close to LiF surface. The electrolyte is consisted with DMC and EC molecule, the salt is Li$^+$P6$^-$, and the simulation is carried out in 600 K, up to 60 ps.

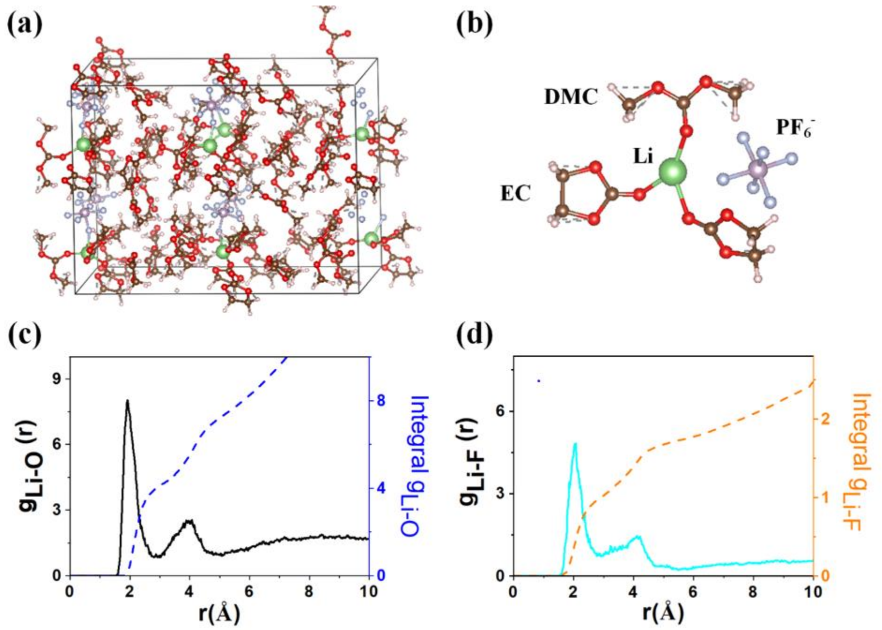

Figure 50. (a) Side view of schematic representation of liquid electrolytes. (b) One representative local structure of the coordination environments around a lithium ion. (c) Li-O and (d) Li-F pair correlation functions (solid lines) and their integrals (dash lines) for liquid electrolyte (a) from constant number, volume, and temperature (NVT) *ab initio* molecular dynamic simulation at 600 K.

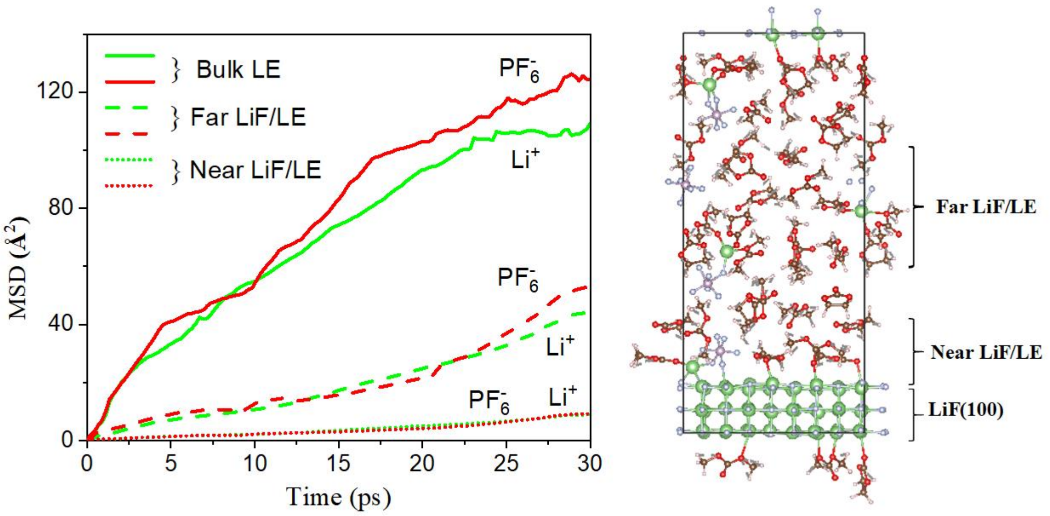

Figure 51. Mean square displacement (MSD) plots of Li-ion and PF$_6$-ion taken from 30 ps constant number, volume, and temperature (NVT) at 600 K simulations in bulk liquid electrolyte (LE) and LiF/LE interface.

In this simulation, Li^+ and PF_6^- are always close to each other, as shown in the Li-F correlation function in Figure 50d. The diffusion between these two species is correlated. The team has investigated the local structure of Li-O and Li-F. Different atomic configurations of the local structure are identified.

The electrolyte system is then placed on top of a LiF slab, with LiF(100) surface. If the Li^+ is close to the surface, it tends to bind to surface F. The Li^+ diffusion mobility depends sensitively on the distance between Li^+ and LiF surface. If the Li-LiF distance is short, the diffusion constant is significantly reduced. It gradually increases to bulk value with the Li-LiF distance approach to 20 A. This has implication for the lithium diffusion in the liquid electrolyte in a confined space. The team plans to investigate more of such behavior, including a systematic study of lithium diffusion in a confine cavity or porous structure. Such lithium diffusion in porous structure is important for many experimental Li-S cathodes using, for example, black carbon.

Patents/Publications/Presentations

Publications

- Chen, D., J. Jie, M. Weng, S. Li, D. Chen, F. Pan, and L.W. Wang. "High Throughput Identification of Li Ion Diffusion Pathways in Typical Solid State Electrolytes and Electrode Materials by BV-Ewald Method." *Journal of Materials Chemistry A* 7 (2019): 1300.
- Tsao, Y., M. Lee, E. C. Miller, G. Gao, J. Park, S. Chen, T. Katsumata, H. Tran, L. W. Wang, M. F. Toney, Y. Cui, and Z. Bao. "Designing a Quinone-Based Redox Mediator to Facilitate Li_2S Oxidation in Li-S Batteries." *Joule* 3 (2019): 872.

Task 3.8 – *In Operando* Thermal Diagnostics of Electrochemical Cells (Ravi Prasher, Lawrence Berkeley National Laboratory)

Project Objective. Effective heat dissipation in batteries is important for multiple reasons including performance, reliability, and safety. Currently, the thermal management of battery cells is provided at the system level by either forced air or liquid cooling, leading to reduced system-level energy densities and more failure-prone complex system designs. Furthermore, even given theoretically infinite system-level cooling applied to the external battery surface, peak temperature rise within a cell would still easily exceed acceptable threshold values due to poor thermal transport properties within the cell itself. It has not yet been possible to thermally profile a real cell during operation to provide a spatially resolved map of heat transfer properties throughout the cell. The objective of this research is to create a metrology capable of spatially resolved *in operando* thermal property profiling, and then use this tool to reveal the largest thermal bottlenecks within a functioning Li-ion cell and create a complete materials-level cell thermal model.

Project Impact. The intrinsic thermal resistance of Li-ion cells is currently far higher than the theoretical value predicted by simply combining the known thermal properties of each macro component into an appropriate thermal model. The spatially resolved thermal transport property measurements from this project will reveal what key piece of information is missing. Preliminary data suggest that more than 75% of the total battery thermal resistance may be due to a single interface between the cathode and separator, previously unknown. An accurate understanding of the cell internal thermal transport is necessary to successfully optimize cell thermal performance to meet the challenges of extremely fast charging, mitigating thermal runaway, and improving battery performance, reliability, and safety.

Approach. To accomplish the project goals, the team will utilize two state-of-the-art thermal metrology techniques. They will build an in-house adapted 3-omega technique to measure thermal transport properties throughout the bulk of a Li-ion cell while it is in operation, without affecting the operation of the cell. The 3-omega system will work by using mm-scale sensors on the electrode current collectors to send variable-frequency thermal waves into the operational battery to quantitatively measure heat transport through different layers and interfaces. The team will also use the ultrafast optical time domain thermoreflectance (TDTR) technique to measure nanoscale thermal transport properties of constituent components of the cathode composite. They will then combine these results to create an “all-scale” accurate thermal model of the cell that—unlike existing models—agrees with the empirical measurements of cell thermal performance.

Out-Year Goals. In outgoing years, the project will design, build, and implement the adapted 3-omega metrology. This will involve developing and testing the metrology itself along with accompanying theory, designing compatible battery samples, and applying the technique to live cells. The team will use the TDTR system at LBNL to measure epitaxially grown cathode materials provided by collaborators. Combined, this will provide enough data to construct and validate a realistic all-scale thermal model of the battery.

Collaborations. This project collaborates with two LBNL groups: V. Battaglia’s for cell assembly for 3-omega studies, and R. Kostecki’s for pristine battery active material growths for TDTR studies.

Milestones

1. *Ex situ* high-accuracy measurements of thermal conductivity of individual battery components. (Q1, FY 2019; Completed)
2. Robust thermal model development. (Q2, FY 2019; Completed)
3. *In situ* battery 3-omega thermal measurements from anode and cathode side. (Q3, FY 2019; On schedule)
4. Detailed *in operando* thermal measurements performed. (Q4, FY 2019; On schedule)

Progress Report

The team has successfully performed *in situ* battery 3-omega thermal measurements from both the anode and cathode sides. Yield rate of the sensors was generally lower for anode-side measurements, but the data and data analysis for those sensors that survived worked equally as well. The summary of measurements from the cathode side of two pouch cells and the anode side of another pouch cell is given in Figure 52.

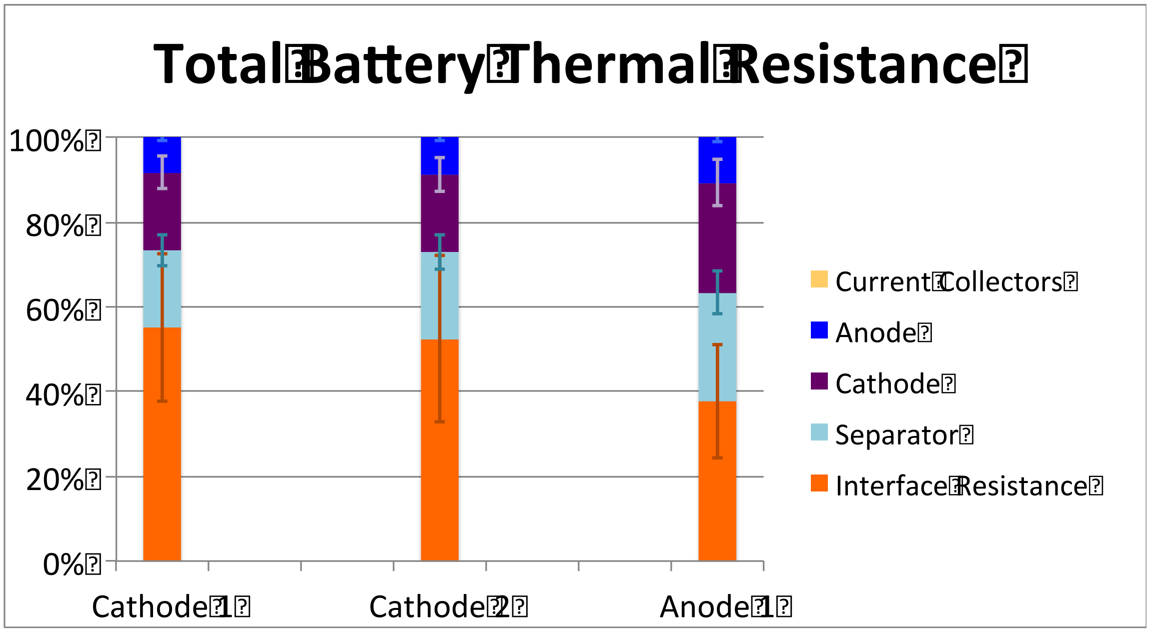

Figure 52. Relative contribution of each relevant layer and interface to the total thermal resistance of Li-ion pouch cells, measured using 3-omega sensors. The sensor was placed on the cathode side for two samples and on the anode side for a third sample.

Figure 52 shows that the team sees agreement between the cathode and anode side sensors within the uncertainty of the measurement. The anode active material and current collector are significantly different thermal conductivities and thicknesses as compared to the cathode. Such close agreement between anode and cathode side sensors (including with sample-to-sample variability mixed in) therefore indicates the validity of the robust thermal model that the team developed last quarter.

Patents/Publications/Presentations

The project has no patents, publications, or presentations to report this quarter.

Task 3.9 – Multi-Scale Modeling of Solid-State Electrolytes for Next-Generation Lithium Batteries (Anh Ngo, Larry A. Curtiss, and Venkat Srinivasan, Argonne National Laboratory)

Project Objective. This project is part of a multi-scale modeling effort to obtain an in-depth understanding of the interaction of the electrode and the solid electrolyte aimed at developing highly efficient SSE batteries for vehicle applications. Input parameters needed for mesoscale (continuum) level calculations are being obtained from atomistic calculations including DFT and classical MD simulations. This atomistic input will enable a multi-scale computational procedure for SSEs that is capable of successfully capturing the physicochemical aspects during charge and discharge process including lithium transport mechanisms, interfacial phenomena during the insertion and extraction of lithium ions, and mechanical deformation of SSE.

Project Impact. A major safety concern experienced with commercially available Li-ion batteries under some scenarios is leakage of the liquid electrolyte, which can potentially catch fire. Replacement of the liquid electrolyte is necessary to decrease the fire hazard and improve safety associated with present-day Li-ion batteries. In addition, use of solid electrolytes provides a path to prevent dendrites in Li-metal anodes, thereby leading to batteries with significantly higher energy density. The impact of this project will be to help in development of good SSEs as a replacement for the commercially used organic liquid electrolytes to improve safety and energy density in Li-ion batteries.

Approach. Parameters needed for mesoscale modeling of GI, GB, and electrode-electrolyte interface will be calculated by DFT-based calculations along with Monte Carlo (MC) and MD simulations. The calculations will be used to determine properties of the electrode with the solid electrolyte as well as in GB regions of the solid electrolyte. This will include calculations of structure, stability, ionic conductivity, Young's modulus, fracture toughness, exchange current density, and other properties.

Out-Year Goals. The out-year goals of this work are to calculate other properties such as fracture toughness and include other SSEs and coatings in the multi-scale modeling.

Collaborations. This project collaborates with Y. Cui at Stanford.

Milestones

1. Computation of elastic. Conductivity properties of interfaces between LLZO with lithium as function of applied electric field for input into multiscale modeling. (Q1, FY 2019; Completed)
2. AIMD and interfacial binding energies calculations of the interface structure of the LLZO solid electrolyte and NMC-622 cathode material. (Q2, FY 2019; Completed)
3. Calculations of lithium migration barriers at interface LLZO/NMC cathode material for estimation of exchange current density NMC/LLZO interfaces. (Q3, FY 2019; Completed)
4. Continuum-level mesoscale calculations for LLZO/NMC cathode materials. (Q4, FY 2019; Initiated)

Progress Report

The use of ceramic solid electrolytes to create all solid-state batteries can enable the use of lithium metal by preventing propagation of lithium dendrites, therefore enhancing safety and decreasing capacity fade. The interfaces between the cathode and solid electrolyte must be stable to enable the use of these materials in batteries. Multi-scale modeling can provide insight into the mechanism for dendrite growth and other instabilities for guidance into how to prevent them. Mesoscale (continuum) modeling requires atomistic level input from theory or experiment to accurately capture physicochemical aspects during charge and discharge processes.

Even under equilibrium conditions (zero applied overpotential), a current of a certain magnitude flows between the electrode and electrolyte. The anodic and cathodic components of this current are equal in magnitude, and they cancel each other, resulting in zero net current flow between the electrode and electrolyte. The magnitude of this current that flows under the equilibrium condition is known as the exchange current density. This quantity is important in material research for batteries in the sense that it provides a measure of the reaction kinetics occurring at the interface of two different materials. A higher magnitude of exchange current density indicates that the reaction at the interface is kinetically favorable, whereas a smaller magnitude of exchange current density denotes the necessity to apply a larger overpotential for the particular interfacial reaction to occur.

For an NMC electrode and SSE LLZO interface, the magnitude of exchange current density i_0 can be given as:

$$i_0 = Fk_{ref} \cdot (c_{Li^+})^{\alpha_a} \cdot c_{Li}^{\alpha_c} \cdot \left(c_{Li,max} - c_{Li}\right)^{\alpha_a}, \text{ where, } k_{ref} = k_0 \cdot \exp(-\Delta G/(k_B T)). \qquad (1)$$

Here, F indicates Faraday's constant, c_{Li^+} stands for Li-ion concentration within the electrolyte, α_a is the cathodic component of transfer coefficient (assumed to be 0.5 in the present research), k_0 is the reaction rate pre-factor, ΔG indicates thermodynamic energy barrier at equilibrium, k_B is the Boltzmann's constant, and T denotes temperature in Kelvin scale. Among all the parameters and constants mentioned here, ΔG and k_0 can be extracted directly from the DFT calculations, and Li-ion concentration within the electrolyte can be estimated from analysis of DFT calculations.

This quarter, the team focused on the LLZO-based SSE to understand the charge transfer process between the NMC-622 electrode and the lowest energy LLZO surface [(100) lithium terminated]. The energy barrier obtained from DFT is shown in Figure 53, which indicates that the magnitude of ΔG is around 0.48 eV. Calculations were carried out with the PBE functional with a plane wave basis, and both GGA and GGA+U calculations were performed. The stability of the interface between the NMC-622 electrode and the lowest energy LLZO surface [(100) lithium terminated] was investigated first with AIMD simulations. All production runs of the AIMD trajectories were obtained after 2 ps of thermal equilibration. The magnitude of the pre-factor k_0 can be extracted from DFT, which depends on the attempt frequency $= \frac{1}{2\pi}\sqrt{\frac{k}{m}}$, where k is the spring constant and m is the mass of the lithium atom. Using GGA+U calculations, the team obtains $k_0 = 5.51 \times 10^5$ cm^2 / s and $k_0 = 8.91 \times 10^5$ cm^2 / s for the LLZO/NMC (10-11) and NMC (10-14) interfaces, respectively. These results will be used to investigate exchange current densities at NMC/LLZO interfaces for use in continuum studies.

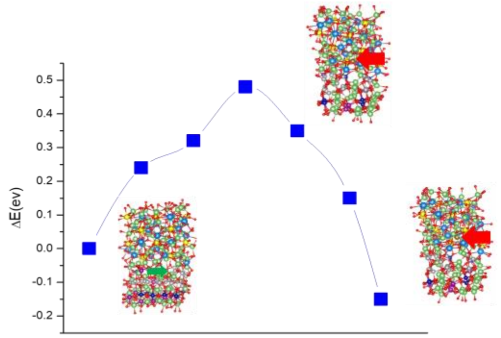

Figure 53. Energy barrier obtained from density functional theory analysis as a lithium atom travels from an NMC-622 (10-14) electrode to a LLZO electrolyte. The magnitude of ΔG obtained from the PBE-GGA calculation is 0.48eV.

Patents/Publications/Presentations

Publications

- Barai, P., K. Higa, A. T. Ngo, L. A. Curtiss, and V. Srinivasan. "Mechanical Stress Induced Current Focusing and Fracture in Grain Boundaries." *Journal of the Electrochemical Society* 166 (2019): A1752–A1762.
- Barai, P., A. T. Ngo, B. Narayanan, K. Higa, L. A. Curtiss, and V. Srinivasan. "Multiscale Modeling of Current Focusing and Crack Propagation at Lithium/LLZO Interface." Under preparation; for submission in *Journal of the Electrochemical Society*.

TASK 4 – METALLIC LITHIUM

Summary and Highlights

The use of a metallic lithium anode is required for advanced battery chemistries like Li-ion, Li-air, and Li-S to realize dramatic improvements in energy density, vehicle range, cost requirements, and safety. However, use of metallic lithium with liquid and polymer electrolytes has so far been limited due to parasitic SEI reactions and dendrite formation. Adding excess lithium to compensate for such losses effectively negates the high energy density for lithium in the first place. For a long lifetime and safe anode, it is essential that no lithium capacity is lost either (1) to physical isolation from roughening, dendrites, or delamination processes, or (2) to chemical isolation from side reactions. The key risk and current limitation for this technology is the gradual loss of lithium over the cycle life of the battery.

BMR, Battery500, and other DOE programs are addressing this challenge with many innovative and diverse approaches. Key to all is the need for a much deeper analysis of the degradation processes and new strategies to maintain a dense, fully connected lithium and a dendrite-free electrolyte so that materials can be engineered to fulfill the target performance metrics for EV application, namely 1000 cycles and a 15-year lifetime, with adequate pulse power. Projecting the performance required in terms of just the lithium anode, this requires a high rate of lithium deposition and stripping reactions, specifically about 30 μm of lithium per cycle, with pulse rates up to 10 and 20 nm/s (15mA/cm^2) charge and discharge, respectively, with little or no excess lithium inventory. This is daunting in the total mass and rate of material transport that must be achieved without failures.

The efficient and safe use of metallic lithium for rechargeable batteries is then a great challenge, and one that has eluded R&D efforts for years. This project takes a broad look at this challenge for both solid-state batteries and batteries continuing to use liquid electrolytes. For the liquid electrolyte batteries, Massachusetts Institute of Technology (MIT), with Carnegie Mellon, is investigating fluoridated components and other additives to form self-healing SEI coatings at the lithium surface. At University of Pittsburgh, alternatives to a standard Li-metal anode are being explored, including metal alloys and templated structures. Researchers at PNNL are pivoting from liquid electrolytes to hybrid electrolytes, with addition of a polymer component to a concentrated solvent-in-salt electrolyte. For solid-state batteries, programs are addressing both the electrolytes and the lithium interface. The stability of the garnet ceramic electrolyte with lithium is being investigated at ANL with materials from University of Michigan; this is now expanding to other solid electrolytes. The different mechanical and electrochemical mechanisms leading to the formation of shorting lithium features through the solid electrolytes is under study at ORNL, University of Michigan, and Michigan Technological University. New ceramic-polymer composite electrolytes formed with scalable processing are being investigated to reveal the properties of both the ceramic electrolyte / polymer electrolyte interface and contacts of the solid electrolyte with the solid composite cathode and thin lithium anode.

Highlights. The highlights for this quarter are as follows:

For solid and hybrid electrolyte systems:

- Interesting work continues for a hybrid electrolyte that is largely LiFSI salt, with small additions of PEO polymer (0.6 mole) and wet by DME solvent (0.6 to 1.2 mole per mole salt). Recent work demonstrates promising high-voltage stability by 3-contact sweep voltammetry and by cycling a Li//NMC-333 battery. For compositions with lower DME content, reasonable cycling was obtained for 300 cycles with a 4.4 V charge cutoff. (Task 4.1)

- Symmetric Li//Li cycling was examined for LLZO ceramic electrolyte stabilized with aluminum, tantalum, and niobium. As shown before, the niobium is not stable, and XPS reveals reduced Nb^{+4} and Nb^{+2} throughout the bulk. Cycling of the Al- and Ta- doped LLZO, however, is stable even to 2 mA/cm^2 current density. This is a higher current than for most reports of a critical current density for LLZO. Several possible distinctions include the short duration DC steps, only 100 sec, and the fabrication of vacuum-deposited lithium contacts on the LLZO covered with a piece of lithium foil. (Task 4.6)
- Cycling of full cells with composite electrolytes, composed of dry-polymer and dispersed ceramic particles, is reported. The anode is a thin lithium film; the cathode is a composite of $LiFePO_4$ particles with a dry-polymer electrolyte. For reasons that remain unclear, best cycling is obtained when the cathode is coated by a single-ion conducting electrolyte. Promising alternative polymer and composite electrolytes are reported that covalently bind the anions to provide single Li^+ ion conduction. One polymer also has a low interface resistance between the polymer and ceramic electrolytes. Such an electrolyte may replace the PEO-based electrolytes in future cell tests. (Task 4.4)

For lithium anode and liquid electrolytes:

- Lithium was reversibly plated and stripped from a copper current collector that was coated with one of two candidate Li-ion absorption (LIA) coating materials. Both coatings reduced the driving force to initiate dendrites and lead to > 99.5% CE. The most effective coating prevented dendritic shorts for more than 230 cycles at currents up to 1 mA/cm^2. (Task 4.3)

Task 4.1 – Lithium Dendrite Prevention for Lithium Batteries
(Wu Xu and Ji-Guang Zhang, Pacific Northwest National Laboratory)

Project Objective. Enable lithium metal to be used as an effective anode in rechargeable Li-metal batteries for long cycle life. The investigation in FY 2019 will focus on effects of various organic solvents, inorganic solid electrolytes, and polymers on ionic conductivity, lithium CE, lithium anode morphology, and battery performances in terms of long-term cycling stability and rate capability at room temperature and elevated temperatures. The compatibility of such electrolytes with 4-V, high-Ni NMC cathode will also be investigated.

Project Impact. Lithium metal is an ideal anode material for rechargeable batteries. Unfortunately, uncontrollable dendritic lithium growth and limited CE during repeated lithium stripping/deposition processes have prevented practical application. This work will explore the new hybrid composite electrolytes that can lead to dendrite-free lithium deposition with high CE. The success of this work will increase energy density of Li-metal and Li-ion batteries and accelerate market acceptance of EVs, especially of PHEVs as required by the EV Everywhere Grand Challenge.

Approach. The approach will encompass several areas. (1) Develop appropriate high-concentration electrolytes (HCEs) that have high lithium CE over 99% and are stable with high-Ni NMC (for example, NMC-532) cathodes. (2) Add a small amount of inorganic solid electrolytes and proper polymers into the HCEs to form uniform mixtures, which will be cast into thin films. (3) Solid-state polymer-in-salt electrolyte will be prepared through the hot-pressing method. The effects of the type and content of inorganic fillers and polymers on the ionic conductivity, the electrochemical window, the lithium CE, and the morphology will also be tested.

Out-Year Goals. The long-term goal of the proposed work is to enable lithium and Li-ion batteries with > 120 Wh/kg (for PHEVs), 1000 deep-discharge cycles, 10-year calendar life, improved abuse tolerance, and less than 20% capacity fade over a 10-year period.

Collaborations. This project collaborates with C. Wang of PNNL on characterization by TEM/SEM; Drs. K. Xu and M. Ding of U. S. Army Research Laboratory (ARL) on solvent purification and differential scanning calorimetry (DSC) measurements; and Dr. B. Polzin at ANL on coated electrode sampling.

Milestones

1. Achieve over 300 cycles for 4-V Li||NMC batteries with ~ 2 mAh/cm^2 cathode loading. (Q4, September 30, 2018; Completed)
2. Investigate effects of high-concentration electrolytes on lithium CE and deposited lithium morphology. (Q1, January 15, 2019; Completed)
3. Investigate effects of polymers in hybrid electrolytes on lithium CE and deposited lithium morphology. (Q2, March 31, 2019; Completed)
4. Develop an HCE with lithium CE > 98% and oxidation potential up to 4.4 V. (Q3, June 30, 2019; Completed)
5. Achieve over 100 cycles for Li||NMC-532 batteries with medium cathode loading. (Q4, September 30, 2019; In progress)

Progress Report

This quarter, the oxidation stability of hybrid polymer electrolytes, lithium CE, and cycling stability of Li||NMC-333 batteries with different cutoff voltages were investigated. The main results of this work are summarized below.

- With the decrease of the molar ratio (x) of the DME solvent in the polymer-in-"quasi ionic liquid" electrolytes (PQILEs) $Li(DME)_xFSI\text{-}PEO_{0.6}$, the anodic stability limit shifted to a more positive potential (where the initial oxidation voltage is defined as the voltage value when the current density reaches 5 µA cm^{-2}). The irreversible oxidative current for $Li(DME)_{1.2}FSI\text{-}PEO_{0.6}$ started to flow at around 4.2 V versus Li/Li^+, while the oxidation voltage of $Li(DME)_{0.7}FSI\text{-}PEO_{0.6}$ was increased to above 4.5 V (Figure 54a). Both $Li(DME)_{0.6}FSI\text{-}PEO_{0.6}$ and $Li(DME)_{0.7}FSI\text{-}PEO_{0.6}$ showed an oxidation potential around 4.7 V.
- The average lithium CE of the PQILEs was tested in Li||Cu cells at 60°C. The lithium CE of $Li(DME)_xFSI\text{-}PEO_{0.6}$ with Celgard 3501 was 95.5%, 95.9%, 96.6%, and 97.8% for x = 0.6, 0.7, 0.8, and 0.9, respectively; the maximum CE of $Li(DME)_{0.9}FSI\text{-}PEO_{0.6}$ was 98.4% (Figure 54b). The lithium CE showed a monotonous increase with DME, but PQILEs with higher DME ratio were not tested due to a phase separation. On further decrease in test temperature to 45°C, the lithium CE of $Li(DME)_{0.9}FSI\text{-}PEO_{0.6}$ increased to 98.6%. The main reason for such a difference is likely that at high-temperature the Li^+-coordinated DME and Li^+ associated FSI^- are more labile and easily dissociate into free DME, FSI^-, and Li^+, thus leading to more side reactions with lithium metal.
- Li-metal cells with a NMC-333 cathode were cycled with different cutoff voltages. A capacity retention of 88.4% after 300 cycles was achieved with the charge cutoff voltage of 4.2 V at C/3 charge rate and 1C discharge rate (where 1C = 2 mA cm^{-2}) (Figure 54c). The cell overpotential increased only slightly after 300 cycles. When the charge cutoff voltage was increased to 4.3 V, the cell showed a capacity retention of 86.7% after 300 cycles. Even when the cell was charged to 4.4 V, it still retained 79.2% of the initial capacity after 300 cycles, which is remarkable for PEO-based electrolytes under such a high voltage. Both the cells charged to 4.3 V and to 4.4 V showed only a small increase in cell overpotential. When the cell charge voltage was further increased to 4.5 V, a continuous capacity fading was observed and about 60% capacity decreased, indicating the decomposition of the hybrid polymer electrolyte.

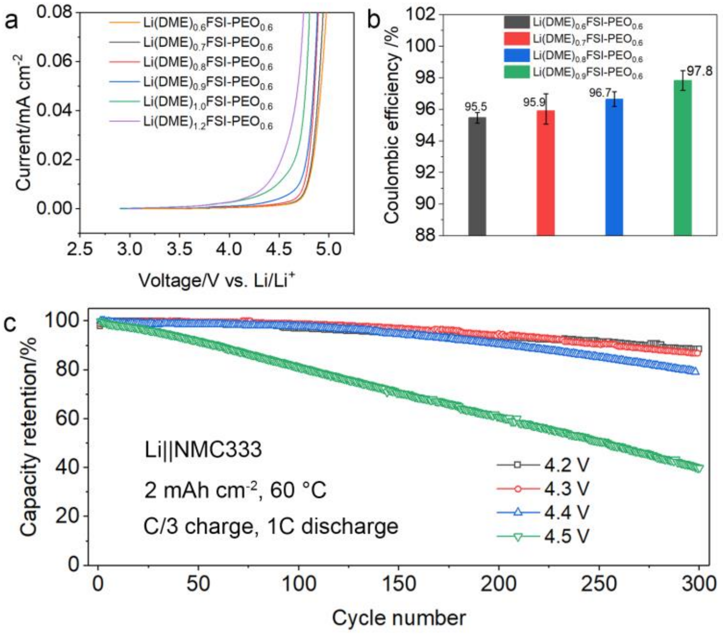

Figure 54. (a) Linear sweep voltammetry curves of polymer-in-"quasi ionic liquid" electrolytes (PQILEs) of $Li(DME)_xFSI\text{-}PEO_{0.6}$ on platinum electrode in a three-electrode cell with a scan rate of 0.5 mV s^{-1}. (b) Average lithium Coulombic efficiency values of $Li(DME)_xFSI\text{-}PEO_{0.6}$ at 60°C with Celgard 3501. (c) Cycling performance of Li||NMC cells using $Li(DME)_{0.7}FSI\text{-}PEO_{0.6}$ under different charge cut-off voltages.

Patents/Publications/Presentations

Presentations

- Beyond Lithium Ion XII, Golden, Colorado (June 25–27, 2019): "High-Voltage Lithium-Metal Batteries Enabled by PEO-Based Gel Electrolytes"; H. Wu, Y. Xu, X. Ren, B. Liu, M. Engelhard, M. S. Ding, P. Z. El-Khoury, L. Zhang, Q. Li, C. Wang, K. Xu, C. Wang, J-G. Zhang, and W. Xu.*
- DOE VTO AMR Meeting, Arlington, Virginia (June 10–13, 2019): "Lithium Dendrite Prevention for Lithium Batteries"; W. Xu* and J-G. Zhang.
- 235th ECS Meeting, Dallas, Texas (May 26–30, 2019): "Polymer-in-'Quasi Ionic Liquid' Electrolytes for High-Voltage Lithium Metal Batteries"; H. Wu,* Y. Xu, X. Ren, B. Liu, M. Engelhard, M. Ding, P. Z. El-Khoury, L. Zhang, Q. Li, K. Xu, C. Wang, J-G. Zhang, and W. Xu.

Task 4.2 – Self-Assembling and Self-Healing Rechargeable Lithium Batteries (Yet-Ming Chiang, Massachusetts Institute of Technology; Venkat Viswanathan, Carnegie Mellon University)

Project Objective. The project objectives are as follows: (1) investigate formation of lithium halide containing SEI, (2) characterize the structure and composition of the SEI surface film and morphology of the electrochemically deposited lithium, and (3) develop combinations of electrolytes (solvents + salts) and electrolyte additives that produce a highly Li-ion conducting, mechanically robust, and self-healing SEI to suppress lithium dendrite formation and improve CE.

Project Impact. Efforts to achieve practical use of the Li-metal anode in rechargeable lithium batteries have long been plagued by lithium dendrite formation and low CE. Lithium dendrites cause battery short-circuits, leading to serious safety hazards. The low CE of Li-metal anodes demands use of excess lithium to offset the lithium loss during cycling, which lowers the overall energy density of the battery. If successful, this project will enable self-forming and self-healing SEI containing alkali and/or alkaline earth halides that can suppress dendrite formation and improve CE. This will eventually enable high-energy-density (> 400 Wh/kg) and long-cycle-life (> 500 cycles, 80% capacity retention) Li-metal batteries.

Approach. The project approach involves the following: (1) identifying suitable combinations of solvents, Li-electrolyte salts, and halide and other additives that can produce highly Li-ion conducting, mechanically robust, and self-healing SEI, (2) using integrated theory and experiment, and (3) assembling and testing symmetric and asymmetric cells and Li-metal batteries comprising a high areal-capacity cathode (> 3 mAh/cm^2) and a capacity-limited Li-metal anode (< 130% lithium excess).

Out-Year Goals. The project will down-select electrolyte compositions, develop designs for prototype full cells of > 10 mAh capacity, and fabricate/deliver cells to DOE-specified laboratories for testing and evaluation.

Collaborations. This project collaborates with 24M Technologies Inc. on 18 cm^2/80 cm^2 pouch cell fabrication and tests.

Milestones

1. *Go/No-Go Decision*: Demonstrate Li-Li symmetric cells that meet established criteria cycling at ≥ 3 mAh/cm^2 at C/5 rate over 30 cycles. (Q1, FY 2019; Completed ahead of schedule)
2. Demonstrate at least one Li-Li symmetric cell that cycles ≥ 3 mAh/cm^2 at C/5 rate over 50 cycles without short-circuit. (Q2, FY 2019; Completed)
3. Build 12 baseline cells of > 10 mAh capacity for testing under different stack pressures. (Q3, FY 2019; Completed)
4. Establish quantitative criteria for solid-electrolyte/liquid electrolyte combinations that exhibit self-healing functionality. (Q4, FY 2019; In progress)

Progress Report

Last quarter, the team reported Li-$LiCoO_2$ full-cell cycling results utilizing the electrolytes developed in this project and also demonstrated the effect of lithium anode thickness. The $LiCoO_2$ full cell containing the 1 M $LiPF_6$ FEC-DMC showed 80 cycles to 80% of initial capacity, and the 1 M $LiPF_6$ FEC-DMC + DTD electrolyte showed 130 cycles, where DTD is 1,3,2-dioxathiolan-2,2-oxide. The team also made full cells with a 50-µm-thick lithium anode, and it showed 250 cycles for the same FEC-DMC+DTD electrolyte.

This quarter, the team has built 10-mAh cells to be studied under different applied stack pressures. They will evaluate the cycle life as a function of stack pressure for the above mentioned electrolytes. Cycling tests are in progress and will be reported next quarter.

Last quarter, the team reported the DFT simulation results of the decomposition of EC, DMC, FEC, difluoroethylene carbonate (DFEC), 1-(trifluoromethyl)ethylene carbonate (CF_3-EC), and DTD on lithium surfaces and their comparison with the XPS measurements. Here, the team reports two descriptors to quantify a high-performance, self-formed SEI based on DFT calculations. Two key factors are (1) the ionicity of the SEI, which is needed for ensuring low electronic conductivity, and (2) the porosity of the SEI, which will control the morphology and packing density of the inorganic and organic phases. The team proposes to use the number of electrons transferred from the lithium surface to the electrolyte molecule as a descriptor for the iconicity of the SEI. This descriptor is intuitive, as the more ionic the SEI is, the more electrons should be transferred from the lithium surface, as shown in Table 3. The team proposes that the volume of the organic species left behind from the decomposition is a good descriptor for the ability to form a compact SEI. This volume can be quantified by the Bader Volume of the largest SEI species, typically the organometallic salt component. These two descriptors, used in conjunction, can rationalize the experimentally observed trends. Based on the descriptor for the ionicity of the SEI, the team nearly achieves the performance trend correctly, with the exception of DFEC. However, when now considering the compactness descriptor, the team can justify that the formation of larger moieties results in DFEC performing worse than FEC and DTD.

Table 3. Theoretical descriptors for solvent decomposition on lithium metal.

Solvent	Electrons Transferred	Bader Volume of Largest SEI Specie (Å^3)
DMC	2.0	145
EC	2.5	132
FEC	3.3	89
DFEC	4.4	125
CF_3EC	0.5	169
DTD	4.1	97

Patents/Publications/Presentations

Publication

- Hong, Z., and V. Viswanathan. “Prospect of Thermal Shock Induced Healing of Lithium Dendrite.” *ACS Energy Letters* 4, no. 5 (2019): 1012–1019.

Task 4.3 – Engineering Approaches to Dendrite-Free Lithium Anodes (Prashant Kumta, University of Pittsburgh)

Project Objective. This project will yield Li-metal anodes with specific capacity ≥ 2000 mAh/g (≥ 4 mAh/cm^2), ~ 1000 cycles, and CE ≥ 99.99% with superior rate capability. The goal is to (1) systematically characterize different approaches for generation of dendrite-free Li-metal anodes while also providing understanding of the scientific underpinnings, and (2) evaluate the microstructure and electrochemical performance of dendrite-free Li-metal anodes. Generation of high-performance, dendrite-free Li-metal anodes will successfully demonstrate generation of novel sulfur cathodes, affording fabrication of Li-S batteries meeting the targeted gravimetric energy densities ≥ 350 Wh/kg and ≥ 750Wh/l with a cost target $125/kWh and cycle life of at least 1000 cycles for meeting the EV Everywhere Grand Challenge blueprint.

Project Impact. Dendrite formation in electrochemical systems occurs due to inhomogeneous current densities coupled with local diffusion gradients, surface roughness, and kinetic roughening. Lithium dendrite formation and growth are, however, not well understood; adding to the complexity is SEI formation. Control and elimination of lithium metal dendrite formation are challenging. If overcome, this would render universal adoption of Li-anode batteries for stationary and mobile applications. This project is a scientific study of novel approaches to address dendrite formation in Li-anode batteries, electrolyte decomposition, and associated cell failure. Development of dendrite-free, high-performance lithium anodes will enable use of Li-free cathodes, opening a myriad of possibilities to push the envelope in terms of cathode capacity and battery energy density.

Approach. This project will explore several approaches focused on engineering new structurally isomorphous metallic alloys (SIA) combined with engineering the surface of metallic lithium as well as the current collectors, including development of novel high Li-conducting conjugated polymers and composite structures. The unifying theme is to initiate a uniform nucleation with homogenous growth, eliminating preferential reversible plating and de-plating and thus resulting in dendrite-free, high-energy-density Li-metal anodes for Li-metal batteries.

Out-Year Goals. This project comprises three major phases to be successfully completed in three years:

- Year 1 – Synthesis, characterization, and scale up of suitable porous foams (PF) for use as current collectors for lithium anodes and Li-ion conductor (LIC) materials to prepare multilayer porous foams (MPF).
- Year 2 – Development of Li-rich SIA anodes. Generation of composite multilayer anodes (CMAs).
- Year 3 – Advanced high-energy-density, high-rate, extremely cyclable cell development.

Collaborations. The project works with Dr. M. K. Datta and Dr. O. I. Velikokhatnyi (University of Pittsburgh) as co-PIs. It also collaborates with Dr. A. Manivannan (Global Pragmatic Materials), XPS analysis; Dr. D. Krishnan Achary (University of Pittsburgh), solid-state magic angle spinning NMR (MAS-NMR) characterization; and Dr. J. R. Gaines (Kurt Lesker), thin-film system fabrication / characterization.

Milestones

1. Integrated electrode (IE) generation to encompass the three paths of development, that is, coating development/PF, development of CMA and SIA exploration including optimizing the maximize lithium content in SIA with no dendrite formation over extended cycling, especially at high rates to demonstrate high capacity. (October 2019; In progress)
2. Fabrication/characterization of for 10-mAh cell configurations. (October 2019; In progress)

Progress Report

Rigorous theoretical calculation of mass transfer of lithium ions under the influence of potential gradient (G_L) and concentration gradient (G_c), as well as interface perturbation and dendrite kinetics analyses, indicates that the driving force for lithium metal dendrite formation depends on the concentration gradient at the Li-metal/electrolyte interface, whereas the resistance to dendrite formation is governed by the Gibbs Thomson parameter or the interfacial energy between the current collector and the plated lithium metal. Novel current collectors exhibiting high interfacial energy were hence developed, as detailed in prior quarterly reports, displaying excellent cyclability along with excellent CE (≥ 99.7%). In this report, significant studies were further conducted to reduce the perturbation driving force minimizing the interfacial concentration gradient and improving the perturbation resistance. Accordingly, novel materials exhibiting highly reversible LIA are identified and coated on copper substrates, minimizing the interfacial Li-ion concentration gradient. The coated LIA also exhibits high interfacial energy and Gibbs Thomson parameter with lithium metal resisting deformation. Cycling of coated LIA in coin cell using 1 M LiTSFI, 0.1 M $LiNO_3$ in 50v:50v DOL:DME electrolyte shows the Li-metal plating/stripping potential change with time tested at a current density of 0.5 mA/cm^2 and areal capacity ~ 0.5 mAh/cm^2 for a representative LIA-coated copper foil (LIA-1); see Figure 55.

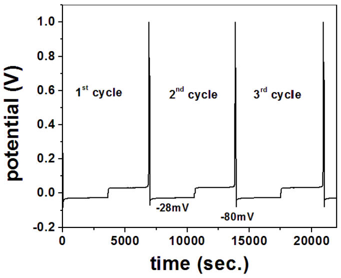

Figure 55. Li-metal plating and stripping behavior of Li-ion absorption 1 (LIA-1) coated on copper foil.

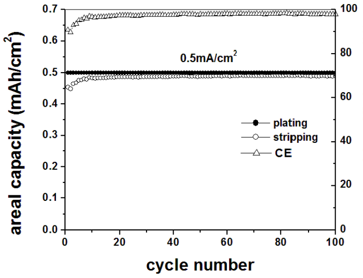

Figure 56. Variation of areal capacity and Coulombic efficiency of Li-ion absorption 1 (LIA-1) for 100 cycles.

Figure 55 shows Li-metal nucleation and growth occurring at an underpotential of -80 mV and -30 mV, respectively, comparable with bare copper current collector. Figure 55 also shows absence of intermetallics formation during Li-metal plating, suggesting the Li-ion non-reactivity of LIA to form intermetallics or solid solution. The variation of areal capacity with cycling (Figure 56) to 100 cycles of studied LIA-1 coated copper foil tested at a current density of 0.5 mA/cm^2 for 1 h of plating shows excellent cyclability with CE > 99.5% after the 10th cycle, whereas traditional copper current collector exhibits poor cyclability after a few cycles. Further, the growth potential of lithium metal (Figure 57), cycled at a current density of 0.5 mAh/cm^2 for 1 h, shows no significant growth potential change (~ 30 mV) with time or cycling, suggesting minimal potential hysteresis of LIA-1 coated copper foil. Based on the above, an improved LIA (LIA-2) exhibiting higher Li-ion absorption than LIA-1 was studied to further improve performance. The variation of areal capacity with cycle numbers up to 230 cycles of LIA-2 coated copper foil tested at areal capacity of 0.5 mAh/cm^2, 1 mAh/cm^2, and 2 mAh/cm^2 (Figure 58) shows excellent cyclability, with CE > 99.5%. The above results clearly suggest that novel materials exhibiting high Li-ion absorption (that is, minimizing the driving force of perturbation) and high Gibbs Thomson parameter coated on copper current collector is a promising way to improve Li-metal battery performance without formation of dendrites. A detailed morphological analysis study is in progress and will be described in future reports.

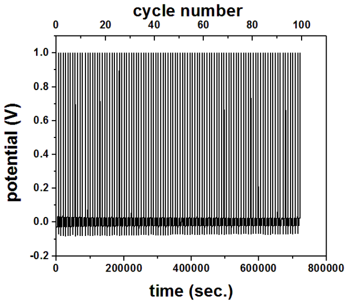

Figure 57. Variation of growth potential of lithium metal during cycling of Li-ion absorption 1 (LIA-1).

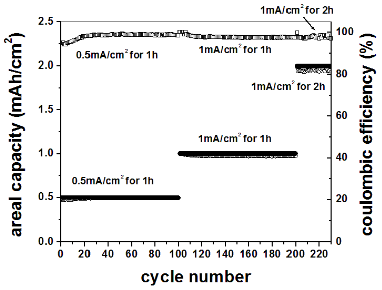

Figure 58. Variation of areal capacity and Coulombic efficiency of Li-ion absorption 2 (LIA-2) coated on copper foil.

Patents/Publications/Presentations

Presentations

- DOE VTO AMR Meeting, Arlington, Virginia (June 10–13, 2019): "Engineering Approaches to Dendrite Free Li-Metal Anodes"; P. N. Kumta.
- Beyond Lithium Ion XII, Golden, Colorado (June 25–27, 2019): "Novel Engineering Approaches to High Energy Density Lithium Metal Batteries"; P. N. Kumta. Invited.

Task 4.4 – Composite Electrolytes to Stabilize Metallic Lithium Anodes
(Nancy Dudney and X. Chelsea Chen, Oak Ridge National Laboratory)

Project Objective. The project has several objectives: (1) prepare composites of representative polymer and ceramic electrolyte materials to achieve thin membranes that have the unique combination of electrochemical and mechanical properties required to stabilize the metallic-lithium anode while providing for good power performance and long cycle life, (2) understand the Li-ion transport at the interface between polymer and ceramic solid electrolytes, which is critical to effective conductivity of the composite membrane, (3) identify key features of composite composition, architecture, and fabrication that optimize performance, and (4) using practical and scalable processing, fabricate thin electrolyte membranes to use with a thin metallic lithium anode to provide good power performance and long cycle life.

Project Impact. A stable lithium anode is critical to achieve high energy density with excellent safety, lifetime, and cycling efficiency. This study will identify key design strategies that should be used to prepare composite electrolytes to meet the challenging combination of physical, chemical, and manufacturing requirements to protect and stabilize the Li-metal anode for advanced batteries. By utilizing well characterized and controlled component phases, design rules developed for composite structures will be generally applicable toward substitution of alternative and improved solid electrolyte component phases as they become available. Success will enable DOE technical targets: 500-700 Wh/kg, 3000-5000 deep discharge cycles, and robust operation.

Approach. This project seeks to develop practical solid electrolytes to provide stable, long-lived protection for the Li-metal anode. Current electrolytes have serious challenges when used alone; oxide ceramics are brittle, sulfide ceramics are air sensitive, polymers are too resistive and soft, and many electrolytes react with lithium. Composites provide a clear route to address these issues. While work continues to emphasize study of ceramic electrolyte/polymer electrolyte interfaces, this effort has expanded to address (1) practical processing routes to fabricate full batteries using better composite electrolytes with a composite cathode and thin Li-metal anode, and (2) introduction of alternative polymer and ceramic phases to replace well-known model materials and develop improved composite electrolytes. In addition to solid-state devices, hybrid batteries are investigated using a fluid or gel catholyte within the porous cathode. Coatings have also been employed to stabilize electrode interfaces. These directions increase complexity of the studies, but are needed to improve cycling stability and rate performance and to advance practical implementation of the solid electrolyte and Li-anode technology.

Out-Year Goal. The goal is to use advanced manufacturing processes where the architecture of the composite membrane can be developed and tailored to maximize performance and cost-effective manufacturing.

Collaborations. Work is conducted by Dr. Y. Zhang and Dr. X. Chen. Ceramic electrolyte powders are obtained from Ohara Corporation and Prof. J. Sakamoto (University of Michigan). Polymer electrolytes are provided by Prof. Z. Bao (Stanford University) and T. Saito (ORNL) and Prof. Jennifer Schaefer (University of Notre Dame). The team will work with new partners from U. S.–German Cooperation on Energy Storage.

Milestones

1. Fabricate full cell using thin evaporated lithium anodes. Compare full-cell performance using thick and thin evaporated lithium anodes. (Q1, FY 2019; Completed)
2. Fabricate gel composite electrolytes with a target room-temperature conductivity of 1×10^{-4} S/cm. Evaluate ion transport, and thermal and structural properties. (Q2, FY 2019; Completed, achieved target)
3. Expand composite materials to include non-PEO type of polymer electrolytes. Identify promising polymer ceramic systems with interfacial area specific resistance (ASR) < 10 ohm. (Q3, FY 2019; Completed)
4. Work with partners from U. S.–German Cooperation on Energy Storage on WP3-polymer electrolyte. Complete milestones as detailed in the proposal. (Q4, FY 2019)

Progress Report

last quarter, the team reported that cells with 6 µm lithium on copper foil anode showed the highest CE (0.99) at cycle 1; the cell is Cu/Li/PE/CPE/PE/LFP/Al, where PE is a thin polymer coating, CPE a composite electrolyte of Ohara's LMTP particles in a polymer, and LFP a $LiFePO_4$ composite cathode. Interestingly, after the 1st cycle, the charge capacity exceeds the theoretical capacity for 5 cycles (Figure 59, left). To understand this behavior, the team is examining the cycling and oxidation state of titanium in the CPE. Assuming the excess capacity is largely attributable to the reduction of Ti^{4+} to Ti^{3+}, the excess capacity is indeed comparable to the titanium content (Figure 59, inset). However, this is not supported by the XAS (7-BM at NSLSII) where the titanium K-edge is unchanged for the cycled electrolytes (Figure 59, right). Alternatively, there is a possibility of an electronic leakage path.

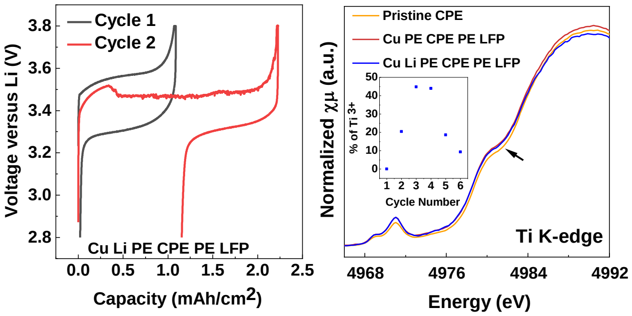

Figure 59. (left) Comparison of cycles 1 and 2 for Cu/Li/PE/CPE/PE/LFP cell, where PE is a thin polymer coating, CPE a composite electrolyte of Ohara's LMTP particles in a polymer, and LFP a $LiFePO_4$ composite cathode. (right): Titanium K-edge of pristine CPE and CPE after cycling from the cell Cu/PE/CPE/PE/LFP and Cu/Li/PE/CPE/PE/LFP. Inset: Percentage of Ti^{3+} calculated from the extra charge capacity of each cycle.

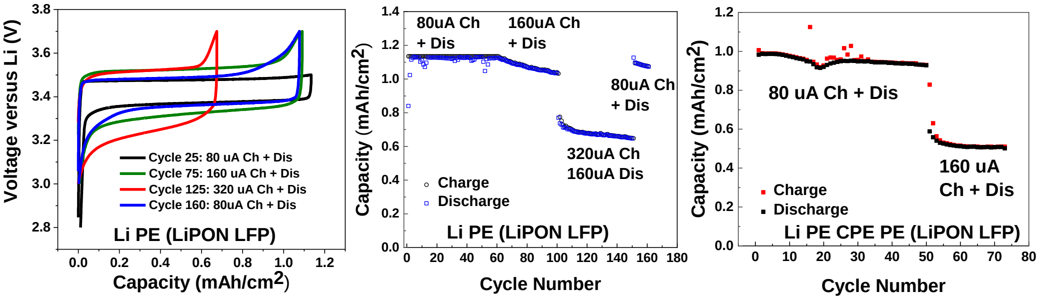

Figure 60. (left) Voltage profiles at cycle 25, 75, 125, and 160 for Cell Li PE (LiPON LFP), where PE is a thin polymer coating and LFP a $LiFePO_4$ composite cathode. (middle) The cycling and rate performance of Li PE (LiPON LFP) cell. (right) Li/PE/CPE/PE (LiPON LFP) cell, where CPE is a composite electrolyte of Ohara's LMTP particles in a polymer. Note: The area of the electrode is 1 cm^2.

Long-term cycling is only observed, so far, with addition of a thin LiPON (300 nm) layer on the LFP cathode and use of a thicker (> 6 µm) lithium. The cell polarization increased with increasing current density (Figure 60, left) and the realized capacity decreased (Figure 60, middle). With addition of a CPE electrolyte (Figure 60, right) there is only minimal overcharge, unlike above. The cell achieved the expected 1.0 mAh/cm^2 capacity. The role of the LiPON layer to block either reaction with the PE or transport of electrons or anions is under investigation.

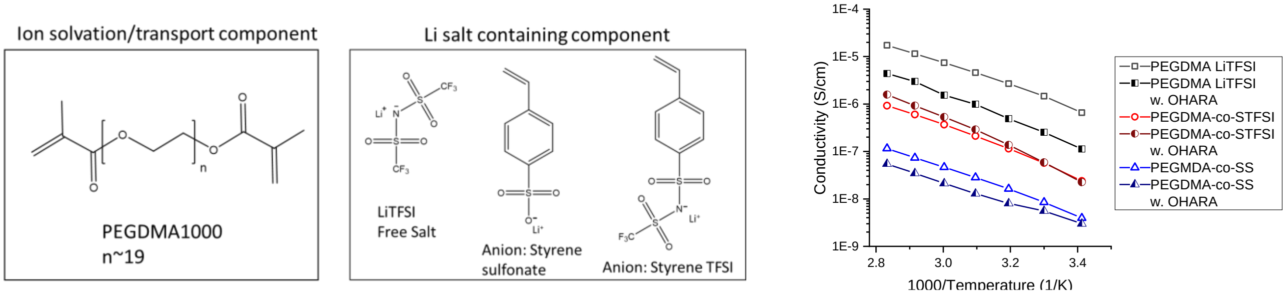

Figure 61. Composites consisting of Ohara ceramic and three different polymers: polyethylene glycol dimethacrylate (PEGDMA) crosslinked with LiTFSI free salt, with covalently bound styrene sulfonate anion and with covalently bound styrene TFSI anion. (right) Ionic conductivity of the polymers and their respective composite with 50 wt% Ohara ceramic.

The team expanded the project's polymer portfolio and examined three polymers (collaboration with Prof. Jennifer Schaefer). The ion solvation/transporting component of these polymers is polyethylene glycol dimethacrylate (PEGDMA). The methacrylate group can be covalently connected to an anion-containing component. The team compared three types of anions: TFSI free anion, covalently bound styrene sulfonate anion (SS^-), and covalently bound styrene TFSI anion ($STFSI^-$) (Figure 61). The ionic conductivity of the dry polymers and their composites with 50 wt% Ohara ceramic is shown in Figure 60(right). An order of magnitude decrease in conductivity was observed in the composite containing free LiTFSI salt compared to the neat polymer; this is consistent with past results on dry composites. In contrast, the composite of Ohara and PEGDMA-co-LiSTFSI polymer is more conductive than the neat single-ion conducting polymer, indicating a low interfacial ASR (milestone 3).

Patents/Publications/Presentations

Publications

- Palmer, M. J., S. Kalnaus, A. S. Westover, N. J. Dudney, and X. C. Chen. "A Three-Dimensional Interconnected Structure of LATP/PEO as a Thin Film Composite Solid Electrolyte." In preparation.
- Zhang, Y., et al. "Thin Evaporated Li in the Cycling of Composite Solid-State Batteries." In preparation.
- Zhang, Y., et al. "Thin LiPON Electrolyte to Stabilize the Solid Electrolyte Interphase between Polymer Electrolyte and Cathode." In preparation.

Task 4.5 – Lithium Batteries with Higher Capacity and Voltage
(John B. Goodenough, University of Texas at Austin)

Project Objective. The project objective is to develop an electrochemically stable alkali-metal anode that can avoid SEI layer formation and alkali-metal dendrites during charge/discharge. To achieve the goal, a thin and elastic solid electrolyte membrane with a Fermi energy above that of metallic lithium and an ionic conductivity $\sigma > 10^{-4}$ S cm^{-1} will be tested in contact with alkali-metal surface. The interface between the alkali-metal and the electrolyte membrane should be free from liquid electrolyte, have a low impedance for alkali-metal transport and plating, and keep good mechanical contact during electrochemical reactions.

Project Impact. A safe alkali-metal anode that can be plated/stripped reversibly at low resistance and high rates over many thousands of charge/discharge cycles would maximize the volumetric energy density for a given cathode of a rechargeable battery for powering an all-electric road vehicle. Such a battery could also be used for stationary back-up storage of electric power from energy sources other than fossil fuels.

Approach. The project will design, make, and test cells. The approach is to introduce a solid-electrolyte interfacing the anode and a coating on the anode current collector that is wet by a lithium anode. The solid electrolyte should also be wet by the anode to create a bond that is strong enough to constrain the anode volume changes to be perpendicular to the anode/electrolyte interface.

Out-Year Goals. The out-year goal is to develop coin cells that are safe and low-cost with a long cycle life at a voltage $V > 3.0$ V that can compete with the internal combustion engine for powering a road vehicle.

Collaborations. This project collaborates with A. Manthiram at UT Austin and K. Zaghib at HQ.

Milestones

1. Test a new, low-cost ceramic separator concept with a liquid electrolyte and an alkali metal anode. (Q1, FY 2019; Completed)
2. Test redox energies and cyclabilities of novel NASICON-structured cathode materials in a Na-ion battery. (Q2, FY 2019)
3. Synthesize and evaluate solid sulfide electrolytes. (Q3, FY 2019)
4. Investigate oxygen redox chemistry for reversible high-voltage Na^+ intercalation. (Q4, FY 2019)

Progress Report

Synthesis and Evaluation of Sulfide Solid Electrolyte (Y. Li and J. B. Goodenough)

The team prepared Li_6PS_5Cl sulfide solid electrolyte (SE) by mechanical milling and subsequent heat treatment; the structure and characteristic of this electrolyte are shown in Figure 62. In Figure 62a, the XRD pattern of Li_6PS_5Cl is the same as that of Li_7PS_6, both of which belong to the argyrodite crystalline phase. Li_6PS_5Cl is a typical representative of argyrodite. Figure 62b-c shows the Nyquist plots of Li_6PS_5Cl electrolyte at different temperatures and the temperature dependence of the Li-ion conductivity. At ambient temperature, Li_6PS_5Cl SE exhibits an ionic conductivity of 1.29×10^{-3} S cm^{-1}, and activation energy of 0.32 eV. The team also evaluated the electrochemical stability of Li_6PS_5Cl solid electrolyte with linear CV of steel/SE/Li cell at a constant scan rate of 5 mV s^{-1} in the voltage window of -0.5 to 5 V (Figure 62d). Except for the lithium plating at -0.5 V and the lithium stripping at 0.3 V, no additional current peak is detected in the whole scanning voltage range, indicating that Li_6PS_5Cl has a wide and stable electrochemical window. Figure 62e shows the SEM images and corresponding element mapping; the average size of Li_6PS_5Cl solid electrolyte is ~ 5μm.

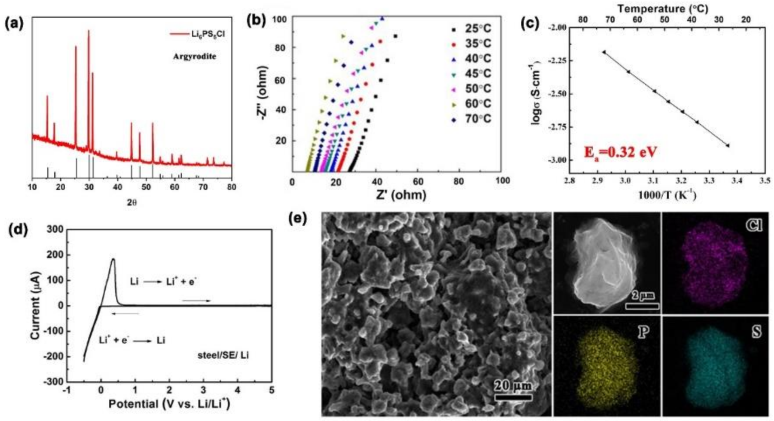

Figure 62. The structure and characteristic of Li_6PS_5Cl sulfide solid electrolyte. (a) X-ray diffraction. (b) The Nyquist plots at different temperatures. (c) Temperature dependence of the ionic conductivity. (d) Cyclic voltammogram of stainless-steel/solid-electrolyte/Li cell at a scanning rate of 0.5 mV/s between -0.5 V and 5 V. (e) Scanning electron microscopy images and corresponding element mapping.

The team also evaluated the electrochemical performance of Li_6PS_5Cl in an all-solid-state $Li_2S/Li_6PS_5Cl/Li$ battery (Figure 63a). The capacity of this battery is 320 mAh g^{-1} at ambient temperature, and it can be increased to ~ 600 mAh g^{-1} at 55°C. The optimization of the cell, especially the electrolyte/electrodes interfaces, will be studied to further improve cycling.

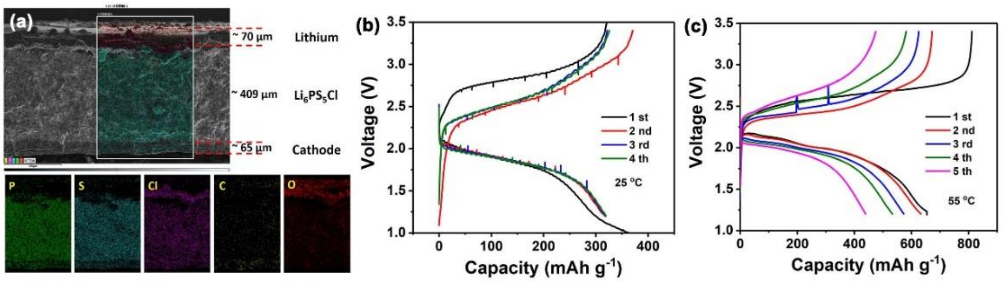

Figure 63. (a) The structure of $Li_2S/Li_6PS_5Cl/Li$ battery. (b-c) Electrochemical performance of $Li_2S/Li_6PS_5Cl/Li$ battery at 25°C and 55°C, respectively.

Patents/Publications/Presentations

The project has no patents, publications, or presentations to report this quarter.

Task 4.6 – Advancing Solid-State Interfaces in Lithium-Ion Batteries
(Nenad M. Markovic and Larry A. Curtiss, Argonne National Laboratory)

Project Objective. The project objectives are multifaceted, including development of a new mechanically and chemically stable and Li-ion conductive ($\geq 2 \times 10^{-4}$ S/cm at 298 K) solid electrolyte for a solid-state battery encompassing a Li-metal anode, Li-oxide-based cathode, and nonflammable crystalline and amorphous solid electrolytes that can operate at cathode potentials > 5 V (denoted as a S_{Li}-S_{EL}-S_{C} system).

Project Impact. Protective organic and inorganic compounds can enhance stability of the interface, improve Li-ion interfacial transport, minimize dendrite formation, and increase safety in Li-ion batteries.

Approach. The project proposes to develop and use interdisciplinary, atomic-/molecular-level insight obtained from integrating both experimental- and computational- based methodologies to define the landscape of parameters that control interfacial properties for a new generation of the Li-ion solid-solid battery systems. The strategy will involve transferring knowledge gained from well-characterized thin-film materials to real-world materials. This strategy forms a closed loop wherein the knowledge gained from model systems is used to design more complex, real-world materials, and vice versa. The work will focus on utilizing existing in-house synthesis and characterization methods to enable rapid transition from fundamental science to realistic cells.

Out-Year Goals. The out-year goals are to use and develop the physical and chemical synthesis methods for design of solid-solid interfaces with unique chemical/mechanical/conductivity properties. The proposed work will develop and exploit a variety of *ex situ* and *in situ* experimental optical and surface sensitive techniques and electrochemical methods to explore and explain bulk and interfacial properties of the selected materials. The results will serve to unravel many puzzling bulk and interfacial properties of S_{Li}-S_{EL}-S_{C} systems, including various types of ceramic and glass materials.

Collaborations. This project funds work at ANL and collaboration with J. Sakamoto at University of Michigan.

Milestones

1. Understand the impact of different dopants in LLZO (niobium versus tantalum versus aluminum) on reactivity by surface and bulk sensitive techniques and spectroscopic methods. (Q1, FY 2019; Completed)
2. Determine the impact of solid electrolyte crystallinity (single crystal versus polycrystalline versus amorphous) on electrolyte reactivity by surface- and bulk-sensitive techniques and spectroscopic methods. (Q2, FY 2019; Completed)
3. Distinguish chemical versus electrochemical reactivity at the interface and bulk of model solid-state electrochemical systems with Li-metal anodes and $LiCoO_2$ cathodes by electrochemical testing and characterization. (Q3, FY 2019; Completed)
4. Determine dopant-dependent impact on chemical reactivity of different interfaces of solid-state electrolytes with lithium metal by computational characterization. (Q4, FY 2019).

Progress Report

Li-LLZO Symmetric Cell Cycling. The team carried out electrochemical testing of Li/LLZO interfaces with different dopants to compare interfacial and bulk changes during electrochemical cycling with the chemical reactivity observed from UHV lithium deposition studies. Electrochemical cycling was done in the symmetric (Li-S_{EL}-Li) coin cell configuration. Thicker lithium films were vacuum-deposited on both sides of UHV-annealed LLZO pellets using the project's Li-LLZO interface preparation procedure, and a clean lithium foil was placed on the freshly deposited lithium films. Symmetric cells were then assembled inside the glove box and tested at room temperature without any stack pressure applied.

Galvanostatic cycling of Li/doped LLZO/Li at 8 μA cm^{-2} (Figure 64a, left) and 2 mA cm^{-2} (Figure 64b, right) exhibit Ohmic behavior for both Al- and Ta- doped samples (based on the charge transfer resistance, ≈50 and ≈25 Ω cm^2, respectively). This indicates that Al- and Ta- doped LLZO are stable against lithium during high current density cycling. Nb-doped LLZO (initial charge transfer resistance ≈ 400 Ω cm^2) displayed higher polarization and significantly longer cycle times needed to reach QSS conditions, consistent with the chemical reactivity with lithium observed previously. Results show that introducing a thin film of vacuum-deposited lithium metal improves electrochemistry at the Li/LLZO interface, yielding a low charge transfer resistance and enabling higher critical current densities during cycling than have been demonstrated thus far.

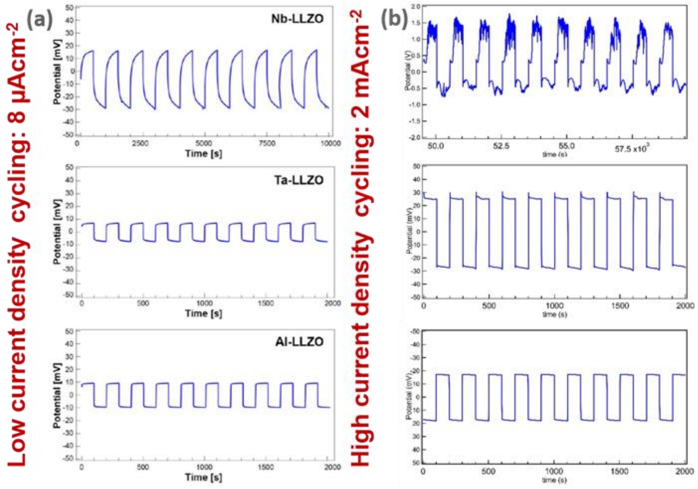

Figure 64. Galvanostatic cycling of Nb- (Top), Ta- (middle) and Al-doped (bottom) LLZO at (a) 8 μA cm^{-2} and (b) 2 mA cm^{-2}. Higher polarization and significantly longer cycle times are needed to reach quasi-steady-state conditions for Nb-doped LLZO.

Electrochemical Stability. After cycling with high current density (> 2mA cm^{-2}), symmetric cells were opened inside a glove box for characterization. LLZO was separated from lithium foil and then polished to remove hundreds of microns of material from the surface and access the bulk. Lanthanum, zirconium, and dopant core level XPS spectra were collected to see if the high current density cycling causes chemical changes inside the solid electrolyte. There is no obvious reduction of zirconium (Figure 65a) or lanthanum (Figure 65b) for all three doped LLZO samples. Nb-doped LLZO showed discoloration, and XPS revealed significant reduction of niobium, as shown in Figure 65c. However, reduction of niobium in the bulk is not necessarily the result of high current cycling, as the same reduction and discoloration happened for Nb-doped LLZO in contact with lithium foil over three days as well. Overall, XPS characterization showed Al- and Ta-doped LLZO are chemically stable to cycling at high current densities when the Li-LLZO interface is generated using lithium thin films.

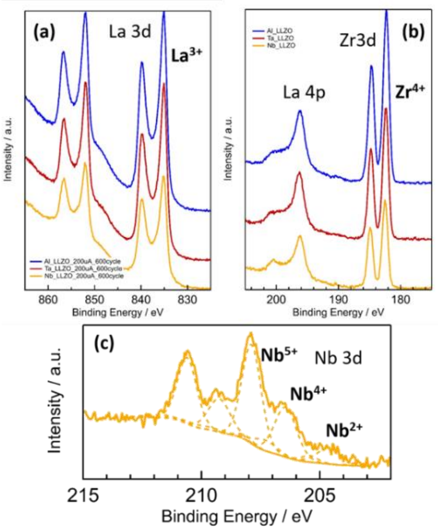

Figure 65. Lanthanum 3d (a), zirconium 3d (b), and niobium 3d (c) core-level X-ray photon spectra from Al-doped (blue), Ta-doped (red), and Nb-doped (yellow) LLZO samples cycled at 2 mA cm^{-2} and then polished to remove ~ 0.3 mm from surface reveal no reactivity of lanthanum and zirconium, but reduction of niobium in the bulk.

Patents/Publications/Presentations

Publication

- Zhu, Y., J. G. Connell, S. Tepavcevic, P. Zapol, R. Garcia-Mendez, N. J. Taylor, J. Sakamoto, B. J. Ingram, L. A. Curtiss, J. W. Freeland, D. D. Fong, and N. M. Markovic. "Dopant-Dependent Stability of Garnet Solid Electrolyte Interfaces with Lithium Metal." *Advanced Energy Materials* 9 (2019): 1803440.

TASK 5 – SULFUR ELECTRODES

Summary

The collected work reported for this quarter involves six projects that have focused on the following:

- Conducting focused fundamental research on the mechanism of “shuttle effect” inhibition for rechargeable Li-S batteries.
- Developing electrode and electrolyte systems that can mitigate the “shuttle effect” so the low self-discharge and long cycle life can be achieved.
- Synthesizing sulfur composite materials with an emphasis on polymer sulfur composite materials.
- Developing creative electrode-making processes to improve processability and aerial capacity; for example, polymeric sulfur composites may not be suitable for the traditional slurry casting process.
- Developing a novel S_xSe_y cathode material for rechargeable lithium batteries with high energy density and long life, as well as low cost and high safety.
- Delivering an electrochemically responsive self-formed hybrid LIC as a protective layer for Li-metal anodes, enabling Li-metal anodes to cycle with a high efficiency.
- Developing high-energy, low-cost Li-S batteries with long lifespan.

Task 5.1 – Novel Chemistry: Lithium Selenium and Selenium Sulfur Couple (Khalil Amine, Argonne National Laboratory)

Project Objective. The project objective is to develop a novel S_xSe_y cathode material for rechargeable lithium batteries with high energy density and long life, as well as low cost and high safety.

Project Impact. Development of a new battery chemistry is promising to support the goal of PHEV and EV applications.

Approach. The dissolution of lithium polysulfides in nonaqueous electrolytes has been the major contribution to the low energy efficiency and short life of Li-S batteries. In addition, the insulating characteristics of both end members during charge/discharge (sulfur and Li_2S) limit their rate capacity. To overcome this problem, sulfur or Li_2S is generally impregnated in a carbon-conducting matrix for better electronic conductivity. However, this makes it difficult to increase the loading density of practical electrodes. It is proposed to solve these barriers using the following approaches: (1) partially replace sulfur with selenium, (2) nano-confine the S_xSe_y in a nanoporous conductive matrix, and (3) explore advanced electrolytes with suppressed shuttle effect.

Out-Year Goals. This new cathode will be optimized with the following goals:

- A cell with nominal voltage of 2 V and energy density of 600 Wh/kg.
- A battery capable of operating for 500 cycles with low capacity fade.

Collaborations. This project engages in collaboration with the following: Professor C. Wang of UMD, Dr. Y. Ren, and Dr. C. Sun of Advanced Photon Source (APS) at ANL, and Dr. L. A. Curtiss at ANL.

Milestones

1. Parasitic reactions study of Li/Se and Se-S systems in different electrolytes. (Q1, FY 2019; Completed)
2. Characterization on the solvation chemistry of concentrated siloxane based electrolytes. (Q2, FY 2019; In progress)
3. Interfacial understanding on the Li/Se-S batteries in different electrolytes. (Q3, FY 2019; Completed)
4. Modify the electrode/electrolytes interface using atomic layer deposition (ALD) and molecular layer deposition (MLD). (Q4, FY 2019; In progress)

Progress Report

In the last two years, the team has developed two kinds of advanced electrolytes to effectively eliminate polysulfides/polyselenides shuttle; one is fluorinated ether-based electrolytes, while the other is concentrated siloxane-based electrolytes. This quarter, by using XPS characterization, the team has conducted the interfacial understanding on the Se-S cathode and lithium metal in different electrolytes to unravel the compositional/structure characteristics of the interfacial layers and the related ionic transport across the interface in Li/Se-S batteries.

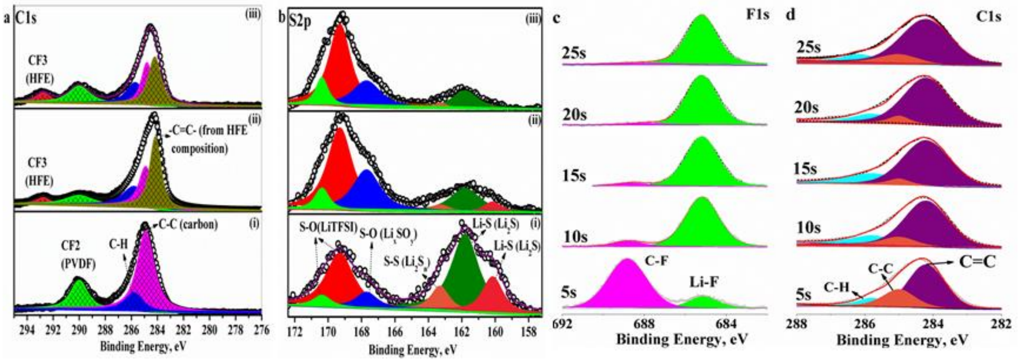

Figure 66. (a) C1s and (b) S2p X-ray photoelectron spectroscopy (XPS) spectra of first discharged $S_{22.2}Se$/KB cathode in (i) DME-based and (ii) HFE-based electrolyte, and (iii) first discharged S/KB cathode in HFE-based electrolytes. XPS spectra of (c) F1s and (d) C1s of first discharged $S_{22.2}Se$/KB cathode in HFE-based electrolytes after different etching time.

Figure 66a-d shows the XPS characterization result of discharged $S_{22.2}Se$/KB cathode in different electrolytes. Compared to the one in DME-based electrolyte, there is an obvious formation of SEI layer on the surface of $S_{22.2}Se$/KB cathode material when discharged in the HFE-based electrolyte. This can be confirmed by evolution of C1s peaks for -CF3 (~ 294 eV) and -C=C- (~ 284 eV) bond due to the decomposition of HFE solvent and also enhanced S2p peaks of sulfate and sulfite (166-172 eV) due to the increased reduction of LiTFSI salt. XPS sputtering experiment further confirmed that the formed SEI layer is robust. Therefore, the origin of different lithiation mechanisms in two electrolytes for the same cathode structure should come from the *in situ* formed SEI layer, which can act as a physical barrier between electrode and electrolytes. In the HFE-based electrolyte, the formed robust SEI layer can de-solvate Li^+ and prevent the attack of solvent molecules toward Se-S, thus leading to the solid-solid lithiation process. In the DME-based electrolytes, there is no such SEI formation, and the solvated Li^+ can easily penetrate into the Se-S active material, thus leading to formation of polysulfides/polyselenides and the solid-liquid-solid lithiation process.

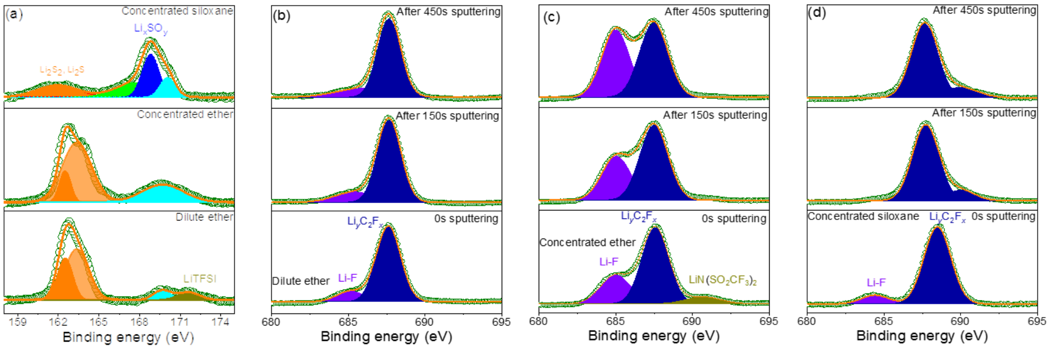

Figure 67. (a) S2p spectra of lithium metal in the Li/S battery after 20 cycles in different electrolytes at C/10. F1s spectra of lithium metal in Li/S battery after 20 cycles in different electrolytes: (b) dilute ether, (c) concentrated ether, and (d) concentrated siloxane.

It has been found that the formation mechanism and the nature of the SEI layers derived from concentrated electrolytes could be fundamentally distinct from those of the traditional SEI and thus enable unusual functions that cannot be realized using regular electrolytes. Hence, the team further examined the interfacial layer on the lithium metal side. During cycling of the Li/Se-S and Li/S battery, the reactivity of lithium metal toward the electrolytes would also dramatically affect cycle performance. The team has therefore conducted XPS characterization on the lithium metal after 20 cycles in different electrolytes. To elucidate the distinct SEI layer as a function of depth in different electrolytes, the team has conducted further XPS characterization using argon sputtering at various times. As shown in Figure 67a, in the ether-based electrolytes (both dilute and concentrated), one can observe a severe accumulation of Li_2S/Li_2S_2 on the surface of lithium metal, while the amount of Li_2S/Li_2S_2 is significantly suppressed in the concentrated siloxane-based electrolytes. This is a clear indicator for the formation of polysulfides even during cycling in the concentrated ether-based electrolytes. Furthermore, depth profiles analysis showed that the SEI layer in the dilute and concentrated ether electrolytes is much thicker than that in the concentrated siloxane electrolyte. Even after 450 s sputtering, LiF, a common SEI component derived from the decomposition of LiTFSI, still existed in the SEI layer. Correspondingly, the SEI after cycling in the concentrated siloxane-based electrolytes is much denser, but thinner; the SEI layers in the ether-based electrolytes are much thicker and porous. This could be attributed to the suppressed reactivity of lithium metal toward concentrated electrolytes.

Next quarter, the team will further work on cathode structure development (surface/interface modification and host structure optimization). In combination with the electrolytes the project has developed, the team will focus on development of long-life and high areal capacity Li/Se-S batteries.

Patents/Publications/Presentations

Patent

- Xu, G., and K. Amine. “Rechargeable Lithium Batteries.” U. S. Patent application; in preparation.

Task 5.2 – Development of High-Energy Lithium-Sulfur Batteries
(Jun Liu and Dongping Lu, Pacific Northwest National Laboratory)

Project Objective. The project objective is to develop high-energy, low-cost Li-S batteries with long lifespan. All proposed work will employ thick sulfur cathode ($\geq$ 2 mAh/cm^2 of sulfur) at a relevant scale for practical applications. The diffusion process of soluble polysulfide out of thick cathode will be revisited to investigate cell failure mechanism at different cycling. The fundamental reaction mechanism of polysulfide under the electrical field will be explored by applying advanced characterization techniques to accelerate development of Li-S battery technology.

Project Impact. The theoretical specific energy of Li-S batteries is ~ 2300 Wh/kg, which is almost three times higher than that of state-of-the-art Li-ion batteries. The proposed work will design novel approaches to enable Li-S battery technology and accelerate market acceptance of long-range EVs required by the EV Everywhere Grand Challenge.

Approach. The project proposes to (1) identify and address key issues of applying high-energy sulfur cathodes including materials, binders, electrode architectures, and functional electrode additives, (2) advance mechanism study of sulfur cathode and electrolyte by using *in situ*/*ex situ* techniques and custom-designed hybrid cell setup, and (3) verify effectiveness of the new approaches with coin/pouch cells by using high-loading electrodes (> 4 mg/cm^2), limited lithium (< 200% lithium excess), and lean electrolyte (E/S < 4 µL/mg).

Out-Year Goals. This project has the following out-year goals:

- Fabricate Li-S pouch cells with thick electrodes to understand sulfur chemistry/electrochemistry in environments similar to real application.
- Leverage the Li-metal protection project funded by the DOE and PNNL advanced characterization facilities to accelerate development of Li-S battery technology.
- Develop Li-S batteries with a specific energy of 400 Wh/kg at cell level, 1000 deep-discharge cycles, improved abuse tolerance, and less than 20% capacity fade over a 10-year period to accelerate commercialization of EVs.

Collaborations. This project engages in collaboration with the following: Dr. X-Q. Yang (BNL), Dr. D. Qu (University of Wisconsin at Madison), Dr. G. Zhang (University of Alabama), and Dr. J. Tao (PNNL).

Milestones

1. Synthesize high Li$^+$ conductivity sulfide-based Li$^+$ conductors with room-temperature conductivity > 1 mS/cm for sulfur cathodes. (Q1, FY 2019; Completed)
2. Develop electrode preparation method for sulfur/Li$^+$-conductor cathodes with sulfur mass loading > 4 mg/cm^2 and sulfur > 75 wt% in whole electrode. (Q2, FY 2019; Completed)
3. Complete electrode composition and architecture optimization for low porosity sulfur electrodes (electrode density >1 g/cm^3). (Q3, FY 2019; Completed)
4. Complete electrochemical evaluation of high-loading sulfur electrodes (> 4 mg/cm^2) at E/S < 3 µL/mg, and identify compatible liquid electrolytes with the cathodes. (Q4, FY 2019; In progress)

Progress Report

The interfacial stability and transport properties of the low-temperature phase $Li_7P_2S_8Br_{0.5}I_{0.5}$ (LT-LPSBI) Li^+ conductor were studied last quarter. To build solid/liquid hybrid Li^+ conduction networks for high-energy Li-S cells by utilizing these novel solid Li^+ ion conductors, the LT-LPSBI particles were further incorporated into sulfur electrode architecture through a new electrode fabrication process. To facilitate sulfur reactions by the interconnected solid Li^+ ion conductor networks, an optimal contact among the triple phases of active sulfur, carbon additive, and the Li^+ conductor is required. Based on a solvent-free electrode processing approach, key factors that affect electrode structure and cell performance were investigated. The availability of the LT-LPSBI for building an efficient Li^+ ion conduction network in high-loading sulfur cathode was first investigated in an all-solid-state Li-S cell. It was found that the types of sulfur host materials and carbon conductors, as well as material mixing procedures, all play critical roles in improvement of sulfur utilization rate while minimizing the LT-LPSBI content in the whole electrode.

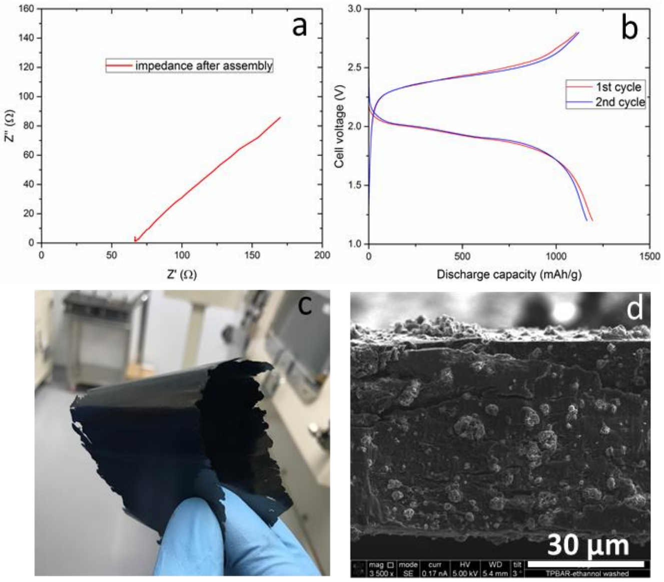

Figure 68. (a) Nyquist plot of a S/SE/Li cell, where SE is solid electrolyte, at room temperature for the frequency range of 100 kHz to 0.01 Hz (voltage modulation was 5 mV, SE=LT-LPSBI). (b) First two-cycle charge/discharge curves of the S/SE/Li cell. (c) Photo image of the high-loading and free-standing sulfur cathode. (d) Cross-section scanning electron microscopy of the high-loading and free-standing sulfur electrode.

Figure 68a shows a typical Nyquist plot of the solid state Li-S cell at optimized conditions. The low overall cell resistance indicates an optimal triple-phase contact inside the electrode with the carefully selected materials and optimized composition. With a sulfur content of 44 wt% and a mass loading of 3.8 mg/cm^2, the solid Li-S cell delivers a reversible capacity > 1200 mAh/g at 0.1 mA/cm^2 at room temperature. Observation of the single discharging plateau at ~ 2.0 V proves the solid-solid sulfur reactions at a relatively low polarization, demonstrating the effectiveness of the LPSBI in building effective Li^+ conduction frameworks. The fully overlapped charge/discharge curves (Figure 68b) indicate robust electrode structure and stable S/C/SE interfaces. Of note, the content of LT-LPSBI in the solid cell is still high (40 wt%), which is expected to be reduced to a reasonably low level through the proposed hybrid electrode design.

The other significant challenge of using the sulfide-based Li^+ ion conductor is the complicated electrode preparation procedure due to moisture sensitivity. In particular, it is very difficult to prepare thin and flexible electrodes because of the very limited binders and solvents that are compatible with sulfide-based electrolytes. A modified solvent-free approach was developed and applied for the sulfur cathode preparation after successfully addressing the binder compatibility and distribution problems. With only 1 ~ 5 wt% binder, free standing and flexible sulfur electrodes can be prepared with controllable thicknesses and sulfur mass loadings. Figure 68c shows a photo image of such a flexible sulfur cathode, which has a sulfur loading > 4.4 mg/cm^2 and a measured electrode density of ~ 2 g/cm^3. The cross section SEM image (Figure 68d) reveals a dense electrode architecture with uniformly distributed LT-LPSBI particles, which is critical for sulfur reactions through a solid-solid pathway. In ongoing research, a rational electrode design with controlled porosity will be developed to demonstrate the concept of the hybrid electrode.

Patents/Publications/Presentations

Presentation

- 235th ECS meeting, Dallas, Texas (May 26–30, 2019): "Understanding of Failure Mechanism of High Energy Lithium-Sulfur Pouch Cells"; L. Shi, D. Lu, C. Niu, X. Ren, J. Xiao, and J. Liu.

Task 5.3 – Nanostructured Design of Sulfur Cathodes for High-Energy Lithium-Sulfur Batteries (Yi Cui, Stanford University)

Project Objective. The charge capacity limitations of conventional TM oxide cathodes are overcome by designing optimized nano-architectured sulfur cathodes. This study aims to enable sulfur cathodes with high capacity and long cycle life by developing sulfur cathodes from the perspective of nanostructured materials design, which will be used to combine with Li-metal anodes to generate high-energy Li-S batteries. Novel sulfur nanostructures as well as multi-functional coatings will be designed and fabricated to overcome issues related to volume expansion, polysulfide dissolution, and the insulating nature of sulfur.

Project Impact. The capacity and the cycling stability of sulfur cathode will be dramatically increased. This project's success will make Li-S batteries to power EVs and decrease the high cost of batteries.

Approach. The approach comprises the three main parts shown below, with primary activities listed.

- ***Advanced Nanostructured Sulfur Cathodes Design and Synthesis.*** (1) Engineer empty space into sulfur cathode to solve the problem of electrode volume expansion. (2) Develop novel sulfur nanostructures with multi-functional coatings for the confinement of S/Li polysulfides to address the issues of active materials loss and low conductivity. (3) Develop/discover optimal nanostructured materials that can capture the polysulfide dissolved in the electrolyte. (4) Develop space efficiently packed nanostructured sulfur cathode to increase the volumetric energy density and rate capability. (5) Identify the interaction mechanism between sulfur species and different types of oxides/sulfides, and find the optimal material to improve the capacity and cycling of sulfur cathode.
- ***Structure and Property Characterization.*** (1) *Ex situ* SEM. (2) XPS analysis. (3) *In operando* XRD and optical microscopy.
- ***Electrochemical Testing.*** (1) Coin cells and pouch cells. (2) A set of electrochemical techniques.

Out-Year Goals. The cycle life, capacity retention, and capacity loading of sulfur cathodes will be greatly improved (200 cycles with 80% capacity retention, > 0.3 mAh/cm^2 capacity loading) by optimizing material design, synthesis, and electrode assembly.

Collaborations. This project engages in collaboration with the following: BMR PIs; SLAC National Accelerator Laboratory: Dr. M. Toney *(In situ* X-ray); and Stanford: Prof. Nix (mechanics) and Prof. Bao (materials).

Milestones

1. Build *in situ* characterization platform to monitor nucleation/dissolution of sulfur/Li_2S_n. (Q1, FY 2019; October 2018, Completed)
2. Develop a noninvasive imaging method with sub-micron, sub-second resolution for Li-S battery in label-free, native organic liquid electrolyte. (Q2, FY 2019; January 2019, Completed)
3. Demonstrate the substrate-dependent electrochemical formation of super-cooled liquid sulfur and crystals, as well as rapid solidification of a super-cooled sulfur droplet. (Q3, FY 2019; April 2019, Completed)
4. Provide direct evidence about a long-debated reaction pathway of surface mechanism versus solution mechanism for sulfur and the current collector effect on sulfur evolution. (Q3, FY 2019; Completed)
5. Investigate the sulfur growth behaviors on different current collectors and correlate the results with their electrochemical performance. (Q4, FY 2019, October 2019; In progress)

Progress Report

Last quarter, the team reported on the rapid solidification of a super-cooled sulfur droplet and suggested the reaction pathway of sulfur nucleation and growth in Li-S batteries. In this report, they systematically investigate sulfur growth behaviors on different current collectors and correlate the results with electrochemical performance.

To evaluate the effect of current collector material on electrochemical performance, Ni-coated (~ 50 nm) aluminum foil was fabricated through e-beam evaporation (denoted as Ni), commercial carbon-coated aluminum (denoted as C), and aluminum foils (denoted as Al) were used as current collectors for Li-S batteries. Coin cells were assembled with lithium polysulfide catholyte using lithium metal as the anode and different planar current collectors at the cathode. The cycling performance of Li-S batteries based on Ni, C, and Al electrodes are shown in Figure 69a. A capacity of 0.98 mAh cm^{-2} was delivered for the Ni electrode at a current density of 0.05 mA cm^{-2}, which retained 95% of its capacity (0.93 mAh cm^{-2}) after 50 cycles (Figure 69b), demonstrating good cycling stability. However, the capacity decayed quickly from 1.12 to 0.16 mAh cm^{-2} for the C electrode with a capacity retention of only 14% when tested at the same conditions. This capacity decay is mainly ascribed to the weak binding between carbon and lithium polysulfides causing the dissolution of polysulfides. Meanwhile, almost no redox reactions occurred on the aluminum surface, which showed a capacity close to zero after three cycles, indicating the non-active surface of aluminum foil. When current density was increased 5 times to 0.25 mA cm^{-2}, the battery with a Ni electrode still delivered a capacity of 0.77 mAh cm^{-2}, 69% of the capacity obtained at 0.05 mA cm^{-2} (Figure 69c), indicating a fast charge/discharge capability; C and Al electrodes could not work at this current density. EIS was performed to further understand the charge transfer and resistance of these electrodes. Figure 69d and inset show the Nyquist plots of the cells with Ni, C, and Al electrodes at open circuit before cycling. The depressed semicircle represents the charge transfer resistance (R_{ct}) on the electrode surface. It can be clearly seen that the R_{ct} of the Ni electrode is much lower than that of the C and Al electrodes (Figure 69d). The smaller resistance indicates that the Ni layer exhibits faster charge transfer compared to that of the other electrodes, which will be further confirmed by theoretical calculations of the Li-ion charge transfer kinetics in later discussion.

To further understand the significantly different battery performance of these electrodes, *in situ* optical observation and *ex situ* experimental characterizations are combined to reveal the underlying mechanism. As sulfur species are sensitive to the atmosphere (for example, water and oxygen), electron beam, and X-ray irradiation, *in situ* optical microscopy is a mild and effective methodology to monitor the morphology evolution of sulfur species on different current collectors. As demonstrated in Figure 70, distinct sulfur growth behaviors were observed on Ni, C, and Al electrodes. As seen from Figure 70a-c, there was no sulfur growth or Li_2S deposition on the surface of Al over the entire range of applied voltage (from 1.0 to 3.0 V), suggesting the inertness of Al surface for sulfur redox. In contrast,

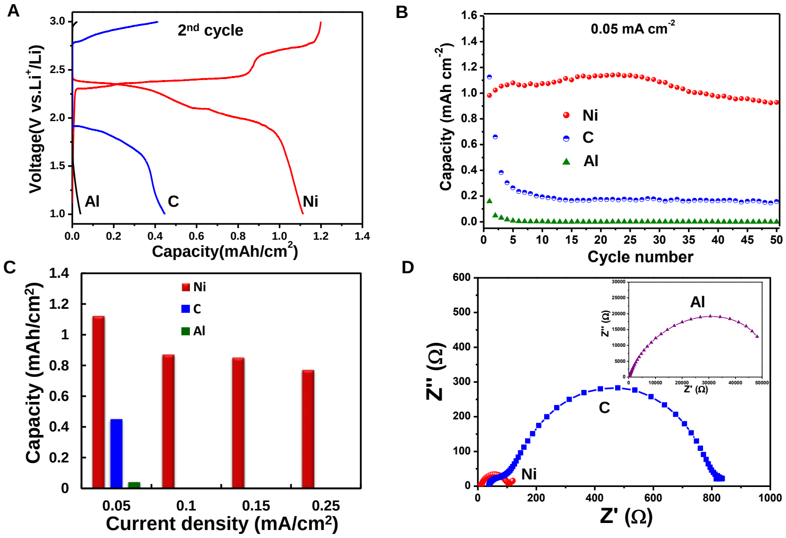

Figure 69. (A) Charge/discharge voltage profiles of the Ni, C, and Al electrodes at a current density of 0.05 mA cm^{-2}. (B) Cycling stability of the Ni, C, and Al electrodes at a current density of 0.05 mA cm^{-2} for 50 cycles. (C) Comparison of the rate capacity of the Ni, C, and Al electrodes. (D) Nyquist plots of the Ni and C electrodes at open circuit before cycling at room temperature. Inset is the Nyquist plot of the Al electrode at open circuit before cycling at room temperature.

many sulfur crystals (highlighted by the red circle) emerged and grew on the surface of the C electrode during charging (Figure 70e). The subsequent discharge process was also monitored, and a large number of flocculent, blurry particles precipitated out during the process (Figure 70f). Most strikingly, spherical liquid sulfur droplets gradually nucleated and grew on the Ni substrate during charging, and all of the sulfur droplets dissolved and finally disappeared from the Ni surface during the discharging process (Figure 2g-i). No clear features of Li_2S were visible after discharge, suggesting that the size of the Li_2S is possibly below the resolution limit of the optical microscope. Therefore, SEM was employed to investigate the morphology change for the sulfur species on different substrates.

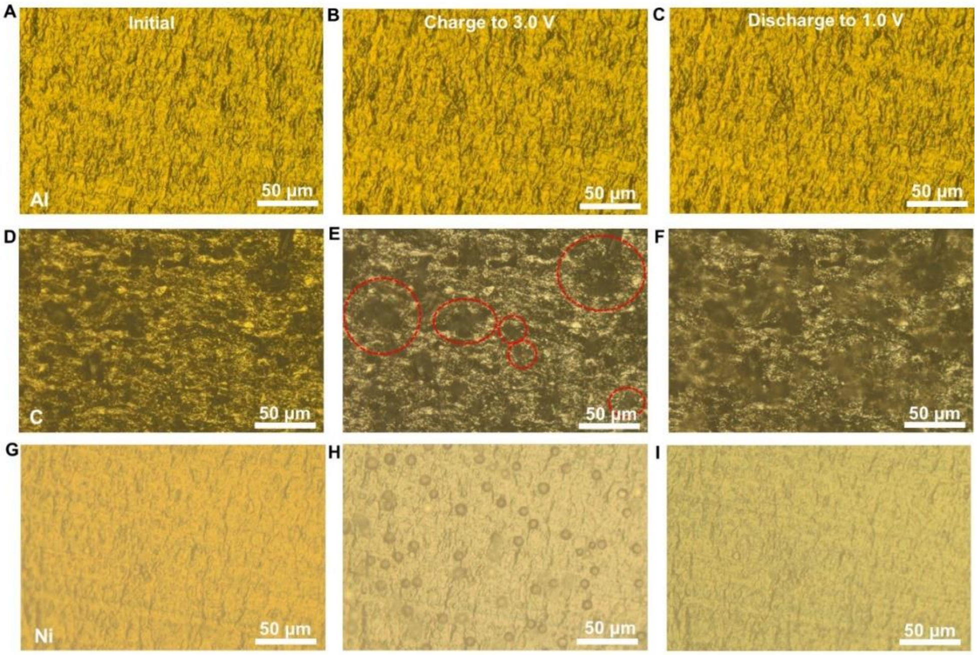

Figure 70. Optical images of the aluminum electrode in lithium polysulfide electrolyte (a) at initial state, (b) after charging to 3.0 V, and (c) after discharging to 1.0 V. Optical images of the carbon electrode in lithium polysulfide electrolyte (d) at initial state, (e) after charging to 3.0 V, and (f) after discharging to 1.0 V. Optical images of the nickel electrode in lithium polysulfide electrolyte (g) at initial state, (h) after charging to 3.0 V, and (I) after discharging to 1.0 V.

Patents/Publications/Presentations

The project has no patents, publications, or presentations to report this quarter.

Task 5.4 –Investigation of Sulfur Reaction Mechanisms (Deyang Qu, University of Wisconsin at Milwaukee; Xiao-Qing Yang, Brookhaven National Laboratory)

Project Objective. The primary objectives are:

- To continue conducting focused fundamental research on the mechanism of "shuttle effect" inhibition for rechargeable Li-S batteries;
- To continue developing the electrode and electrolyte systems that can mitigate the "shuttle effect" so low self-discharge and long cycle life can be achieved.
- To synthesize sulfur composite material with an emphasis on polymer sulfur composite materials.
- To develop creative electrode making processes to improve processability and aerial capacity; for example, polymeric sulfur composite may be unsuitable for the traditional slurry casting process.

The ultimate goal is to develop a practical rechargeable Li-S battery that meets the challenges of powering the next generation of EVs beyond Li-ion technologies.

Project Impact. With development of unique *in situ* electrochemical high-performance liquid chromatography (HPLC)/MS and *in situ* electrochemical microscopic techniques, the mechanisms of all reactions in a Li-S cell can be further understood. Better understanding the sulfur redox reaction will lead to mitigation of the "shuttle effect." The project results will thus guide development of polymer sulfur cathode and Li-S designs for EVs.

Approach. This project will use *in situ* electrochemical HPLC/MS, XPS, SEM, and XRD to study electrochemical reactions associated with sulfur electrodes. Electrochemical techniques such as AC impedance, rotation ring disk electrode, and galvanostat will be used to study the electrode process kinetics. The project will use an *in situ* electrochemical optical method to investigate the surface of lithium anode during cycling of a Li-S cell. It will develop thicker sulfur electrode with high areal capacity using dry process.

One-Year Goals. The one-year goals include the following areas: (1) complete investigations of new electrolytes for mitigating the "shuttle effect" and improving Li-anode performance, and (2) complete preliminary design of new electrode processes and tests of polymeric sulfur composite electrodes.

Collaborations. The PI, D. Qu, is the Johnson Controls Endowed Chair Professor; thus, the team from University of Wisconsin at Madison and BNL has close collaboration with Johnson Controls' scientists and engineers. This collaboration enables the team to validate outcomes of fundamental research in pilot-scale cells. This team has been closely working with top scientists on new material synthesis at ANL, LBNL, and PNNL, with U. S. industrial collaborators at GM, Duracell, and Johnson Controls as well as international collaborators in China, Japan, and South Korea. These collaborations will be strengthened and expanded to give this project a vision on both today's state-of-the-art technology and tomorrow's technology in development, with feedback from the material designer and synthesizers upstream and from industrial end users downstream.

Milestones

1. Literature review and molecular design of polymeric sulfur compounds. (Q1, FY 2019; Completed)
2. Complete screening electrolyte and additives for the Li-S batteries. Start synthesis of polymeric sulfur compounds. (Q2, FY 2019; Completed)
3. Complete preliminary designs of electrode manufacture process and start to explore feasibility for the synthesized polymeric sulfur composite. (Q3, FY 2019; Completed)
4. Complete initial design of electrode manufacture processes and tests of synthesized polymeric sulfur materials. (Q4, FY 2019)

Progress Report

This quarter, while continuing chemical synthesis of different new sulfur-containing copolymer materials, the team started to investigate the impacts of organic sulfide additives in the electrolyte and TM sulfide additives in the polymer sulfur cathode. All experiments were done in coin cells with sufficient amounts of electrolyte.

Additives to Electrolyte. Seven small organic sulfides were investigated: CH_3SCH_3, $C_2H_5SC_2H_5$, $C_3H_7SC_3H_7$ (mono-sulfide); CH_3SSCH_3, $C_2H_5SSC_2H_5$, $C_3H_7SSC_3H_7$ (di-sulfide); and CH_3SSSCH_3 (tri-sulfide). Two types of sulfur cathodes were tested: a typical elemental sulfur cathode (prepared by infusing elemental sulfur S_8 into carbon matrix at 170°C) was tested as a control; a polymeric sulfur cathode (prepared by polymerizing sulfur and monomer organic substrate under heated condition) was also tested. Figure 71a-b shows cycling results for the control and polymeric sulfur cathodes, respectively. Evidentially, small organic sulfides, including dimethyl sulfide (DMS), diethyl sulfide (DES), dipropyl sulfide (DPS), dimethyl disulfide (DMDS), diethyl disulfide (DEDS), dipropyl disulfide (DPDS), and dimethyl trisulfide (DTS) have little influence on the cycle-performance of Li-S (S_8) and Li-PS (polymeric sulfur) batteries.

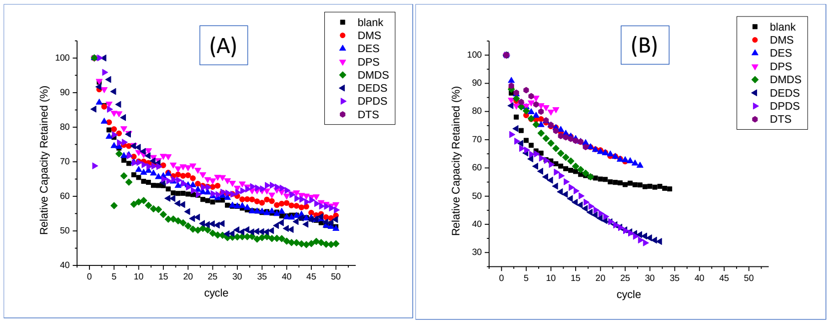

Figure 71. (a) The sulfur cathode is a polymeric sulfur (co-polymerization with monomer) electrode; the averaged capacity is 0.805 mAh discharge/charge. (b) The sulfur cathode is an elemental sulfur electrode; the averaged capacity is 2.075 mAh discharge/charge at 50 uA between 1.8 to 2.8 V.

Metal Sulfide Additives in a Sulfur Cathode. Due to specific interaction between some TMs such as mercury, silver, and copper with elemental sulfur and polysulfides, it is conceivable that sulfides or polysulfides of those metal elements, as a cathode additive, could either effect the redox mechanism of sulfur or localize the polysulfide intermediates within the cathode matrix. Either way, the polysulfide "shuttle effect" could be alleviated. As shown in Figure 72, the Hg/S mixture as an additive has observable influence on cycling performance of Li-S batteries. For the polymeric sulfur cathode without an additive, capacity kept decreasing throughout the entire duration of cycling, even though initial capacity retention was better. Capacity decay of a polymeric sulfur cathode with an additive was mainly observed at the beginning. After the 50th cycle, however, capacity remained relatively steady. The mechanisms of such improvements are still under investigation.

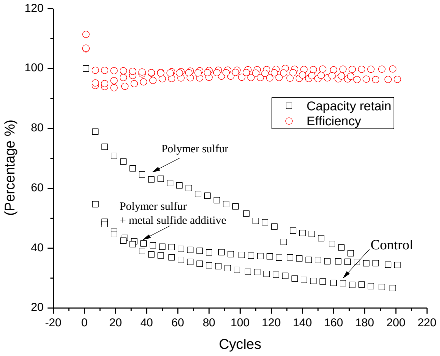

Figure 72. Cycle life of sulfur and polymer sulfur cathodes with metal sulfide additives.

Patents/Publications/Presentations

The project has no patents, publications, or presentations to report this quarter.

Task 5.5 – Electrochemically Responsive, Self-Formed, Lithium-Ion Conductors for High-Performance Lithium-Metal Anodes
(Donghai Wang, Pennsylvania State University)

Project Objective. The project objective is to develop and deliver an electrochemically responsive self-formed hybrid LIC as a protective layer for Li-metal anodes, enabling Li-metal anodes to cycle with a high efficiency of ~ 99.7% at high electrode capacity (> 6 mAh/cm^2) and high current density (> 2 mA/cm^2) for over 500 cycles. The project will also demonstrate prototype ~ 300 mAh Li-S battery cells with energy densities of ~ 200 Wh/kg and ~ 80% capacity retention for ~ 300 cycles at ~ 80% depth of discharge using Li-metal anodes with this protective layer.

Project Impact. This project aims to develop a new hybrid LIC that enables safe and high-performance Li-metal anodes. Use of these anodes in turn enables Li-S batteries with high energy density and long cycling life. Such anodes can also lead to a 50% increase in the energy density of conventional Li-ion batteries with Li-metal oxide cathodes. Meeting the technical targets will potentially develop a new high-energy-density lithium battery, promote increased adoption of EVs and PHEVs, and reduce petroleum consumption in the transportation sector by helping battery-powered vehicles become accepted by consumers as a reliable source of transportation.

Approach. The novel multiphase organo-Li_xS_y or organo-$Li_xP_yS_z$ hybrid ion conductors with tunable multi-functional organic components and controlled Li_xS_y and $Li_xP_yS_z$ inorganic components will be designed and prepared, and thus enable safe use of lithium metal with high CE. In the third year, the team will develop the organo-Li_xS_y/organo-$Li_xP_yS_z$ composite lithium protection layers with tuned functionality: (1) finding appropriate composition, (2) developing appropriate synthesis and fabrication methods, and (3) optimizing organo-Li_xS_y/organo-$Li_xP_yS_z$ components in a protection layer to improve CE and Li-S battery performance.

Out-Year Goals. The project is working toward developing the organo-Li_xS_y/organo-$Li_xP_yS_z$ composite lithium protection layers with tuned functionality. Characterization, performance, and compatibility tests on materials and systems will be conducted. Uniform, dendrite-free lithium deposition under protection of organo-Li_xS_y/organo-$Li_xP_yS_z$ composite lithium protection layers will be demonstrated; CE will be improved.

Collaborations. There are no active collaborations.

Milestones

1. Develop the organo-Li_xS_y/organo-$Li_xP_yS_z$ composite lithium protection layers with tuned functionality. Conduct characterization and performance tests on the materials. (Q1, FY 2019; Completed)
2. Demonstrate uniform and dendrite-free lithium deposition under protection of the organo-Li_xS_y/organo-$Li_xP_yS_z$ composite lithium protection layers. (Q2, FY 2019; Completed)
3. Optimize the organo-Li_xS_y/organo-$Li_xP_yS_z$ composite lithium protection layers and demonstrate lithium anodes cycling with ~ 99.4% CE for ~ 200 cycles. (Q3, FY 2019; Completed)
4. Demonstrate lithium anodes with optimized organo-Li_xS_y/organo-$Li_xP_yS_z$ composite lithium protection layers and ~ 99.7% CE for ~ 300 cycles. (Q4, FY 2019)

Progress Report

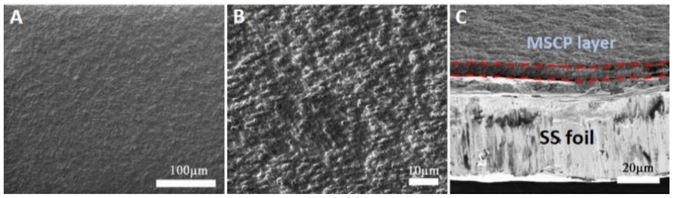

Figure 73. (a-b) Top-view and (c) side-view scanning electron microscopy images of the as-prepared multifunctional sulfur-containing polymer (MSCP) film on stainless-steel foil.

The team is developing a multifunctional sulfur-containing polymer (MSCP); during lithium plating/stripping, the polymers react with lithium metal and *in situ* release lithium sulfides and $Li_xP_yS_z$ at the interface of polymer and lithium metal to form organo-Li_xS_y/organo-$Li_xP_yS_z$ composite protection layer. The morphology of MSCP was investigated by using SEM. As shown in Figure 73, the optimized MSCP film appears to have a uniform coating layer on the substrate with a thickness of around 6.0 µm. The morphology of deposited lithium with an MSCP protection film was investigated. As shown in Figure 74, for lithium deposition on the MSCP film protected SS foil, the MSCP layer on the top surface keeps intact and uniform after cycling (Figure 74d-e). Also, a sandwich cross-section structure can be observed that consists of a top layer of the MSCP film, a middle layer of the deposited dense lithium, and a bottom layer of the SS foil (Figure 74f). The results demonstrate that the MSCP protective layer can provide effective protection for Li-metal anode and enable dendrite-free lithium plating/stripping after long-term cycling.

Chemical components of the SEI layer (MSCP-SEI) using MSCP protection film have been investigated by XPS characterization. As shown in Figures 75 and 76, the chemical components of MSCP-SEI and control SEI layers are analyzed through the deconvoluted S 2p, P 2p, Cl 2p, Li 1s, C 1s, F 1s, and N 1s XPS spectra. In MSCP-SEI, peaks at 160.5 and 161.3 eV in S 2p spectra (Figure 75a) can be ascribed to the inorganic sulfide components Li_2S, Li_2S_2, and Li_3PS_x. The existence of Li_3PS_x components can be confirmed from the P 2p spectra (Figure 75b). The peak at 163.3 eV in S 2p spectra corresponding to S−S and C−S bonds can be ascribed to the inorganic polysulfides (Li_2S_n, $n \geqslant 3$) and the polymer-tethered organo(poly)sulfide. The existence of polymer-tethered organo-(poly)sulfide can also be verified from the C−S bond in C 1s spectra (Figure 76a). In addition, inorganic salts such as LiCl, LiF, and Li_xNO_y can be observed from Cl 2p (Figure 75c), F 1s (Figure 76b), and N 1s (Figure 76c) spectra, respectively. The existence of multiple lithium salts and lithium sulfides can also be confirmed from the Li 1s spectra (Figure 75d). The MSCP-SEI shows a higher content of carbon (36.82%), sulfur (10.16%), phosphorus (3.48%), and chlorine (1.19%), but a lower content of oxygen (28.24%), lithium (16.52%), nickel (1.51%), and fluorine (2.08%), compared with that of control SEI (carbon, 11.63%; sulfur, 3.16%; phosphorus, 0%; chlorine, 0%; oxygen, 42.14%; lithium, 35.44%; nickel, 11.63%; and fluorine, 5.83%), as shown in Figure 75i. The higher content of carbon in MSCP-SEI implies polymer-dominant SEI rather than inorganic-dominant SEI, which is attributed to significant participation of MSCP into the SEI formation. The contribution of MSCP to MSCP-SEI also manifests at a higher content of sulfur species in MSCP-SEI due to chemical/electrochemical decomposition of the sulfur species from MSCP at the interfaces. The higher content of phosphorus species in MSCP-SEI particularly indicates the

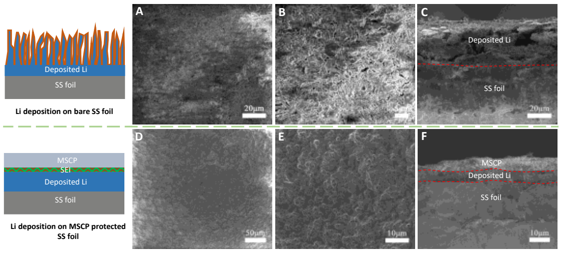

Figure 74. (a-b) Top-view and (c) side-view scanning electron microscopy (SEM) images of deposited lithium on bare stainless-steel foil after 10 cycles. (d-e) Top-view and (f) side-view SEM images of deposited lithium on multifunctional sulfur-containing polymer (MSCP) film protected stainless-steel foil after 10 cycles. The cells were cycled at 2 mA cm^{-2} and 2 mAh cm^{-2}.

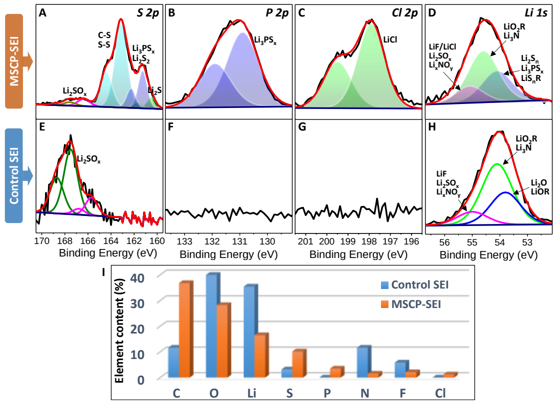

Figure 75. S 2p, P 2p, Cl 2p, and Li 1s X-ray photoelectron spectroscopy (XPS) spectra of (a-d) multifunctional sulfur-containing polymer (MSCP) SEI and (e-h) control SEI. (i) Elemental composition comparison of control SEI and MSCP-SEI calculated on the basis of the XPS spectra.

presence of Li_3PS_x species in the SEI. On the other side, lower content of nickel and fluorine in MSCP-SEI indicates an alleviated decomposition of LiTFSI and $LiNO_3$ salts by using MSCP, as LiTFSI is the only source of fluorine and both LiTFSI and $LiNO_3$ are the only sources of nickel in the electrolyte. Furthermore, the lower content of lithium and oxygen in MSCP-SEI indicates a reduced consumption of the lithium salt as well as electrolyte by using MSCP.

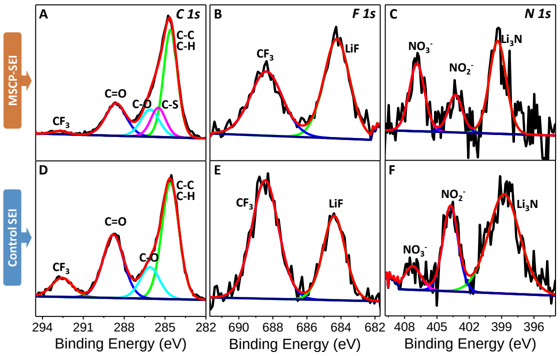

Figure 76. C 1s, F 1s, and N 1s X-ray photoelectron spectra of (a-c) multifunctional sulfur-containing polymer (MSCP) SEI and (d-f) control SEI.

The team evaluates electrochemical cycling performance of lithium deposition using the MSCP protection layer to illustrate its advantages. As shown in Figure 77, compared with the fast drop of CE using bare SS foil, cells using MSCP protected SS foil can maintain high CE for prolonged cycle life. Specifically, an average CE of 98.7% for over 950 cycles at 1 mA cm^{-2} and 1 mAh cm^{-2} (Figure 77a) and an average CE of 98.5% for over 460 cycles at 2 mA cm^{-2} and 2 mAh cm^{-2} (Figure 77b) can be achieved for cells using the MSCP-protected SS foil. Even at higher capacities of 3 and 4 mAh cm^{-2}, very stable cycling can also be achieved (Figure 77c-d), respectively. Figure 78a shows voltage profiles as a function of time of two Li||Li symmetric cells using bare or MSCP protected Li-metal foils. The cell using MSCP-protected Li-metal foils shows lower voltage overpotential (< 120 mV) and stable cycling for more than 800 h without an obvious voltage fluctuation compared with control cells. Finally, the MSCP protection for Li-metal anode was further evaluated in full cells using LFP (~ 2.4 mAh/cm^2) cathode and the MSCP-protected Li-metal anode. As shown in Figure 78b, the cell with MSCP protected Li-metal anode shows significantly increased cycling performance, with a capacity retention of ~ 89.4% even after 500 cycles and an improved average CE of ~ 99.9%. Furthermore, the team found that an anode-free cell using MSCP-protected SS foil as anode and using LFP as cathode shows remarkably improved cycling stability over that in a bare SS foil anode-free cell (Figure 78c).

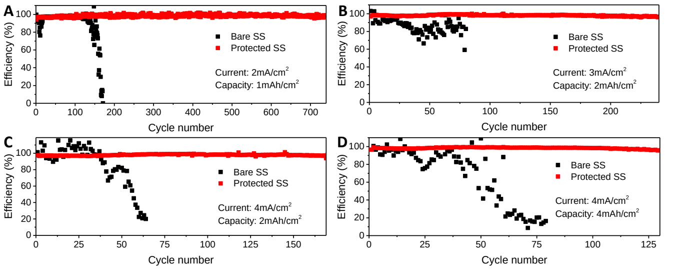

Figure 77. Coulombic efficiency of cells using bare (black) and multifunctional sulfur-containing polymer (MSCP) protected (red) stainless-steel foil versus cycle number at (a) 1 mA cm^{-2} and 1 mAh cm^{-2}, (b) 2 mA cm^{-2} and 2 mAh cm^{-2}, (c) 2 mA cm^{-2} and 3 mAh cm^{-2}, and (d) 2 mA cm^{-2} and 4 mAh cm^{-2}.

The team is also developing a high-zeta-potential porous film containing nano/submicron-sized pores, called a leaky film, to promote electrokinetic phenomena for enhancement of the Li-ion transport (Figure 79a) and to enable uniform deposition of Li-metal anodes. The leaky film was composed of crosslinked polyethylenimine (PEI)-based polyurea (PEIPU), PEO, and SiO_2 nanoparticles (PEIPU–PEO–SiO_2, designated as PPS). PPS leaky films on copper or lithium substrates (designated as PPS@Cu or PPS@Li, respectively) were prepared by successive coating of PEI–SiO_2–PEO colloidal solution and hexamethylene diisocyanate (HDI) solution onto the substrate, followed by *in situ* crosslinking between PEI and HDI. SEM images (Figure 79b–d) display a rough surface morphology of the polymer composite film on the copper

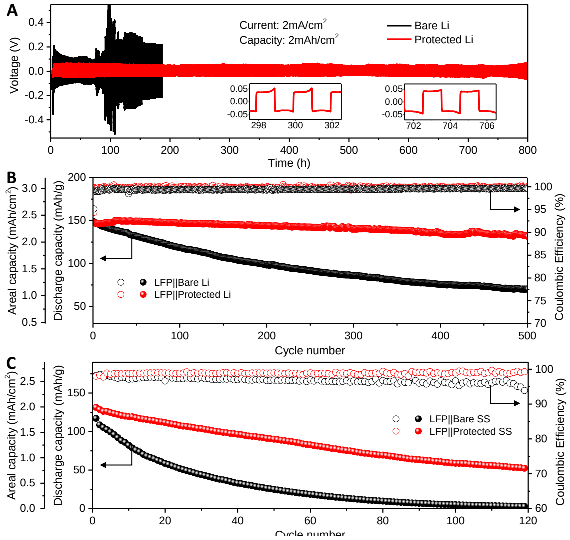

Figure 78. (a) Cycling performance of symmetric cells using bare (black) or multifunctional sulfur-containing polymer (MSCP) protected (red) Li-metal foils cycled at 2 mA cm^{-2} and 2 mAh cm^{-2}. (b) Cycling performance of Li||LFP full cells using bare (black) and MSCP protected (red) Li-metal as anode at 0.5 C (1 C = 170 mAh/g). (c) Cycling performance of anode-free stainless-steel (SS)||LFP cells using bare SS foil (black) and MSCP protected (red) SS foil as anode at 0.5 C.

foil containing submicron-sized pores, which endow the film with a “leaky” property; the measured leaky rate is ≈ 2.82 mL cm^{-3} s. Due to the unique chemical structure and Li-ion affinity, PPS leaky film cannot only self-concentrate the lithium ion, but also induce electrokinetic phenomena to enhance Li-ion transport, which can be directly demonstrated by linear sweep voltammetry (LSV). As shown in Figure 79e, the higher current density of PPS leaky film electrode at voltages of −0.4 and −1.1 V is attributed to improved local Li-ion concentration in the leaky film, owing to its Li-ion affinity to adsorb lithium ion. The Li-ion affinity also drives formation of EDL on the leaky film surfaces, evidenced by measured zeta potential of + 36 mV in the electrolyte [1.0 m lithium hexafluorophosphate ($LiPF_6$) in EC and diethyl carbonate (DEC); V/V = 1]. The existence of EDL induces electrokinetic surface conduction within the leaky film under an electric field. The electrokinetic surface conduction can enhance the Li-ion transport to overcome the diffusion-limited current under strong Li-ion depletion conditions, which are manifested by dramatic increase of current density of PPS leaky film electrode above −1.1 V in LSV.

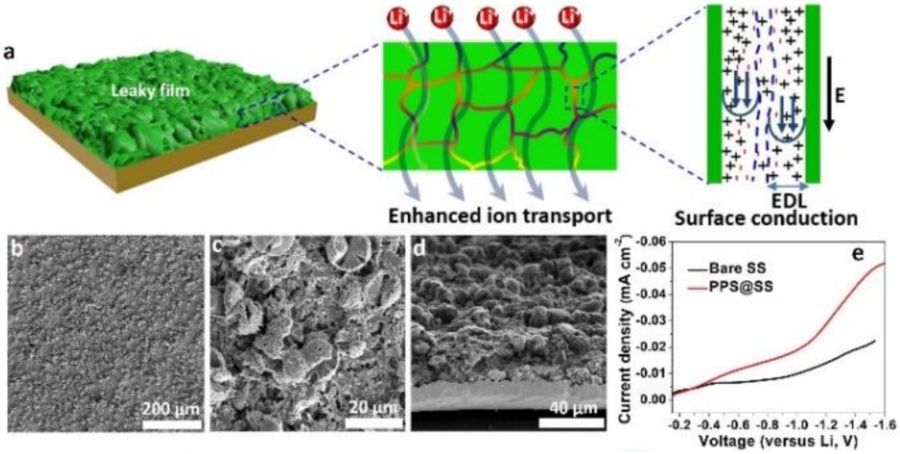

Figure 79. (a) Electrokinetic phenomena (that is, electrokinetic surface conduction) enhance Li-ion transport in the leaky film under applied electric field in the electrolyte. (b-d) Scanning electron microscopy morphology of the PPS leaky film. (e) The linear sweep voltammetries of PPS@stainless steel (PPS@SS) and bare SS electrodes.

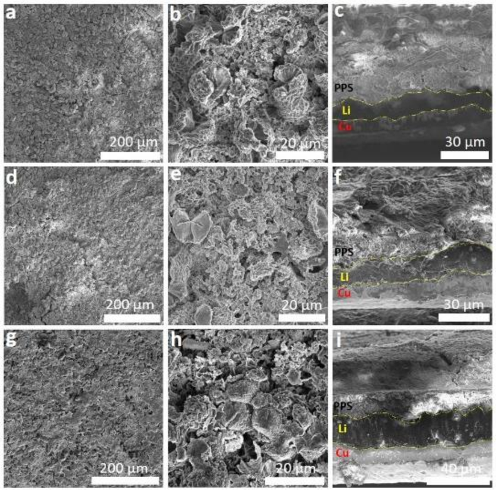

Figure 80. Morphologies of lithium metal deposited on PPS@Cu at different deposition capacities and current densities. (a–c) 2 mAh cm^{-2} and 1 mA cm^{-2}. (d–f) 4 mAh cm^{-2} and 2 mA cm^{-2}. (g–i) 6 mAh cm^{-2} and 2 mA cm^{-2}.

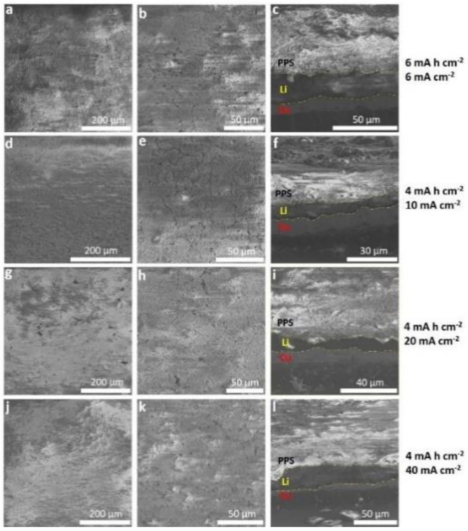

Figure 81. Morphology of lithium metal deposited on PPS@Cu at different deposition capacities and current densities. (a-c) 6 mA h cm^{-2} and 6 mA cm^{-2}. (d-f) 4 mA h cm^{-2} and 10 mA cm^{-2}. (g-i) 4 mA h cm^{-2} and 20 mA cm^{-2}. (j-l) 4 mA h cm^{-2} and 40 mA cm^{-2}.

The Li-ion transport enhancement PPS leaky film can effectively suppress the growth of dendritic lithium at high deposition capacities and high current densities in a carbonate-based electrolyte. As shown in SEM images, the deposited lithium demonstrates a uniform, compact, and dendrite-free morphology without penetrating the PPS layer under various deposition capacities and current densities (2 mAh cm^{-2}, 1 mA cm^{-2} in Figure 80a–c; 4 mAh cm^{-2}, 2 mA cm^{-2} in Figure 80d–f; 6 mAh cm^{-2}, 2 mA cm^{-2} in Figure 80g–i; 6 mAh cm^{-2}, 6 mA cm^{-2} in

Figure 81a–c). Notably, even at high rates of 2.5 C (4 mAh cm^{-2}, 10 mA cm^{-2} in Figure 81d–f), 5 C (4 mAh cm^{-2}, 20 mA cm^{-2} in Figure 81g–i) and 10 C (4 mAh cm^{-2}, 40 mA cm^{-2} in Figure 81j–l), the uniform and compact lithium layer can still be achieved under the PPS leaky film.

The uniform and dendrite-free deposition of lithium enabled by PPS leaky film leads to an improvement of the lithium plating/stripping CE. At a deposition capacity of 2 mAh cm^{-2} and a current density of 1 mA cm^{-2}, the cells containing PPS leaky film deliver an enhanced average CE of 97.8% over 150 cycles (Figure 82a). When deposition capacities increased to 4 mAh cm^{-2} (Figure 82b) and 6 mAh cm^{-2} (Figure 82c) at a current density of 2 mA cm^{-2}, the cells containing PPS leaky film still maintained high average CE of 97% over 100 cycles and 96.9% over 90 cycles, respectively. In contrast, the bare copper electrodes show very poor CE and cycling stability. Figure 82d shows the cycling stability of symmetric Li-metal cells at a current density of 1 mA cm^{-2} and a deposition capacity of 2 mAh cm^{-2}. Compared with the bare Li-metal anodes exhibiting a gradual increase in hysteresis over cycles by almost 250% after 800 h, Li-metal anodes with PPS leaky film show good cycling stability with a low overpotential at ≈ 40 mV for over 1000 h.

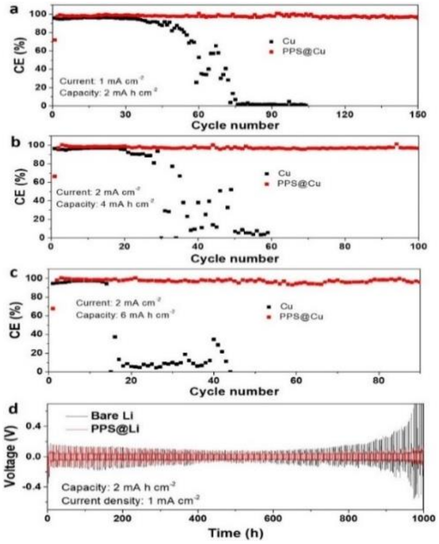

Figure 82. Electrochemical performance of PPS@Cu and bare copper foil electrodes. Coulombic efficiency of lithium plating/stripping on PPS@Cu and bare copper foil at a current density of 1 mA cm^{-2} and a deposition capacity of 2 mA h cm^{-2} (a), at a current density of 2 mA cm^{-2} and a deposition capacity of 4 mA h cm^{-2} (b), and at a current density of 2 mA cm^{-2} and a deposition capacity of 6 mA h cm^{-2} (c). (d) Cycling stability of symmetric cells using PPS leaky film protected lithium metal as electrodes.

The stable Li-metal anodes enabled by the PPS leaky film ensure their high performance in Li-metal batteries. Full cells were assembled using thin PPS@Li foil (≈ 120 µm) as anodes and high-areal-capacity NCM-811 (≈ 4.2 mAh cm^{-2}) (PPS@ Li|NCM-811) as cathodes. When flooded electrolyte was used (Figure 83a), the cells with PPS@Li delivered a high initial discharge capacity of 165.4 mAh g^{-1}, and still maintained the capacity of 132.8 mAh g^{-1} after 200 cycles (80.3% capacity retention) with an average CE of 99.4%, while the control cells show a fast capacity decay after 100 cycles. Under lean electrolyte conditions, it is expected that the cells exhibit worse cycling performance than that of cells with flooded electrolyte, as the reduced electrolyte greatly decreases cycling life. The team found that the cells with PPS@Li anodes still exhibit improved cycling stability, capacity retention, and CE compared with control cells under the lean electrolyte condition, as shown in Figure 83b (5 µL mAh^{-1}) and Figure 83c (3 µL mAh^{-1}).

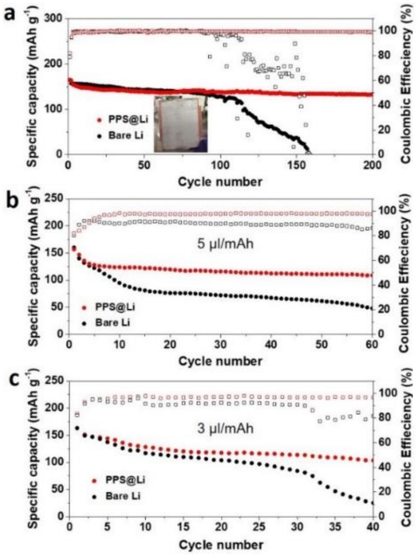

Figure 83. Cycling performance of full cells using PPS leaky film protected lithium metal as anodes and NCM-811 as cathodes. (a) Flooded electrolyte. (b) Lean electrolyte of 5 µl/mA h. (c) Lean electrolyte of 3 µl/mA h. The photo image of lithium foil protected by PPS leaky film (20 cm × 15 cm) is shown as an inset in (a); the thickness of lithium foil is 120 µm. The areal capacity of NCM-811 cathode is around 4.2 mA h cm^{-2}.

Patents/Publications/Presentations

Publications

- Zhao, Y. M., G. X. Li, Y. Gao, D. W. Wang, Q. Q. Huang, and D. H. Wang. "Stable Li Metal Anode by a Hybrid Lithium Polysulfidophosphate/Polymer Cross-Linking Film." *ACS Energy Letters* 4 (2019): 1271–1278.
- Li, G. X., Z. Liu, D. W. Wang, X. He, S. Liu, Y. Gao, A. AlZahrani, S. H. Kim, L. Q. Chen, and D. H. Wang. "Electrokinetic Phenomena Enhanced Lithium-Ion Transport in Leaky Film for Stable Lithium Metal Anodes." *Advanced Energy Materials* 9 (2019): 1900704.

Task 5.6 – New Electrolytes for Lithium-Sulfur Battery
(Gao Liu, Lawrence Berkeley National Laboratory)

Project Objective. The project objective is to develop new electrolytes, additives, and electrode compositions for Li-S battery with high ion-conductivity, stable toward polysulfide and promoting the polysulfide affiliation with the electrode substrate to prevent polysulfide dissolution.

Project Impact. This work will address the high cost and low energy density of the Li-ion rechargeable batteries. The emerging Li-S batteries could be both high energy density and low cost. This project enables the applications of the low-cost, abundant sulfur element as a major chemical component for electrical energy storage. This project will develop new approaches for electrolytes and electrode compositions of Li-S rechargeable batteries.

Approach. This project aims to develop new electrolytes and additives for Li-S battery. The properties of the ideal electrolyte for sulfur electrode would be high ion conductivity, stable towards polysulfide, and promoting the polysulfide affiliation with the electrode substrate to prevent polysulfide dissolution. The project is designed to first understand the electrode substrate interaction with the polysulfides in different electrolytes. This will lead to better understandings of the polysulfide nucleation and precipitation mechanisms in common electrolytes. The second stage of the project will focus on chemically modifying the structures of the solvent and salt electrolyte molecules to increase electrolyte stability and ionic conductivity and to prevent polysulfide dissolution and promote polysulfides precipitation.

Out-Year Goals. The team will also investigate the contribution of Li-metal electrodes to the overall Li-S battery performance and develop methods to stabilize Li-metal surface.

Collaborations. This project collaborates with Dr. J. Guo and Dr. W. Yang (ALS/LBNL), Prof. A. Minor (National Center for Electron Microscopy at LBNL/UC Berkeley), Dr. L-W. Wang (LBNL), and Prof. P. Balbuena, TAMU.

Milestones

1. Identify the baseline electrolyte compositions and electrode composition and configuration for Li-S study. (Q1, FY 2019; Completed)
2. Develop polymer binders with different affiliation functional groups with polysulfides, and use baseline electrolytes to investigate dissolution and precipitation of polysulfides. (Q2, FY 2019; Completed)
3. Develop *in situ* cells for synchrotron analysis with improved spatial resolution. (Q3, FY 2019; Completed)
4. Formulate one composition of the new electrolyte for Li-S battery and test its performance. (Q4, FY 2019)

Progress Report

This quarter's research is focused on understanding sulfur composite materials and the effect of binder. A new approach was proposed and developed by the team to use nucleophilic substitution reaction between the dissolved polysulfides and leaving groups on the polymer binder to immobilize polysulfides on to the electrode [*Nano Energy* 38 (2017): 82]. Polymer binders that form strong electronic static interaction or covalent binding with the polysulfide have been investigated this quarter. Polyisoprene (PIP) is a promising new binder material for sulfur electrode. PIP can play a dual role as composite with sulfur materials and as a binder for the composite electrode. A polyisoprene-sulfur (PIPS) copolymer and nano-sulfur composite material (90 wt% sulfur) is synthesized through inverse vulcanization of PIP polymer with sulfur micron-size particles for high areal capacity Li-S batteries. To evaluate the properties of PIPS and sulfur nanocomposite materials, HRTEM images are collected, as shown in Figure 84. A typical polycrystalline structure, Debye rings in Figure 84b/e, is presented through inverse FFT. The Debye rings originated from Figure 84a/d clearly demonstrate the success of copolymerization and the incorporation of nano-domain sulfur in connection with the sulfur crosslinkers. The homogeneous distribution at nano-scale is verified by the randomly distributed polycrystalline without preferred orientation.

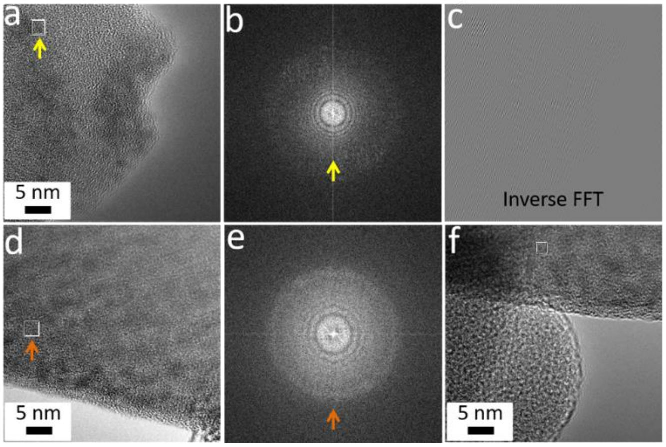

Figure 84. Transmission electron microscopy images of the PIPS and sulfur nanocomposite materials. The polycrystalline structure is verified by the Debye rings in 1b and 1e, corresponding to the square area pointed by the arrow in 1a and 1d, respectively. Panel (c) shows the inverse fast Fourier transform (FFT) of the square area pointed in (f).

The branched PEI polymer with a high density of amine groups was also further investigated to trap lithium polysulfides through the interaction between –NH in the amine group and soluble Li_2S_x, as shown in Figure 85. To boost this interaction, cationization was achieved through nucleophilic substitution with CH_3I, where the cationic PEI (denoted as MPEII) exhibited enhanced affinity to polysulfides. MPEII attracted not only lithium polysulfide through Li–N and Li–I attraction, but also S_x^{2-} by electrostatic attraction of the positively charged nitrogen after cationization. The cell with MPEII binder exhibited better performance than that with PEI in the self-discharge test.

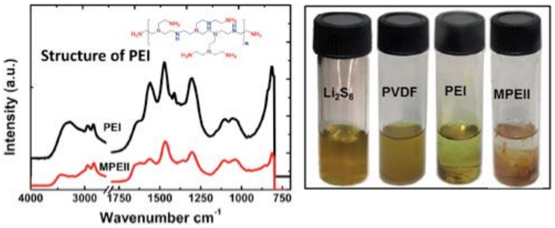

Figure 85. (a) Infrared spectra of polyethylenimine (PEI) polymer and cationic PEI (MPEII). (b) The polysulfide adsorption force comparison.

Patents/Publications/Presentations

Publications

- Liu, G., et al. "Polyisoprene Captured Sulfur Nanocomposite Materials for High Areal-Capacity Lithium Sulfur Battery." *ACS Applied Polymer Materials* 1 (2019): 1965−1970.
- Liu, G., et al. "Recent Advances in Polysulfide Mediation of Lithium-Sulfur Batteries via Facile Cathode and Electrolyte Modification." *APL Materials* 7 (2019): 080902.

TASK 6 – AIR ELECTRODES / ELECTROLYTES

Summary and Highlights

High-density energy storage systems are critical for EVs required by the EV Everywhere Grand Challenge. Conventional Li-ion batteries still cannot fully satisfy the ever-increasing needs because of their limited energy density, high cost, and safety concerns. As an alternative, the rechargeable lithium-oxygen (Li-O_2) battery has potential to be used for long-range EVs. The practical energy density of a Li-O_2 battery is expected to be ~ 800 Wh kg^{-1}. The advantages of Li-O_2 batteries come from their open structure; that is, they can absorb the active cathode material (oxygen) from the surrounding environment instead of carrying it within the batteries. However, the open structure of Li-O_2 batteries also leads to several disadvantages. The energy density of Li-O_2 batteries will be much lower if oxygen must be provided by an onboard container. Although significant progress has been made in recent years on fundamental properties of Li-O_2 batteries, research in this field is still in an early stage, with many barriers to be overcome before practical applications. These barriers include:

- Instability of electrolytes—The superoxide species generated during discharge or O_2 reduction process is highly reactive with electrolyte and other components in the battery. Electrolyte decomposition during charge or O_2 evolution process is also significant due to high over-potentials.
- Instability of air electrode (dominated by carbonaceous materials) and other battery components (such as separators and binders) during charge/discharge processes in an O-rich environment.
- Corrosion of Li-metal anode in an electrolyte saturated with oxygen.
- Low energy efficiency associated with large over-potential and poor cyclability of Li-O_2 batteries.
- Low power rate capability due to electrode blocking by the reaction products.
- Absence of a low-cost, high-efficiency oxygen supply system (such as oxygen selective membrane).

The main goal of this Task is to provide a better understanding on the fundamental reaction mechanisms of Li-O_2 batteries and identify the required components (especially electrolytes and electrodes) for stable operation of Li-O_2 batteries. This task will investigate several new approaches to improve stability of Li-metal anode in Li-O_2 batteries:

- Li-metal anodes will be protected using two approaches: (1) *in situ* formation of a stable SEI layer before Li-O_2 cell operation through various electrolyte formulations and treatment protocols, and (2) *ex situ* formation of stable inorganic/polymeric hybrid electrolyte layers through dip-coating or tape-casting method to coat the inorganic/polymeric hybrid electrolyte layer on Li-metal surface.
- A joint theoretical/experimental approach for design and discovery of new cathode and electrolyte materials will act synergistically to reduce charge overpotentials and increase cycle life. Synthesis methods, in combination with design principles developed from computations, will be used to make new cathode architectures. Computational studies will be used to help understand decomposition mechanisms of electrolytes and how to design electrolytes with improved stability.
- A new cathode will be developed based on high-efficiency catalyst such as two-dimensional TM dichalcogenides. These cathode materials will be combined with new electrolyte blends and additives that work in synergy to reduce charge potentials and increase stability of the Li-air system.

State-of-the-art characterization techniques and computational methodologies will be used to understand charge and discharge chemistries. Success of this Task will establish a solid foundation for further development of Li-O_2 batteries toward practical applications for long-range EVs. The fundamental understanding and breakthrough in Li-O_2 batteries may also provide insight on improving performance of Li-S batteries and other energy storage systems based on chemical conversion process.

Highlights. The Task highlights for this quarter are as follows:

- Amine and Curtis confirmed through EIS studies that the electronic conductivity of LiO_2 is higher than that of Li_2O_2, which can lead to reduced charge over-potentials in batteries forming this discharge product.
- Curtiss, Ngo, and Salehi systematically investigated 24 redox mediators as effective additives for Li-O_2 batteries and will use some of these in future development of Li-O_2 batteries.
- The Zhang and Xu group found that protected Li-C composite anode leads to more stable cycle performance of Li-O_2 cells.

Task 6.1 – Rechargeable Lithium-Air Batteries
(Ji-Guang Zhang and Wu Xu, Pacific Northwest National Laboratory)

Project Objective. The objective of this project is to develop rechargeable lithium-oxygen ($Li\text{-}O_2$) batteries with long-term cycling stability. In FY 2019, the team will pay more attention to lithium anode stabilization and building a more stable $Li\text{-}O_2$ battery based on the protected lithium anode and optimized air-electrodes to develop practical $Li\text{-}O_2$ batteries with stable, long-term cycling capability.

Project Impact. Li-air batteries have a theoretical specific energy more than five times that of state-of-the-art Li-ion batteries and are potential candidates for use in next-generation, long-range EVs. Unfortunately, the poor cycling stability and low CE of Li-air batteries have prevented their practical application. This work will explore well-protected Li-metal anodes, new electrolytes, and high-loading air-electrodes that could lead to long cyclability and high CE in high-energy Li-air batteries that can be used in the next-generation EVs required by the EV Everywhere Grand Challenge.

Approach. Li-metal anodes will be protected using highly elastic and stable protective composite layers and gel-polymer crosslinked electrolytes. These membranes will be prepared through dip-coating or tape-casting method to coat the inorganic/polymeric hybrid electrolyte layers. Stable host structures for lithium metal will also be investigated to stabilize Li-metal anode in oxygen atmosphere. The electrochemical performances of $Li\text{-}O_2$ batteries using the protected Li-metal anodes and the previously developed carbon/catalyst composite air electrodes based on carbon nanotubes (CNTs) and TM oxides such as RuO_2 will be evaluated. The lithium anodes, air-electrodes, and $Li\text{-}O_2$ cells at different stages of cycling (including as-prepared, after discharge, after recharge, and after cycling) will be analyzed by microscopy and spectroscopy techniques such as SEM, EDX, TEM, XRD, and XPS.

Out-Year-Goals. The long-term goal is to enable rechargeable Li-air batteries with a specific energy of 800 Wh/kg at cell level, 1000 deep-discharge cycles, improved abuse tolerance, and less than 20% capacity fade over a 10-year period to accelerate commercialization of long-range EVs.

Collaborations. This project collaborates with C. Wang of PNNL on characterization of cycled air electrodes by TEM/SEM.

Milestones

1. Develop highly elastic and stable protective composite layers for lithium anode in $Li\text{-}O_2$ batteries. (Q1, FY 2019; Completed)
2. Protect Li-metal anode by using gel-polymer crosslinked electrolytes $Li\text{-}O_2$ batteries. (Q2, FY 2019; Completed)
3. Develop stable host structure to protect lithium anode in oxygen rich environment. (Q3, FY 2019; Completed)
4. Complete evaluation of cycling performance of $Li\text{-}O_2$ batteries with protected Li-metal anodes and optimized air-electrodes. (Q4, FY 2019)

Progress Report

This quarter, a protected host structure for anode used in Li-O_2 batteries was investigated. Both conductive carbon matrix and protection layer have been used to stabilize Li-metal anode, as shown in Figure 86. A carbon paper (see Figure 86a) was used as a conductive matrix; it was treated by ammonium hydroxide solution in 24 h to functionalize the surface for facile Li-metal soaking. After functionalization of carbon fabric, it was transferred in argon-filled glove box and soaked by molten lithium metal at 300°C for 30 min (Figure 86b). After lithium infiltration, additional lithium was removed, and Li-C composite was cooled down. A Nafion-Al_2O_3 composite layer (NCL) was prepared and coated on Li-C composite as a stable protective composite layer to protect Li-C composite anode in an oxygen-rich environment. Nafion was selected because it can form a stable polymer against the reactive oxygen. Figure 86c-d shows optical images of anode before and after NCL coating. The smooth side of the anode is coated with NCL.

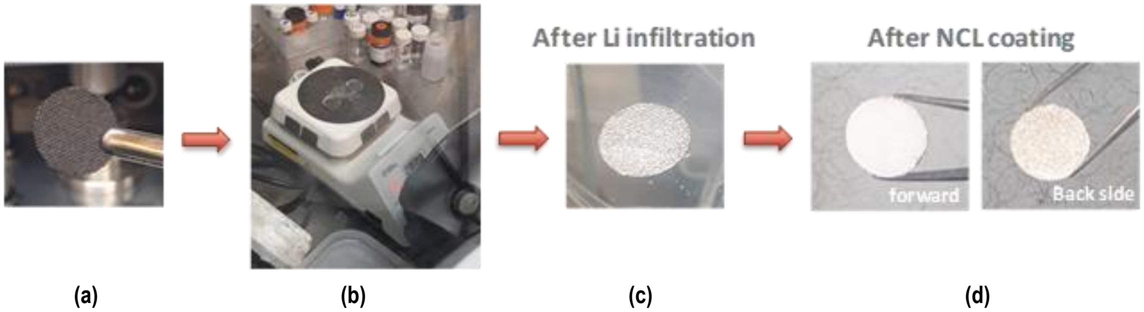

Figure 86. Process of Li-C composite fabrication by lithium infiltration in surface functionalized carbon fabric and protective layer (Nafion-Al_2O_3 composite layer, or NCL) coating.

Lithium triflate (LiTf) and tetraethylene glycol dimethyl ether (TEGDME) have been proven as relatively stable salt and solvent, respectively, for rechargeable Li-O_2 batteries. Using the RuO_2-CNT cathode and 1 M LiTf-TEGDME electrolyte, Li-O_2 cells composed of Li-metal anode and protected Li-C composite anode have been cycled at 25°C at a current density of 0.1 mA cm^{-2} under a capacity protocol of 1,000 mAh g^{-1}. More stable cycle performance of Li-O_2 cells can be observed with protected Li-C composite anode (Figure 87c) compared to that of Li-O_2 cell using bare lithium metal (Figure 86a) and Li-C composite anode without protection (Figure 87b). However, cycle life of Li-O_2 cell was limited to about 40 cycles, although protected Li-C composite was used as a host for lithium anode. To reveal the failure mechanism in these Li-O_2 batteries, the morphological change of protected Li-C composite anode after 40 cycles was further investigated. It is found that the amount of lithium source at the Li-C composite was significantly reduced after cycling. This means that part of the lithium has irreversible loss due to the side reaction at the cathode side and cannot move back to the anode side during cycling. In other words, it is confirmed that reversibility of lithium anode depends not only on the anode/electrolyte reaction, but also on the cathode/electrolyte/O_2 reaction. To improve stability of lithium anode in Li-O_2 batteries, optimization of the full cell structure, including improvement of cathode reversibility, is required.

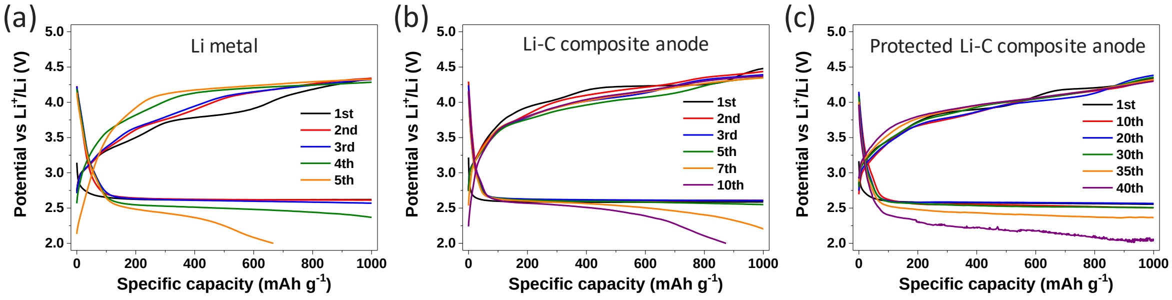

Figure 87. Cyclic stability tests based on Li-O_2 cells composed of RuO_2-CNTs air-cathodes and 1 M LiTf-TEGDME electrolyte at 25°C at a current density of 0.1 mA cm^{-2} under a capacity protocol of 1,000 mAh g^{-1} with (a) Li-metal anode, (b) Li-C composite anode, and (c) protected Li-C composite anode.

Patents/Publications/Presentations

The project has no patents, publications, or presentations to report this quarter.

Task 6.2 – Lithium-Air Batteries
(Khalil Amine and Larry A. Curtiss, Argonne National Laboratory)

Project Objective. This project will develop new cathode materials and electrolytes for Li-air batteries for long cycle life, high capacity, and high efficiency. The goal is to obtain critical insight that will provide information on the charge and discharge processes in Li-air batteries to enable new advances to be made in their performance. This will be done using state-of-the-art characterization techniques combined with state-of-the-art computational methodologies to understand and design new materials and electrolytes for Li-air batteries.

Project Impact. The instability of current nonaqueous electrolytes and degradation of cathode materials limits performance of Li-air batteries. The project impact will be to develop new electrolytes and cathode materials that are stable and can increase cycle life and improve efficiency of Li-air batteries.

Approach. The project is using a joint theoretical/experimental approach for design and discovery of new cathode and electrolyte materials that act synergistically to reduce charge overpotentials and increase cycle life. Synthesis methods, in combination with design principles developed from computations, are used to make new cathode architectures. Computational studies are used to help understand decomposition mechanisms of electrolytes and how to design electrolytes with improved stability. The new cathodes and electrolytes are tested in Li-O_2 cells. Characterization, along with theory, is used to understand the performance of materials used in the cell and make improved materials.

Out-Year Goals. The out-year goals are to find catalysts that promote discharge product morphologies that reduce charge potentials and find electrolytes for long cycle life through testing and design.

Collaborations. This project engages in collaboration with Prof. K. C. Lau (UC at Norridge), Prof. Y. Wu (Ohio State University), Dr. D. Zhai (China), and R. Shahbazian-Yassar (UIC).

Milestones

1. Synthesis and testing of low-cost TM catalysts that give low charge potentials in Li-O_2 batteries. (Q1, FY 2019; Completed)
2. Investigations of the role of mass and charge transport in discharge and charge reactions in Li-O_2 batteries. (Q2, FY 2019; Completed)
3. Characterization of electronic conductivity in discharge products via electrochemical impedance measurements. (Q3, FY 2019)
4. Investigation of dependence of discharge product properties on electrolytes with additives for Li-anode protection. (Q4, FY 2019)

Progress Report

The mechanism or underlying reasons for differences in charge potentials in Li-O_2 cells are still not well understood, but this knowledge is important for advancing this type of beyond Li-ion battery technology. In particular, the effect of the composition on the electronic conductivity is still not clear. To clarify this, the team has carried out a careful experimental study of effect of composition on electronic conductivity using cathode materials that can control composition. Theoretical calculations have indicated that LiO_2 has a higher electronic conductivity compared to Li_2O_2. Experimental evidence to prove these calculations has not been previously reported. EIS can be used to quantify the increase in charge transfer resistance of the oxygen reduction reactions in Li-O_2 batteries due to discharge product passivation of the cathode. In this work, the first experimental evidence indicating that LiO_2 has increased electronic conductivity compared with Li_2O_2 is found. Galvanostatic discharge and charge experiments coupled with three electrode impedance measurements were used to investigate the charge transfer impedance for LiO_2 discharge product compared to that of Li_2O_2, which is insulating in the bulk form. Iridium – reduced graphene oxide (Ir-rGO) was used as a cathode material, which the team has shown gives LiO_2 as the discharge product.

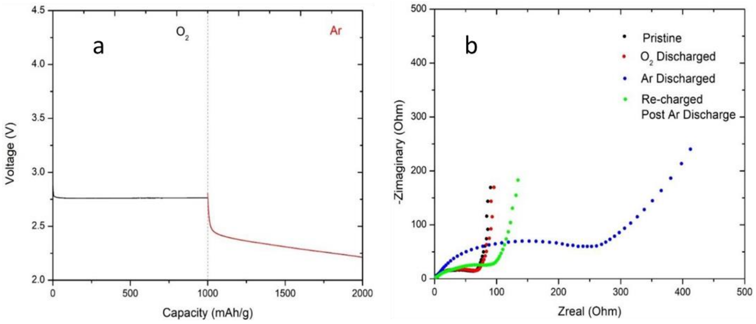

Figure 88. (a) Discharge profile of iridium – reduced graphene oxide (Ir-rGO) under O_2 followed by discharge profile under argon flow. (b) Electrochemical impedance spectroscopy measurements performed on pristine cathode, after O_2 discharge, after argon discharge, and after re-charge of the discharged cathode.

In the experiment shown in Figure 88, the discharge was carried out first in O_2 ($O_2 + Li^+ + e^- \rightarrow LiO_2$) to form LiO_2 and then in argon ($LiO_2 + Li^+ + e^- \rightarrow Li_2O_2$) to form Li_2O_2. The observed cathode potential during O_2 discharge was constant at ~ 2.75 V versus Li/Li^+ with discharge capacity of 1000 mAh/g. On discharge in argon, voltage readily dropped to 2.2 V versus Li/Li^+ with a discharge capacity of 1000 mAh/g. The discharge capacity above 2.0 V versus Li/Li^+ of the same cathode in argon without a prior discharge in O_2 is < 100 mAh/g. This indicates that the capacity obtained during the argon discharge in Figure 88a is derived from reduction of the LiO_2 discharge species formed during prior O_2 discharge. Raman and titration analysis were performed; results indicate that LiO_2 was formed during discharge with O_2 and that it was converted to Li_2O_2 by the discharge in argon.

Nyquist plots show that the impedance spectra of the cathode after the O_2 discharge is similar to the pristine cathode, as shown in Figure 88b. The impedance of the cathode after discharge in argon is larger than that measured after the initial O_2 discharge. The impedance of the cathode measured after recharge is reduced in comparison to that of the discharged cathode. These results demonstrate that the impedance increase in Figure 88b results from the change from LiO_2 to Li_2O_2. Investigation of other Li-O_2 cells without iridium, where Li_2O_2 is formed as the discharge product, confirms this increase in impedance. The key insight from the EIS studies is the increased electronic conductivity of LiO_2, which can lead to reduced charge over-potentials in batteries forming this discharge product found in previous studies. Ongoing work is aimed at investigating the impact of LiO_2 and Li_2O_2 discharge products on the impedance throughout multiple cycles and at different discharge rates along with quantifying discharge product conductivity.

Patents/Publications/Presentations

Publication

- He, K., Y. Yuan, X. Bi, T. Foroozan, J. Lu, and R. Shahbazian-Yassar. "Study of the Li-Oxygen Battery Discharging and Charging Process using *In-situ* TEM." *Microscopy and Microanalysis* 24, S1 (2018): 328–329.

Task 6.3 – Lithium Oxygen Battery Design and Predictions
(Larry A. Curtiss/Anh Ngo, Argonne National Laboratory; Amin Salehi-Khojin, University of Illinois at Chicago)

Project Objective. The objective of this work is to develop new materials for Li-O_2 batteries that give longer cycle life and improved efficiencies in an air environment. New electrolyte blends and additives will be investigated the can reduce clogging and at the same time promote the cathode functionality needed to reduce charge overpotentials. New cathode and anode materials will be investigated that can work in conjunction with the electrolytes to improve cycle life in the presence of air components.

Project Impact. Li-air batteries are considered as a potential alternative to Li-ion batteries for transportation applications due to their high theoretical specific energy. The major issues with the existing Li-O_2 systems include degradation of the anode electrode, reactions with air components, clogging of the cathode, and electrolyte instability. Thus, this project is using a comprehensive approach to improve cycle life and efficiency through development of new materials for electrodes, anodes, and electrolytes that work in synergy.

Approach. The experimental strategy is to use cathode materials based on 2D TM dichalcogenides (TMDCs) that the team has found to be among the best oxygen reduction and evolution catalysts. These cathode materials will be combined with new electrolyte blends and additives that work in synergy to reduce charge potentials and increase stability of the Li-air system. DFT and AIMD simulations are used to gain insight at the electronic structure level of theory of the electrolyte structure and function both in the bulk and at interfaces with the cathode, anode, and discharge product. Classical MD is used to obtain understanding at longer length and time scales of processes occurring in the electrolyte and growth mechanisms of discharge products. The team will also utilize a high-throughput screening strategy based on experiment and theory to develop a large database of properties and outcomes of electrolyte combinations that can be analyzed using machine learning to predict electrolytes and additives that will have the best performance.

Out-Year Goals. The out-year goals are to find electrolytes that give high capacities and long cycle life in an air atmosphere using high throughput screening.

Collaborations. This project engages in collaboration with Z. Zhang (ANL), R. Assary (ANL), B. Narayanan (University of Louisville), J. G. Wen (UIC), and R. Klie (UIC).

Milestones

1. Investigate possible lithium anode protection additives and redox mediators (RMs) for electrolyte blends that can work with MoS_2 cathode to extend cycle life and reduce charge overpotentials of Li-O_2 cells. (Q1, FY 2019; Completed)
2. Assess electrolyte blends and additives that will work in concert with MoS_2 cathode in Li-O_2 cells. (Q2, FY 2019; Completed)
3. Evaluate, using experiment and theory, properties of RMs for electrolyte blends to lower charge potentials for increased efficiency of Li-O_2 cells. (Q3, FY 2019; Completed)
4. Develop first-generation electrolytes that work in concert with MoS_2 cathode for increased CE of Li-O_2 cells running in a realistic air environment. (Q4, FY 2019; In progress)

Progress Report

Li-O_2 batteries are regarded as an advanced energy storage system that could provide a much higher specific energy than Li-ion batteries for electrical transportation. Thus far, research on the Li-O_2 battery has generally found short life cycle in a pure oxygen environment. In the presence of actual components of air such as nitrogen, carbon dioxide, and moisture, the issues of side reactions become more complex since the small concentrations of these species can react with discharge products at the cathode or with lithium anode. This project is exploring new avenues to improve on a Li-O_2 battery, based on a MoS_2 cathode catalyst, that can operate in a realistic air environment [*Nature* 555 (2018): 502]. To do this, the team has carried out a systematic investigation of a wide range of RM additives that could lower the charge potential for the MoS_2 cathode used in the Li-air battery. This study also provides useful data for high throughput studies of Li-O_2 battery system to identify the descriptors for improved performance.

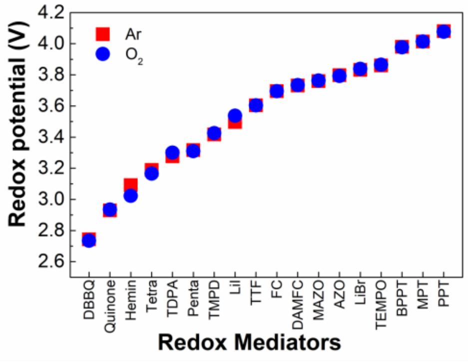

DBBQ: 2,5-di-tert-butyl-1,4-benzoquinone
Quinone: p-Benzoquinone
Hemin: Chloro(protoporphyrinato)iron(III)
Tetra: 5,10,15,20-Tetraphenyl-21H,23H-porphine iron(III) chloride
TDPA: tris[4-(diethylamino)phenyl]amine)
Penta: 5,10,15,20-Tetrakis(pentafluorophenyl)-21H,23H-porphyrin iron(III) chloride
TMPD: tetramethyl-p-phenylenediamine
LiI: Lithium iodide
TTF: Tetrathiafulvalene
FC: Ferrocene
DAMFC: (Dimethylaminomethyl)ferrocene
MAZO: 1-methyl-2-azaadamantane-N-oxyl
AZO: 2-azaadamantane-N-oxyl
LiBr: Lithium Bromide
TEMPO: 2,2,6,6-Tetramethyl-1-piperidinyloxy
BPPT: 10-(4-biphenylyl)phenothiazine
MPT: 10-Methylphenothiazine
PPT: 10-isopropylphenothiazine

Figure 89. Redox potentials (versus Li^+/Li) of redox mediators measured from cyclic voltammetry experiments in dimethyl sulfoxide solvent.

RMs are additives that can homogeneously dissolve in the electrolyte solutions to assist oxidization of discharge products (Li_2O_2), that is, by having oxidation potentials less than 3.5 V. There have been numerous investigations of existing RMs. However, none of these have systematically investigated the performance of a large number of RMs within one specific Li-O_2 battery system. The team has studied 24 RMs in terms of chemical characteristics such as redox potential with dimethyl sulfoxide (DMSO) and TEGDME electrolytes. The team also collected data on the separation of cathodic and anodic peaks and intensities of the peaks, correlating with reversibility and electron transfer rates. Results for redox potentials collected from electrochemical CV experiments for DMSO electrolyte for 18 of the RMs are shown in Figure 89.

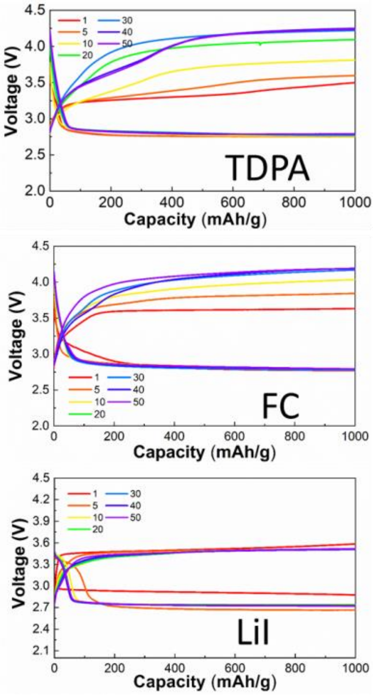

Figure 90. Voltage profile of three selected redox mediators (lithium iodide, ferrocene, and tris[4-(diethyl-amino)phenyl]amine]) measured in dimethyl sulfoxide with MoS_2 as a catalyst.

Nine of the best RMs were selected based on an integrated comparison of results from the CV studies; these nine are as follows: ferrocene (FC), lithium iodide (LiI), tetramethyl-p-phenylenediamine (TMPD), (dimethylaminomethyl)ferrocine (DAMFC), lithium bromide (LiBr), p-benzo-quinone (Quinone), tetrathiafulvalene (TTF), tris[4-(diethyl-amino)phenyl]amine] (TDPA), and 2,5-di-tert-butyl-1,4-benzoquinone (DBBQ). Galvanostatic cycling tests on these RMs were performed in Li-O_2 batteries in Swagelok cells. The results for three (FC, LiI, and TDPA) are shown in Figure 90. The results for all nine show that halides such as LiI and LiBr exhibit much better performance compared with the organic based on the charge potentials. The organic ones and TM complexes tend to have increasing charge potentials with number of cycles, as shown in Figure 90 for TDPA and FC. This may be due to the reaction with singlet O_2, which may be present during charge. However, the presence of the discharge plateau (reduction of I_3^- to I^-) at higher concentrations of LiI and LiBr (not shown here) restrict their state of charge when compared to other RMs. To solve the issue, the team reported last quarter using $LiNO_3$ as an additive to bypass the non-functional fraction of capacities.

Selected organic RMs such as TTF and TDPA reveal more effective results than halides for suppressing charge over-potentials, yet their instabilities are a major challenge, especially in the presence of singlet oxygen that may be formed during discharge.

The team has also carried out density functional calculations on the RMs considered in the experimental studies. This has included calculation of the redox potentials, which were in agreement with the experimental measurements. In addition, regarding the organic RMs having oxidation potentials less than 3.5 V, the team used these as base molecules for adding functional groups to expand the set of possible RMs. Some of these have oxidation potentials less than 3.5 V and may be effective as RMs.

In sum, the team has systematically investigated 24 RMs as effective additives for Li-O_2 batteries and will be using some of these in future development of Li-O_2 batteries.

Patents/Publications/Presentations

Publication

- Ahmadiparidari, A., M. Asadi, R. E. Warburton, L. Majidi, A. Chammani, J. R. Jokisaari, S. Rastegar, Z. Hemmat, B. Sayahpour, R. S. Assary, B. Narayanan, P. Abbasi, P. C. Redfern, A. Ngo, M. Vörös, J. Greeley, R. Klie, L. A. Curtiss, and A. Salehi-Khojin. “Long Cycle Life Lithium-CO_2 Battery with Carbon Neutrality.” *Advanced Materials*. In press.

Presentation

- Beyond Lithium Ion XII, Golden, Colorado (June 25–27, 2019): “Li-O_2 Batteries: Challenges and Recent Progress”; A. Salehi-Khojin.

TASK 7 –SODIUM-ION BATTERIES

Summary

During FY 2019, the BMR will add five new projects, including several in the area of Na-ion batteries. Progress on four of these new projects is described in this report; the fifth project will begin reporting next quarter. The Na-ion battery will require investigations to identify optimal electrode materials, electrolytes, separators, and binders to reach its full potential. The BMR program will therefore have a limited effort directed toward identifying Na-ion battery materials that have potential value for vehicle applications. More detailed information on this BMR Task will be provided in upcoming reports.

Highlights. The highlights for this quarter are as follows:

- The Doeff group at LBNL found significantly improved cycling for low-voltage sodium titanate anodes with carboxymethyl cellulose binders (CMC) compared to those made with PVDF, achieving a reversible capacity of about 190 mAh/g for a derivative of $NaTi_3O_6(OH)$ (sodium nonatitanate).
- The Zhang group at PNNL found that sodium-based non-flammable localized high-concentration electrolyte (LHCE) (NaFSI:TEP:BTFE in a molar ratio of 1:2:2) leads to a high initial CE of 97.9% and subsequent CE of > 99% for Na||O_3-$NaCu_1/9Ni_{2/9}Fe_{1/3}Mn_{1/3}O_2$ (Na-CNFM) cells.
- The Johnson group at ANL reported a high-performance phosphorus-based anode material with high reversible capacity of 2000 mAh/g, high initial CE of > 90% and excellent cycle stability by high-energy ball milling. A U. S. patent application was filed.
- The Yang group at BNL found that in $Na_{0.7}[Cu_{0.2}Fe_{0.2}Mn_{0.6}]O_2$ cathode, the increase in copper content in the lattice will enhance the metal-to-ligand charge transfer (MLCT) effect between copper and oxygen, but will relatively mitigate such an effect between iron and oxygen. Therefore, Cu–O becomes the redox center to compensate for charge neutrality on deep desodiation at high charging voltage. One paper was published in *Chemistry Materials*.

Task 7.1 – Exploratory Studies of Novel Sodium-Ion Battery Systems (Xiao-Qing Yang and Enyuan Hu, Brookhaven National Laboratory)

Project Objective. The objective of this project is to develop new advanced *in situ* material characterization techniques and apply these techniques to explore the potentials, challenges, and feasibility of new rechargeable battery systems beyond the Li-ion batteries, namely the Na-ion battery systems for EVs, such as PHEV and BEV. To meet the challenges of powering PHEVs and BEVs, new rechargeable battery systems with high energy and power density, low cost, good abuse tolerance, and long calendar and cycle life need to be developed. This project will use the synchrotron based *in situ* X-ray diagnostic tools, combined with TEM and STEM imaging techniques developed at BNL, to evaluate the new materials and redox couples to obtain fundamental understanding of the reaction mechanisms of these materials aiming for improvement of and guidance for new material and new technology development regarding Na-ion battery systems.

Project Impact. In the VTO MYPP, the goals for battery were described as: “Specifically, lower-cost, abuse-tolerant batteries with higher energy density, higher power, better low-temperature operation, and longer lifetimes are needed for the development of the next-generation of HEVs, PHEVs, and EVs.” The knowledge learned from diagnostic studies and collaborations with U. S. industries through this project will help U. S. research institutions and industries to develop new materials and processes for a new generation of rechargeable battery systems, namely Na-ion battery system, in their efforts to reach these VTO goals.

Approach. This project will use the synchrotron-based *in situ* X-ray diagnostic tools developed at BNL to evaluate the new materials and redox couples to enable a fundamental understanding of the mechanisms governing performance of these materials and provide guidance for new material and new technology development regarding Na-ion battery systems.

Out-Year Goals. Complete the synchrotron based *in situ* XRD and *ex situ* absorption (XAS) studies of low-cost P2-type iron-based cathode materials ($Na_{0.7}[Cu_{0.15}Fe_{0.3}Mn_{0.55}]O_2$) as new cathode materials for Na-ion batteries during charge-discharge cycling.

Collaborations. The BNL team has been closely working with top scientists on new material synthesis at ANL, LBNL, and PNNL and with U. S. industrial collaborators at General Motors and Johnson Controls, as well as international collaborators.

Milestones

1. Complete *in situ* XRD studies of new low-cost P2-type iron based cathode materials ($Na_{0.7}[Cu_{0.15}Fe_{0.3}Mn_{0.55}]O_2$) for Na-ion batteries during charge-discharge cycling. (Q1, December 2018; Completed)
2. Complete the synchrotron-based XAS studies and XAS analysis of $Na_{0.7}[Cu_{0.15}Fe_{0.3}Mn_{0.55}]O_2$ and $Na_{0.7}[Cu_{0.2}Fe_{0.2}Mn_{0.6}]O_2$ electrodes at different SOCs at iron K-edge, copper K-edge, and manganese K-edge. (Q2, March 2019; Completed)
3. Complete the sXAS studies of $Na_{0.7}[Cu_{0.15}Fe_{0.3}Mn_{0.55}]O_2$ and $Na_{0.7}[Cu_{0.2}Fe_{0.2}Mn_{0.6}]O_2$ electrodes at different SOCs at iron L-edge, copper L-edge, and oxygen K-edge. (Q3, June 2019; Completed)
4. Complete *in situ* XRD studies of new stabilized global P2 phase cathode material ($Na_{0.72}[Li_{0.24}Mn_{0.76}]O_2$) for Na-ion batteries during charge-discharge cycling. (Q4, September 2019; In progress)

Progress Report

This quarter, the second milestone was completed. BNL has been focused on the synchrotron-based soft XAS studies and XAS analysis of $Na_{0.7}[Cu_{0.15}Fe_{0.3}Mn_{0.55}]O_2$ and $Na_{0.7}[Cu_{0.2}Fe_{0.2}Mn_{0.6}]O_2$ electrodes at different SOCs to gain more fundamental insights into the correlation between different TM elements and oxygen participation in electrochemical reactions. Soft XAS was performed on the TM L-edge as well as oxygen K-edge of both $Na_{0.7}[Cu_{0.15}Fe_{0.3}Mn_{0.55}]O_2$ (Figure 91a–c) and $Na_{0.7}[Cu_{0.2}Fe_{0.2}Mn_{0.6}]O_2$ (Figure 91d–f) electrodes. Detailed results on copper L-edge, iron L-edge, and oxygen K-edge spectra of the two electrodes at different SOCs in both the 1st and 15th cycle are shown in Figure 91a–f. To highlight the spectral differences in battery cycling, only the L3 edge, which evolves due to 2p3/2–3d state transition of TM L-edge XAS, is shown. As for copper L-edge and iron L-edge XAS, the most evident change is the rise and decay of a metal-to-ligand charge transfer (MLCT) feature, as shown in the shaded area. Such a MLCT feature has been verifed in previous reports in TM oxide systems and is supported by theoretical simulations. It should be noted that the increase in copper content in the lattice will enhance the MLCT effect between copper and oxygen, but relatively mitigate such an effect between iron and oxygen. Therefore, Cu–O becomes the redox center to compensate for charge neutrality on deep desodiation at high charging voltage. Oxygen K-edge XAS further supports the perturbation on the TM–O hybridization feature on sodium removal with excess copper doping. The surface sensitive total electron yield (TEY) results, as shown by dotted lines, are in contrast to the bulk-sensitive total fluorescence yield (TFY) results, implying particular surface layer-formation on battery cycling. In the case of $Na_{0.7}[Cu_{0.2}Fe_{0.2}Mn_{0.6}]O_2$, where drastic voltage decay occurs, it was found that the 15th charged cathode at 4.3 V basically reproduced the 1st charge 3.9 V state, which is consistent with the dynamic origin of the voltage decay phenomenon. Based on sXAS characterization, it can be concluded that superior battery performance in $Na_{0.7}[Cu_{0.2}Fe_{0.2}Mn_{0.6}]O_2$ can be interpreted from interactive correlation among inherent iron, substituting TM elements and ligand oxygen.

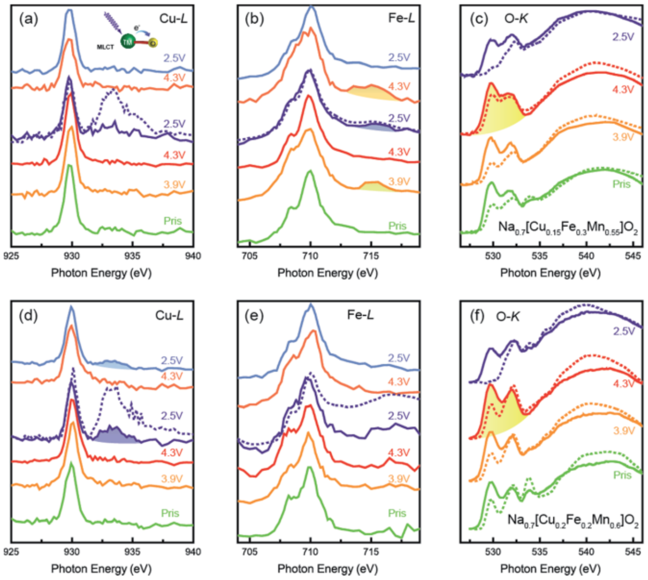

Figure 91. Soft X-ray absorption (sXAS) of $Na_{0.7}[Cu_{0.15}Fe_{0.30}Mn_{0.55}]O_2$ (a–c) and $Na_{0.7}[Cu_{0.20}Fe_{0.20}Mn_{0.60}]O_2$ (d-f) samples. The copper L-edge (a/d), iron L-edge (b/e), and oxygen K-edge (c/f) sXAS data for the $Na_{0.7}[Cu_xFe_yMn_{1-x-y}]O_2$ cathode were collected at different cycle states, including pristine, charge 3.9 V, charge 4.3 V, and discharge 2.5 V during the 1st cycle and charge 4.3 V and discharge 2.5 V during the 15th cycle. The spectra in solid lines were collected in total fluorescence yield mode, while those in dotted lines demonstrate sXAS collected in total electron yield mode. Schematic of metal-to-ligand charge transfer (MLCT) is shown in the inset of (a). The spectral evolution is highlighted with shaded areas.

Patents/Publications/Presentations

Publication

- Song, B., M. Tang, E. Hu, O. J. Borkiewicz, K. M. Wiaderek, Y. Zhang, N. D. Phillip, X. Liu, Z. Shadike, C. Li, L. Song, Y-Y. Hu, M. Chi, G. M. Veith, X-Q. Yang, J. Liu,* J. Nanda,* K. Page,* and A. Huq.* "Understanding the Low-Voltage Hysteresis of Anionic Redox in $Na_2Mn_3O_7$." *Chemistry of Materials* 31, no. 10 (2019): 3756-3765. doi: 10.1021/acs.chemmater.9b00772. Publication Date (Web): May 1, 2019.

Task 7.2 – Development of a High-Energy Sodium-Ion Battery with Long Life (Chris Johnson and Khalil Amine, Argonne National Laboratory)

Project Objective. The project objective is to develop a high-energy Na-ion battery with long life. Moreover, the battery chemistry should utilize low-cost materials. The energy density target is 200 Wh/kg and/or 500 Wh/L, wherein the anode and cathode capacity targets are 600 $mAhg^{-1}$ and 200 $mAhg^{-1}$, respectively.

Project Impact. A Na-ion battery on par with the energy density of a Li-ion battery can have a high impact in the transportation sector with the assumption that the cost is significantly below $85/kWh and the battery pack provides a 300-mile range. The consumer is not concerned about the battery chemistry employed if these metrics can be met. Development of these battery chemistries will situate the U.S. in a strong position as relates to new low-cost energy storage systems beyond Li-ion.

Approach. In a team approach, the Na-ion battery group will create a versatile Na-ion battery chemistry with beneficial advantages such as low cost, safety, recycling, and sustainability of materials used. The team will work in a synergistic way so that the final design is the culmination of advances in phosphorus carbon composites mated with optimized lead or other highly dense metalloids, such as tin and/or antimony and derivatives thereof, for the recyclable anode. Synthesis and optimization of such blended composite anodes will be conducted in parallel to diagnostic characterization of structures, phase formation, and cycling stability. Cathode work will begin at the end of the first year and will involve (1) gradient cathodes consisting of Fe-Mn compositions, and (2) intergrowths of layer stacking sequenced oxides. If resources allow, the team also will attempt to stabilize cathode surfaces using ALD methods, particularly for the benefit of staving off dissolution of manganese and iron / electrolyte reactivity. Electrolytes will be partly procured from Dr. H. Pan at PNNL.

Out-Year Goals. The state-of-the-art Na-ion battery in the literature has now been surpassed by this team, but performance is still too low for commercialization. Thus, the goal is to move forward and continually invent the most superior Na-ion battery chemistry that can compete worldwide through work output from this project.

Collaborations. Researchers from PNNL who are developing electrolytes for Na-ion batteries will provide this project with formulations to test with the various electrode combinations investigated at ANL. The team also exchanges commercial samples with Dr. J. Barker of Faradion Ltd. in the United Kingdom. The project collaborates with Dr. Y. Ren (high-energy XRD, APS at ANL), Dr. C. Sun (XAS, APS at ANL) and Dr. Y. Liu (TEM, Center for Nanoscale Materials at ANL) for advanced structure characterization.

Milestones

1. Report on the BatPaC cell cost and energy density for the proposed Na-ion battery cell couple. (Q1, FY 2019; Completed).
2. Report on the synthesis, characterization, and initial cycling performance data on relevant Na-ion anode battery materials. (Q2/Q3, FY 2019; Completed)
3. Optimize anode composites produced in Q3. Continue characterization of materials for understanding. (Q3/Q4, FY 2019)
4. Demonstrate cycle life of optimized anode. (Q4, FY 2019)

Progress Report

This quarter, the team has worked on optimization of phosphorus as a Na-ion battery anode. Such a material has attractive theoretical capacities of up to 2596 mAh g^{-1}, but the volume change on (de)sodiation is problematic. For this reason, the team has developed an advanced ball-milling strategy to overcome the limitations of electrical conductivity, sodium cation diffusion, and volume swelling/shrinking issues. Black phosphorus (BP) or red phosphorus (RP), Ketjenblack (KB), and multi-walled carbon nanotubes (MWCNT) are ball-milled together to make a nano-composite, which is coined BPC.

The XRD in Figure 92a shows that after ball milling, the strong diffraction peaks of bulk BP became broad, indicating the formation of nanocrystalline BP. A similar result was seen in the Raman test (Figure 92b). The microstructures of the BP and BPC composite were characterized by electron microscopy (Figure 93). The particle size of bulk BP is about hundreds of micrometers (Figure 93a). After high-energy ball milling, these large BP particles cannot be observed. They are homogeneously assembled with Ketjenblack and MWCNTs and form a unique nanostructure. Secondary particles with a size of about hundreds of nm to 1 μm can be observed (Figure 93b). The high-magnification TEM image of the BPC composite in Figure 93c clearly shows that BP nanoparticles with crystal lattices (marked by dashed circles) uniformly distributed in the amorphous carbon matrix, which confirms the nanocrystalline property of BP in the BPC composite. The interval between lattices was measured to be 0.334 nm from the HRTEM image (Figure 93d), coinciding with the *d*-spacing for the (021) plane of BP (PDF no. 76-1962).

The electrochemical performance of the BPC composite anode was evaluated by assembling into coin cells with sodium as reference and counter electrode. The optimal electrolyte was 1 M $NaPF_6$ in PC with 2 vol% FEC, in which FEC has been widely used as an additive to protect the electrolyte decomposition. The initial charge/discharge profile of the BPC anode is shown in Figure 94a. The initial discharge capacity was measured to be 2206.7 mAh g^{-1}, corresponding to 85% phosphorus utilization compared to the theoretical capacity of phosphorus. The first reversible capacity was 2011.1 mAh g^{-1}, corresponding to an initial CE as high as 91.1%. Such a high CE is very important when coupling an anode with a cathode material in a full cell system. The average working voltage of the BPC anode is around 0.5 V versus Na/Na^+, which is good for the consideration of both energy density and reactivity toward electrolytes. Figure 94b illustrates CV of the BPC anode. A weak and broad peak occurs at around 1.0 V in the first cathodic scan and is attributed to the reduction of electrolytes to form the SEI layer. In subsequent scans, a new peak centered at around 0.95 V appeared, which should be attributed to the initial sodiation of BP. When the potential was further scanned from 0.8 to 0.01 V, a major cathodic peak appeared at about 0.45 V, which corresponds to Na-ion insertion and formation of Na_xP ($1 < x \leq 3$). The curves overlapped after the 2nd cycle, indicating excellent cycle stability. As shown in Figure 94c, the BPC anode maintained stable capacities of around 2000 mAh g^{-1} within 50 cycles at 0.416 A g^{-1}. At a much higher charge/discharge current density of 1.3 A g^{-1}, the BPC anode illustrates excellent cycle stability, which could deliver a high reversible capacity of about 1700 mAh g^{-1} after 100 cycles.

The effect of sodium salts on the cycle performance of BPC anode has also been examined. As shown in Figure 95, the BPC anode demonstrates higher reversible capacity and better cycle stability in the $NaPF_6$-based electrolytes than $NaClO_4$-based electrolytes. This is probably due to the higher ionic conductivity and better stability of $NaPF_6$. Due to the high cost of BP, the team also examined the electrochemical performance of red phosphorus-carbon (RPC) composite using a similar synthetic process. Figure 96 showed that the RPC anode exhibits lower initial CE (87.8%), lower reversible capacities, and higher capacity fading rate in 50 cycles, which may be due to its lower electronic conductivity than BPC. However, it should be noted that the sodium storage performance of RPC anode is still comparable to most P/C composites, demonstrating the advantages of Ketjenblack-MWCNTs network used in this work. Also, results indicate that a blend of black and red phosphorus could simultaneously achieve high capacity and lower the cost.

Overall, the team has demonstrated a high-performance nanostructured anode material for room-temperature Na-ion batteries. The BPC anode the project developed has an ultra-high initial CE of > 90%, high reversible capacity of ~ 2000 mAh g^{-1}, and excellent cycle stability when used as anode of Na-ion batteries. However, several key issues need to be further addressed: (1) the cause for the ultra-high initial CE of the BPC; (2) the conflict between highly reversible capacity of the BPC and the huge volume expansion; (3) the balance between specific capacity and cycle life, as 2000 mAh g^{-1} is too high to couple with a cathode material; and (4) the limitation of the high cost of BP for practical use. The team will deploy cutting-edge characterization techniques and optimize the anode structure (composition and morphology) to address the above issues. Moreover, items 3 and 4 can be addressed by incorporation of lead Pb/Pb-oxide into the matrix to up the volumetric energy density and to cut the cost of this modified BPC composite. The Pb/Pb-oxide composite was presented last quarter.

Next quarter, the team will begin to combine components of Pb/Pb-oxide composite with RPC and/or BPC.

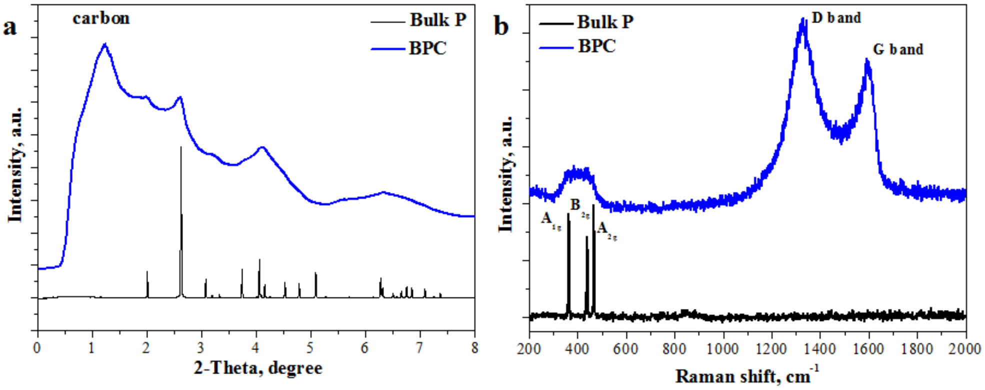

Figure 92. X-ray diffraction and Raman spectra of black phosphorus-carbon composite.

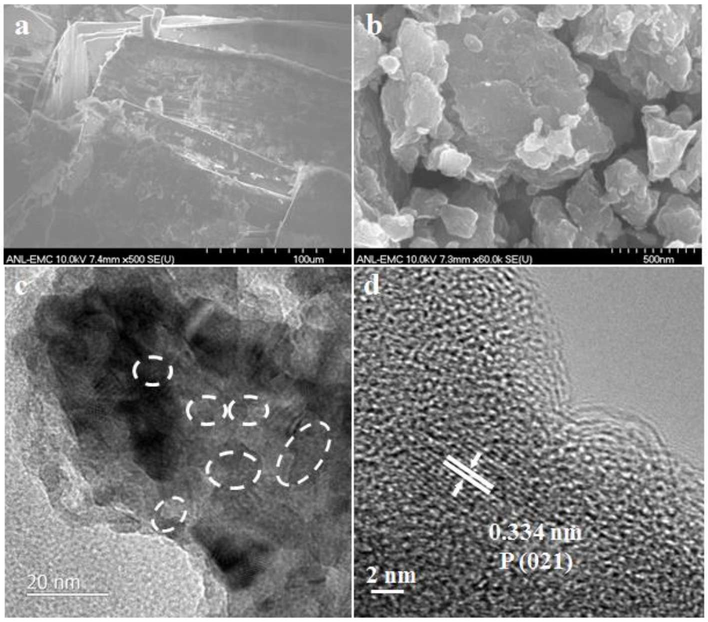

Figure 93. Scanning electron microscopy images of (a) bulk phosphorus and (b) black phosphorus-carbon composite, (c) high magnification, and (d) high-resolution transmission electron microscopy images of black phosphorus-carbon composite (70% black phosphorus).

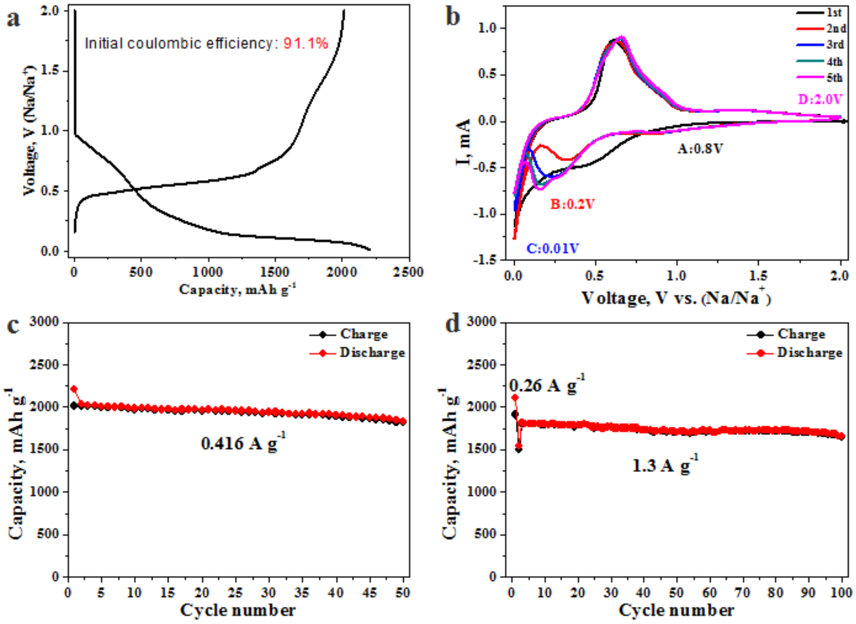

Figure 94. (a) Initial voltage profile of black phosphorus-carbon (BPC) composite at 0.416 A g^{-1}. (b) Cyclic voltammogram of BPC composite at 0.1 mV s^{-1}. (c-d) Cycle performance of BPC composite anode at (c) 0.416 A g^{-1} and (d) 1.3 A g^{-1}. The specific capacities were calculated based on the mass of black phosphorus.

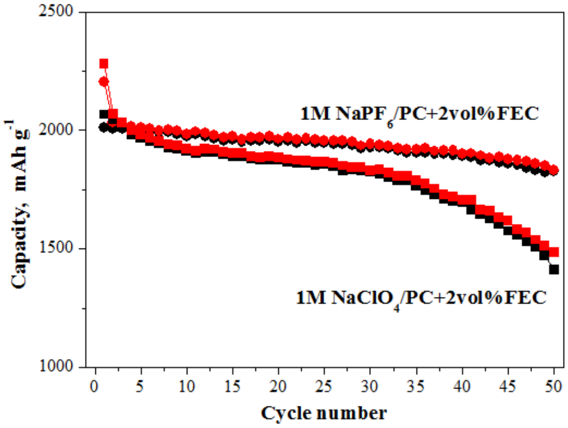

Figure 95. The effect of sodium salts on the cycle performance of black phosphorus-carbon composite anode using different electrolytes at 0.416 A g^{-1}.

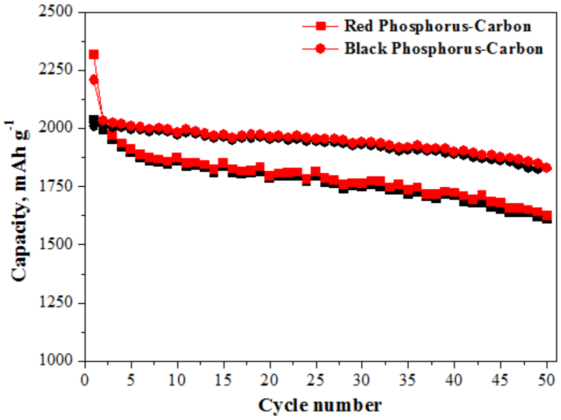

Figure 96. Comparison for the cycle performance of red phosphorus-carbon and black phosphorus-carbon composite at 0.416 A g^{-1}.

Patents/Publications/Presentations

Patent

- Xu, G., Z. Chen, and K. Amine. “Phosphorus-Carbon Composites as Battery Anode Materials.” U. S. Patent App. 15/006, 456, pending.

Task 7.3 – High-Capacity, Low-Voltage Titanate Anodes for Sodium-Ion Batteries (Marca Doeff, Lawrence Berkeley National Laboratory)

Project Objective. The objectives are to understand differences in the sodium intercalation mechanism of various sodium titanate anodes through an array of synthetic, electrochemical, and structural characterization techniques, and to overcome practical impediments to their use, such as the high first-cycle Coulombic inefficiencies that are currently observed. The ultimate goal is to produce a 200-250 mAh/g anode that cycles reversibly.

Project Impact. Although several suitable cathode materials for Na-ion batteries exist, there are few suitable anode materials due to their low potential instabilities. Therefore, sodium titanate variations will be synthesized through different routes to develop materials with various morphologies and dopants. Decreasing the first-cycle inefficiencies and improving cycling performance has the ability to enable technology for a practical high-energy Na-ion battery.

Approach. Candidate stepped layered titanates will be synthesized by appropriate routes (hydrothermal, solid state routes, etc.). Materials will then be characterized electrochemically and physically. Structure-function relationships will be built to correlate the effect of changing structure (for example, step size) on electrochemical properties.

Out-Year Goals. A series of synchrotron characterization techniques will be used to further develop sodium titanate anode materials with stable cycling while delivering high capacities.

Collaborations. TXM is done in collaboration with Dr. Y. Liu (SSRL). Synchrotron hard, sXAS, and X-ray Raman efforts are in collaboration with Dr. D. Nordlund and Dr. D. Sokaras (SSRL). Electrolyte design is done in collaboration with Dr. K. Xu (ARL).

Milestones

1. Hydrothermal synthesis of sodium nonatitanate (NNT). (Q1, FY 2019; Completed)
2. Ion exchange sodium NNT with magnesium. (Q2, FY 2019; Completed – *No Go*)
3. Complete synchrotron XRD and XAS analysis on sodium NNT. (Q3, FY 2019; Completed)
4. *Go/No-Go Decision*: Magnesium exchange; stop if electrochemical properties are not improved. (Q4, FY 2019)

Progress Report

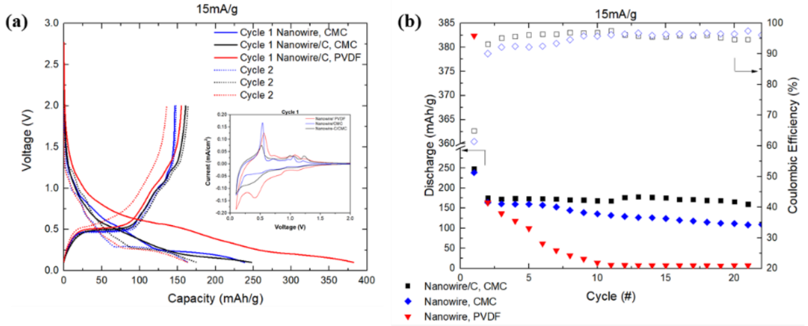

Figure 97. (a) 1st and 2nd cycles of sodium nonatitanate (NNT) and carbon-coated NNT cells with carboxymethyl cellulose binders or polyvinylidene fluoride binders. (b) Capacity and Coulombic efficiency as a function of cycle number for the same cells.

Electrode engineering has played an important role in determining the electrochemical performance of NNT (Figure 97). By simply changing the binder from PVDF to CMC, the cycling performance and CE have dramatically improved. Additionally, carbon coating by sucrose pyrolysis improves the electronic conductivity and limits the side reactions. Side reactions contribute to the initial Coulombic inefficiency, which is much higher for the PVDF-containing electrodes than the CMC ones. After the first charge, the CMC-containing electrodes have two voltage plateaus, which are also seen as peaks in the CV curves (Figure 97a, insert). CMC allows for the full activation of NNT during electrochemical cycling by forming a conformal coating with all the electrode components, thereby reducing the effects associated with volume changes and particle disconnection during cycling. The capacity retention can be further improved by reducing the current (4 mA/g). Continuing to optimize the electrode can lead us closer to reaching the ~ 200 mAh/g reversible capacity of sodium titanates.

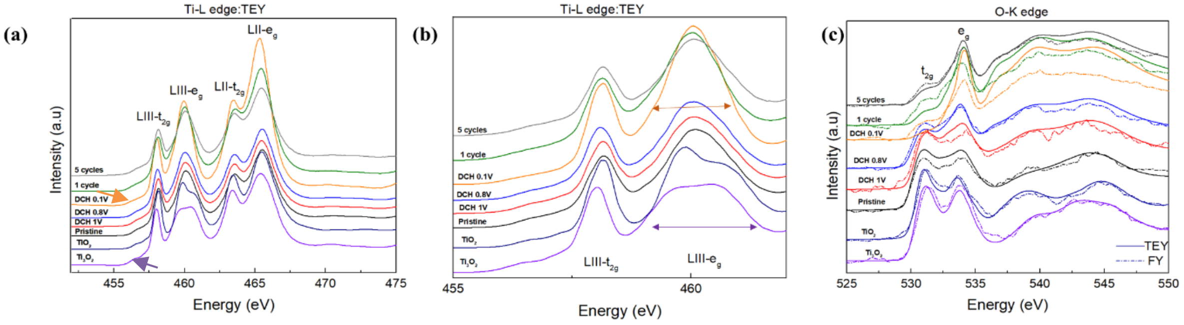

Figure 98. soft X-ray absorption spectroscopy of the (a) Ti-L edge. Zoomed in image (b) and the (c) O-K edge of the nonatitanate nanowires at different states of charge.

Figure 98 shows the soft XAS spectra for the titanium L-edge at different SOCs along with Ti^{4+} and Ti^{3+} references. The spectra consist of a L3 peak between 455-463 eV that is associated with the 2p3/2 core hole and a L2 peak between 463-468 eV that corresponds to the 2p1/2 core hole. The ligand field causes a splitting of both the L3 and L2 peaks, resulting in t2g and eg peaks. The pristine NNT shows characteristics of both Ti^{4+} and Ti^{3+} when comparing to the reference profiles. On discharge to 0.1 V, there are subtle changes that indicate a $Ti^{4+}/^{3+}$ redox couple: (1) a slight L3-t2g peak shift to lower energy; (2) a shoulder appearing at lower energy, shown with arrows in Figure 98a; and (3) broadening of the L3-eg peak (double head arrows in Figure 98b). The oxygen K-edge shows peak intensity changes in the titanium 3d-oxygen 2p region (528–536 eV). The t2g peak decreases significantly during discharge in both the TEY and FY mode. The intensity ratios of the t2g and eg peak do not return to the pristine state after charging, indicating some titanium is still in the trivalent state. Both the titanium L-edge and oxygen K-edge show conclusively that titanium is reduced during cell discharge, consistent with hard XAS data reported last quarter.

During discharge, the titanium coordination becomes a distorted octahedra that can be seen in both titanium L-edge and oxygen K-edge. The analysis of *operando* XRD is in progress, which would aid in understanding the intercalation and deintercalation of sodium into NNT and will further validate the XAS experiments.

Patents/Publications/Presentations

The project has no patents, publications, or presentations to report this quarter.

Task 7.4 – Electrolytes and Interfaces for Stable High-Energy Sodium-Ion Batteries
(Huilin Pan and Ji-Guang Zhang, Pacific Northwest National Laboratory)

Project Objective. This project will develop innovative electrolytes and enable fundamental understanding on the interface between electrode and electrolyte for stable operation of high-energy Na-ion batteries for potential application in EVs. The proposed research will enhance the achievable capacities of both anode and cathode for Na-ion battery and improve the stability of electrodes/electrolyte interface, build correlation (electrolyte design rule) between electrochemical performances of Na-ion batteries and the electrolyte/interface properties, and enable long cycle life and safe operation of high-energy Na-ion batteries.

Project Impact. This project will enable a fundamental understanding on the electrolyte/electrode interface in Na-ion battery systems. Successful project execution will improve their energy density, cycle and calendar life, and safety. The project will provide a solid contribution to development of Na-ion battery technology and promote its practical application as a competitive alternative to the current Li-ion batteries, as well as greatly reduce the cost of energy storage systems for EVs.

Approach. This project will optimize the electrolyte components and concentrations to develop innovative electrolyte and additives with improved physical and (electro) chemical properties. *In situ* and *ex situ* spectroscopy methods will be used to unravel the origin of the SEI at the dynamic interface, providing guidance for the electrolyte and interface design and enabling high achievable capacity and long life of Na-ion batteries.

Out-Year Goals. This project will select the electrolyte compounds and use *in situ* and *ex situ* techniques to identify the formation of interfacial SEI layer and its effect on the electrode materials. It will also provide guidance to electrolyte optimization to improve the hard carbon anode capacity to > 300 mAh g^{-1} and enable its long-term stable operations.

Collaborations. This project will collaborate with ANL and LBNL and other leading scientists in the field of cathode and anode materials for Na-ion batteries. It will collaborate with Dr. C. Wang and Dr. M. Engelhard for TEM and XPS characterization.

Milestones

1. Determine the physical-chemical properties of carbonate-based electrolytes, and identify the key factor affecting the stability of these electrolytes in sodium batteries. (Q1, FY 2019; Completed)
2. Design new phosphate-based electrolyte with improved electrochemical and thermal stability in sodium batteries. (Q2, FY 2019; Completed)
3. Characterize chemical coordination structure of selected carbonate- and phosphate-based electrolytes for sodium batteries. (Q3, FY 2019; Completed)
4. Demonstrate improved capacity, CE, and cyclic stability of electrode materials using the electrolytes developed in this work; achieve hard carbon capacity of > 250 mAh g^{-1}, initial CE > 85%, and cycle life > 200 times. (Q4, FY 2019; In progress)

Progress Report

The milestones for this quarter have been accomplished. The chemical coordination structures of optimized carbonate- and phosphate-based electrolytes for sodium batteries have been characterized by Raman and NMR. For carbonate electrolyte, the pure solvent (EC and DMC) shows ^{13}C resonance for carbonyl group at range of 158-156 ppm. After adding 1 M $LiPF_6$ salt into EC and DMC co-solvent (1:1 in mass), the ^{13}C resonance shifts to higher frequency because of coordination between Na^+ and carbonyl oxygen nuclei (Figure 99a). The change of the chemical shift of EC upon Na^+ coordination is greater than that for DMC, indicating more EC coordinated to Na^+ cation. The chemical shift of the ^{13}C carbonyl resonance is plotted for five kinds of solvents in Figure 99b. By comparing the chemical shift, coordination ability sequence of solvent is: PC ~ EC > DMC. From Raman spectra of electrolyte with EC and DMC co-solvent (1:1 in mass) in Figure 99d, Na^+ can coordinate with both EC and DMC, but the peak shift of EC is more obvious than DMC, which also indicates stronger coordination of EC than DMC. The low coordination ability of DMC with Na^+ leads to more free DMC decomposition and accounts for low initial CE (32%) of Na||Hard carbon (HC) cells with 1 M $NaPF_6$ in DMC. With strong coordination of EC in co-solvent of EC+DMC (1:1 in mass), the amount of free solvents is reduced so SEI formation in HC surface is minimized, leading to higher CE, lower SEI resistance, fast ion transport, and better rate and cycling performance.

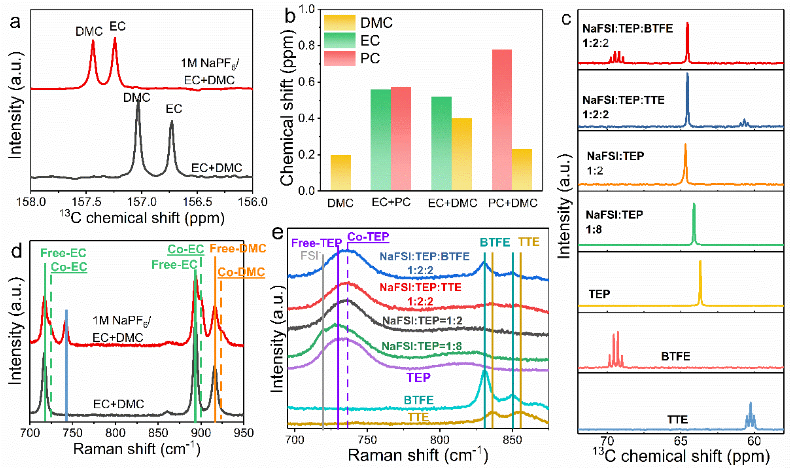

Figure 99. (a) ^{13}C NMR spectra of 1 M $NaPF_6$ in ethylene carbonate / dimethyl carbonate (EC/DMC) co-solvent. (b) Change in chemical shift for ^{13}C in five kinds of solvent with 1 M $NaPF_6$ salt. (c) ^{13}C NMR spectra of pure triethyl phosphate based electrolyte. (d) Raman spectra of 1 M $NaPF_6$ in EC/DMC co-solvent. (e) Raman spectra of triethyl phosphate based electrolyte.

For phosphate-based electrolytes, there is a ^{13}C NMR peak at 63.6 ppm for pure triethyl phosphate (TEP) solvent, as demonstrated in Figure 99c. As the molar ratio increases, the ^{13}C NMR peak position shifts to higher frequency, indicating increased coordination of Na^+ and TEP. In Raman spectra (Figure 99e), dilute electrolyte of TEP:NaFSI (8:1) exhibits an absorption band at 722 and 730 cm^{-1}, indicating the presence of a large amount of uncoordinated FSI^- and TEP. With increasing molarity, TEP: NaFSI (2:1) shows upshift Raman peak at 737 cm^{-1}, indicating coordinated-TEP and coordinated-FSI^-. With higher molarity, the number of free TEP molecules is minimized and TEP decomposition is inhibited. When this electrolyte is used in Na-metal batteries with a high-energy cathode of O_3-$NaCu_{1/9}Ni_{2/9}Fe_{1/3}Mn_{1/3}O_2$ (Na-CNFM), an initial CE of as high as 97.6% is obtained. For the localized high-concentration electrolyte (LHCE) formed by adding diluent bis(2,2,2-trifluoroethyl) ether (BTFE) or 1,1,2,2-tetrafluoroethyl-2,2,3,3-tetrafluoropropyl ether (TTE) into TEP-based electrolyte, there is no observable change in the coordinated-TEP ^{13}C NMR peak (64.6 ppm) and Raman shift peak. Therefore, sodium-based, non-flammable LHCE not only exhibits lower overall salt molarity, lower viscosity, and safety, it can also preserve the Na^+-coordinated TEP solvation structure and lead to higher initial CE of 97.9%, therefore outperforming the high-concentration electrolyte.

Patents/Publications/Presentations

The project has no patents, publications, or presentations to report this quarter.

Innovation Center for Battery500
(Jun Liu, PNNL; Yi Cui, Stanford University)

Project Objective. The project aims to develop commercially viable lithium battery technologies with a cell-level specific energy of 500 Wh/kg through innovative electrode and cell designs that enable the extraction of the maximum capacity from advanced electrode materials. In addition to achieving high specific energy, the project aims to be able to achieve 1,000 cycles for the developed technologies.

Project Impact. The Battery500 Consortium will develop next-generation lithium battery technologies that will significantly increase energy density, improve cycle life, and reduce cost. This will greatly accelerate deployment of EVs and reduce carbon emission associated with fossil fuel consumption. The consortium will utilize first-class expertise and capabilities in battery research in the United States and develop an integrated and multidisciplinary approach to accelerate development and deployment of advanced electrode materials in commercially viable high-energy batteries. The advances made in this consortium will also benefit the improvement of current Li-ion battery technologies.

Approach. This project will utilize an assortment of national resources located at the national laboratory level and university level. The lithium anode combined with a compatible electrolyte system and two cathodes—one high-Ni $LiNi_xMn_yCo_zO_2$ and another sulfur—will be studied and developed to reach high-energy density. The project focus is to design novel electrode and cell architectures to meet the 500 Wh/kg goal. The consortium will work closely with R&D companies, battery/materials manufacturers, and end users/OEMs to ensure that the developed technologies are aligned with industry needs and can be transitioned to production.

Out-Year Goals. This project aims for the following out-year goals. (1) Integrate materials and components developed in FY 2018 into 1-Ah pouch cell and demonstrate 400-Wh/kg cell with more than 30 charge discharge cycles, and provide analytical results for materials selection, cell design and fabrication, and further refinement for FY 2019. (2) Evaluate the seedling projects for key findings.

Collaborations. Collaboration among consortium team members will be well coordinated by the leadership team, which includes the keystone project leads and co-leads along with PIs at all member institutions. Collaboration with the community outside of this consortium and with industry will be facilitated by the executive committee, the advisory board, and the industry committee.

Milestones

1. Synthesize high-nickel layered oxide cathodes (nickel content > 90%) with a capacity of > 210 mAh/g and test. (Q1, FY 2019; Completed)
2. Implement lithium protection approaches to demonstrate 20% cycle life improvement. (Q2, FY 2019; Completed)
3. Fabricate and test a pouch cell capable of 350 Wh/kg and 250 cycles. (Q3, FY 2019; Completed)
4. Fabricate and test a pouch cell capable of 400 Wh/kg and 30 cycles. (Q4, FY 2019; In progress)

Progress Report

This quarter, the third milestone was completed, and progress toward fourth quarter milestones was made. Pouch cells with 350 Wh/kg energy density with cyclability of 250 cycles have been successfully fabricated and achieved. One international patent application was filed by the UW consortium member. In addition, PIs of the consortium delivered 31 invited talks and published 12 papers in peer-reviewed journals.

The technical portion of this report is organized under three Keystone projects, as presented below.

Keystone Project 1: Materials and Interfaces

The goal of Keystone 1 is to provide the materials and chemistry support for Keystone projects 2 and 3. This quarter, Keystone 1 developed an ether-based liquid electrolyte for the Li||NMC-811 cell that is enabling attainment of long life and high energy density; determined the impact of coatings on the NMC-811 electrode; and developed the capability to make large batches of NMC-811 in-house.

An ether-based LHCE was developed that can greatly enhance the stability of a Ni-rich NMC-811 cathode under 4.4 V and 4.5 V with an effective protection interphase enriched in LiF. Four electrolytes were investigated: conventional electrolyte 1 M $LiPF_6$ in EC-EMC (3:7 by wt.) with 2 wt% of VC; dilute electrolyte (LiFSI-9DME); high-concentration electrolyte (HCE, LiFSI-1.2DME), and LHCE (LiFSI-1.2DME-3TTE). Li||NMC-811 cells with a medium high cathode areal loading of 1.5 mAh cm^{-2}, a thick lithium anode, and an excess electrolyte were first assembled and cycled under high voltages. Figure 100a shows, for the Li||NMC-811 cells charged to 4.4 V, the superior behavior of the LHCE over the conventional electrolyte. The synergistic effect between the LiFSI salt and the DME solvent plays an important role in stabilizing the highly reactive NMC-811 cathode. The LHCE also shows the highest CE. Even at a cutoff voltage of 4.5 V, the LHCE was superior, holding over 82% of the initial capacity after 250 cycles. XPS data further indicate that a more stable SEI layer and CEI layer are formed on the Li-metal anode and NMC-811 cathode in LHCE. The superior stability of lithium anode and NMC-811 cathode in this electrolyte enables dramatically improved cycling performances of Li||NMC-811 batteries under highly challenging conditions, that is, 1.1 times excess lithium anode and an extremely limited electrolyte amount.

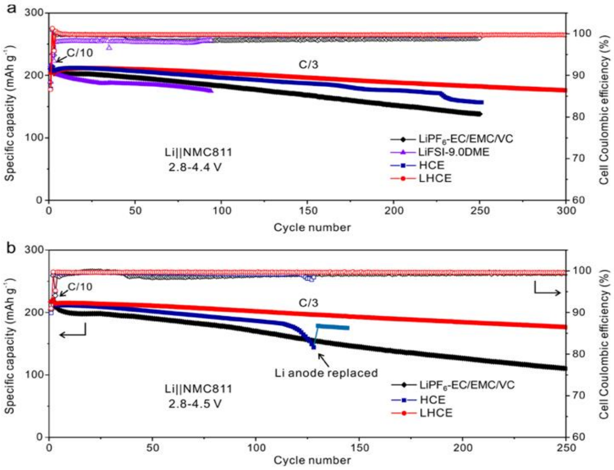

Figure 100. Cycling performances of Li||NMC-811 batteries in different electrolytes (conventional electrolyte (1 M $LiPF_6$ in EC-EMC (3:7 by wt.) with 2 wt.% of VC); dilute electrolyte (LiFSI-9DME); HCE (LiFSI-1.2DME), and LHCE (LiFSI-1.2DME-3TTE) under the charge cutoff voltage of 4.4 V (a) and 4.5 V (b), respectively. The electrolyte amount in each coin cell is 75 µl.

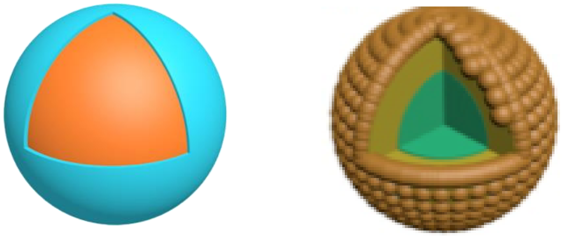

Figure 101. a range of coatings and surface substitution studies were performed. As shown, these can be just a coating (left) or a coating with penetration into the surface layers (right).

As noted in previous reports, high-Ni NMC is very reactive with both the environment and the electrolytes, and also has a large capacity loss of 10-15% on the first cycle. To remediate this, a range of coatings and surface substitution studies was performed. As shown in the schematic in Figure 101, these can be just a coating or a coating with penetration into the surface layers. Niobium- and boron-based coatings were studied.

The results of cell performances are shown in Figure 102. The use of a niobium oxide coating/substitution reduced the 1st cycle loss, while at the 1% level, it slightly increased capacity of the cell. The capacity retention and rate capability were also improved. The use of boron-coated NMC-811, using LiDFOB (Li difluoro oxalato borate), resulted in higher rate capability and capacity retention. A boron-based coating was also found to protect an ultra-high nickel NMC, $LiNi_{0.94}Co_{0.06}O_2$, against environmental degradation. Figure 102 (right) compares the superior rate capability of the boron-coated NMC versus the uncoated NMC after storage. The capacity is also improved.

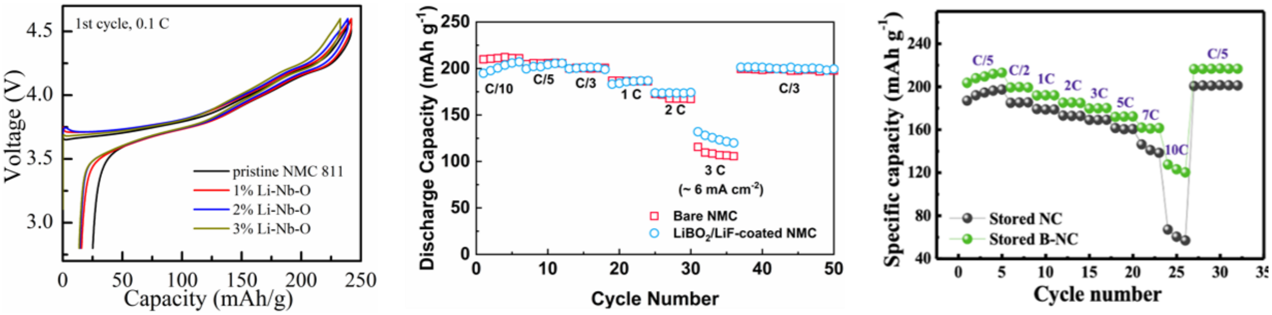

Figure 102. (left) 1st cycle behavior of NMC-811 in voltage range 2.8-4.6 V. (middle) Rate capability of NMC-811 with a $LiBO_2$/LiF coating in voltage range 2.8-4.6 V. (right) Rate capability of $LiNi_{0.94}Co_{0.06}O_2$ after storage in voltage range 2.8-4.4 V.

Most of the research performed to-date used commercial sources of 622 and 811 NMC. A goal of the Battery500 effort was to shift to an in-house source of material so that any coatings or lattice substitutions are known (vendors do not normally disclose this information). Figure 103 shows that large batches, 220 g, of NMC-811 can now be made that show the same behavior as small batches.

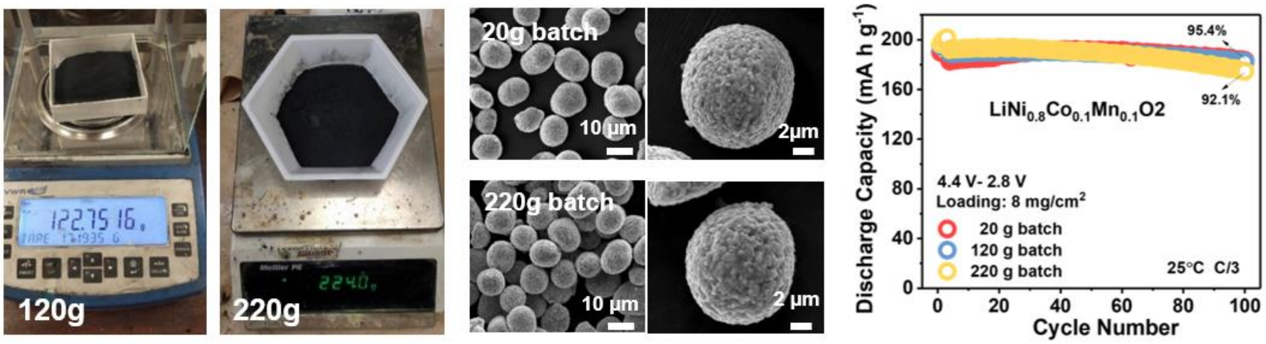

Figure 103. Large-scale synthesis of NMC-811, showing (left) the material formed; (center) the uniformity of the "meatballs" formed: top is 20 g batch and bottom is 220 g batch; and (right) the consistency of discharge capacity and capacity retention between the different sized batches.

The use of thick electrodes demands that the team builds the capabilities to study their behavior. Many of these capabilities are now in place, and are described in Figure 104. Results on these thick electrodes will be the subject of the next quarterly report.

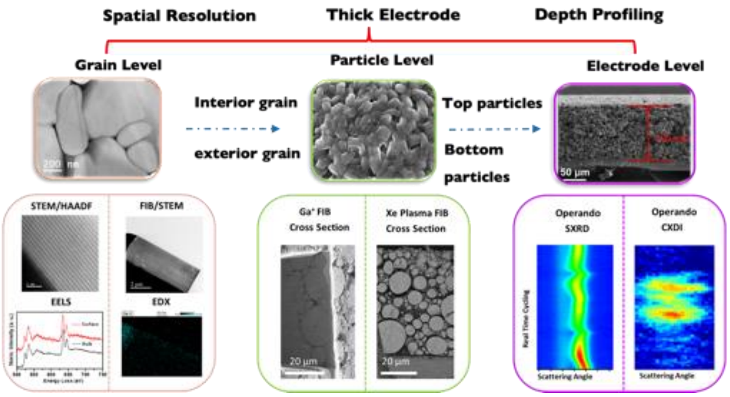

Figure 104. Schematic of the tools Battery500 are employing to study thick electrodes.

Highlights of Keystone Project 1

The highlights for this quarter are as follows:

- An ether-based liquid electrolyte has been developed to give much improved performance over the standard carbonate-based electrolytes in Li||NMC-811 cells.
- Coatings on high-nickel NMC have been shown to enhance capacity retention and rate capability, reduce 1st cycle loss, and mitigate effects of environmental degradation on storage.
- NMC-811 can now be made in-house in a reproducible manner, for use by the Battery500 team.

Keystone Project 2: Electrode Architecture

The goal of Keystone 2 is to design, model, fabricate, and characterize the effect of electrode architecture on electrode and cell performance in support of reaching the project goal of 500 Wh/kg cell specific energy. Included in this Keystone are architecture design of thick cathodes (UCSD), Li-metal electrode architectures (PNNL, UCSD, and Stanford), inorganic (UT-Austin) and polymer (Stanford) electrolytes, and electrode performance modeling (UW). Highlighted this quarter are recent advancements at multiple institutions in understanding the importance of Li-metal architecture and developing approaches to address the failure mechanisms.

Work at the Meng Group at UCSD has focused on development of a methodology to quantify how much of the lithium is lost to reactions with electrolyte to form the SEI and how much is lost as metallic lithium to electrical isolation. The method is based on analyzing hydrogen gas production after reacting the electrode with water; only isolated lithium metal will produce hydrogen. The method is applied to correlate the origin of inactive lithium with the CE in Li||Cu half cells. Two representative electrolytes, the HCE (4.6 m LiFSI + 2.3 m LiTFSI in DME) and commercial carbonate electrolyte (CCE, 1 M $LiPF_6$ in EC/EMC), were compared at three stripping rates (0.5, 2.5, and 5.0 mA cm^{-2}; all plating was done at 0.5 mA cm^{-2} for 1 mAh cm^{-2}). Figure 105a-b shows average CE and representative voltage profiles during the 1st cycle. The small error bars indicate good consistency among the cells. As expected, the HCE exhibits higher CE than the CCE. The total amount of inactive lithium is equal to the capacity loss between the plating and stripping processes, displaying a liner relationship with CE in Figure 105d. The content of the metallic Li^0 was directly measured by the hydrogen evolution method. As summarized in Figure 105c, in the HCE, the capacity loss from inactive metallic Li^0 is about 60% at different stripping rates. This is consistent with the similar CE at various stripping rates, whereas, in the CCE, it contributes over 90%, especially at high stripping rate. Surprisingly, the amount of unreacted metallic Li^0 exhibits a linear relationship with loss of CE, as shown in Figure 105e, which is almost independent from the testing conditions. This implies that the CE loss is governed by the formation of inactive metallic Li^0. Thus, the SEI Li^+ amount (Figure 105f) deducted from above remains low and relatively constant under various stripping rates. Based on these analyses, the team identifies the unreacted metallic Li^0, rather than the (electro)chemically formed Li^+ in SEI, as the dominating cause for the inactive lithium and capacity loss in Li-metal batteries, clearing the long-term misconception in the field that the low CE is caused by the continuous repairing of SEI fracture that consumes both electrolyte and active lithium.

The analysis results obtained at UCSD thus argue for approaches to effectively connect lithium metal to prevent formation of isolated metallic lithium. In this regard, PNNL developed a mesoporous carbon framework that is highly lithiophilic that encourages the filling of the mesopores with lithium metal, thus promoting self-wetting and self-smoothing. As a result, a Li-metal battery with a NMC-811 cathode showed excellent cycle life, even in lean electrolyte and low N/P ratio conditions (Figure 106).

In a collaboration between Stanford and PNNL, another 3D host employed a silicon pillared graphene oxide, or SirGO. Silicon makes the host more lithiophilic and prevents the collapse of the GO structure upon Li-metal stripping. This design is proven to be effective in ensuring Li-metal incorporation into the host rather than on the outer surface. On removal of lithium, the thickness of the electrode is maintained, demonstrating the effectiveness of design (Figure 107).

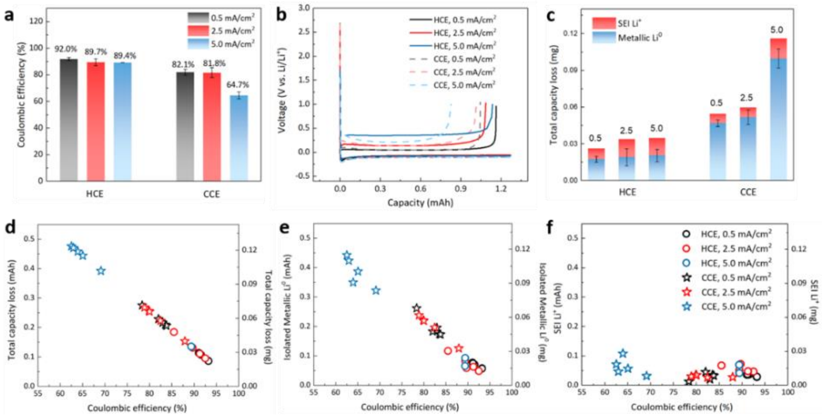

Figure 105. Quantitative differentiation of inactive lithium by the hydrogen evolution method. (a) Average Coulombic efficiency (CE) of Li||Cu cells under different testing conditions. (b) Representative voltage profiles of Li||Cu cells under different testing conditions in the 1st cycle. (c) Summarized quantitative contribution of capacity loss from the SEI Li^+ and metallic Li^0. (d) Total capacity loss as a function of CE. (e) Inactive metallic lithium amount measured by the titration gas chromatography method as a function of CE. (f) Calculated SEI Li^+ amount as a function of CE.

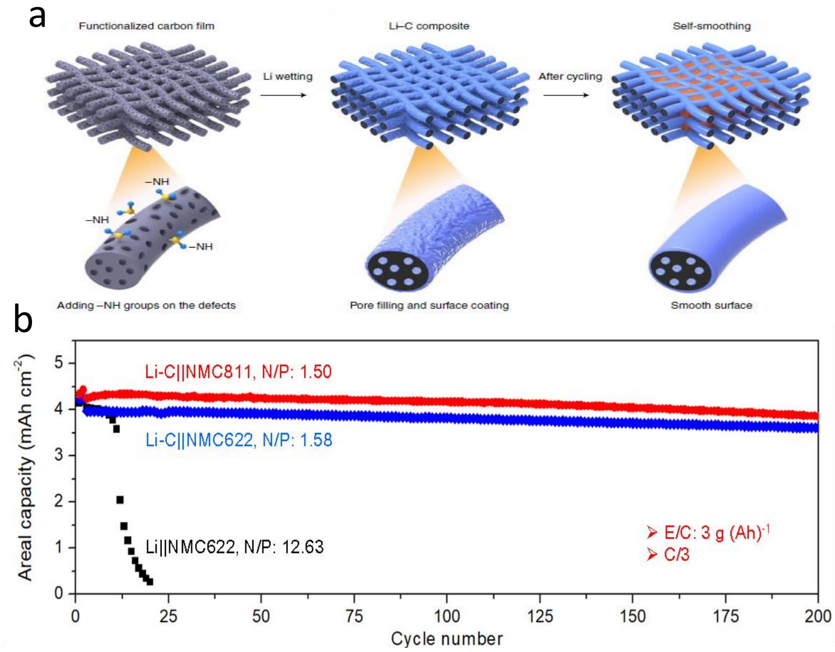

Figure 106. (a) Schematic of the structure of a 3D mesoporous carbon host that encourages lithium wetting and pore filling. (b) Capacity retention of Li||NMC cells with cycling. NMC-622 is $LiNi_{0.6}Co_{0.2}Mn_{0.2}O_2$, NMC-811 is $LiNi_{0.8}Co_{0.1}Mn_{0.1}O_2$, and E/C is electrolyte/ capacity ratio.

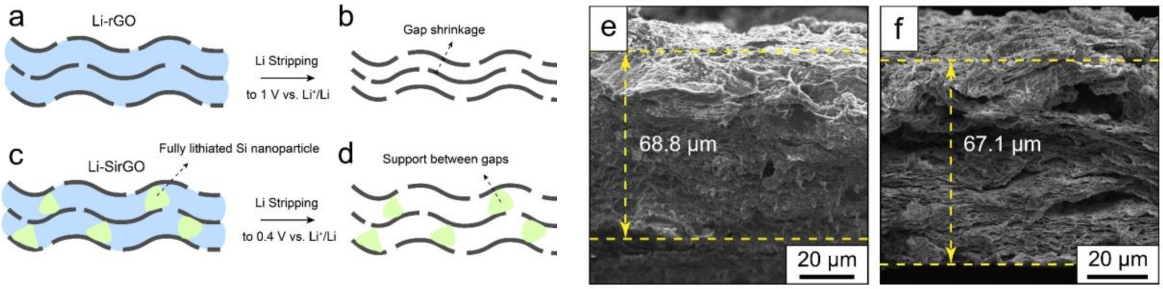

Figure 107. A schematic comparison of the structure of Li-rGO (reduced graphene oxide) and Li-SirGO (silicon pillared graphene oxide), where the presence of silicon between the GO layers helps to maintain the gaps (a-d). (e-f) Scanning electron microscopy images of electrode cross-section, demonstrating that the Li-SirGO structure maintains its overall thickness after removal of 1 mAh/cm^2 of lithium.

Highlights of Keystone Project 2

The highlights for this quarter are as follows:

- Significant advancement in understanding the importance of Li-anode architectures was made. The role of isolated lithium metal in determining capacity loss is confirmed by a new chemical analysis method.
- With this new insight, numerous design approaches have been undertaken to fabricate 3D architectures that minimize production of isolated lithium metal. These advancements will play a pivotal role in developing long-life Li-metal batteries.

Keystone Project 3: Cell Fabrication, Testing, and Diagnosis

Understanding cycle life and ways to life extension is a key concern for enabling high-energy, rechargeable Li-metal batteries; this has been the focus this quarter. Using different sets and designs for Li||NMC cells, the Battery500 team has been investigating ways to extend cycle life using multiple routes and cell characterization approaches. The result of these activities has been development of a 2.5 Ah cell with 350 Wh/kg capable of 250 cycles with less than 20% fade (Figure 108). The team is validating this performance and developing an early understanding of the state of calendar life for this round of cells. Initial work on previous designs has shown over one year of calendar life with low capacity fade. As part of the validation activities and prior assessment of calendar and cycle life, key differences in performance are being evaluated.

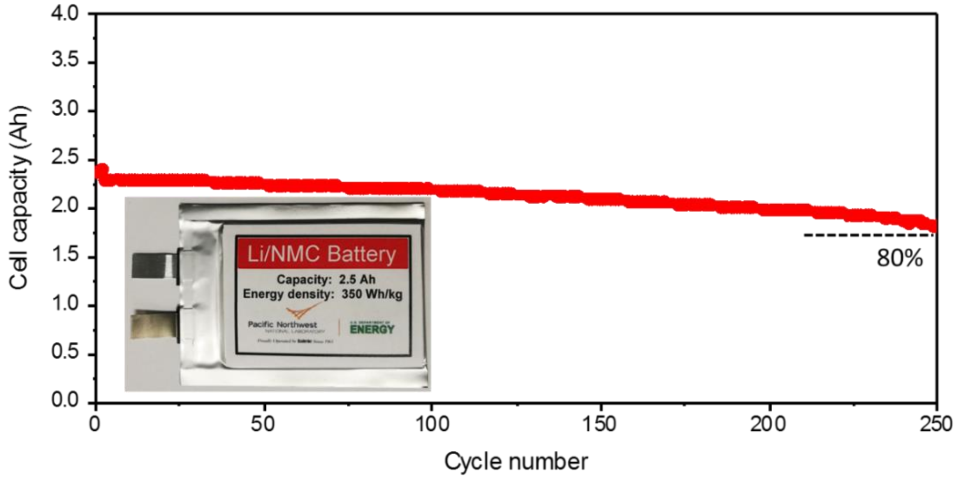

Figure 108. Cycle life data for a 2.5 Ah Li||NMC cell. Cycling was at a C/10 charge and a C/3 discharge.

One area that has helped facilitate the long cycle life in full pouch cells has been a refined understanding of pressure and pressure conditions for fixturing cells. A key finding from earlier this fiscal year that was applied to the 2.5 Ah pouch cell was the uniform use of pressure and tracking pressure evolution as cycling advanced. In response, as activities related to cell design and use conditions evolved, the team has developed additional standard testing protocols including single-layer pouch cell procedures. The combination of coin cell and single-layer pouch cell procedures provides a means to better understand the processes of both materials as well as to more directly understand charging and mechanical differences in cell design. The standard procedures for single-layer pouch cells include prescribed cathode loading, with electrolyte volume similar to the standard coin cell procedures. The single-layer pouch procedures also include means for fixturing cells and additional safety-related information.

As shown in Figure 109, the team is now starting to more discretely evaluate pressure uniformity as a function of the materials being used in the cell and how the associated design impacts electrochemical performance. On the left side, differential capacity for cells at three different pressures shows a distinct shift in response and utilization as cycling progresses. On the right, computational assessment of the impact of surface roughness on local current density is shown. For the assessment, characterization of electrode surface roughness was used to import into the model. As shown, increasing roughness of the electrode leads to current density variation, which subsequently increases the localized pressure distribution in the cell during cycling.

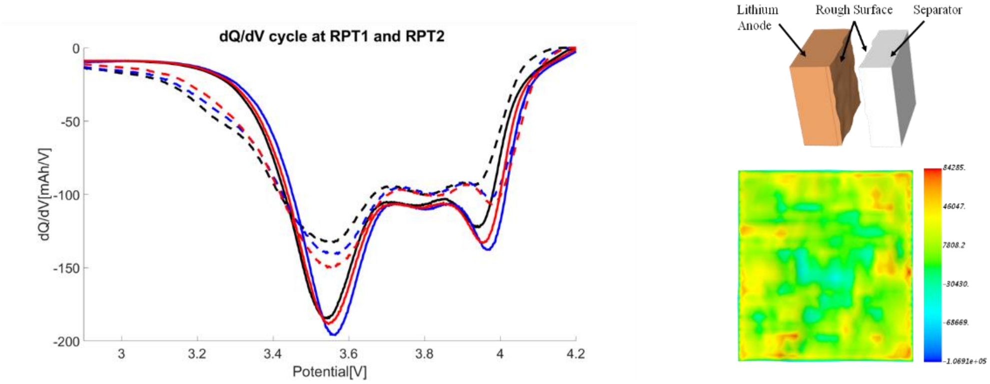

Figure 109. (left) Differential capacity analysis on the impact of three different pressure regimes for cycling of a single-layer Li||NMC pouch cell. (right) Model framework and predicted, local current density for real electrode during early cycling.

Highlights of Keystone Project 3

The highlights for this quarter are as follows:

- Achieved 250 cycles at 350 Wh/kg cells with less than 20% fade.
- Began validation testing to understand cycle and calendar life.
- Studied and increased understanding of the impact of local pressure in cell by electrode design.

Patents/Publications/Presentations

Patent

- Wang, S., H. Pan, J. Xiao, J. Liu, and J. Yang. “Battery Separator with Lithium Ion Conductor Coating.” International Patent Application No. PCT/US2019/037988, June 19, 2019. Filed by UW.

Publications

- Shadike, Z., H-S. Lee, C. Tian, K. Sun, L. Song, E. Hu, I. Waluyo, A. Hunt, S. Ghose, Y. Hu, J. Zhou, J. Wang, P. Northrup, S-M. Bak, and X-Q. Yang. “Synthesis and Characterization of a Molecularly Designed High-Performance Organodisulfide as Cathode Material for Lithium Batteries.” *Advanced Energy Materials*. doi: 10.1002/aenm.201900705. Publication Date (Web): April 10, 2019.
- Lin, R., E. Hu, M. Liu, Y. Wang, H. Cheng, J. Wu, J-C. Zheng, Q. Wu, S-M. Bak, X. Tong, R. Zhang, W. Yang, K. A. Persson, X. Yu, X-Q. Yang, and H. L. Xin, “Anomalous Metal Segregation in Lithium-Rich Material Provides Design Rules for Stable Cathode in Lithium-Ion Battery.” *Nature Communications* 10 (2019): 1650. doi: 10.1038/s41467-019-09248-0. Publication Date (Web): April 9, 2019.
- Liu, D., Q. Yu, S. Liu, K. Qian, S. Wang, W. Sun, X-Q. Yang, F. Kang, and B. Li.* “Evolution of Solid Electrolyte Interface on TiO_2 Electrodes in an Aqueous Li-Ion Battery Studied Using Scanning Electrochemical Microscopy.” *Journal of Physical Chemistry C* 123, no. 20 (2019): 12797–12806. doi: https://doi.org/10.1021/acs.jpcc.9b01412. Publication Date (Web): May 1, 2019.
- Qiu, Q-Q., Z. Shadike, Q-C. Wang, X-Y. Yue, X-L. Li, S-S. Yuan, F. Fang, X-J. Wu, A. Hunt, I. Waluyo, S-M. Bak,* X-Q. Yang,* and Y-N. Zhou.* “Improving the Electrochemical Performance and Structural Stability of the $LiNi_{0.8}Co_{0.15}Al_{0.05}O_2$ Cathode Material at High-Voltage Charging through Ti Substitution.” *ACS Applied Materials & Interfaces* 11, no. 26 (2019): 23213–23221. doi: 10.1021/acsami.9b05100. Publication Date (Web): June 11, 2019.
- Chen, H., A. Pei, D. Lin, J. Xie, A. Yang, J. Xu, K. Lin, J. Wang, H. Wang, F. Shi, D. Boyle, and Y. Cui. “Uniform High Ionic Conducting Lithium Sulfide Protection Layer for Stable Lithium Metal Anode.” *Advanced Energy Materials* 9, no. 22 (2019): 1900858. doi: 10.1002/aenm.201900858. Publication Date (Web): April 30, 2019.
- Li, W., A. Dolocan, J. Li, Q. Xie, and A. Manthiram. “Ethylene Carbonate-Free Electrolytes for High-Nickel Layered Oxide Cathodes in Lithium-Ion Batteries.” *Advanced Energy Materials* (2019): 1901152. doi: 10.1002/aenm.201901152. Publication Date (Web): June 25, 2019.
- Bewley, R., E. J. Dufek, S. E. Egan, D. J. Jamison, C. Ashton, C. H. Ho, M. C. Evans, and T. L. Bennett. “Safety Aspects of Energy Storage Testing.” *Journal of the Electrochemical Society* 166, no. 8 (2019): E263–265. doi: 10.1149/2.1271908jes. Publication Date (Web): May 21, 2019.
- Fang, C., X. Wang, and Y. S. Meng.* “Key Issues Hindering a Practical Lithium-Metal Battery.” *Trends in Chemistry* 1 (2019): 152–158. Publication Date: May 2019.
- Zhou, H.,* H. Liu, * Y. Li, X. Yue, X. Wang, M. Gonzalez, Y. S. Meng, and P. Liu.* “In-Situ Formed Polymer Gel Electrolytes for Lithium Batteries with Inherent Thermal Shutdown Safety Features.” *Journal of Materials Chemistry A* 7 (2019): 16984–16991. doi: 10.1039/C9TA02341K. Publication Date (Web): June 25, 2019.
- Dawson-Elli, N., S. Kolluri, K. Mitra, and V. R. Subramanian. “On the Creation of a Chess-AI-Inspired Problem-Specific Optimizer for the Pseudo Two-Dimensional Battery Model Using Neural Networks.” *Journal of the Electrochemical Society* 166, no. 6 (2019): A886–A896. doi: 10.1149/2.1261904jes. Publication Date (Web): March 15, 2019.

- Ren, X., L. Zou, X. Cao, M. H. Engelhard, W. Liu, S. D. Burton, H. Lee, C. Niu, B. E. Matthews, Z. Zhu, C. Wang, B. W. Arey, J. Xiao, J. Liu, J-G. Zhang,* and W. Xu.* "Enabling High-Voltage Lithium-Metal Batteries under Practical Conditions." *Joule* 3 (2019): 1662–1676. doi:10.1016/j.joule.2019.05.006. Publication Date (Web): June 5, 2019.
- Niu, C., H. Lee, S. Chen, Q. Li, J. Du, W. Xu, J-G. Zhang, M. S. Whittingham, J. Xiao,* and J. Liu.* "High-Energy Lithium Metal Pouch Cells with Limited Anode Swelling and Long Stable Cycles." *Nature Energy* 4 (2019): 551–559. doi:10.1038/s41560-019-0390-6. Publication Date (Web): May 13, 2019.

Presentations

- Materials Science and Engineering Department Seminar, University of California, Irvine, California (May 24, 2019): "Advanced Diagnosis and Characterization for Next Generation Energy Storage Materials"; Y. S. Meng. Invited.
- University of California, Department of Chemistry, Santa Cruz, California (April 1, 2019): "Chemistry and Architectures for Energy Storage"; P. Liu. Invited.
- Advanced Automotive Battery Conference (AABC), San Diego, California (June 24, 2019): "Long Life and Safe Lithium Batteries"; P. Liu. Invited.
- MRS Spring Meeting, Phoenix, Arizona (April 26, 2019): "Stable High-Voltage Lithium Metal Batteries Enabled by Ether-Based Electrolytes"; W. Xu,* X. Ren, S. Jiao, and J-G. Zhang. Invited.
- 257th American Chemical Society (ACS) National Meeting, Orlando, Florida (April 2, 2019): "Enabling Ether-Based Electrolytes for High Voltage Lithium Metal Batteries"; W. Xu,* X. Ren, S. Jiao, and J-G. Zhang. Invited.
- 235th ECS Meeting, Dallas, Texas (May 26–30, 2019): "The Fundamental Mechanism behind the Stability of Li Metal Anodes in Non-Aqueous Electrolytes"; J-G. Zhang,* X. Cao, X. Ren, and W. Xu. Invited.
- Beyond Lithium Ion XII, Golden, Colorado (June 25–27, 2019): "Non-Flammable Electrolytes for Lithium Metal Batteries"; J-G. Zhang. Invited.
- TMS Annual Meeting & Exhibition, San Antonio, Texas (March 10–15, 2019): "Identification and Visualization of Chemical Outliers through Scientific Data Mining in Nanoscale Spectro-Microscopic Study of NMC Electrode"; E. Hu, Y. Liu, H. Xin, and X-Q. Yang. Invited.
- CERC-CVC, Xining, China (June 23, 2019): "Understanding Capacity Fade in High-Nickel Content Cathode Materials for Lithium Batteries"; R. Lin, Z. Shadike, S-M. Bak, E. Hu, H. Xin, X. Huang, Y. Shin, H-S. Lee, Y. S. Chu, Y. Liu, and X-Q. Yang.* Invited.
- Cornell Energy Systems Institute (CESI), Chemical Engineering, Cornell University (April 10, 2019): "What are the Materials Limitations to Advancing Lithium Batteries to the Next Level?"; M. S. Whittingham. Invited.
- Willem Prins Memorial Lecture, Syracuse University, Syracuse, New York (April 16, 2019): "What are the Chemistry and Materials Limitations to Advancing Lithium Batteries to the Next Level?"; M. S. Whittingham. Invited.
- MRS Meeting, Phoenix, Arizona (April 2019): "Key Parameters for Solid Electrolytes – Learnings from Beta-Alumina and Future Opportunities"; M. S. Whittingham. Invited.
- Cornell Center for Materials Research (CCMR) Symposium, Cornell University, Ithaca, New York (May 22, 2019): "How Far Can We Push the Limits of Intercalation Batteries?"; M. S. Whittingham. Invited.
- Center for Research in Extreme Batteries (CREB) Spring Biannual Meeting, Electric Flight Batteries, University of Maryland, College Park, Maryland (June 14, 2019): "Battery500 Consortium: Revisiting and Addressing the Fundamental Challenges of Rechargeable Li Metal Batteries"; J. Xiao and J. Liu. Invited.

- 235th ECS Spring Meeting, Dallas, Texas (May 27, 2019): "Battery500 Consortium: Addressing the Fundamental Challenges to Enable High-Energy Rechargeable Li Metal Batteries"; J. Xiao and J. Liu. Invited.
- Nanotechnology Seminar Organized by Graduates in Nanotechnology, Georgia Institute of Technology, Atlanta, Georgia (April 8, 2019): "Nanomaterials Design for Energy and Environment"; Y. Cui. Invited.
- MRS Spring Meeting, Symposium QN05, Phoenix, Arizona (April 22–26, 2019): "Thermal Materials and Science in Textile and Batteries"; Y. Cui. Invited.
- 4th Lithium Battery International Summit (LBIS), Shenzhen, China (May 6–9, 2019): "Lithium Metal Anode: Host Materials Design and Solid Electrolyte Interphase"; Y. Cui. Invited.
- Donghua University Seminar, Shanghai, China (May 8, 2019): "Nanomaterials Design for Energy, Environment and Textile"; Y. Cui. Invited.
- Department of Materials Science and Engineering Seminar, Seoul National University, Seoul, South Korea (May 9, 2019): "Nanomaterials and Interface Design for Energy Storage"; Y. Cui. Invited.
- 23rd Annual Interdisciplinary Symposium, Miller Institute, Marconi Conference Center, Marin County, California (June 7–9, 2019): "Reinventing Batteries: What's Possible?" Y. Cui. Invited.
- 6th Nano Today Conference, Lisbon, Portugal (June 16–20, 2019): "Nanomaterials Design for Energy and Environment"; Y. Cui. Invited Plenary.
- Dan Maydan Prize in Nanoscience, Hebrew University of Jerusalem, Jerusalem, Israel (June 18, 2019): "Nanomaterials Design for Energy Storage"; Y. Cui. Invited Award Talk.
- World New Energy Vehicles Congress, Hainan, China (June 30, 2019): "Next Generation High Energy Batteries"; J. Liu. Invited.
- AABC, San Diego, California (June 23, 2019): "Addressing Li Problems in High Energy Batteries"; J. Liu. Invited.
- Euro Mediterranean Conference on Materials and Renewables, Marrakesh, Morocco (June 14, 2019): "Next Generation High Energy Batteries for Electrification"; J. Liu. Invited.
- Huazhong Agricultural University, Wuhan, China (May 6, 2019): "Next-Generation Battery Technologies"; A. Manthiram. Invited.
- Zhengzhou University, Zhengzhou, China (May 7, 2019): "A Perspective on Electrical Energy Storage"; A. Manthiram. Invited.
- Nankai-Cambridge International Symposium on Advanced Materials, Nankai University, Tianjin, China (May 19–21, 2019): "Advanced Materials for Next-Generation Batteries"; A. Manthiram. Invited.
- SSI-22, Pyeongchang, South Korea (June 16–21, 2019): "High-Nickel Layered Oxide Cathodes for Lithium-Ion Batteries"; A. Manthiram. Invited Keynote Talk.
- AABC, San Diego, California (June 24–27, 2019): "High-Nickel, Low-Cobalt Cathodes for Lithium-Ion Batteries"; A. Manthiram. Invited.